Department of Architecture and
Built Environment

The University of
Nottingham

A NOVEL CLEAR FOIL CUSHION CONSTRUCTION INCORPORATING AN ADDITIONAL WATER LAYER

By

Fei Xie, ***BArch, MArch***

Thesis submitted to the University of Nottingham
for the degree of Doctor of Philosophy
June 2011

A NOVEL CLEAR FOIL CUSHION CONSTRUCTION INCOPORATING AN ADDITIONAL WATER LAYER

71,658 words in total.

5.11.2011

Fei Xie
BArch, MArch

The University of Nottingham

Department of Architecture and Built Environment

ABSTRACT

Pneumatic clear foil cushion systems, notably as ETFE foil cushions have been developed as an alternative technology to large-scale glass glazing systems for wide-span buildings. The systems display better thermal performance and have advantagies of extremely low dead-weight constructions comparied to conventional glazing systems, and thereby the increasing popularity of foil cushion cladding systems have been witnessed in the last decades. However due to their lightweight and thinness, the thermal behaviour of architectural foil membranes exhibits a high responsiveness to variations in external conditions. For this reason, it is argued that the reliable prediction of the thermal environment experienced in a space enclosed by a tensile membrane skin construction would require a bespoke modelling of the dynamic thermal behaviour of such a construction at first.

Building envelopes clad with such cushions, such as the famous Eden project in the UK, need a dynamic system to control overheating in summer. A cooling liquid layer constructed within a clear multi-layer foil cushion envelope is proposed in this thesis. It enables rapid cooling effects on the building envelope. The system is based on an evaporative cooling mechanism and is integrated with the inflated cushion to provide desired cooling effect eco-friendly. The implications of the forms and configurations of clear foil cushion constructions with and without a cooling liquid layer in the overheating control were evaluated in this research project. Data were collected from a series of experiments to ascertain the effects of the additional cooling water layer on heat transfer processes within the foil skin construction. The results demonstrated that the thermal behaviour of a foil penal depended mainly on surface convection and radiation heat transfer and the cooling performance of the water layer within the foil skin constructions was evident. The initial experimental outcomes were valuable for the design of such novel dynamic cooling systems.

In order to assess the effect that different pneumatic foil skin constructions with a water layer might have on thermal conditions inside the enclosed space, the thermal behaviour of full-scale indoor double-layer foil cushion en-

closure and triple-layer foil skin construction, with varying evaporative cooling integrative ways and foil skin constructions, were tested during the course of this research. The test datasets were compared according to the research objectives and with the environmental control strategy proposed at the initial design stages.

The investigated thermal behaviour of the foil skin constructions incorporating a water layer serves as a reference basis for the analytic modelling of the tested double and triple-layer foil skin constructions in order to predict their surface temperatures and the solar radiation directed into the space they enclose. The approach is based on a detailed modelling of the radiative and convective heat transfer processes affecting the membrane surfaces. These prediction results derived from the model were compared against the environmental data obtained on the test rigs.

The developed analytical model is only tentative, as some thermal transfer processes, such as long wave radiation exchanges between the foil sheets, have not been accounted for in this model. Further work is required to develop this model in order to appreciate the thermal performance of such novel foil cushion constructions more precisely and extend their building applications.

KEYWORDS: Clear Foil Cushion, Pneumatic Structure, Foil Skin Envelope, Thermal Performance, Over-heating Control, Cooling Liquid Layer, Evaporative Cooling, Constructional Integration System

ACKNOWLEDGEMENT

This thesis is the result of all the support, help, patience and friendship from many people involved in these four years of my PhD study in the University of Nottingham. I would like to express my sincere gratitude to:

- My supervisor, Dr. Siddig Omer, for his support on the accomplishment of this research project.
- My second supervisor, Prof. Saffa Riffat, for his invaluable assistance to make this study possible at the first place and to be developed.
- The Collaborative Research Personnel Training Programme, which organised by the University of Nottingham and Mr. Jianguo Zhong, the financial sponsor, for such a good opportunity to study PhD and to have invaluable international academic training in the United Kingdom.
- The board of Directors of the Hunan University, P.R. China, for the generous grant that allowed me to survive and accomplish this formidable research work.
- The staff of the Department of Architecture and Built Environment for providing help, information and experiment facilities required for this project, especially to Mr David Oliver, and Ms Amante-Roberts Zeny.
- The precious help and friendship from the Nottingham friends, Fidel, Ricardo, for sharing their experience on how to develop a interdisciplinary research work as an independent academic at the early stage, and specially to Deborah Adkins for proofreading and valuable comments.
- My beloved family, i.e. Diyu, Isabel, Timothy..., in particular, my parents, Sanyuan Fang, Bingyan Xie, for their most profound love, great patience and believing in me.

Of course, this research work is a strenuous task I have completed, but all of your consistent encouragement and love give me strength and courage to go through any tough stage of the research and understand:

> "*When the going gets tough, the tough get going.*"
> ---English Proverb

TABLE OF CONTENTS

LIST OF FIGURES

LIST OF TABLES

NOMENCLATURE

A	Area [m^2]
d	Dameter of the air conduit [m]
D_e	Hydraulic diameter of the noncircular duct [m]
ε	Hemispherical emissivity of a grey body surface
E	Emissivity factor
h	Heat transfer coefficient [$W.m^{-2}.K^{-1}$]
ha, hr	Surface convective heat transfer coefficient, surface radiative heat transfer coefficient [$W.m^{-2}.K^{-1}$]]
$hr0$	Radiative coefficient for a black-body [$W.m^{-2}.K^{-1}$]
h_{in}, h_{out}	Enthalpy of air flow at the inlet or outlet [kJ/kg]
H	The height of the volume [m]
i_{sp}	Angle of incidence between solar and panel normal [degrees]
I, I_{direct}	Incident light, direct beam radiation on panel [$W.m^{-2}$]
I^o_{en}	Transmitted light incident on the internal surfaces of a room
k	Conductivity of the layer [$W.m^{-1}.K^{-1}$]
L	Height of vertical surface [m]
M	Local membrane tension [Pascal]
P	Air pressure [Pascal], [$N.m^{-2}$]
Pr	Prandtl number [dimensionless]
q	Total energy gains [$W.m^{-2}$]
Q	Heat gains [$W.m^{-2}$]
Q_e	Evaporative cooling rate [$W.m^{-2}$]
Q_w	Water convective heat transfer [$W.m^{-2}$]
r	Curvature ratio in a sphere radius [m]
R	Core resistance of glazing layer [$m^2.K.W^{-1}$]
R_{si}, R_{so},	Combined radiative and convective thermal resistance of the internal and external surfaces respectively [$m^2.K.W^{-1}$]
Re	Reynolds number [dimensionless]

$SHGC(i)_{test}$	Solar heat gain coefficient at incidence angle *i*
$SHGC(i)_{ref}$	Heat gain coefficient of a standard glazing at incidence angle *i*
t, T	Temperature [°C]
T_a, Tr	Air temperature, mean radiant temperature [°C]
Δt, ΔT	Mean temperature difference [°C]
Ug	U value of a particular glazing [$W.m^{-2}.K^{-1}$]
V	Air flow rate [$m.s^{-1}$]
Vol	Volumetric flow rate [m3. s^{-1}]
V_F	View factor of surface [dimensionless]
W	Moisture content [$Kg.Kg^{-1}$]
τ ,α ,ρ	Transmittance, absorptance, reflectance of a body for a spectrum range
α_s, α_z	Solar altitude, solar azimuth [degrees]
β, β_z	Inclination of panel (tilt from horizontal), panel azimuth [degrees]
η_{sat}	Saturation Efficiency
ρ	Air density [kg. m^{-3}]
σ	Stefan-Boltzmann constant [5.6697x10-8 W. $m^{-2}.K^{-4}$]
ϕ	Relative humidity of incoming air [dimensionless]
φ	Equivalent surface coverage factor of water [dimensionless]
θ	Thickness of the layer [m]
τ^k , ρ^k	Generic angular solar transmittance factor, reflectance factor
ν	Kinematic viscosity [$m^2.s^{-1}$]
ω_{sp}	Panel solar azimuth [degrees]
λ	Thermal conductivity [$W.m^{-1}k^{-1}$]
m	Air mass flow rate [kg. s^{-1}]
C_p	Specific heat [$J.kg^{-1}.K^{-1}$]

SUBSCRIPTS

0,1,2,3	Recording stations along with the height from top to bottom
ao, ai, aca,	Outside, Internal air and cavity air
ad, aw	Air temperature in the dry channel and the wet channel [℃]
-A, -B	Distance to the reference (centre) line-A, reference (centre)
c	Center layer
cav	Cavity
cavo, cavi	Outlet , inlet of the cavity
db, wb	Air dry bulb and wet bulb temperature [℃]
dp	Dew point temperature [℃]
en	Entering enclosure
ext, int	External, internal
int, out	Inter, Outlet/outer
i/in,o/out	Inside/inner, outside/outer
LW	longwave length radiation
m	Mean values/membrane penal
net	Net energy gains
re	Rejcted
se, g	Surface of surroundings, ground
so, sc, si	Outer layer ,centre layer, Inner layer surface temperature
sw	Water layer temperature on the layer surface
SL	Shortwave length radiation
wf	combined water layer and foil layer

ACRONYMS

NIR	Near Infrared wavelength range
Far-IR	Far Infrared wavelength range

CHAPTER 1
INTRODUCTION

> *"Judge a man by his questions rather than by his answers"*
> --- Voltaire François-Marie Arouet (1694–1778)

The ability to create locally clement climate places for human activities is largely reliant on human knowledge of building constructions and on understanding of nature and the built environment in the space. Using wide-span structures to modify the local climate has only been a recently practice. In consideration of energy and environmental problems faced by mankind, the role of low-energy microclimate modification using large enclosures has become the focus of interest to both in the academic and industrial building communities.

Glazed atria, building roofs, and enclosures, etc. are all popular practices in modern design in order to create human immediate clement climate places. However high embedded-energy, heavy structure and the greenhouse effect, are deterring glass enclosures to develop further in the energy efficient wide-span architecture nowadays.

An alternative to large-span glass enclosures appears to be tensile surface membrane structures, of which the inflatable foil cushion is one derivation. The constructional industrial product of foil cushion is dominated by the use of the foil film, i.e. ETFE (Ethylene Tetra Fluoro Ethylene), a fluoro-carbon based thermoplastic polymer in the same chemical group as Teflon™ (i.e. PTFE).

1.1 Problem Statement and Objectives of Study

In the modern design of public or office buildings, large glazed areas are becoming a common feature. The application of large glazed areas in buildings is justified mainly by the argument that there is an improvement of natural lighting within the internal space enclosed by such envelop. However, these types of envelop still add significant heat gains and heat losses to the total energy consumed for heating and cooling[1].

Compared to glass glazing, foil cushion constructions display better thermal performance as the air entrapped between the layers provides good thermal properties to the cladding system (see Figure 1-1), in spite of their extremely low mass of only 2-3.5 kg/m^2 generally. A typical thermal conductance (U value) of 1.96 W/m^2.K can be reached for a triple-layer cushion, compared to 3.2 W/m^{2}K for double-glazing. For these materials with high absorption properties to long infrared radiation can add extra value to save energy consumption in the heating. Therefore, the concept of foil cushion cladding system offers reduced U-value and extreme lightweight for glazed envelopes with large glazed area. However, due to high light transmission of clear foil cushion, the risk of over-heating exists and yet the field of over-heating control is under study.

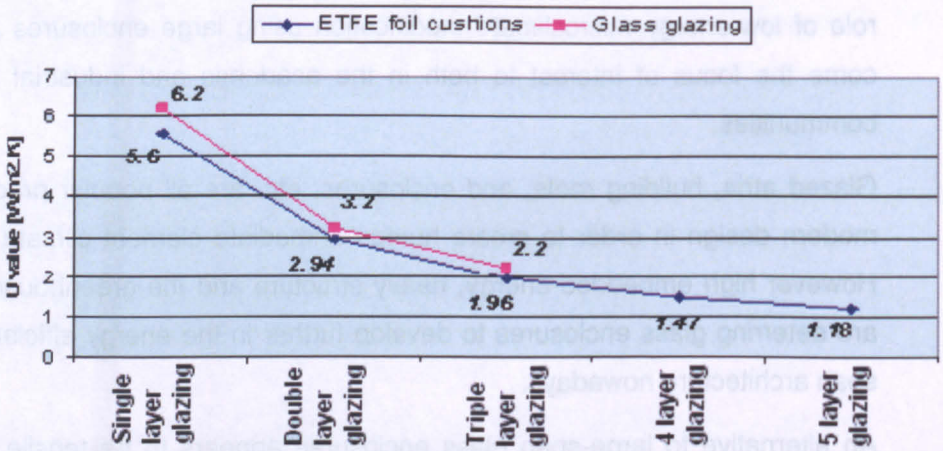

Figure 1-1: Comparisons of U values between ETFE foil cushions[3],[4] and glass [2] glazing systems with different constructions [5] [6]. [NB. the caculation is for a standard foil sheet of 100μm in thickness, weighing175g/m^2]

The common commercial available solution on solar control is surface treatment of the foil cushion to modify it transmission and consequently reduce solar gain. This measurement is at the expense of reducing day light level; meanwhile build-up heat caused by thermal radiation still remains unsolved.

An alternative, dynamic system by forming thin liquid layer on a clear plastic membrane is presented and investigated in this project to reduce cooling load while reject solar gain as a latent heat of water vapour. This concept claims to be compatible with the lightweight nature of foil cushion at the same time, to enhance thermal radiation control, and provides both cooled envelope and a good level of day-lighting.

Previous study on the liquid cooling process within a transparent building roof has not considered combining the convective cooling effect of airflow created

within the air spaces of the multi-layer foil skin building envelope. Yet the consequence of such an evaporative-cooled envelope could be on the internal buoyancy cooling of the enclosed space, and on overheating control by proper design of pneumatic clear foil cushion constructions.

In addition, the lightweight property of foil membrane constructions exhibits a high thermal response to the surrounding environment, which increases the difficulty for thermal environment control within foil cushion enclosures. The large scale of these enclosures can even worsen the situation if they are designed without careful concern about their thermal characteristics. In current foil cushion industries, there is a demand for holistic methods to improve their thermal environment in an environmentally friendly and integrative manner. Some researchers have already proposed some solutions to those enquiries. Therefore, the objectives of this research project are as follows:

- Review on the environmental performance of existing foil cushion envelope systems and architectural forms favouring indoor thermal conditions.
- Understand the cooling processes underlying the thermal performance of the proposed systems
- Assess the performance of the integration, and impact that these variable constructions may have on the thermal environment of the enclosed space by experimental simulation.
- Develop an analytical tool or at least tentative one to gain some informative data for a better appreciation of its performance

1.2 Scope of the Research and General Approaches Adopted

Considering the breadth of the subject and the limited existing body of knowledge available, it was decided to restrict the scope of the research presented in this thesis to the following aspects:

- Only pneumatic or frame-supported foil membrane enclosures were considered. Air-supported membrane enclosures were not included in this investigation, since their detailing and internal environment demonstrates features were specifically pressurised.
- Translucent foils similar to ETFE foil sheet were dealt with in this research

- This research was restricted to double-layer and triple-layer foil skin constructions and did not encompass the application of insulating materials such as fibrous insulation.
- Emphasis was put on the climatic aspects of Northern Europe.

The approaches have been adopted in this project:

- Analysis of the thermal properties of a foil penal coupling with/without water film---parameter study
- Experimental assessment on the overall thermal behaviour of the proposed constructions in various configuration---experimental simulation
- Assessment on the tentative computer simulation techniques vs. experiment results---comparative study of experiments and computer modelling

1.3 Outline of the Thesis

The overall structure of the research is illustrated in the following a 'map' of the thesis:

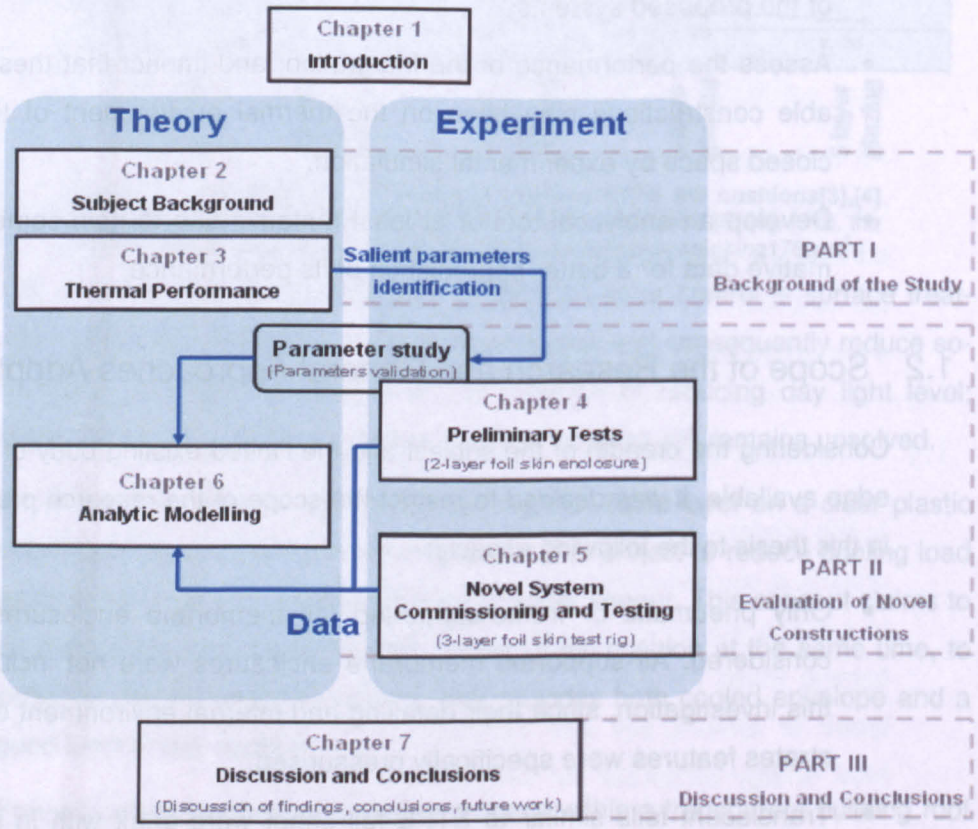

Figure 1-2: The format of the research work

PART I BACKGROUND OF THE STUDY

| SUBJECT BACKGROUND

| THERMAL PERFORMANCE

The foil cushion envelope has become an established form in the modern architecture. However, the issue of overheating is a challenge to be addressed in foil cushion architecture. The study presents the overview of the foil cushion technology and its thermal environment. A novel integration system of liquid cooling and foil cushion construction has been introduced to abate the overheating and enhance the thermal control of a foil cushion enclosure in this part.

CHAPTER 2
SUBJECT BACKGROUND

> *"I have built little. But I have built many castles in the air"*
> --- Frei Paul Otto (1925–)

2.1 Introduction

During the last decades, architects, engineers and designers have shown concern about the impact of the built environment on the natural environment; as a result, interest in the application of passive and active solar energy systems in buildings has increased leading to potential reductions in the use of fossil fuels as energy sources. Therefore, the concept of 'green' or 'sustainable' architecture has become widely acceptable among the building industry all over the world.

According to several authors, sustainability issues incorporate every level of decision-making affecting social, economic and environmental aspects of human life. Although there have been many definitions for the term 'sustainability', there is one used by the Brundtland Commission on Sustainable Development (1987) which is broadly accepted: "Development that meets the needs of the present without compromising the ability of future generations to meet their own needs".

In the building sector, a building envelop acting as a skin-layer relates to, and separates the external and internal environments. It is one of the main parts of the building, which is responsible for most of its energy consumption during the building's life span. Achieving highly efficient envelopes is something of a key issue in building related disciplines in this sustainable age. Some researchers have developed the concept of the responsive envelope, which has a controlled reaction to the variations that occur between the exterior and the internal spaces, providing comfort by adjusting itself automatically. Thus, the building envelope serves as an enclosure, which protects against the weather [1]. This concept opens the way and sets up design criteria for future development.

Glass is a very common and popular construction material for modern building envelop. Due to transparency of glass being associated with concepts of clear corporative and modern images, fully glazed buildings or glazed with large area have witnessed the continuant popularity within building designers. When buildings like these kinds are exposed to daily thermal variation and solar radiation, most of the heat received by the internal spaces is transmitted through the glazed areas of the envelope, resulting in over heating and increasing the cooling load for the internal space. Some technologies have been introduced into the glass glazing, such as double skin façade technology, adaptive building façade etc., to improve or enhance the environmental and energy performance of envelopes glazed in glass, becoming responsive or so called intelligent to the changes of the surrounding environment [8].

A double-skin façade system is developed to improve the thermal performance of glass- glazed envelope. The system is *"a pair of glass skins separated by an air corridor ranging in width from 20cm to several meters"*. [9] The cavity of the facade as a thermal buffer, which improves the thermal insulation, reduces heat losses and allows passive solar heating through the envelope [9]. There are some other advantages to this system, which is so called as one type of modern responsive envelope, but the disadvantages in terms of energy and thermal performance of such glazing material are still evident and make them not appropriate for the envelop of a large scale building (Figure 2-1). From the figure, the over-weight and over-cost of the double façade constructions have identified as major disadvantages by those previous researchers by up to 50%.

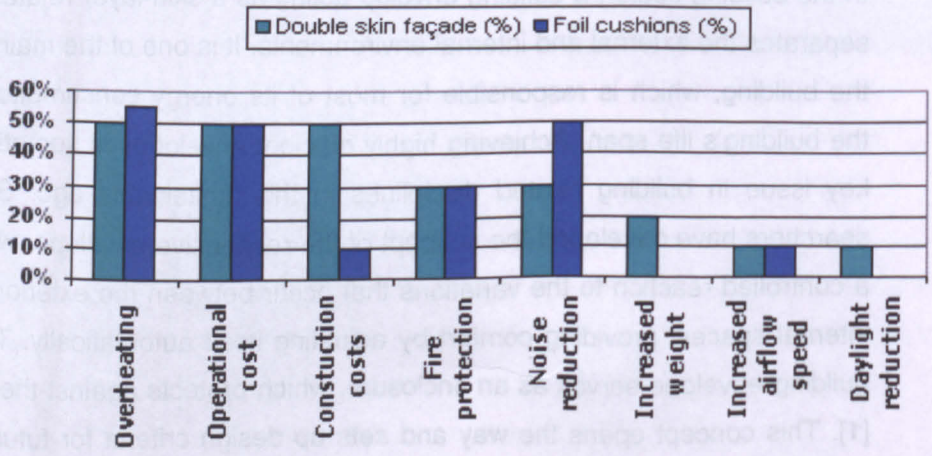

Figure 2-1: Disadvantages of the Double Skin Facades and foil cushions identified by some of the authors on previous literature in percentage

Some alternative technologies have been developed along with the glass glazed envelop. Tensile membrane structural architecture is a type of building driven by a different design concept to save energy during the whole of the building's life cycle. By reducing the overall dead-weight and construction costs in the building envelope, tensile membrane structures have become one of the new forces in the construction market of energy efficient envelopes.

The current commercial successful cladding system employing the membrane structure technologies is foil cushion constructions. This system sharing with the similar values to the glass glazing, such as transparency, natural light or aesthetics, also exhibit better thermal behaviour in comparison with the double glass glazing, however facing the same problems, specifically the over-heating in the hot seasons.

Until recently, designers have paid little attention to the environment inside membrane skin buildings. Their complex geometry and the small thickness of the membrane structures have made it difficult to understand and properly study their environmental behaviour. Previous research highlighted that the two major characteristics that affect the internal environment in a space enclosed by a foil membrane were:

- A membrane surface can gain heat very easily, and
- It can also lose heat almost instantaneously when the heat source is removed.

A number of researches focusing on thermal control and the performance of cooling techniques of membrane skin buildings were developed by firstly the University of Seville [10], Cardiff University [11], the University of Nottingham [12], and some other professional from the membrane industries [13]. As the membrane skin envelopes, especially foil cushion systems, are a relatively new area in the construction sector, the availability of research source and design tools is so limited that the work on detail researching of their thermal control is far behind the point where they may be used to inform the design process.

Generally, the respective advantages and disadvantages of foil and glass as glazing materials are vice versa in some cases. Both materials have their specific application fields and sometime preclude each other's use. But for the architectural vision of large facades and roofed areas, foil cushion have a great of advantages due to its lightness and economic structures. Now the glazing

industry has developed a new glazing solution, called FoilGlass [14], to combine the specific advantages of both materials to achieve synergy effect and result in better performance than that done by single materials alone.

2.2 Brief Background of Foil Cushions

The idea of using minimum energy structures in our daily life and with many possibilities of being recycled have been developed in order to save energy. The work is focused on lightweight structures and fibre-reinforced materials with the main aim to save energy from the construction process thus reducing the impact on the environment. Tensile surface membrane structure, commonly called tent, is one important player among the family group of lightweight structures in modern architecture.

One of the first architects working with lightweight structures was the American Buckminster Fuller, who introduced new concepts to the architectural vocabulary such as: tensegrity (continuous tension compensated with discontinuous compression), developed with Kenneth Snelson; and dymaxion (maximum benefit with minimum energy) [15]. Then Rice, P. [16] has classified lightweight structures into five main types:

- Tents and pre-stressed cable networks
- Air supported structures
- Pneumatic structures (inflatable air beam, foil cushion etc.)
- Grid shells
- Heavyweight cable roofs

Tents, air support and pneumatic structures are based on the tensile surface technical membranes to enclose space for human activities. But until the end of the 18th century, there was little development of the tent due to the limitations of fabric or foil film, including limited tensile strength and problems of making joints capable of transmitting significant force. Typically, the foil cover, normally a cheap temporary substitution for glass in greenhouse applications, was best known as a poly-tunnel cover for plants growth. With the emergence of the durable ETFE (ethylenetetrafluoroethylene) foil material, which first used for building applications in the 1970s, foil cushion technologies started to be widely accepted in architectural context and changing the image of foil from a flimsy material to an innovative glazing alternative to glass in building en-

velop constructions. The main advantage of foil membranes is that they are extremely light and low in embodied energy, which reduces the incurrence of environmental burden at their construction stage and impact of buildings in their lifetime (see Table 2-1). By constrast, a glass roof without accounting for the substantially larger support system that is required supporting it weighs upwards 50,000 grams/m^2 [5].

Table 2-1: Comparison of foil cushion and float glass in some aspects [5]

	ETFE Foil	6 mm Float Glass	Ratio Value of ETFE Foil to Glass	Special Information
Embodied Energy [GJ/ ton]	26.5	20		
Embodied Energy per m^2 [MJ/ m^2]	27	300	9%	
System Weight /Unit [kg / m^2] *	0.45	50	<2%	
Ultimate Tensile Strength [N/ m^2]	40-46	16 [c]	288%	
Power Input to Maintain Pressure /Cladding Area	50W/1000m2	----		A constant pressure of a foil cushion (is maintained by two 50W fans (one for back-up)
Commercial Retail Price	£25 /m^2 @ e=0.25mm [a]	Around £5/m^2 [b]	500%	

Notes:
a: the latest price was obtained from the website: http://www.alibaba.com/product-gs/326715853/Sell_4_6mm_Dark_Green_Float.html [Accessed by 08/2011]
b: the latest price is from the ETFE foil product supplier: http://www.professionalplastics.com/TEFZEL-ETFESHEETSRODS [Accessed by 08/2011]
c: the specification of the material properties was from: http://www.matbase.com/material/glass/float-glass/properties [Accessed by 08/2011]
** : Typical ETFE foil has a weight of approximately 175 g / m^2 for a foil thickness of 100 microns [18]. While an entire foil cushion system is 10%-50% of the glass façade structure*

Nonetheless, glass glazed building envelop is still leading the mainstream of the glazing systems. The foil cushion envelop has become an established form in the building cladding construction. But it is still relatively unusual one as opting for foil cushion architecture is not a decision for the architect or the engineer alone, and persuading a client to commit to this form of construction needs to be strongly supported by the proven engineering and environment performance of such inflatable envelopes. This involves the development of different topics such as materials technology, energy conservation, building construction, geometry, orientation and design and it is necessary to design them for a specific climate and a suitable activity.

2.2.1 Modern Lightweight Foil Cushion Envelope

2.2.1.1 Innovations during the Twentieth Century

After the Second World War the development of more light and flexible membrane materials in architecture, allowed the design and construction of more stable pre-stressed membrane structures.

Vandenberg R. [19] recognised two prime innovators of modern tensile membrane structures, such as, the architect and engineer Frei Otto, who in 1957 founded the Centre for the Development of Light-weight Construction in Berlin, followed in 1964 by his Institute for Lightweight Structures at Stuttgart University, and Peter Stromeyer, whose family firm has been one of Europe's most important manufacturers of large tents since 1872. According to Erger, H. [20], Frei Otto clearly understood the indispensable principles of thin membrane architecture:

- The structural and architectural forms are inseparable
- Flexibility is strength not weakness
- The surface material must be more flexible than the supporting elements

Architectural foil material has not been used in the long-lasting external envelopes and was not a feasible proposition until the flouropolymers were developed, and the most successful one is ETFE foil. Table 2-2 lists the most physical advantages of the foil.

ETFE was the optimal choice for cladding the enormous gardens of the Eden Project. The ETFE entails substantially less primary support structure: minimizing material, transportation, and monetary and environmental costs. Finally, the ETFE cladding uses less than 1% by volume of the double glazed glass required to cover the Eden Project. Alan Jones [22], chairman of Anthony Hunt Associates and project engineer for the Eden Project, also highlights geometric and size flexibility, ease of ma intenance and repair, ultraviolet light transmission, and lifespan as attractive attributes of ETFE foil for use in the greenhouse project.

Prestigious and successful building projects employing ETFE foil cushion technology, especially Eden project, began drawing the public attention to such technology and made it regarded as one of symbols representing innovative building technologies in the twentieth century.

Table 2-2: The main advantages of EFTE foil physical characteristics

Performance of ETFE Foil	Property Description	Special Information
Transparency	• 95% visible light transmission • 85% ultraviolet light transmission	• Functional coating applied allowing certain adjustment on the heat/light transmission control
Weather Resistance	• Low gas and water vapour permeability • Low water absorption • Extreme weather resistance • Excellent chemical and solvent resistance • Wide service temperature range (-200℃ -150 ℃)	• 0.01% water absorption for 24 hours soaked • 122 seconds for air resistance
Flammability	• Low flammability • Self extinguishing • No experience of molten drips of foil	• Flash-ignition temperature =470 ℃ • HB-no visible combustion
Mechanical Property	• Excellent tearing resistance • Excellent mechanical and dielectric properties /good insulator • good elongation and elastic behaviour	• tensile strength at break=34,000-7,000psi • Elongation at break=45/650%
Cleaning& Maintenance	• Anti-adhesive characteristics/self clean • Extruded material with smooth surface	• No external cleaning need • 5-10 years internal cleaning cycle.

Notes:
The foil cushion displays excellence self vent in fire emergence.
The higher thermal control can be achieved by multi-layered cushion constructions.
The information tabulated above is referring to the publications [21], [4]

2.2.1.2 Structure concept and geometry

Foil cushions are cladding elements constituted of generally two or three layers of foil films, such as the most common architectural film ETFE foil, clamped in aluminium profiles and maintained inflated mechanically. Figure 2-2 shows the typical detailing of a foil cushion system.

Foil cushions are pneumatic, that is, they rely on the pressure inside the cushion to stabilise its surfaces and withstand environmental loads (wind, snow) and imposed live loads. The structural stability is based on two fundamental concepts: pre-stress (**P**) and curvature (**r**) (Figure 2-3). The components of a tensile structure need to be arranged in a specific geometric form while being subjected to a specific pre-stress pattern, which require a high point presented in the system. Depending on the type of pre-stress created by the air pressure inside the foil skin, the tensile forces of the membrane reaches the equilibrium and spherical, cylindrical or shapes in between are emerging, otherwise external loads causing the undesirable deformation of membranes.

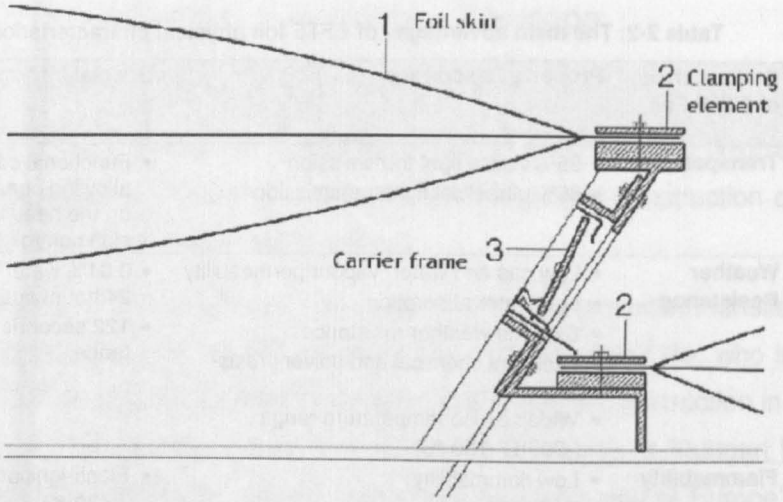

Figure 2-2: Typical detailling of foil cushion [3]

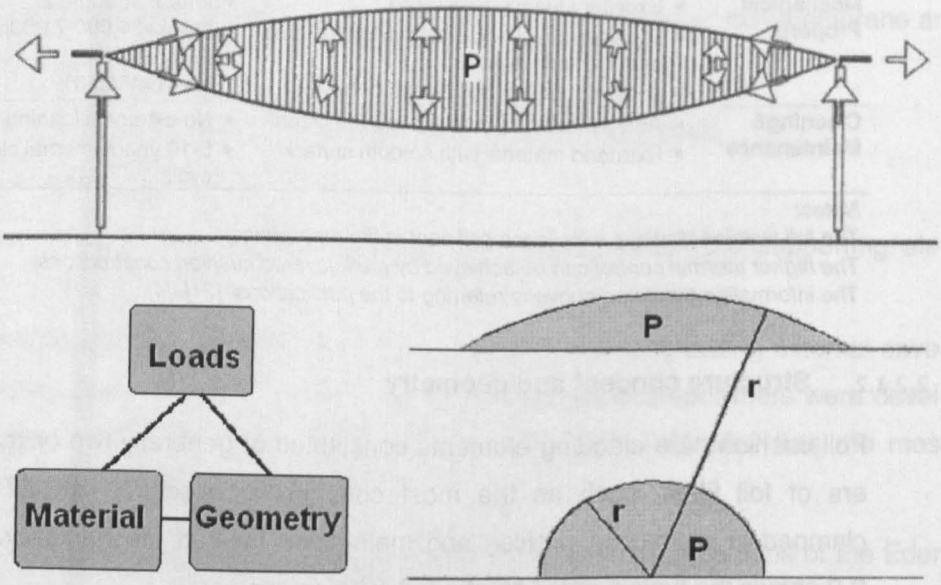

Figure 2-3: Schematric illustration of interrelationshiop between surface curvature/geometry, cladding material and internal pre-press/loads of a foil cushion.

The local stress distribution caused by the internal air pressure is related to the local curvature of the membrane. The fundamental relation of those can be expressed as:

$$M = P \times \frac{r}{2}$$

M	*Local membrane tension [Pascal]*
P	*A leve of pre-stress inside of inflated cavity [Pascal]*
r	*Surface curvature ratio in a sphere radius [m]*

Equation 2-1: Membrane tension in relation to inflated air pressure and surface curvature [23]

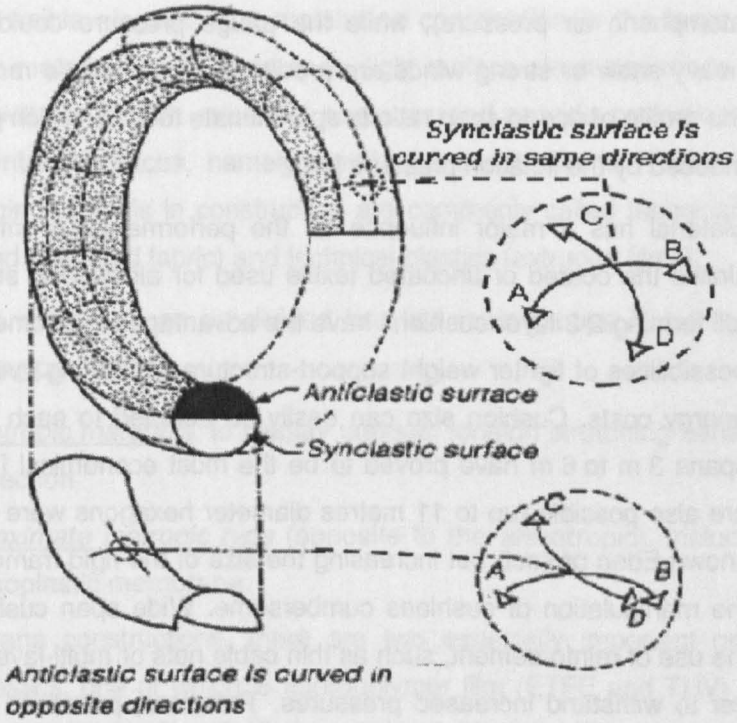

Figure 2-4: Anticlastic and synclastic surfaces. [Reproduced by author]

As the cushion is inflated, foil membrane tension (M) increases to reach a desired level of pre-stress (P, in Pascals), which is transmitted onto the perimeter framing of the cushion. The level of stress depends on the internal pressure and on the external loads carried. The perimeter frame members have to be designed to withstand these forces.

The pre-stressing forces and forces from loads in membrane structures are carried in both directions of sheet, generally generating a type of Gaussian curvature surface when the tensile forces reach the balance level. The Gaussian curvature of the membrane surface can be positive (synclastic surface) or negative (anticlastic surface) (Figure 2-4). Synclastic membrane shapes have the centres of the radii of the principal curvatures on the same side of the surface while those for the anticlastic surfaces have the inverse relationship.

Under wind suction, the outer layer is more highly stressed and its thickness should be chosen to ensure adequate safety against plastic elongation. Under snow loads, this layer will also tend to invert once the load exceeds the nominal inflation pressure. Increasing the pressure inside the cushions provides additional stability but also increases the stress level in the foils and in the perimeter support. The foil cushions are subject to permanent pressure of between 250 Pa (or 200 pa) and 400 Pa (a gauge pressure, which is relative to

atompheric air pressure), while the gauge pressure could be increased if heavy snow or strong winds are predicted. For a simple rectangle foil panel, the profile of rise-to-span ratio is approximate to 1:10, which purely from strain induced by the inflation pressure [24].

Material has a major influence on the performance of inflatable structure. Unlike the coated or uncoated textile used for air-support structure, the pure foil forming 2-3 layer cushions have the advantages in geometric flexibility and possibilities of lighter weight support-structures, reducing overall financial and energy costs. Cushion size can easily be adapted to each design, although spans 3 m to 6 m have proved to be the most economical [25]. Larger sizes are also possible (up to 11 metres diameter hexagons were used in the well-known Eden project) but increasing the size of the rigid frames tends to make the manipulation of cushions cumbersome. Wide span cushions will require the use of reinforcement, such as thin cable nets or multi-layer foil skins, in order to withstand increased pressures. Therefore, patterned cushions will be preferred in the case of complex geometry with short radii of curvature, to avoid unsightly foil wrinkles under inflation.

It is concluded that the trinity between geometry, loads and materials is essential for designing inflatable structures (see Figure 2-3). The optimum combination of these parameters is a determining factor for the success of the design.

2.2.2 Technical Description of Foil Cushion Constructions

2.2.2.1 Foil membrane materials

Plastic membranes, for instance, clear foils can function as diversely from as an insulation element separating the air gap in high-insulation widows to as glass laminates. But in the field of membrane constructions, membrane plastics have achieved their eminent importance only in the recent years, although these constructions have been known long before the mid-twentieth century. The great leaps due to the development in the field of material and production technology indicate that an enormous potential in the area of materials today. The momentum to develop a new standard products often arise directly during the work on a project, where the project team, like the architects, engineers, and companies involved, are working as equal partners. Such synergies are especially evident and contribute to the dynamic growth of new technical applications of membrane materials.

The most visible element of a membrane construction is the large area of membrane materials itself. Wide span, light surface structures made of such materials will serve both structural purposes and provide protection against environmental influences, namely membrane constructions. These kinds of skin-like thin materials in construction are commonly called technical textiles (coated and uncoated fabric) and technical plastics (extruded films).

Membrane materials can be divided into two main groups in terms of their load-bearing properties:

- *Anisotropic materials*, to display unequal tension stretching behaviour in all direction
- *Approximate Isotropic type* (opposite to the anisotropic), including thin thermoplastic membrane.

In membrane constructions, there are two especially important groups of thermo-plastics, one of which is fluoropolymer film (ETFE and THV) and another polyvinylchloride film (PVC) (see Table 2-3). Among these listed materials, the common economical cladding film, namely PE film, can be fluoridised to improve its weather performance by methods, such as thermal insulati on, UV resistance etc.

Table 2-3: A selection of current commercial plastic films used in the transparent building constructions

		Synthetic Materials: Thermoplastic (no cross-linking)	
Categories		Polymerisation	Copolymerisation
Membrane: Closed-pore Materials	ETFE film		• ETFE: ethylene tetrafluoro-ethylene Copolymer • EFEP: modified ETFE.
	THV film	• THV: Tetrafluoroethylene hexafluoropropylene vi-nylidene fluoride terpolymer	
	PVC film	• PTFE: polytetrafluoroethylene polymer • PVC: (PVC-U, PVC-P) polyvi-nyl chlorides	
	PE film	• PE: Polyethylene • LDPE: low-density polyethyl-ene for plastic cladding film.	

Notes:
The film materials listed above, except PVC, are all fluoro-thermoplastics, exhibiting excellent chemical resistance, light fast, self-cleaning, thermal stability and incombustible. Pneumatic clear constructions often use ETFE, THV film, and PTFE is usually used for coatings of textile membrane. But these thermoplastics are hydrophobic resulting the difficulty in bond with adhesives [26]

Table 2-4: Material qualities of selected technical films for building applications

Technical film	ETFE Film [b]					THV Film [b]	PVC film [c]	PE Film [d]
Thickness [mm]	0.05	0.08	0.1	0.15	0.2	0.5	>=0.25	0.065~0.25
Surface Density [$kg.m^{-2}$] [a]	0.0875	0.14	0.175	0.2625	0.35	0.98	0.2 to 2.0	0.053
Translucency [%]	Up to 96%					Up to 95%	Up to 90%	Up to 90%
UV Resistance	High performance					Good	Adequate	low
Life Span	More than 25 years (generally 30year) Estimated to be over 50 years					More than 20years	About 15-20 years	3-4 years
Building Use Field	Zoo buildings, botanic houses, swimming pools, facades and atriums					Indoor / outdoor use	Indoor use	Greenhouse projects

Notes: surface density = weight per unit area.
a: according to DIN55 352
b: the data in the category referring to "construction materials manual " [26] . The foil is for small spans application
c: the data referred to "Membrane structures" [25]
d: the data referred to "Pneumatic structures" [27]

The light and UV transmittance of plastic foil used in building envelop constructions today cannot be surpassed by any other materials. These membranes are tension-stressed only, reducing the dead weight of the outer layer and minimize the load-bearing system, particular suitable for pneumatic structures.

Table 2-4 presentes a selected qualities of plastic foil in building constructions. For external use, only fluoropolymer based foil can be applied successfully. Fluoroplastic foils are manufactured as flat or blown films. For instance, ETFE foils are flat extruded so as to achieve high quality and consistent material thickness while blow films can achieve the same qualities as ETFE foil for architectural projects and used elsewhere, for example in botanic buildings.

ETFE was first produced in the 1940's and patented in the USA by DuPont. This material became commercially available in the 1970's as cable insulation. Its original purpose was as a friction resistant insulating material for industrial machines. Before their use in the field of building, ETFE foils had been developed as prototypes for solar energy collecting (a solar water heater) and utilizing (the first solar balloon) by the physicists Hans and Jurgen Kleinwachter. ETFE was introduced building sector in 1972 by DuPont (Tefzel®) in the USA and in 1974 by Hoechst (Hostafon® ET) in the European market. Later Asahi Glass (Afon® COP) and Daikin (Neofon® ETFE) in the Japanese market and Nowofol (Nowofon® ET) in Germany followed. At end of 1970s, some pioneer-

ing work with material and processing technology was done by the chemists Herbert Fitz and Herbert Koch and ETFE foils emerged as a new cladding material in building applications. The next generation of foil in the construction industry is believed to be EFEP, a strongly modified ETFE foil, offered by Daikin [28]. Figure 2-5 briefs the developing trend of the ETFE foil product history.

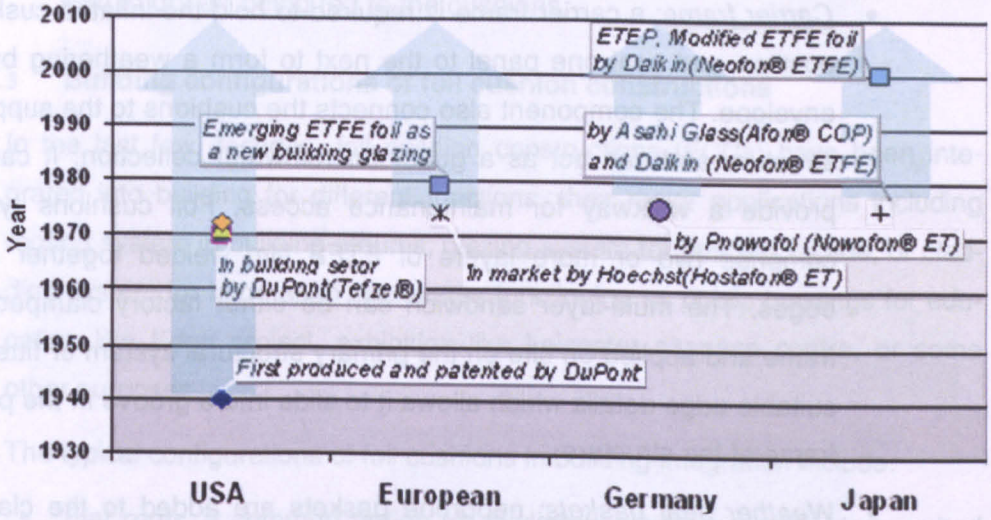

Figure 2-5: Mapping of ETFE produts developing history

2.2.2.2 Components of foil cushion constructions

Technical foils or films forming cushions act as cladding elements as an alternative to glass. Due to the flexibility in geometry, ETFE cushions are available in variety of standard geometries (rectangular, circular, triangular, long strips) or can be tailor-made for specific projects.

Different from the glass skin envelop, foil cushion systems are arranged basically with a similar combination of primary structures, the carrier frame, foil skin, supporting structures etc. Those elements are multi-functional, not only bearing the load existing on them, but providing the shield against the external adverse climate variations.

The spatial assembly of the foil cushion system is described as a main characteristic. These are basically configured by the following main components (see Figure 2-2):

- *Inflated ETFE foil cushions*: at least two, and more generally three, layers of ETFE film, heat welded together along their edges. Intermediary layers are usually porous in order to maintain even pressure in the different compartments. The typical thickness of the external layer is 200 microns as it is highly stressed, and of the inner most layer is in the

range of 150-200 microns. Internal layers in the cushions are made of thinner gauge material less than 100 microns [3].

- *Clamping plate assembly:* essentially made of an extruded aluminium profile to hold the cushion edges in position and to create a labyrinthine profile to limit water and air ingress.
- *Carrier frame*: a carrier frame is required to hold the inflated cushion in position and seal one panel to the next to form a weathering building envelope. The component also connects the cushions to the supporting structure and can act as a gutter for rainwater collection. It can also provide a walkway for maintenance access. Foil cushions typically comprise two or more layers of ETFE film welded together at the edges. The multi-layer sandwich can be either factory clamped on a frame and applied on site on the primary structural system or fitted with suitable edge details which allows it to slide into a groove in the primary frame of the structure.
- *Weather seal gaskets*: neoprene gaskets are added to the clamping system to provide additional air tightness at the perimeter of the cushions. Since the perimeter of the cushion doesn't have to accommodate thermal or structural movement (as is the case with glass panes), high pressure clamping is possible.
- *Supporting structure*: cushions can be held in position by a rigid or flexible supporting structure. Timber, aluminium, steel and GRP may all be used to support the cushions. Rigid structures normally incorporate an integral carrier frame to which the cushions are directly attached. Unframed flexible installations rely on pre-stressed, multi-strand cables spun from high tensile wires, which support a clamping assembly. Wind and snow loads may generate large relative movements in this type of systems.
- *Centrifugal fans*: centrifugal fans are usually used to maintain constant pressure in the cushions, which ranges between 250 and 500 Pa, depending on the size of the cushions and on the loading. Two 50W fans (one for backup) will usually be sufficient for 1000m^2 of cladding. Fans are generally equipped with sensors that monitor air pressure variations and allow fans to auto-top-up pressure in cushions when it falls below the desired range.

- *Air feed system*: a network of flexible hoses connect the fans and cushions, and are equipped with non-return valves to delay accidental deflation in case of air supply failure. An air filter and dehumidifier unit will avoid the entrapment of dirt and condensation inside the cushions. For high humidity environments, air dryers can easily be fitted with the system to dry air being fed to the cushions.

2.2.2.3 Building configurations of foil cushion constructions

In the last few decades, foil cushion constructions (FCCs) have been integrated into building for different functions, their major applications including roofing system in building atriums, glazing system for building façade, or cladding system for large span enclosures functioning as public buildings for education like Eden project, exhibition like Leicester airspace centre, or some other purposes.

The typical configurations of foil cushions in building integration include:

- *Flat roofs:* a common option for skylights, which are particularly suited for the use of standardised geometry. A built example is given in Figure 2-6.

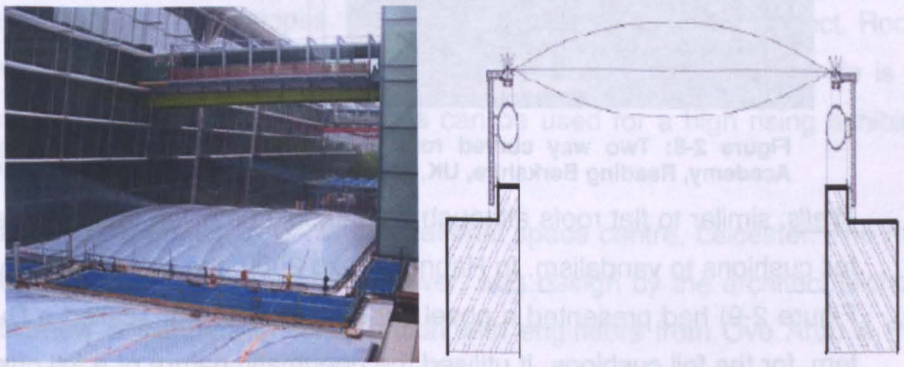

Figure 2-6: Flat foil cushion roofing detail. [Building example: Heathrow terminal 5, London, UK, 2006. Architects: HOK international architects& Richard Rogers partnership]

- *One way curved roofs*: standard long strip cushions (up to 50 m) can be slid into a grooved aluminium profile, supported by arched structures. The cushions can easily accommodate large radii of curvature. Increasing the curvature would usually require the use of patterned cushions to reduce stress and avoid wrinkling. The Figure 2-7 shows the structure concept and an example in the UK.

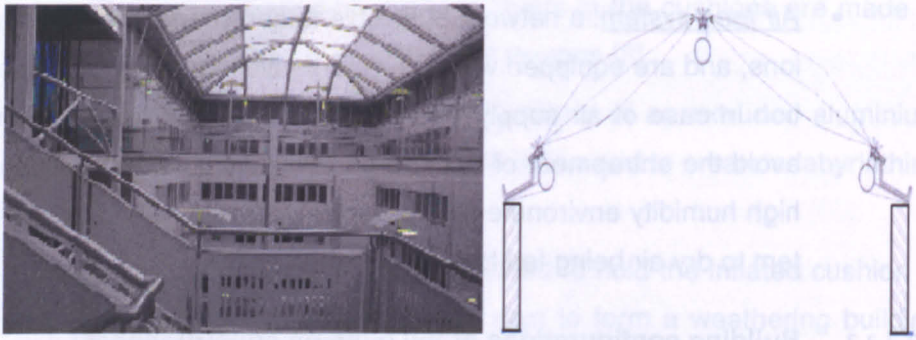

Figure 2-7: Single curvature roofing. [Building example: Westminster & Chelsea Hospital Atrium, London, Uk, 2000. Architects: Sheppard Robson]

- *Two way curved roof*: similar in principle to one way curved systems but more complex to design and detail, as the carrier frame is curved (see Figure 2-8). Careful patterning of the cushions is necessary, especially when considering the derivation of wrinkle-free surface shapes inflated within warped boundaries.

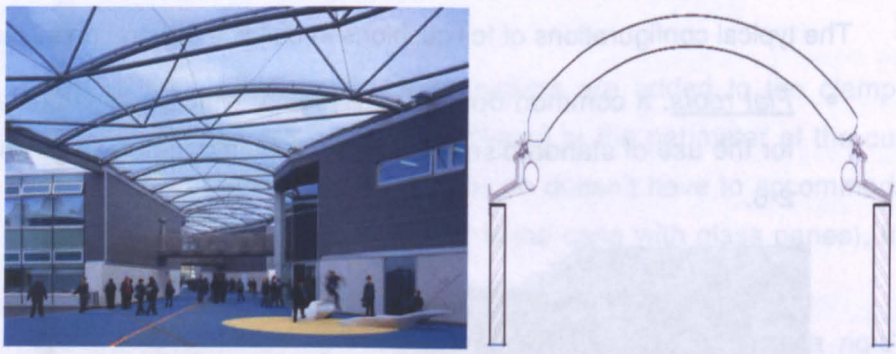

Figure 2-8: Two way curved roof. [Building example: John Madejski Academy, Reading Berkshire, UK, Architects: Wilkinson Eyre Architects]

Walls: similar to flat roofs although care should be given to the vulnerability of foil cushions to vandalism. In Hannover exp 2000, the cycle bowl pavilion (see Figure 2-9) had presented a novel solar control solution, called a Duales system, for the foil cushions. It utilised the pneumatic nature of a foil cushion construction having layers of foil pillow printed with negative and positive pattern and change the transmittance of foil cushions from opaque to translucent by altering air pressure inside the pillow.

Some famous examples of enclosures clad by foil cushions in the UK, (in historical order) will be selected and discussed in the next section to further explore the technical features of the foil cushion envelope.

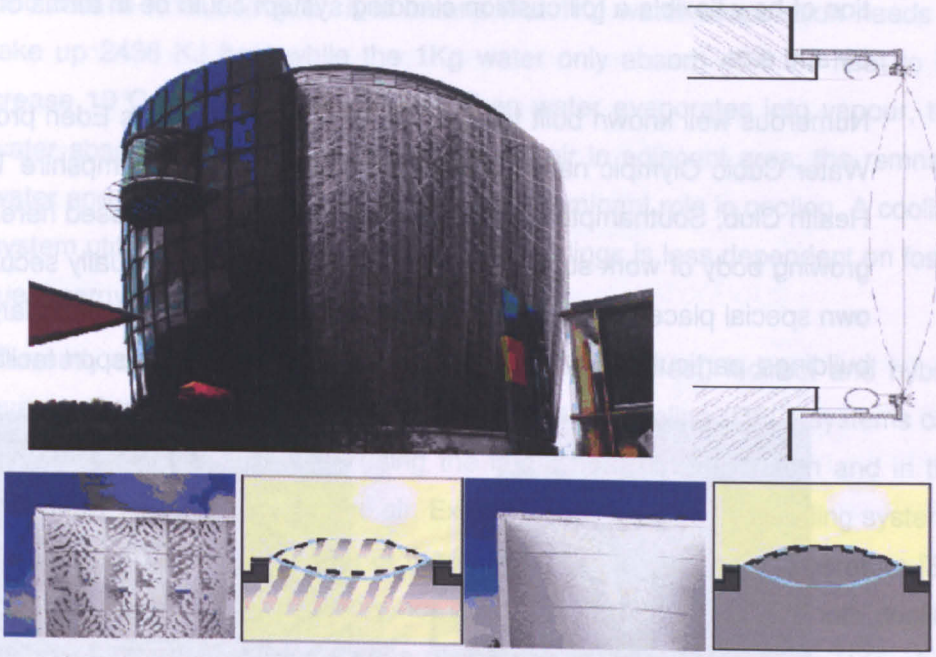

Figure 2-9: Wall cladding detial . [Building example: Cycle bowl Exp 2000 pavilion, Hannover, Germany. Architects: AtelierUweBruckner]

2.2.2.4 Built examples of foil cushion enclosures

Except for those common projects which used foil cushions in building envelopes, the foil cushion has proved its worth in an increasing number of space-enclosing building envelopes. Here a brief introduction to one project, Rocket Tower of the national space science centre, is presented. The centre is the first demonstration that foil cushions can be used for a high rising exhibition building (Figure 2-10).

This bespoke project in UK is the National space centre, Leicester. The main feature of the project, the rocket tower, was design by the architect Nicholas Grimshaw & Partners in collaboration with engineers from Ove Arup & Partners. Triple-layer ETFE foil cushions wrap around a curved 42-meter high exhibition Rocket Tower, creating a continuous band of cushion around the building. The biggest cushion is reported to be 30 m high and 20 m long.

In this exhibition space, the solar control methods are to have the cushions gridded coating and printed silver matrix dots. The inflation system is a network of vertical channels that are installed in the back of the structure. This project confidently marks the potential functional variety of foil cushion enclosures, such as exhibition high-rising building application other than only botanic or green houses. It is a good piece of work triggering people's imagina-

tion of how flexible a foil cushion cladding system could be in terms of geometry and size.

Numerous well known built foil cushion enclosures, such as Eden project, the Water Cubic Olympic national swimming pool in China; Hampshire Tennis & Health Club, Southampton in England, etc., will not be discussed here. But the growing body of work suggests that foil cushions have gradually secured their own special places in the field of glazing constructions for covering large scale buildings, particularly for aquatic centres, botanic and some sport facilities.

Figure 2-10: Exterior and interior view of Rocket tower. [Photos by author]

2.3 Building Integrated Evaporative Cooling

2.3.1 Evaporative cooling

Evaporation is the physical process in which a phase of liquid is transformed into vapour or gas by taking heat from the water and its surrounding air and hence performing cooling to the immediate environment. Santamouris *et al* [29] has defined evaporative cooling as "the process that uses the effect of evaporation as a natural heat sink". The effect of the evaporation of water is that it requires a certain amount of heat in order to occur. This energy is called latent heat of evaporation and varies according to the ambient temperatures.

The cooling performance of using water evaporative cooling is better than cold water. For instance, at normal temperature of 27℃ and pressure of one atm, the latent heat of water vaporization is 2438 KJ/Kg while water sensible spe-

cific heat is 4.18 KJ/Kg.℃. It is means that 1Kg water evaporation needs to take up 2438 KJ heat while the 1Kg water only absorb 41.8 KJ heat to increase 10℃ of water temperature. When water evaporates into vapour, the water absorbs heat from the non-saturated air in adjacent area, the remnant water and immediate surfaces playing a predominant role in cooling. A cooling system utilizing this process to cool down buildings is less dependent on fossil fuel energy and therefore environment friendly.

Currently available systems are basically utilizing direct, indirect and hybrid evaporative cooling processes. Direct evaporative cooling (DEC) systems can lower the temperature of air using the latent heat of evaporation and in the meantime adds moisture to the air. Existing direct evaporative cooling systems are 70-95% effective in terms of the incoming air's wet bulb temperature [30] and suitable for use only in dry hot climates, or rooms needing both cooling and humidification. The process is represented in a psychrometric chart (Figure 2-14) by a displacement along a constant wet bulb temperature line A-B. The indirect evaporative cooling (IEC) process is able to lower the air temperature without adding increase moisture in the air, which are represented as a section of line A-C in Figure 2-14. This feature makes them more attractive than direct systems. An indirect evaporative cooing system uses a heat exchanger to separate the cooled air form working air in wet side. Ideally the product cooled air could reach the wet bulb temperature of the incoming working air if the two airstreams have a good balance of flow-rates and an infinite contact area. However, practical systems have been reported that only 50-60% of the incoming working air wet bulb temperate can be achieved for a typical indirect evaporative cooling system [30]. A hybrid system is basically a combination of direct and indirect evaporative cooling process. A typical process is demonstrated in, represented by two sections of line A-C-D.

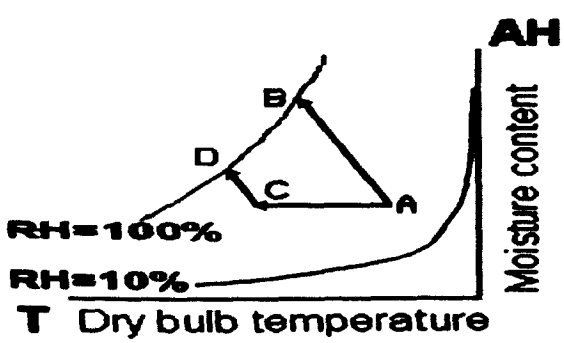

Figure 2-11: Psychrometric chart of DEC process [line section A-B] and IEC process [line section A-C]

Performance assessment of evaporative cooling systems is described as saturation efficiency defined in the equation below:

$$\eta_{sat}=\frac{T_{db,i}-T_{db,o}}{T_{ab,i}-T_{wb,i}}$$

η_{sat}	*Saturation Efficiency*
$T_{db,i}$	*Dry bulb temperature of air at the inlet of a system [℃]*
$T_{db,o}$	*Dry bulb temperature of air at the outlet of a system [℃]*
$T_{wb,i}$	*Wet bulb temperature of air at the inlet of a system [℃]*

Equation 2-2: Saturation Efficiency

It is important to note that the web bulb temperature is the function of dry bulb temperature, air humidity and yet uncorrelated to airflow, the increase of air velocity however cannot reduce the wet bulb temperature of the incoming air, but the total cooling capacity can be influenced by that.

The higher value of saturation efficiency can be obtained by the provision of a greater contact surface and longer contact time between the air and water. In practice, the capabilities of liquid solution or surface materials to increase wet surface area and lengthen the water retaining of the surface are two key parameters taken into account to increase the cooling capacity of an evaporative cooling system.

Table 2-5: Impacts of imperative factors on the rate of the evaporation and total cooling capacity

	Main Factors Influencing the Rate of Evaporation			
Cooling Information	*Air temperature (Tair)*	*Relative humidity (RH)*	*Air movement (Velair)*	*Area of water-air contact surface (A)*
Relationship to Cooling Production	A direct proportion	A inverse proportion	An indirect proportion (as the calculation of wet bulb temperature is irrelative to air velocity)	A direct proportion
Impacts on Cooling Capacity of a System	A big temperature reduction is reached (NB. It is under condition when the air temperature is a high coupling with low relative humidity)	Evaporative cooling is effective (NB. It is under condition in hot arid climate)	Water vapour pressure adjecent to the wet surface is reduced and evaporative rate is increased (NB.The condition is constant incoming drier airflow supplied)	Favourable condition for the evaporation process is created. (NB. The condition is sufficient interact area between air and water provided)

Table 2-5 has are tabulated the important four factors affecting the rate of evaporation and discussed their impacts on the total cooling capacity of a system. In all, in design of an evaporative cooling system, to consider those factors carefully can maximize the cooling capacity of the evaporative cooling system.

2.3.2 Evaporative cooling in clear foil skin constructions

Nowadays building integrated evaporative cooling has been widely used as energy-saving process and low-energy architectural statement around the world. The most common ways to implement this strategy are to introduce vegetation into atria or even interior space, especially trees or potted plants. Pools, fountains, waterfalls, sprays and other water features all add to the evaporative cooling effect. How to incorporate such a low energy method into modern building layout, not only in the environment but into the building construction have become one of the major areas in which modern low energy architecture wants to explore.

Commonly, translucent or transparent foil constructions are applied to the greenhouse project, notably the Eden Project. Taking the advantages of higher transmittance and lighter weight than glass glazing system, a large amount of solar energy infiltrating through the foil envelop can be captured by the vegetation underneath the cover and excess heat can be rejected by the transpiration mechanism (nature evaporative cooling process) in vegetation to keep relative cool environment for themselves, preventing overheating. Unlike machine engineering system whicg are dominated by high temperature and pressure, the living system, including human being, operate at ambient temperature and humidity. In addition, the green vegetation can convert solar radiation into stored hydrocarbon energy at a rate as high (10% to 20%) as the monocrystalline silicone PV cells by means of photosynthesis process. Nowadays greenhouses have been used as a device of harnessing solar energy, incorporating with other nature processes, and then all of solar radiation will be utilized in the ideal condition.

The Watergy project [31], demonstrating such novel concept of sola collector based on a humid air circuit powered by solar thermal energy, has developed two prototypes (Figure 2-12 and Figure 2-13), which combine the process of

evaporation and condensation using solar thermal energy in more efficient way.

Prototype-1 is a single closed greenhouse enclosure, naturally ventilated (see Figure 2-12). The building consists of a 200m^2 greenhouse covered by a clear polyethylene plastic film and a solar chimney in height of 10 m^2. Figure 2-12(right) shows a scheme of the climatization system in side the greenhouse powered by solar energy. Hot and humid air cooled when passing down the solar tower has been circulated back to the crop-growing enclosure, and saline water can be purified in the evaporation process. The average temperature in the greenhouse could be maintained around 30 °C when the cooling system (heat exchanger in the solar tower) is in action.

Prototype 2 (see Figure 2-13) has applied the Watergy concept to a building technology as a solar collector and water treatment device. Its south facing façade area of 40 m^2 is covered with ETFE transparent foil. A heat exchanger has been integrated to transfer the warm humid air to water and store the released thermal energy for the house and greenhouse heat supply in cold seasons.

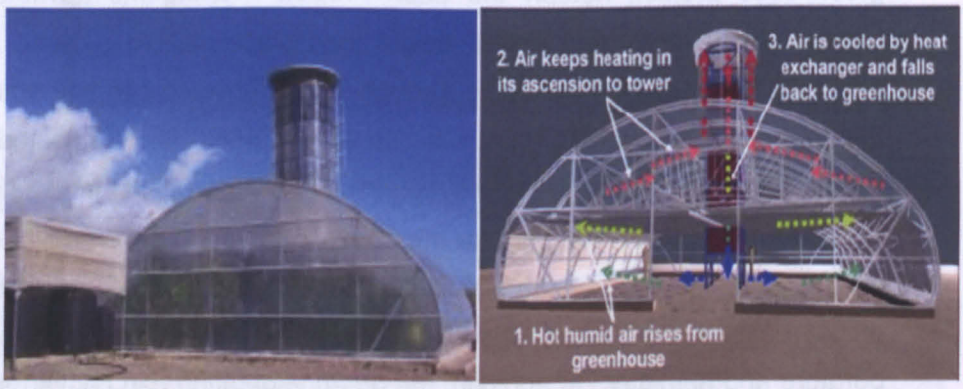

Figure 2-12: Watergy prototype-1 and the scheme of the air circulation inside building.[Location: Almería, Spain]. [31]

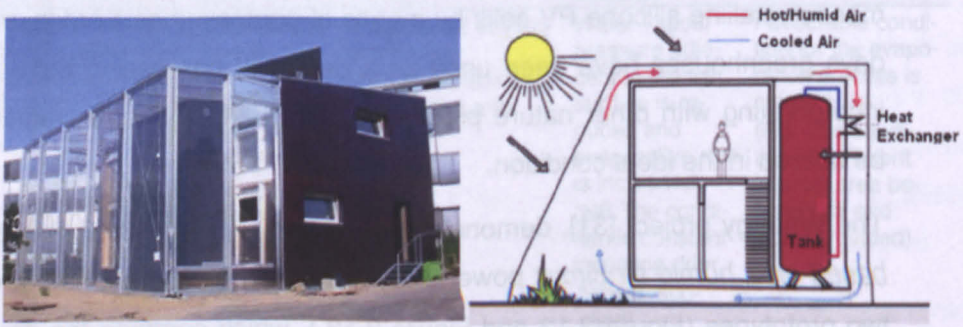

Figure 2-13: Watergy prototype-2 and the scheme of the heat collention in building in Watergy PT2. [Location; Berlin Germany]. [31]

Solar-Roof open source community has initiated innovative liquid bubble insulation and liquid solar technologies to transfer our city and home to sustainable living places, based on the similar concept of the Watergy project. The founder, Richard Nelson and other pioneers, have proposed a concept of active greenhouse as an integral component of the building roof or façade, which so called as solar roof technology [32].

They argued that circulating cool air in conventional buildings was not an efficient measure to take away the heat gain and avoid overheating on hot sunny days in cooling seasons, as the source of the overheating (the overheated building components, building envelop etc) had not been removed and available ambient air was still hot. An alternative means to cool the building is to reduce the temperature of the building envelope directly. Sola-Roof group suggested a more efficient system using a water-based evaporative cooling process in pneumatic transparent foil roof structures. The system is comprised of multi-layers of lower weight (fabric membrane or plastic film, foil) transparent covering materials to form entire or most part of the building envelope. As a result, an enclosed controlled environment for the plants was provided, and so was the control of the interior comfort conditions within the building, which was similar to NASA life science based technologies of Closed Ecological Life Support Systems.

The whole process (see Figure 2-14) is actually a combination of solar energy, plants and cold water resource. The cooling liquid constantly chills the inner skin of the transparent envelop and is claimed that nearly 20% direct and indirect solar infra-red is absorbed by the liquid thin film. The heat absorbed by working liquid is then dissipated to a heat sink such as cold ground water or stored for space heating etc. Some of the blue and red light spectrum is converted into plant growth by photosynthesis; hence the rest of the light entering the building is cool and a natural source for space lighting.

The study of the Solar-Roof projects showed that when the water based liquid was supplied at 15.5 ℃, the typical readings in the building were that the temperature of vegetation leaves was 23 ℃; the air temperature around them was 27 ℃ while the air temperature near the liquid cooled glazing was around 15 ℃. The relative humidity could remain at about 50% if humid air condenses when approaching the cold inner skin. The light level within such a structure is alleged similar to that in conventional single glass buildings with the advan-

tage of double-glazing provided by this system, which thanks to its high transmission, low reflectance and a degree of light diffuse. Those researchers suggested that ideal specification for the Sola Roof is a roof with maximum transparency and would have about 4% reflection, 2% absorption and 94% transmission of the solar radiative spectrum (lies in range of 0.1μm to 4μm wavelength) [32].

The drawbacks of this evaporative chilling process are requiring energy to operate the system and consuming water. But the researchers suggested implementing such a system as an integral part of roof solar thermal and PV system for energy generation on site would balance out the energy consumption.

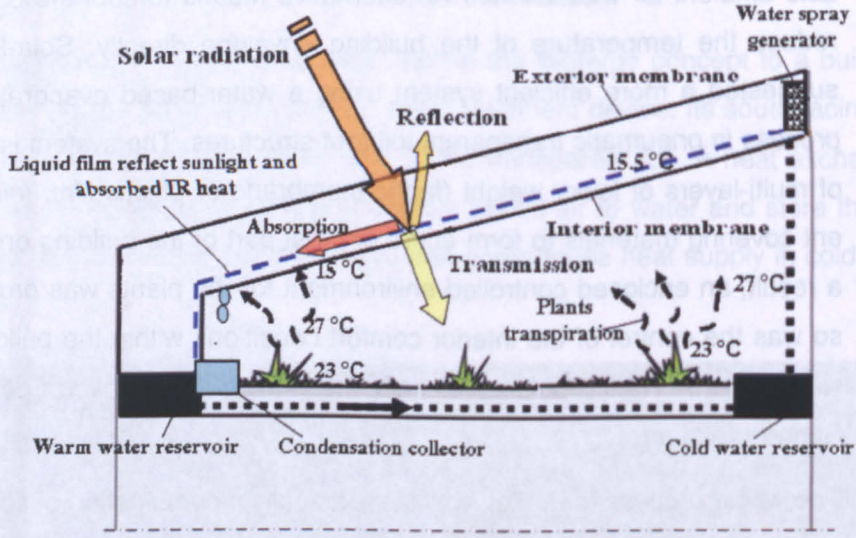

Figure 2-14: Scheme of transparent Solar-Roof system

To sum up, Sola Roof is a very radical concept suggesting transparent living structures using "water working" (the Blue) and living plants (the Green) to provide an integral low-energy climate control process to regulate the building environment. This concept provides a new viewpoint and chance to rethink whether the current uses of transparent construction methods are adapted in an adhoc way. How to develop this concept and its applications is a novel area needing exploration.

2.4 Novel Integration of Evaporative Cooling and Foil Cushion Construction Systems

Foil cushion systems as a recently developed glazing method in the transparent building constructions witnessed increasing popularity in building designers. Evaporative cooling as a best-known passive cooling method is working

well along with membrane structure, normally associated with rooftop mist spraying system, shower-cooling tower etc. However, how to incorporate evaporative cooling into pneumatic foil constructions is still a novel area to explore and very scarce available knowledge on their climatic behaviour handicaps intentions to explore architectural potential of such enclosures.

2.4.1 Introduction

Similar to other glazing systems, foil cushion glazing system is challenged by the question whether, in the sustainable age, the current use of such a glazing system is in an appropriate way or not. In Section 2.3, some researches and solutions have been made by previous researchers and are generating some interests and ideas for the coming followers. This section introduces a scheme attempting to integrate the evaporative chilling concept (part of Solar –Roof concept) to pneumatic foil cushion constructions so as to improve the climate control of these spaces.

The proposed scheme is based on the liquid cooling process where the cooling water chills the inner skin of the foil cushion envelope. The formed water thin film will block out and absorb the incident solar infrared and re-radiated long-wave thermal radiation on the membrane, providing cool nature light and removing a source of overheating, such as a hot building envelope. The chilling water and cool envelop functioning as a heat-sink take heat away from solar energy when passing through the envelope and those generated from inside.

2.4.2 The concept of proposed integration systems

2.4.2.1 Schemes of the proposed systems

To integrate evaporative chilling process in the pneumatic foil constructions was proposed and developed two basic typologies. The first type had two layers and one channel structure (see Figure 2-15, the model at the left top). The cooling liquid supplied from the top side of the channel rapidly chilled down the surface temperature of the inner skin of the channel and consequently cooled down the air temperature in side the space mainly by the effect of heat conduction. In this scheme, working air was ducted in from the same position as the chilling liquid and exhausted from the bottom to the ambient when the air became warm and saturated (see Figure 2-15, the psychrometric chart at the

left bottom). A constantly cool envelop produced by this scheme removed a big source of overheating for such building in hot season.

The second type was developed to construct additional layer within two layers and form a two-channel structure (see Figure 2-15, the model in the middle). When cold liquid film was evenly distributed on the outer side of middle skin, naturally the top channel became wet while another was a dry channel. Air was ducted in and cooled when passing through the dry channel with no increase in moisture. After that, a percentage of air was expected to deliver into the foil-glazed spaces for cooling and ventilation purposes while the rest was saturated and exhausted to atmosphere after travelling through the wet channel to enhance the effect of evaporative cooling taking place (see the Figure 2-15, psychrometric chart at the middle bottom). The more complicated processes influenced the interior climate of buildings integrating such a scheme. Apart from conductive heat transfer, convective and radiative heat exchanges were also involved. This scheme was supposed to produce a cool envelop as well as cool air replacing the hot and humid air generated inside.

2.4.2.2 Description of concept models evaluated in this research

The concept of integrating the cooling water and pneumatic foil skin structures could be derived out a few concept models illustrated in Figure 2-15.

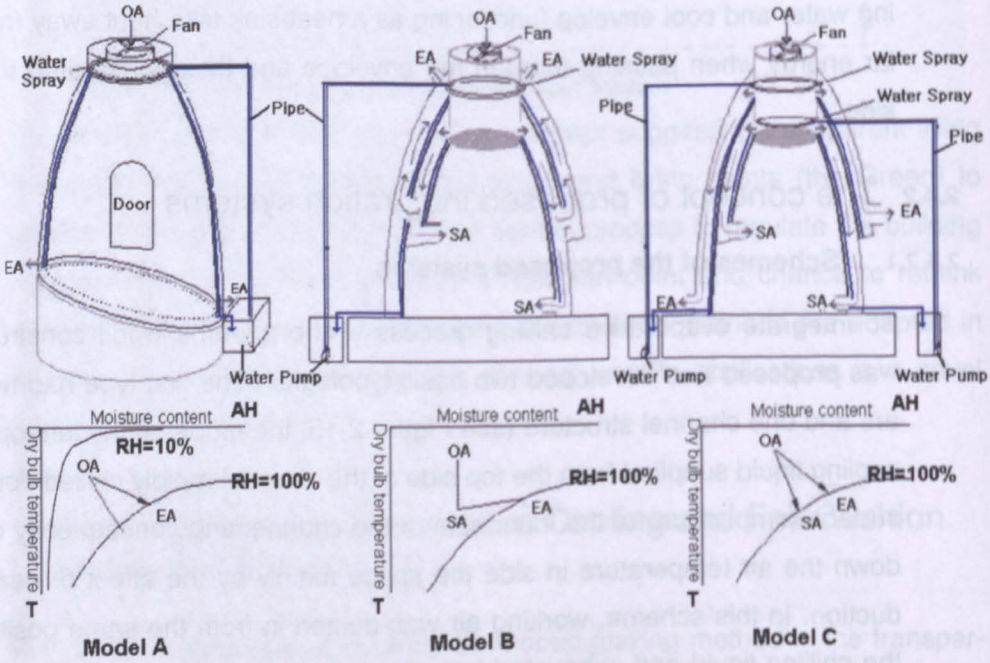

Figure 2-15: Concept model-A, B, and C of novel pneumatice membrane integration constructions. [NB: OA = outside air; EA = exhaust air; SA = supply air]

The basic structures are a two-layer one channel type and a triple-layer two channel type. Both structures are made by an inflatable tent to simulate a pneumatic foil-glazed enclosure. The main features of the tent are listed as follows:

- The structure is pneumatic consisting of multiple clear or translucent foil skins.
- An ancillary structure incorporating a fan or air duct unit at the rooftop of the enclosure connected to the foil layers and guiding the water or air supply lines in the system.
- The air and water is distributed evenly from the top point of the tent to the bottom of the channels.
- A liquid source (such as a tank) connects to a pipe and spray nozzle or tube.
- An incline structure supporting the tent at the base and liquid running down to the bottom of the channels is collected in a tank at the lowest point of the incline.

As shown in Figure 2-15, the concept model A has the inner skin of the channel cooled using directly evaporative cooling mechanism and no air flow enters the enclosed space. The climate condition inside is regulated by the surface temperature of the inner skin by indirect cooling process without ventilation removing the hot air inside the dome.

In concept model B, the climate control of the foil glazed dome has developed from model A, using indirect evaporative cooling mechanism coupling ventilation to enhance the cooling effect in the enclosure.

Concept model C is a variation of model B, which is aiming at giving an example of the flexibility of the proposed schemes which allowing adaptable enclosed environment with slight changes in the construction, but this model will not be explored and evaluated in the scope of the research.

To conclude, the novelty of the proposed systems is integrating the liquid chilling process into transparent inflatable constructions. By means of infiltration solar control on the envelope, not only should the thermal gains and overheating resources be reduced, but also the solar energy picked up by the chilling liquid could be utilized in the building for any appropriate purpose. These sys-

tems are suggested to apply for the climate in UK, and assess in the same condition.

2.5 Discussion and Conclusions

Transparent building envelop has been deemed as an evolutionary step in modern building design. From early famous glazing building "Crystal Palaces" to current glass office towers and Eden projects, transparency is strongly associated with the image of modernity for urban buildings. However the wide applications of glazing envelop have created a great concern about its implications on natural lighting, thermal performance and energy consumption in today contemporary architecture.

Glazing envelopes present the big source of thermal gain, causing overheating and thermal loss, so strict building energy standards have been placed on the area of glazing applied on buildings. For instance, the impact of glass glazing constructions on the internal environment has been a matter of great research for the last decades. But new improvements on their manufactures, physical qualities, and construction technologies, to achieve building energy standards are still the issues. Though the blind, shades, and solar shutters are present, the active control and modulation of solar infiltration through the glazing is still limited.

The foil cushion technology is emerging as an innovative transparent glazing system in building constructions. It has been hitherto the only possible envelop glazing solution providing the decent amount of insulation without loss of transparency. The advantages and physical characteristics of such a construction have been elaborated in Section 2.1 to Section 2.2. The increased insulation and nature-lighting performance of a foil cushion construction are highlighted as some of their benefits in the literatures. But the argument raised that the limitations are on its use in places as the high light transmittance and negligible thermal mass of clear foil materials, which are the relevant factors easily leading to the overheating. Some researchers and professionals have suggested and offered a set of solutions for the solar control, such as foil surface treatment, prints etc., but are not efficient. The author suggests that it is not a very energy efficient cladding system and call for a deep assessment or innovative development in regards of the entire building to improve its thermal per-

formance, especially the overheating control, to reduce energy usage as well as maintaining thermal comfort level.

Most of the literature suggests that evaporative cooling is an energy efficient cooling mechanism for building thermal control, which is working well with membrane materials, including foil sheets (see in Section 2.3). Today the built projects worldwide seeking the integration of evaporative cooling and building constructions are becoming energy efficient architectural statements.

To incorporate evaporative cooling with foil cushion glazing system is a novel concept but a sustainable solution to the overheating. In Section2.3.2 previous attempts and some literature presented that a transparent building structure combining working liquid or humid air re-circuit process and living plants could achieve the synergy effect of both evaporative cooling and photosynthesis in the production of food, water or energy and provision of low energy active controlled climate within a cooled envelop. This break-through concept of glazing systems is considering the transparent envelop and surrounding climate conditions as a whole, acting as active a solar energy collector to modulate the solar penetration and provide cooled envelop reducing risk of the overheating. In the mean time, the collected energy in the systems via working medium can be harvested and recycled for the building environment control, such as the overheating control. Nevertheless the information of site monitoring and built cases of such glazing systems in architectural form are scarce and no sufficient information of their thermal performance during different climatic conditions has been provided. It is a necessity for a study to define which specific environments are suitable for evaporative cooling integrated foil cushion constructions. [33]

Based on the above concept and discussions, this research project contemplates the development of two prototypes (see concept model A and B in Figure 2-15) of foil cushion constructions applied for the critical summer condition in UK. In the project planning, the choice of such foil cushions is pertaining to their architectural, functional, economic factors or far reaching implications in the constructions. However, a very relevant priority influencing the decision should be the climatic conditions and the predicted behaviour of the foil cushion constructions under critical conditions. This requires a detailed study of the foil skin constructions for specific cases and the general knowledge of the underlying thermal climate within the enclosed space.

CHAPTER 3
THERMAL PERFORMANCE OF FOIL CUSHION CONSTRUCTIONS

> *"One moon shows in every pool, in every pool the one moon."*
> --- **Zen proverb**

3.1 Introduction

During the last few decades, designers and engineers have concentrated all their efforts on the development of foil material and structural systems that allow the construction of structures with longer span, more durability, less cost and minimum material such as ETFE foil cushions. Nonetheless, following a literature review, it appeared that the environmental consequences associated with the large spaces enclosed by a lightweight translucent skin remained relatively unexplored, probably the main cause is the complexity of these structures and the wide range of possibilities they offer regarding geometric shapes, flexible materials, translucency, durability, etc. The correct understanding of their environmental properties, especially their thermal properties, and the ability to predict their environmental behaviour would allow the designer to appreciate better the thermal impacts of an additional cooling water layer on a foil cushion construction, and consequently to create more impressive, functional, energy efficient and sustainable foil cushion envelope.

Meanwhile, the increased demand for the integration of foil glazing systems as a part of large permanent building envelopes calls for the development of modelling tools for the exploration of the potential of foil skin constructions to control internal thermal comfort and energy performance.

This chapter presents a review of the existing body of knowledge relating to the thermal behaviour of tensile membrane skins and of the spaces they enclose. This review includes a description of the previous attempts to monitor their thermal environment as well as the modelling approaches that were adopted to model the thermal behaviour of membrane skins.

Most of the theory assessing the performance of a foil cushion cladding system was based on thermal performance models, airflow and daylight simulations. The main thermal aspects relative to the thermal environment basis of foil cushion envelopes are identified in this chapter by the following aspects:

- Thermal/Optical Properties.
- Thermal Performance.
- Thermal Environment.
- Airflow.
- Compatibility of a foil cushion construction and a water layer

3.2 Thermal Behaviour of Foil Membrane Skins

The most relevant characteristic of membrane glazing materials are their translucency or transparency. This gives its quality for light transmission, which closely associated with thermal perforamnce of foil membrane buildings. This section is exporing the correlation of their characteristic optical properties and thermal behaviour.

3.2.1 Thermal-optical properties

The optical parameters are dependent on two basic criteria:

- Wavelength of incident light.
- The angle of incidence of light beam.

When solar radiation strikes a sheet of membrane, light is partly reflected, partly absorbed in the thickness and partly transmitted. Those three parts are represented as the symbols: Reflectance (β), Absorptance (α) and Light transmittance (τ). The thermal-optical properties of a membrane material are expressed by the three parameters in description of their radiative behaviour regarding to correspondent thermal radiation spectrurm.

Given that the selective spectral transmission of a typical window clear glass, the two main catergories of themal radiation are distingushed:

- Solar radiation, the spectral span of 0.28~2.5 μm [1].

- Far-Infrared radiation, the spectrum range of 3~50 μm [infrared, wiki], and most earth surfaces emit their radiation in this range, generally their temperature less than 500 °C.

In a glass glazing system, the total transmittance is a result of the sum of the total solar radiation, which is absorbed and reflected outside and transmitted and absorbed inside the building. This resultant solar radiation described as the total solar energy transmission factor (g-value) [35], which is illustrated in Figure 3-1(left figure). This description has been also suggested to apply in analysis of thermal behavior of foil membrane constructions (see Figure 3-1, right). But this steady simplified model has not taken into account of the internal reflected solar radiation, the diffused solar radiation and impact of convective heat exchange around the surface boundary etc. The accuracy level of this representation reduces in proportion to the increasing importance of variations in boundary heat flow conditions to overall thermal performance of a typical glazing system.

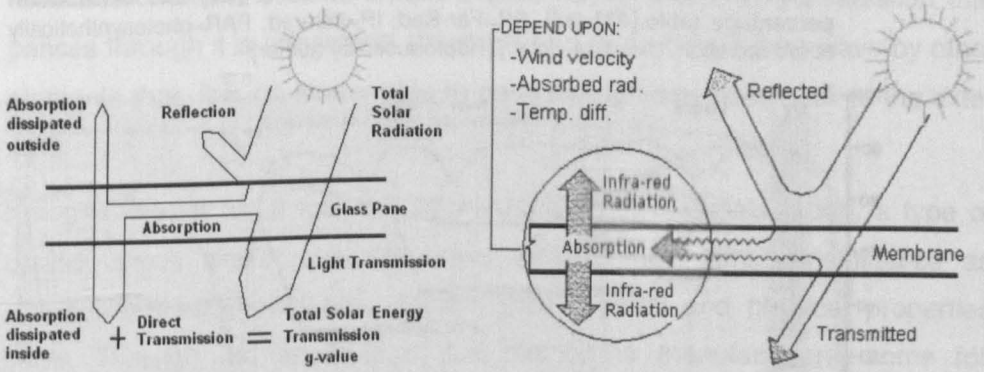

Figure 3-1: Ilustrations of solar energy transmittance through single pane of gass [35] and a sheet of membrane. [36] [Reproduced by author]

For membrane constructions, the thermal-optical properties are suggested to be more representative of their thermal behaviour than the standard thermal properties (i.e. U-values), when investigating the thermal performance of the membrane products or thermal environment of a membrane skin enclosure (see Section 3.2.2).

3.2.1.1 Solar thermal properties

Solar radiation is emitted in various wavelengths, which all together constitute the solar radiation spectrum. The spectrum generally spans from approximately 0.1 to 4.0 micrometers, made up of about 7% of the Sun's emission in

the waveband of ultraviolet (0.1-0.4 micrometers), about 48% in the region of infra-red radiation (0.71 to 4.0 micrometers) and the rest within the range of visible light from 0.38 to 0.78 micrometers. [37] (Figure 3-2)

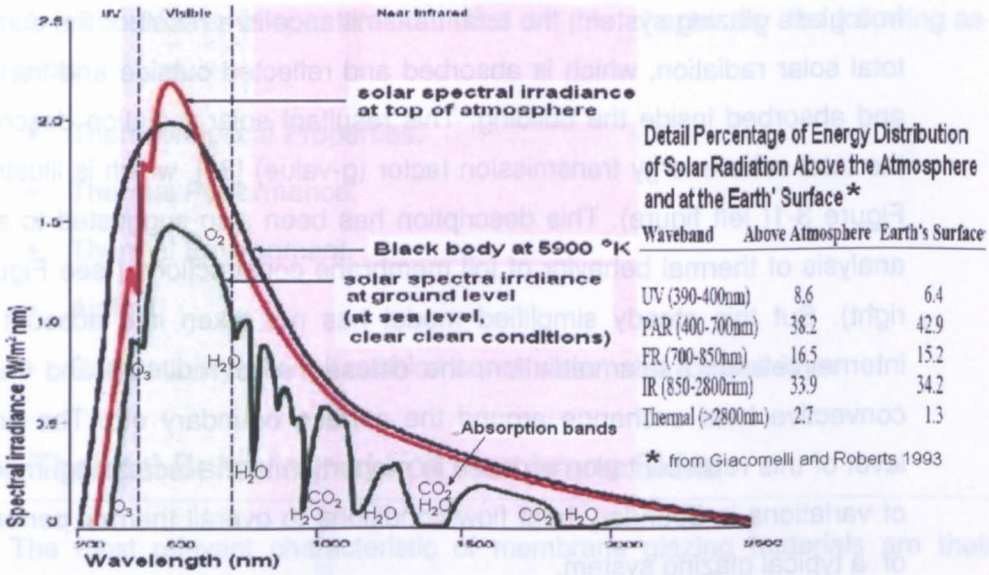

Figure 3-2: Spectral distribution of solar radiation [38] and distribution percentage table.[41] [NB: FR=Far-Red; IR=infrared; PAR=photosynthetically active radiation; UV=ultra-violet] [Reproduced by author]

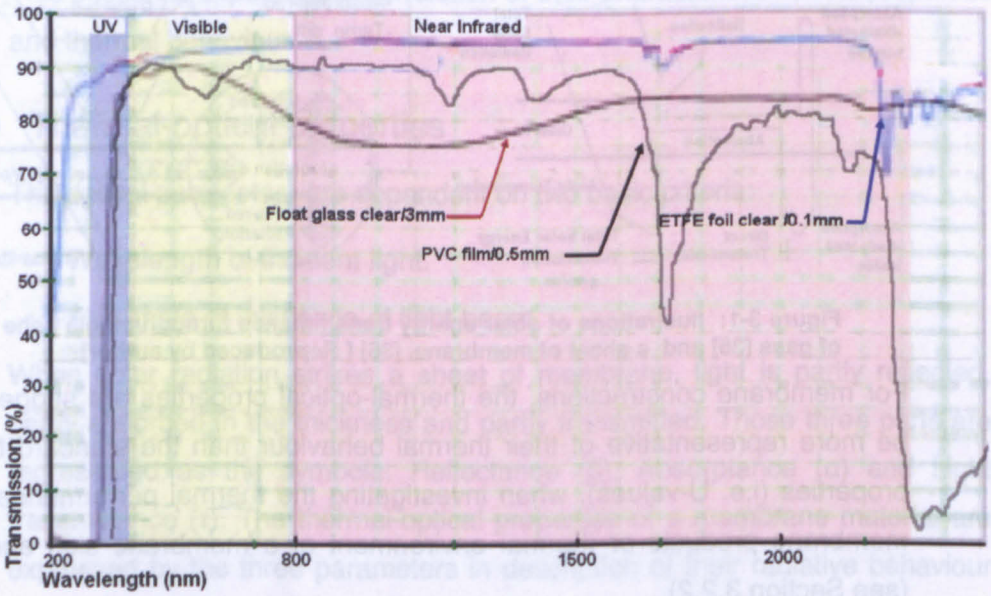

Figure 3-3: Optical properties of typical ETFE clear foil, PVC fim, and glass glazing materials. [42] [43]

Figure 3-2 illustrates the amount of solar energy reaching the earth at the top of the atmosphere and at sea level. The solar irradiance decreases at ground level due to the "greenhouse gases", such as water vapour, oxygen, nitrogen, carbon dioxide and ozone in atmosphere, which are in favour of trapping the

heat near earth surface by and create greenhouse the effect. More than 75% of captured heat in atmosphere is attributed to the action of greenhouse gases that absorbs thermal radiation emitted by the Earth's surface. On this account, the energy absorbed and re-emitted by the Earth's surface in a balanced green house effect is to maintain a constant average temperature suitable for life.

Most transparent media transmit selectively, and their solar thermal transmission is a function of wavelength of the incident solar radiation. In the case of glass and glass-like glazing materials, their constant transmittances of light over total solar spectrum available on the Earth's surface are within the range of 0.3-2.3 micrometers (see Figure 3-2). In general, the glazing materials are substantially opaque for wavelengths greater than 3.0 micrometers and almost completely opaque for wavelength larger than about 4.5 micrometers. This means that the wavelengths below 0.31 and higher than 3.0 micrometers are either reflected or absorbed. Essentially, this is why most glazing materials have the characteristics to create a greenhouse effect as the radiation that passes through it is afterwards absorbed and re-emitted in long-wave by other elements that it is no longer able to pass through the glass back to the exterior.

Foil membranes as a member of inorganic base materials group, a type of plastic, share similar characters like transparency, light transmittance as glass-alike glazing materials, though their thermal and physical properties differ. Through the attempts of foil membrane manufacturers, some foil materials can easily achieve more than 95% of visible light transmittance with good UV-resistance to prolong the life span of the plastic material, i.e. ETFE foil. Figure 3-3 illustrates out those characterisitic in light transmittance of typical membrane foils compared to a glass glazing material.

In foil cushion constructions, ETFE foil is the most relevant material, and it is responsible for the transmission of most of the visible and short wave infrared segments of the spectrum through this type of buildings. ETFE Foil has high transparency about 95% across the entire visible light region (380-780 nm), with scattered light at a proportion of 12 % and direct light at a proportion of 88 % [44], and approximately 85% of total solar radiation. Transmission across the ultraviolet range (320- 380nm) is approximately 83-88% and therefore

leads to a light quality being close to natural light conditions which is favourable for plant growth as well as for human comfort and well-being. It is also important to note that the film absorbs a large proportion of infra-red transmitted (larger than 3.0 mm), a quality which can be exploited to improve a building's energy consumption.

Similar to that in glass, the physical properties of a foil membrane, like colour and chemical composition or surface treatments, determine its total transmittance. The three parameters of thermal radiation, transmittance (τ), absorptance (α) and reflectance (ρ) quantify the proportion of incident solar radiation that is respectively transmitted, absorbed and reflected by the glazing material. These properties are a function of both the wavelength and angle of incidence of the solar radiation. For any wavelength or angle of incidence, the sum of these three properties is always unity. So that the definition of two of these properties is sufficient to describe the thermal-optical behaviour of a body, as:

$$\tau + \alpha + \rho = 1$$

τ	*Transmittance of a body for a spectrum range*
α	*Absorptance of a body for a spectrum range*
ρ	*Reflectance of a body for a spectrum range*

Equation 3-1: Interrelation of thermal-optical properties of a object [39]

Since radiation is directional, these properties may also differ depending on the directionality of the incident radiation. The quantification of these properties can therefore be broken down into three categories:

- Direct beam
- Diffuse, representing radiation incident in many directions
- Hemispherical, referring to the total flux incident from a theoretical hemisphere at the body surface and including both direct beam and diffuse radiation

3.2.1.2 Long-wave infrared properties

Materials have different thermal-optical behaviour responding to long wave infra-red radiation from to the solar radiation. Moreover, almost all objects above 0°K emit, reflect or transmit some thermal radiation. Numerous types of spec-

tral radiation can be distinguished depending upon the nature of the radiation coming from an object.

The main property describing the long-wave thermal radiation behaviour of membrane materials is its long wave infrared absorptance, which expresses as thermal absorption factor (α) to the total incident long wave infrared radiant flux onto the material surface. Kirchoff's law states that, for diffuses radiation, this quantity is equal to the emissive power of the material at a given wavelength λ, which is referred as the emissivity (ε).

However most glazing materials are opaque to long wave thermal radiation, and hereby their transmittance is set as nil. Since the most material bodies in buildings emitted radiation at room temperature within the range 3um to 50um, variations of emittances in such a temperature span are assumed to be small in an acceptable range for engineering. The emittance is thus generally assumedly constant to the temperature changes and the Kirchoff's law is further simplified as:

$$\alpha = \varepsilon$$

α	*Abosorptivity of a grey body for incident thermal energy, at thermal equilibrium*
ε	*The emissivity of a grey body for incident thermal energy, at thermal equilibrium*

Equation 3-2: Kirchoff's law of thermal radiation [40]

Therefore, In building glazing industries, it is a common practice that the use of only an average value of transmittance/reflectance describes the optical behaviour of a glazing material for short wavelengths while an average reflectance or absorption for the long wavelengths.

It is however seen in Figure 3-4 that a common available cladding plastic film for a greenhouse project is not opaque to the long wavelengths. ETFE foil is a type of fluoridised thermoplastics displaying a relative high value in the long-wave transmission, which indicates in Figure 3-5 (this figure has not been confirmed). If applying only one average transmittance for all wavelengths for an ETFT foil glazing system as that for the glass glazing, a considerable underestimation of solar energy input in hot seasons could occur. Harris P. *et al.* therefore suggested that a dynamic thermal performance simulation tool incorporating spectral properties of glazing layers could address difficulties in the energy assessment of the foil cushion glazing system [13]. This argument stresses

on the significant importance of the optical properties of the membrane products on energy optimization studies of membrane structures, particularly for the ETFE foil skins. However, the availability of information on ETFE spectral properties is limited due to the manufacturers tending to treat such information as confidential.

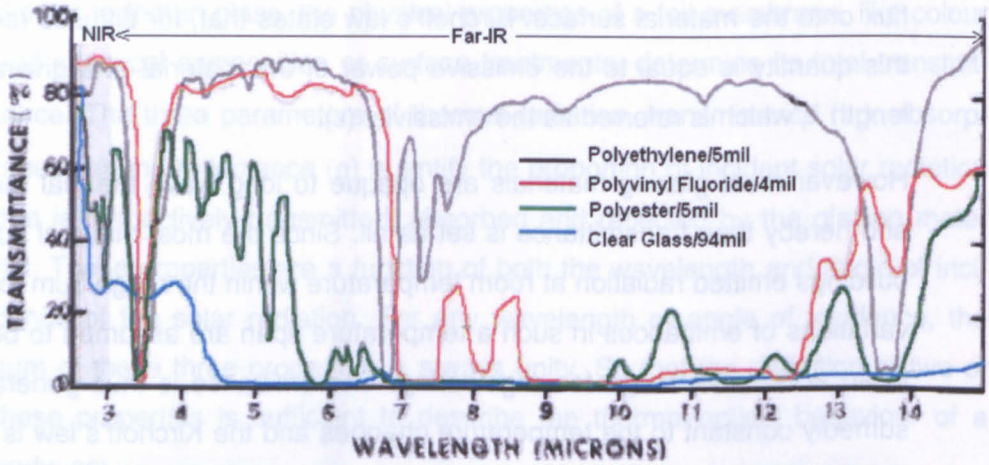

Figure 3-4: Infrared transmittance of various plastic film and a clear glass pane for the wavebane 2.5-15 mm. [45] [Reproduced by author] [NB: NIR=Near Infrared; Far-IR=Far Infrared. Information based on the information from Hanson, K. J. 1963].

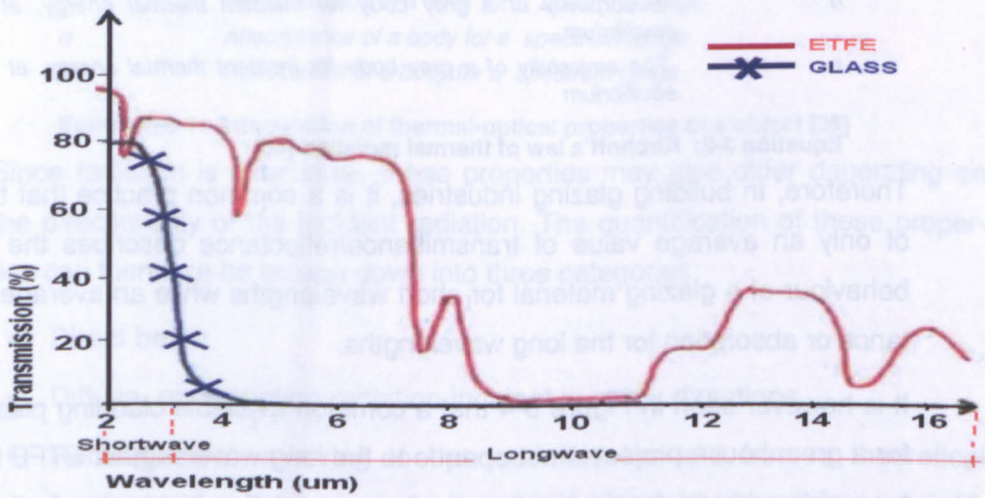

Figure 3-5: Indicative longwave properties of typical ETFE clear foil and glass glazing materials. [Reproduced by the author]

For most building materials, their solar thermal absorptance is not necessary the same as that of long wave infrared. One of the facts is that the solar absorptance of a membrane is influenced by its thickness, its colour and its chemical composition while its emissivity depends on its surface properties and temperature of the body. It is suggested that the factors to effectively con-

trol the infrared thermal radiation through the membrane constructions might be the following:

- modulation of the chemical composition of a membrane material (to control the solar absorptance),
- surface treatment or properties alteration, and
- body temperature control of the material (to influence it emissivity).

3.2.2 Discussion on characteristics of thermal behaviour of architectural foil skins

The thermal transmittance (or U-value) and shading coefficients of membrane materials are the two parameters, which are routinely used to describe their thermal performance. Following the discussion in the previous literature (see Section 3.2.1), some one doubted their applicability to lightweight membrane constructions.

3.2.2.1 Significance of surface heat transfer

It is found that the extreme lightweight and thin film of architectural foils offer little bulk of material to resist the immediate environment changes [46]. As such, the importance factor influencing its thermal properties is not the thermal conductance of material mass but the dynamic conditions of the heat flows on the surface boundary, which are generally described by the physical term surface resistance.

The thermal transmittance, usually referred to as U-Value of a given construction, is described by the British Building Regulations as *a measure of the speed is with which heat is lost through one square metre of a structural element with 1K temperature difference across its faces* [47]. It is commonly quoted to describe the thermal performance of building elements in construction industries.

This property conveniently incorporates the thermal conductance of structural material core along with the surface heat transfer due to convection and radiation. The overall thermal transmittance of the typical multiple glazing can be calculated using Equation 3-3. (Figure 3-9 gives a simple example of the multilayer glazing.)

$$U_g = \frac{1}{R_{si} + \sum_{i=1}^{N} R_i + \sum_{j=1}^{M} R_{Cj} + R_{se}}$$

N	*Number of homogeneous glazing layers in the construction*
M	*Number of air cavity in the construction*
Ri	*Core resistance of glazing layer [$m^2.K.W^{-1}$]*
Rcj	*Thermal resistance of air cavity [$m^2.K.W^{-1}$]*
Rsi, Rso,	*Combined radiative and convective thermal resistance of the internal and external surfaces respectively [$m^2.K.W^{-1}$]*

Equation 3-3: Thermal transmittance (or U-Value) of glazing [48]

The resistance of the material core is a simple function of its thermal conductivity *k* and its thickness *e*, so that:

$$R_i = \frac{\theta_i}{k_i}$$

e_i	*Thickness of the layer i [m]*
k_i	*Conductivity of the layer i [$W.m^{-1}.K^{-1}$]*

Equation 3-4: Material core thermal resistance [48]

The thermal resistance to the combined heat exchange of radiation and convection occurring at the material/air interface is so complex that its calculation involved a number of simplifying assumptions. The values of the internal and external surface resistance quoted in the thermal analysis of a building construction are assumed to quantify the steady state heat conducting through and are independent of the temperatures of construction elements' surfaces and their surrounding. These properties can be calculated from equations:

$$R_s = \frac{1}{Eh_r + h_a}$$

h_r	*Surface radiative heat transfer coefficient [$W.m^{-2}.K^{-1}$]*
h_a	*Surface convective heat transfer coefficient [$m^{-2}.K^{-1}$]*
E	*Emissivity factor*

Equation 3-5: Surface thermal resistance [48]

Table 3-1 presents the calculated results of the comparison between the thermal characters of a typical glass glazing and a membrane constructions.

Table 3-1: Comparison of the heat capacity and the ratio of core thermal resistance to surface resistance in glass and ETFE foil constructions

	Single Glazing Float glass [a]	Single Membrane ETFE Film [b]
Thickness [mm]	6	0.1
Surface Density [kg.m^{-2}]	15@density=2500kg/m^3	0.175@density=1750kg/ m^3
Specific Heat [kJ.kg^{-1}.K^{-1}]	0.72	1.9-2.0
Heat capacity [kJ.m^{-2}.K^{-1}]	10.8	0.35
Core Conductivity [w.m^{-1}.K-$^{-1}$]	1	0.24@23°C
Core Resistance [m.K.W^{-1}]	0.006	0.00042
Total Resistance [m.K.W^{-1}]	0.146 [c]	0.1404 [d]
Ratio of Core Resistance to surface Resistance [%]	4.3%	0.3%
Ratio of Core Resistance to Total Resistance [%]	4.1%	0.3%

Notes:
surface density = weight per unit area.
a: Values in this column taken from [49]
b: Values in this column taken from [the data in the category referring to "construction materials manual [www.goodfellow.com] [50]
c: Assuming the surface resistance design values taken from BS EN ISO 10077,[51]. the external surface thermal resistance Rse=0.04, the internal surface resistance Rsi=0.1 (values for glazing surfaces as glass)
d: value taken from [52], at 15 temperature difference with air velocity of 4m/s

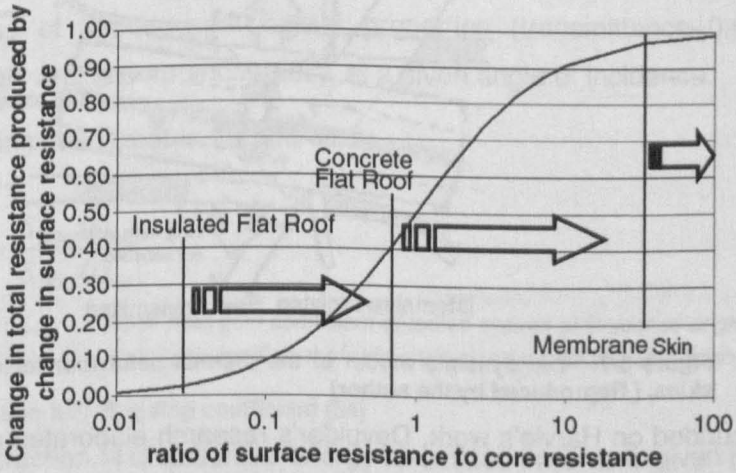

Figure 3-6: Impact of variations in surface resistance for different typical building constructions. [53] [Reproduced by the author]

The heat capacity of the ETFE foil is found in Table 3-1about 3% of that of the glass glazing, that is to say only such a fractional amount of energy input is able to raise a square metre of the temperature of the membrane by 1℃. Moreover, surface resistance of ETFE foil accounts for over 99% of total resistance, which is higher than that of a common glass glazing. These facts imply that significant impact of the variation of the surface thermal resistance on the resultant total thermal resistance of membrane skins and then the thermal performance of the buildings incorporating with the membrane constructions.

Figure 3-6 furthermore suggests that along with the increasing importance of the surface thermal resistance to the total resistance, a higher rate of an unacceptable loss in the accuracy occurs when predicting the thermal performance of membrane constructions by using static thermal concepts like thermal transmission properties, or U value.

Harvie [11] therefore argued that an appropriate thermal method for the membrane skin constructions was required to predict the their thermal performance. It would be able to describe the dynamic thermal behaviour of the membrane skin, which was dominant by the surface heat transfer around the boundary as proposed in his thesis (see Figure 3-7).

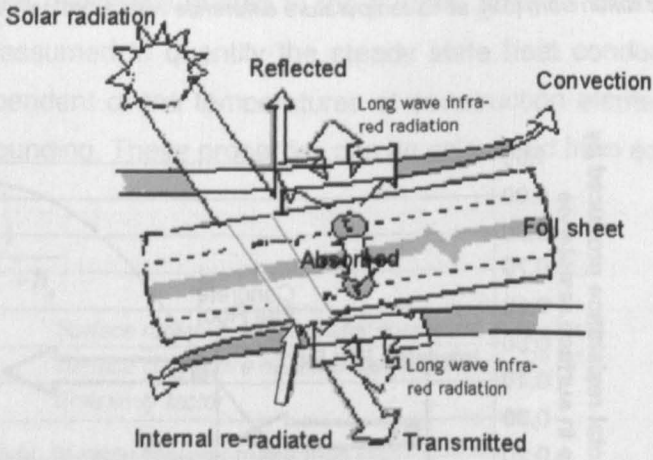

Figure 3-7: The dynamic model of the thermal behaviour for membrane skins. [Reproduced by the author]

Grounded on Harvie's work, Devulder's research elaborated an extreme thermal responsiveness of the membrane constructions and proved that the addition of two or more membrane layers could reduce the amplitude of the temperature fluctuations of the internal skin, but that the thermal behaviour of two or more layers are largely linked by long wave radiation processes.

To summarise, the assumptions underlying the calculation of standard properties (particularly, U-value) are incompatible with the nature of architectural foils to some extent. This inapplicability takes root in three specific aspects of foil skin constructions:

- the minimum thickness of foil material core, which offers little resistance to conductive heat transfer through the construction.
- the extremely low thermal mass of foil membranes, resulting in limited thermal inert effects against external environmental variations and to a extent temperature fluctuation experienced in their enclosed spaces.
- the reduced transparency of multi-layer foil constructions, giving a rise to a increasing amount of solar radiation absorbed and retained between the foil layers and the opportunities for the solar heat passing inwards by their strong longwave radiative heat exchange.

3.2.2.2 Discussions on reliability of shading coefficients

The shading coefficient is based on the solar transmittance of glazing products and the solar energy absorbed by them and reemitted inwards (SHGC, the solar heat gain coefficient). The variation of the type of glazing in such solar heat flow passing inward is then represented as the shading coefficient (SC). This is the ratio of the heat gain through the particular glazing to that through the reference glazing. The reference glazing is generally a single pane of clear float glass of known solar optical properties (transmittance=0.86, reflectance=0.08, and absorptance=0.06), at a given angle of incidence.

The shading coefficient is defined as:

$$Sc = \frac{S_{HGC}(i)_{test}}{S_{HGC}(i)_{ref}}$$

$S_{HGC}(i)_{test}$ *Solar heat gain coefficient of tested system at incidence angle* i

$S_{HGC}(i)_{ref}$ *Heat gain coefficient of reference standard glazing at incidence angle* i

Equation 3-6: Shading coefficient [54]

Then the fraction M of absorbed energy re-emitted inwards is given by

$$M = \frac{U_g}{h_o}$$

U_g	*U value of a particular glazing [W.m^{-2}.K^{-1}]*
h_o	*Heat transfer coefficient of outer surface of glazing, combination of surface radiative and convective heat transfer [W.m^{-2}.K^{-1}]*

Equation 3-7: A fraction of absorbed energy of a glazing [54]

It has been discussed in the previous section that the single use of U-values, a property combining the different heat transfer processes into static values, is incompatible with the nature of thin membrane skins. The calculation of shading coefficient property involving the application of U-values could therefore result in an unrealistic description of the thermal conductive behaviour of foil skins.

For the solar radiant energy penetrated through the glazing surface, such as diffuse and direct solar radiation, the amount of the transmitted and absorbed direct solar radiation is dependent on the solar incidence angle. This means that for any type of glazing on any exposure and at any location the shading coefficient is solar time dependent as the solar incidence angle is changing according to the solar geometry in the sky.

To simplify the calculation procedure, the shading coefficient is reasonably assumed to remain constant as the spectral distribution and the angle of incidence of the incident solar radiation varies. This assumption is verified for most clear and many tinted glazing systems [54].

However for most 'advanced' glazing systems, the use of shading coefficient introduced significant inaccuracy in the prediction of average hourly solar gains in the space. This is the case particularly for all multi-pane glazing at angles of incidence above 60°.

The foil cushion is a double-layer or multi-layer air inflated structure. El-Asfouri *et al* [54] has presented that variation of the shading coefficient of double glazing or multi-sheet glazing constructions were more sensitive to the incidence angle than the single one especially at oblique incidence angles just above 40°.

Regarding the angular dependent light transmission of foil cushion constructions, Ieremia [55] pointed out in a client communication letter that due to the complex curved surface geometry of foil cushion glazing system, the light

transmission figure based on laboratory measurements of a single flat sheet of ETFE foil was substantially different from that of two-layer foil cushion field test. In addition, according to their project reports, the argument he made follows as below:

- The light transmission does appear a difference between the tested foil sample and the reference glazing at the incident angle above 45°.
- The inflated cushion formed by curved surfaces will give an enhanced angle of incidence by up to 20°, if it is treated as flat when the solar elevation is not at its zenith.

As the characteristics of glazing construction and its surface geometry , and the angular optical selectivity of the foil cushion glazing system departs significantly from the conventional reference glazing, one would question whether the shading coefficient provides a reliable basis to evaluate its solar energy performance.

3.2.2.3 Early research attempts

One previous attempt trying to quantify the thermal transmittance of membrane construction by a conventional simplified method was demonstrated by Larsson in 1977 [56]. In his research paper, the calculation of U value ($5.5W.m^{-2}.K^{-1}$, single layer) was derived from the assumption that the air temperature of the enclosure was uniformly distributed. This method was seen to be inapplicable to membrane structures as vertical thermal stratification was easily formed in the membrane enclosures [36].

Another important attempt made by Hirokazu *et al* [52] in 1984 was to measure the thermal conductance of the core membrane specimens and their surface heat transfer coefficients (reciprocal of the surface resistances) separately. One of their aims was to control summer overheating issue, recurrent in membrane enclosures.

The surface heat transfer coefficient *h* of the membrane samples was measured when exposed to a controlled airflow. The observation showed that their surface heat transfer had been influenced more markedly by the air velocity near the surface than the surface-to-air temperature difference.

In the experiment, the controlled variable was essentially air velocity and no clear distinguishment was made between the convective and radiative surface heat transfers. But the test data depicted that the heat transfer coefficient of silver coated membrane was up to 25% lower than that of other test samples, particularly in the surface-to-air temperature difference of 5 ℃ and less, which implied a significant role played by radiative exchanges in the surface heat transfer balance of the membrane samples. In addition, the test results of the membrane samples indicated a strong relationship between the radiation with their environment and their thermal behaviour.

In all, their overall heat transfer coefficients were proved to be determined more predominately by the heat transfer process on the surface than by the thermal conductivity. Croome *et al.* [57] highlighted the insignificance of core thermal resistance for membrane skins, which will been discussed further in the section.

The implication of these findings mentioned above is that the thermal-optical properties are an alternative or more representative indicator of the environmental performance of membrane products.

The main characteristics of heat transmission behaviour on membrane materials are listed as follows:

- the pronounced dependency of its surface heat transfer on air flow in contact with surface
- the significance of long wavelength infra-red radiative exchanges onto overall surface thermal exchanges
- the negligible importance of core thermal resistance and minor body temperature gradient through the membrane skins.

To sum up, the thermal radiation behaviour of membrane constructions implied the priority of the thermal-optical properties of membrane products when assessing the thermal performance of the buildings clad by them. The recent research [13] has further stressed on the importance of detailed models on the spectral properties of a glazing element when assessing the thermal performance of the foil cushion envelop. Harris P. *et al.* suggested that a dynamic thermal-optical model should incorporate in simulation tools, by which the clear detail assessment on the shortwave or longwave transmission contribu-

tion on the resulting thermal performance of the element could be carried out respectively.

Based on the findings mentioned earlier, Harvie and Thaibault had developed a numerical model, which was appropriate for the investigation of the unusual thermal responsiveness of membrane skin buildings. The model developed was found to provide stable predictions when validated against the monitored data of the real buildings:

- A strong thermal coupling existed between the membrane layers provoking the presence of radiant cooling.
- The thermal balance at the additional inner membrane layer was largely governed by infrared radiation transfers. The heat exchange at the internal membrane surface is in proportion to the temperature difference between the internal air and membrane surface temperatures.
- The contribution of the membrane envelope to the thermal behaviour of its enclosed space was primarily the results of the solar radiation transmission into the space.
- The presence of an additional membrane layer and ventilated air cavity between the layers reduced the long-wave radiative heat gains of the external membrane layer from the enclosed space and shifted its heat transfers to the outside of the enclosure.
- The significance of internal convective heat transfer accounted for on average less than 10% of the overall heat exchanges. Therefore the external coupling of this boundary model was appropriate to implement in subsequent flow analysis of the enclosed space and no significant error was reported in this approach.

3.2.3 Multi-layer constructions

3.2.3.1 Thermal-optical properties model

Double-layered construction is a most common type of foil cushion construction. It is suggested in a previous section that the thermal-optical properties are the most relevant parameters to assess the thermal energy performance of foil membrane constructions. Derived from the properties of the individual

foil layers, the overall optical transmittance (τ_m) and reflectance (ρ_m) are modelled as:

$$\tau_m = \frac{\tau_o \tau_i}{1 - \rho_o \rho_i}$$

$$\rho_m = \rho_o + \frac{\rho_i \tau_o^2}{1 - \rho_o \rho_i}$$

τ_o τ_i	*The transmittance of internal and external foil layers respectively.*
ρ_o	*The reflectance of inner surface of the outer foil layer*
ρ_i	*The reflectance of outer surface of the internal foil layer*

Equation 3-8: Calculation of total optical properties of double-layer foil skins [54]

The total absorption can be deducted from Equation 3-8 since the sum of the three properties is unity. In the cases of the clear foil, the daylight transmission is as high as around 0.95 whereas the reflectance varies according to the surface properties with relatively low values in the shortwave region.

For triple layer construction, the optical properties model is expressed as below:

$$\tau_m = \frac{\tau_o \tau_c \tau_i}{(1 - \rho_o \rho_c)(1 - \rho_c \rho_i) - \tau_c^2 \rho_o \rho_i}$$

$$\rho_m = \rho_o + \frac{\rho_c \tau_o^2}{1 - \rho_o \rho_c} + \frac{\rho_i \tau_o^2 \tau_c^2}{(1 - \rho_o \rho_c)(1 - \rho_i \rho_c) - \tau_c^2 \rho_o \rho_i}$$

τ_o τ_c τ_i	*The transmittance of internal, central and external foil layers respectively.*
ρ_o	*The reflectance of inner surface of the outer foil layer*
ρ_i	*The reflectance of outer surface of the internal foil layer*

Equation 3-9: Calculation of total optical properties of triple-layer foil skins [58]

Parting from common glazing materials, ETFE foil products have a considerable amount of longwave transmission. A detailed assessment is suggested to evaluate the thermal-optical effects of the short and long wavelengths on thermal performance of ETFE foil cushion glazed buildings respectively (see Section 3.2.2.3).

As highlighted in Section 3.2.2.1, the thermal radiative exchanges play a prominent role in the overall heat transfer process between the single membrane skin and its surrounding environment. It is because of the high emissivity of most available membrane materials, the typical value is around 0.9. As

results of these characteristics, a strong effect of thermal coupling between the two membrane layers was observed as the surface temperatures appeared similar on the two layers [59], which implied that the dominant infra-red radiation transfer on the membrane skins.

Moreover, because of low thermal mass and predominant thermal radiation behaviour, membrane skins experience a larger temperature swing during the course of a day. Meanwhile the inner layer at the same time has been observed strong radiative exchanges with the internal space. Therefore, it is essential to control the thermal radiation exchange so as to improve the thermal comfort within the membrane enclosed space and reduce the risk of the condensation on the inner skin [59].

3.2.3.2 Environmental performance advantages

In the building glazing industry, the use of multi-layered constructions is a common practice to improve their environment behaviour. Thermal buffer air spaces created between the layers enhances solar protection and allows building insulation against thermal variation. It is particularly true for a membrane enclosure with incremental layers constituting the building envelop, without substantial structural load increased yet.

For foil cushions, their thermal and optical properties can be easily altered by applying the coating, prints, geometry or the building layout surrounding them. Figure 3-8 illustrates the two commercial successful examples available in the construction market.

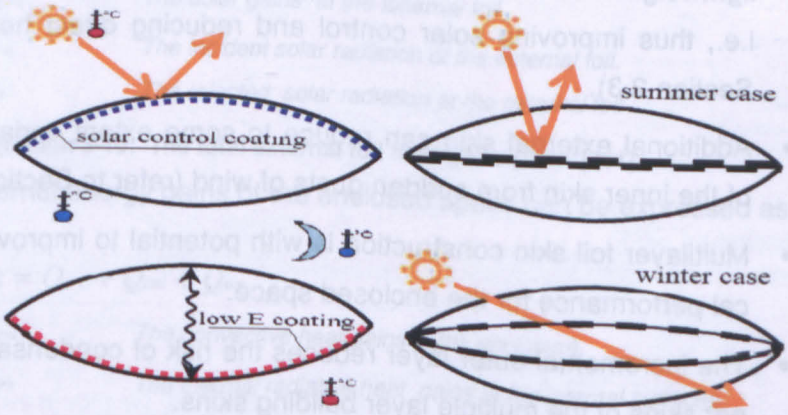

Figure 3-8: Typical examples of optical properties modification in ETFE foil cushions: application of the functional coating (left) and reflective frit at the intermediate layers (right)

The functional coating, which is durable, transparent and specifically suitable for the case of foil cushion, can reduce the thermal heat gain or heat loss according to the environment design strategies. A dynamic concept of solar control is to incorporate additional intermediate layers with offset prints or frits in the cushions. This method can achieve maximum shading or reduce shading when required by alternatively pressurizing the individual chamber (for instance, a built example, the cycle bowl pavilion, Germany, Figure 2-9).

The environmental advantages of constructing multi-layer membrane skins can be justified in following cases:

- The improvement on thermal properties is agreed in most of the literature, especially in winter due to the additional skin and the buffer zone of the cavities.
- Ventilated air space in the multi-layer construction allows heat discharge from the building envelop, enhancing the protection from the thermal variation without compromising daylighting much [60].
- Due to foil properties and air cavity configuration, reduced U-Value and g-value are also a quality highlighted by previous literature (refer to Section 1.1).
- Most authors agree that energy savings can be achieved by the use of multi-layer foil skin. This also means that indirect reduction of environmental impact and CO2 emissions can be achieved.
- The air cavity allows the placement of compatible solar protections, like lightweight insulation material, liquid chilling process, offset prints or frit, i.e., thus improving solar control and reducing direct heat loads (see Section 2.3).
- Additional external skin can reduce to some extent variable pressures of the inner skin from sudden gusts of wind (refer to Section 2.2).
- Multilayer foil skin construction is with potential to improve the acoustical performance for the enclosed space.
- The incremental outer layer reduces the risk of condensation on the inner skins of the multiple layer building skins.

- Additional fire protection of the structural membrane skin, due to the self-distinguishing properties of foil materials and air cavity constructed in between the layers. [44], [21]
- Improved aesthetic value and transparency of building image (see Section 2.2.2).

Multi-layer construction provides thr possibility of use different type of membranes and materials together to take advantage of their synergic effects of their properties.

3.2.4 Heat fluxes in a foil cushion construction

Reflected on the previous discussions on the characteristic thermal behaviours of a membrane skin enclosure, Figure 3-9 illustrates the main contributors to the thermal behaviours of the enclosure and the resulting thermal environment likely incurred under solar radiation.

The heat fluxes through the foil skins enclosure behaviour similar to that in a multi-pane glazing system.

The external foil energy gain (Q_f) (W/m²) is described as:

$$Q_f = Q_{rad} + Q_{con} + Q_{sol}$$

where

$$Q_{sol} = I_{sol} - I_{re}$$

Q_{con}	*The convective heat gains at the external foil.*
Q_{rad}	*The radiative heat gains at the external foil*
Q_{sol}	*The solar gains at the external foil*
I_{sol}	*The incident solar radiation at the external foil.*
I_{re}	*The rejected solar radiation at the external foil*

Equation 3-10: The total external foil heat gains [W/m²] [61]

The internal energy gains of the enclosed space can be expressed as:

$$Q_i = Q_{src} + Q_{cni} + Q_{trs}$$

Q_{cni}	*The convective heat gains in the enclosure.*
Q_{trs}	*The thermal radiative heat gains at the internal surfaces*
Q_{src}	*The transmitted solar irradiance in the enclosure.*

Equation 3-11: The total internal heat gains [W/m²] [61]

The accumulated heat gains in the air cavity of the double-layer foil constructions are described by:

$$Q_{cav} = Q_{ent} + Q_{stc}$$

where

$$Q_{ent} = mCp\Delta T$$

Q_{ent}	*The air enthalpic gains in the cavity.*
Q_{stc}	*The total heat gained from the energy stored in the cavity components.*
m	*The air mass flow rate [kg. s^{-1}]*
C_p	*The air specific heat [J.kg^{-1}.K^{-1}]*
ΔT	*The temperature difference of the controled air volumes and outlet of the volume [K]*

Equation 3-12: The total external foil heat gains [W/m^2] [61]

Then the overall heat balance at the external foil is shown as:

$$Q_f = Q_{cav} + Q_i$$

Equation 3-13: The overal heat balance at the external foil [W/m^2] [61]

The total effective internal heat gains (Q_{total}) of the enclosure are estimated by a function of the net internal gains of the enclosure (net Q_i) taken away the heat loss (Q_{ls}) from the inside.

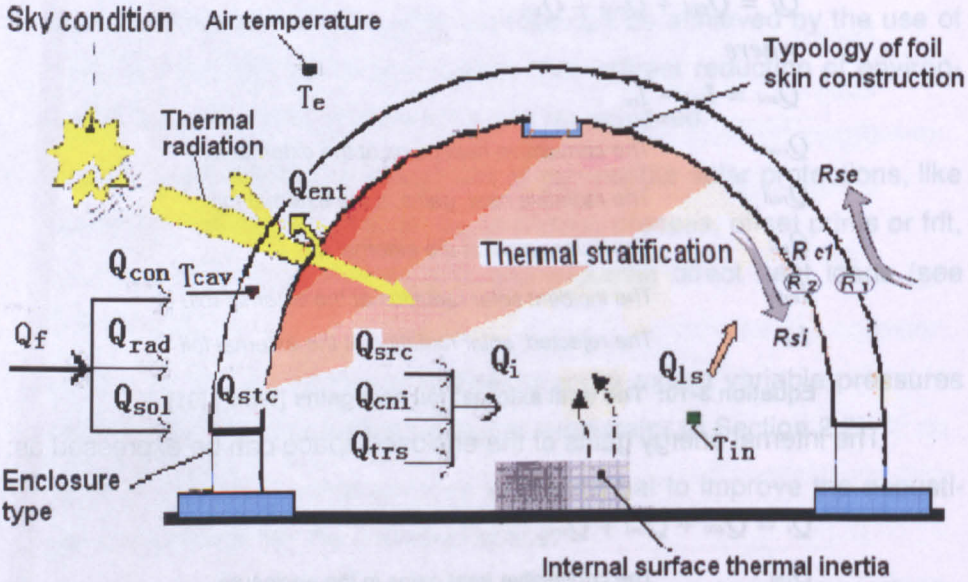

Figure 3-9: Main heat fluxes through the foil skin envelop. [NB. Rc: thermal resistace of air cavity, Rsi/Rse: the thermal resistance of the internal surface and external surface, R1/R2: core resistance of the glazing penal1 and penal2]

It can be seen that the overheating control of a foil skin enclosure is closely associated with the issue of the total heat gains in the enclosure, which is effected by the thermal loads from the envelop construction, thermal loads from the cavity and the heat losses from the enclosure, which is highly dependent on the air movement. While the incident solar irradiance in the enclosure tends to be more influential on the overall internal thermal behaviour and subsequently affect the internal convective heat exchange rates.

3.3 Thermal Environment of Multilayer Foil Skin Enclosures

Previous sections have discussed the general thermal characteristics of the foil skin enclosures. The following sections are about to detail the critical issues about the overheating and explore the existing feasible environment strategies for the foil cushion constructions.

3.3.1 Overheating in foil cushions

The reasons for development of foil cushion cladding system were its lightweight and better thermal properties than that of glass glazing. The air trapped in the cushion creates thermal buffering and reduces heat loss while maintaining most of the benefits of solar gain directly into the building. J. Chilton *et al.* [59] stated that *"the air space reduces heat transfer by convection occurring between the external membrane and the enclosed space"*.

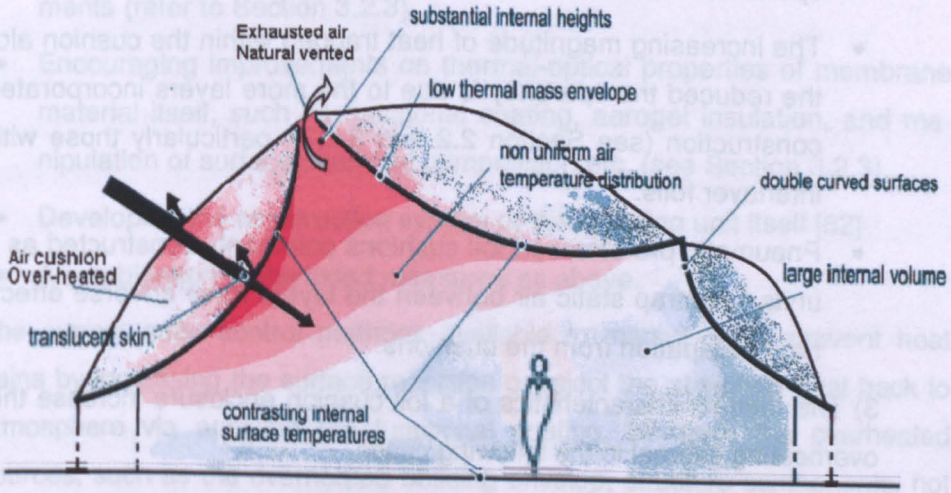

Figure 3-10: Environment particularities inside foil cushion enclosures

In previous sections, the increasing chances of uncontrollable heat built-up in a cushion envelop and the enclosed space have been explored to some extent, in particular regarding the thermal nature of membrane materials and construction configurations.

Figure 3-10 indicates the thermal particularities relating to the over-heating issues in the foil cushion enclosures. The underlying factors can be summarised into the following three categories:

1) The thermal-optical properties of clear foils lead to the presence of high thermal transmission as results of the following facts.

- Foil materials have high light transmission cross the whole solar thermal radiation spectrum, for the ETFE foil sheet allowing a mount of light transmitted in the range of long wave part. (see Section 3.2.1)
- The thermal absorption and emission behaviour of foil materials and fritted foil tend to hold up the heat on the membrane and develop strong radiative heat exchanges with their surroundings.(refer to Section 3.2.3)
- Selective transmission of foils that results in the greenhouse effect is in favour of accumulating the heat in the cushion. (refer to Section 3.2.1)

2) The thermal behaviours of foil cushion constructions favour the tendency of overheating in the cushion envelop because of the below factors.

- Low thermal mass of a foil cushion has low resistance to heat changes in its surrounding environment and thus display immediate thermal responses.
- The increasing magnitude of heat trapped within the cushion along with the reduced transparency is due to the more layers incorporated in the construction (see Section 2.2 and 3.2.3), particularly those with fritted interlayer foils.
- Pneumatic pre-stressed foil cushions commonly constructed as air-tight units to entrap static air between the layers have adverse effect on the heat dissipation from the cushions.

3) The thermal characteristics of a foil cushion enclosure increase the risk of overheating internal in the following cases.

- The high transmission of solar thermal radiation greatly influence the internal environment of the fully cushion glazed enclosure. In summer conditions, the east and west orientations are critical to prevent and assess the overheating.
- High temperature-contrast of the internal surfaces cause the uncomfortable radiant heat and destabilize the favourable vertical thermal layering (see Section3.3.2). In different ambient conditions, a 5-10℃ difference reported between the skins facing the solar radiation and away in the shadow, which is illustrated in Figure 3-10. This behaviour made the asset of buoyancy force unreliable to exploit in the cooling seasons.
- Large volume of the enclosure combining the above two factors might create localized air turbulence aggravate instability of thermal stratification in summer days and cause thermal discomfort in the occupied space if not designed properly.

According to the discussion in the previous sections, it is concluded that the thermal-optical properties of the foils and faulty constructions of the foil cushions are the two main critical contributors to the overheating in the fully foil cushion clad buildings.

To date the improvements of thermal control in a multilayer foil cushion skin envelop have focused on four areas:

- Favouring either air being entrapped or ventilated between the different layers of multi-layer foil skin constructions according to design requirements (refer to Section 3.2.3).
- Encouraging improvements on thermal-optical properties of membrane material itself, such as functional coating, aerogel insulation, and manipulation of surface chemical composition etc. (see Section 3.2.3).
- Developing the construction system of the insulting unit itself [62]
- A combination of the listed measures as above.

The current solar control methods available in market either prevent heat gains by increasing the surface reflection or reject the absorbed heat back to atmosphere via applying the functional coating. However the overheated sources, such as the overheated building envelop, structure components, hot ambient air, are still available in the immediate environment, which favour the

tendency to overheat the buildings. To remove the sources of overheating as a means to mitigate the overheating problem is of particular importance for thermal improvement on the foil membrane envelops due to their strong radiation transfer relationship with their immediate environment (refer to Section 3.2.2).

3.3.2 Temperature stratification

The general type of building applications integrated with a foil cushion construction system is the large scale one, requiring light weight envelop structures with fashion and modern transparent images. Due to the nature of a foil cushion construction there is always a large single volume with substantial internal heights presented in its enclosure. The geometry of the enclosures results in the tendency of temperature stratification within enclosures that have been highlighted in a number of publications.

The heat filtrated and trapped inside the enclosure increases as the density of air develops a difference of pressures and temperatures along the height of such an enclosure. The cold air tends to sink and warm air is to accumulate at the upper part of the enclosed space which increases the risk of heat overloads at the upper part of the enclosed volume and buoyancy cooling at the lower part. This process is well known as thermal buoyancy, and is a value asset in cooling season for the occupied zone on the lower storey of the building (see Figure 3-10).

For a passive cooling building, this natural climate zoning is essential to allow to some extent user thermal comfort zone to be formed below the building envelop. The stability of the natural thermal layering can be both assisted by the solar radiation, which heat up the surface temperature of the foil skin, and by the artificial cooling at the lower spaces of the building or by exploiting thermal inertia of the floor slabs.

However, the following cases can easily disturb the upper warm air layer and then results in turbulent mixing flows in the enclosure [36]:

- High temperature difference between the foil surfaces of the enclosure generating downward flow of cooler air at the points with low surface temperature and producing air turbulence.

- Induced natural ventilation or infiltration is not designed carefully to augment and utilize the thermal stratification to reduce the cooling load

Solar thermal radiation has an adverse effect on the thermal comfort of the space users as a result of high surface temperature. The high emissivity of the foil and its strong long wave radiation behaviour between the foil skin and internal environment can increase the mean radiant temperature experienced by the space users. It is suggested to apply low-emissivity coatings to reduce such a detrimental effect.

The passive driven buoyancy force can be give by an air pressure difference [64]:

$$\Delta P = 0.043 H \Delta t$$

H	*The height of the air enthalpic gains in the volume [m]*
Δt	*The mean temperature difference along the height from the surroudding air [℃]*

Equation 3-14: The air pressure (Pascal) difference of buoyancy force

Passive natural ventilation is driven by the thermal buoyancy, where the surplus hot air flow tends to flow out openings at the top of the enclosure while cool air will flow at the bottom (stack effect). Equation 3-14 describes that the greater mean temperature deviation of the internal and external air as well as the greater height of the enclosed volume can achieve, the more efficient air flow is created. It thus implies that the heat accumulated from solar gains should take place as low down the enclosure as possible to improve such stack effect induced natural ventilation.

3.3.3 Thermal environmental strategies in cooling season

Common building regulation imposes restriction on the energy usage in the large glazed buildings like a foil cushion enclosure. To improve its internal environment and avoid overheating in summer, encouraging natural ventilation is a practical measure to cool foil cushion enclosures passively and reduce the building loads. The following three strategies are considered in this research:

- Exploitation of buoyancy cooling generated by the thermal stratification, by which thermal comfort zone is created in the inhabited zone in the enclosed volume.

- Focus of ventilation strategies beneficial to stabilization of the thermal stratification (more discussion in Section 3.4.3). The configuration of the opening vents is placed carefully in a displacement type, where inducing the cooler air at the floor lever or pre-cooled air through underground channel and discharging the warm air at the rooftop follows the flow pattern as the internal thermal buoyancy force.
- Utilization of the form of a foil-cushion enclosure to enhance wind-driven ventilation through induced airflow.

Chapter two and previous sections in this chapter have mentioned the possibility of employing a number of relevant architectural strategies in a foil skin enclosure, particularly those on the ventilation rate increment and the enhancement on its interior climatic performance in terms of passive cooling. A number of publications [64] reported the implementation of innovative environmental strategies in large-scale membrane skin enclosures at the design stage. Yet the development on the building performance of foil cushion enclosures is still limited and lags behind their extension in architectural applications.

3.4 Enhancing the Internal Environment of the Enclosures

The developments in foil cushion glazing systems principally consider one of the two categories:

- The energy performance of the envelop via the use of solar control and thermal insulation for energy savings (which has been discussed in Section 3.3), or
- Improvements on the built environment of the interiors, such as, the indoor thermal comfort, ventilation (air exchange rates), aesthetic issues, etc.

With the developments on the above areas for the last decades, foil cushions gained popularity in the glazing industries mainly due to the high daylight transmittance, provision of acceptable thermal insulation and the potential for energy savings.

3.4.1 Compatibility of evaporative cooling to foil skin constructions

The overheating problem as highlighted in literatures (see Section 3.3.1) is a critical issue in a foil cushion enclosure, although current passive cooling strategies mentioned in previous literatures can achieve to some extent a gain in building users' comfort. However due to complexity of foil cushions' geometry and dynamic thermal behaviours of architectural foil, the detailed investigation and improvement to fully address the problem seem to be bottlenecked and seeking a novel proposal to ameliorate the situation.

Table 3-2: Physical feasiblity of evaporative cooling integration to foil cushion

	Evaporative Cooling [a]	foil Cushion Constructions [b]	Compatibility
Materials	• Water based liquid	• Hydrophobic foil material/water proof. • Extreme thin film	• Waterproof properties reduce the risk of water damaging the material constructions. • Liquid cooling works effectively with thin membrane structures
Construction Type	• Drop-wise mist • Film-wise water flow	• Multi-layered constructions (double/triple layers)	• Air cavity in foil cushions provides the channels for chilling water flow
Air Movement Provision	• Constant incoming air flow	• Inflation unit • Air dryer (for the humid condition) in place	• Inflation units of foil cushions in-situ help to produce the air-flow for the water cooling process.
Surface Area	• Vast water-air contact surface required	• Tensile surface structure • Advantageous ability of double curve surface covering large space volume	• The large covering surface of foil skin enclosure is in favour of creating large water-air interacting surface.

Notes:
a: the relevant information refer to Section 2.3.1
b: the constructional configuration refer to Section 2.2.2

In Section 2.3 and Section 2.4, a concept was proposed to innovate the foil cushion constructions and enhance the internal environment of the foil cushion buildings. The authors suggested that the use of liquid chilling process in the ventilated air cavity of a multi-layer foil skin construction could offer a rapid cooling on its foil surface and consequently control the rate of the long wavelength radiation on such a building skin.

Utilization of liquid chilling process in the multi-layer foil cushion constructions is based on the possibility of maximizing the water chilling process and enhancing the internal environment of the foil cushion enclosures. Table

3-2discusses the physical compatibility of evaporating cooling process to a foil cushion construction. The evaporative cooling effect on one hand could be enhanced by the massive foil surface provision of a large enclosed volume. On the other hand, the cooled foil layer of the foil cushions in contact with the water film could produce a heat sink for its adjacent area.

The cooling production as a result of this integration is expecting to enhance the thermal control of the foil cushion enclosure in the following aspects:

- Favourable thermal behaviour of foil material can be achieved by taking advantage of the synergic effect of both the cooling water film and foil properties.
- The thermal performance of the foil cushion envelop is improved by this type of fluidized glazing. The cooling liquid in the cavity of the insulating unit (foil cushion) perform both an insulating and solar control function. The solar heat retained between foil layers has been absorbed and taken away by the liquid, by which an over-heated source is removed and a cooled envelope can be produced. (refer to Section 2.3)
- Beneficial impact of this fluidized glazing on the internal environment of the foil cushion enclosure can be attained as the cooling liquid reduces the influencing degree of solar thermal radiation on the internal thermal stratification, and thus the buoyancy cooling effect can be reliable to some extent. The natural ventilation in the building is therefore enhanced by the source of natural buoyancy at the floor level.

It is noted that this concept of fluidized glazing is a challenge of glazing, insulating unit and plumbing technology together which conventional glass glazing manufacturers have not been used to be familiar. But now the demand to exploit this dynamic type of fluidized coating technology in a foil cushion glazing system as well as to improve its thermal performance has pushed the glazing manufacturers to exert themselves ensuring its compatibility and developing practical constructions to meet the constant challenge.

3.4.2 Thermal-optical properties of clear foils covered with a cooling fluid

Once the foil layer constituting the foil cushion envelope is in contact with the fluid, the physical thermal properties of the material surface are modified cor-

respondingly and so are the climate conditions inside the space enclosed by the foil material. The fluid material used in the research project is water. The current literatures regarding the studies of optical properties of thin films combining with water materials are largely pertinent to the greenhouse projects utilizing water condensation or cooling process (Cf. Section 2.3). On the basis of the cladding material similarity to this project, a number of literatures have been reviewed in this section with an intention to gain a general referenced information of the thermal/optical properties of a thin foil incorporating a water layer for the later research work.

3.4.2.1 The nature of plastic cladding films

PE (Polyethylene), PVC (polyvinylchloride), and EVA (ethylene-vinyl acetate) are three major types of commercial successful plastic cladding materials in the greenhouse constructions.

Table 3-3 lists two common films and discusses their relevant differences in particular for greenhouse projects purpose. Giacomelli [41] concluded that the both materials are widely used and performance well for greenhouse glazing

Table 3-3: General physical characteristics of the selected synthetic materials relating to the greenhouse applicatins.

Cladding Materials	PE Plastic Film	PVC Plastic Film	Further Details
Thermal/ Optical Properties [b]	• PAR transmittance up to 90% • Far-infrared transmittance about 80%	• light translucence around 90% • Reduced transparency(<45%) to the far-infrared (better thermal insulation)	• PAR: the spectrual range of solar radiation from 400 to 700 nm.
General Weighta	• Low density:910-930kg/m3 • Thickness around 0.2mm	• High density :1160-1350kg/m3 • Thickness>=0.25mm	• 80% greenhouse cladding film in Japan are PVC films.
Flammability [a]	• High flammability • Experience of molten drips of the film in the event of fire	• Low flammability • Self-extinguishing • Minimal danger of molten drips of the film.	• Service temperatures of both materials are around 80 degree C

Notes:
PAR: Photosynthetically active radiation
a: the physical information refer to the Construction Materials Manual, [65].
b: the relevant information from Giacomelli and Roberts 1993 [41].
Generally speaking, PE film has a limited reduction in the light transmittance during service time while the light transmittance of PVC film reduces considerably at the early stage of its service due to its duct-stick surface. On the other side, PVC films have generally better weather performance than PE synthetic materials.

Table 3-4: Properties of the selected common PE films and ETFE film for green house projectes. [66]

Cladding Materials	LDPE Film	ADCPE Film	DPE Film	ETFE Film*
Thickness [mm]	0.15	0.18	0.18	0.05-0.2
Surface Density [kg.m^{-2}]	0.138	0.17	0.17	0.1-0.35
Transmittance For the Far-Infrared [%]	60	16 (~60)	20	Around 20 (assumed)

Notes:
LDPE: low density polyethylene, which is the ordinary PE plastic film.
ADCPE: Anti-drop condensation polyethylene, with 11% vinyl acetate content (vinyl acetate is a modifying agent to reduce the transmittance of a plastic film for the far-infrared to 16 % in this case.)
DPE: Diffusive photo-selective polyethylene, with 7% vinyl acetate content.
** The data in this column is derived from the information in Section 3.2.1.*

Table 3-4 shows that the far-infrared transmittance of PE film decreases substantially from 60% for LDPE film to 16% for ADCPE film as a small increase in the percentage of modifying agent content. This properties treatment is effectively improving PE film thermal performance in cold seasons. In terms of the thermal properties, the ADCPE/DPE film shares the most similarity with ETFE cladding materials.

Seen from the above tables, both greenhouse cladding materials display similar thermal-optical characters in the wave band from 400-700nm. As most frequent used soft cladding materials in greenhouses, PE films had been selected as the samples studied for their radiation transmittance covered with water condensation. However owing to its unsatisfactory weather resistance, commercial available products of PE film are special-processed or modified by adding chemical agent to improve its weather performance

3.4.2.2 Optical characteristics of plastic films covered with a liquid

Due to the nature of high moisture content and low thermal mass, glazing layers of a greenhouse are generally at risk of water condensation. Consequently the light quantity and quality have been significantly modified by the optical properties of the cladding materials with condensation [67].

Generally two main types of condensation are:

- drop-wise, and
- film-wise

Pollet and Pieter et al [68] had studied in detail on the correlation between the solar radiation transmittance of plastic films (ordinary PE) and the full cycle of

condensation phases (dry, condensation without/with run-off, and evaporation). It was revealed that, at the normal incidence angle, the drop-wise condensation on dry PE film reduced the solar light penetration around 24% (up to 40%) due to droplet scatting effect. For the materials with a good wettability surface, such as anti-drop PE, this effect was negligible as the condensation was generally a film-like shape (Figure 3-11). Therefore, most plastics receive surfactant treatments to promote film shape condensation [69].

However seen from the Figure 3-11, in the wet state, the transmittance of LDPE with a drop-wise condensation is not incident angular dependant from zero to 60 degree, and average value of transmittance for complete test angle range is around 0.6, less than 10% difference to the highest and lowest transmittance. This phenomenon had been further proved in the Pollet's research on the effect of run-off condensation [68]. The relevant summary of PAR optical performance of the selected PE film and glass panes with water covering is illustrated in the Figure 3-11.

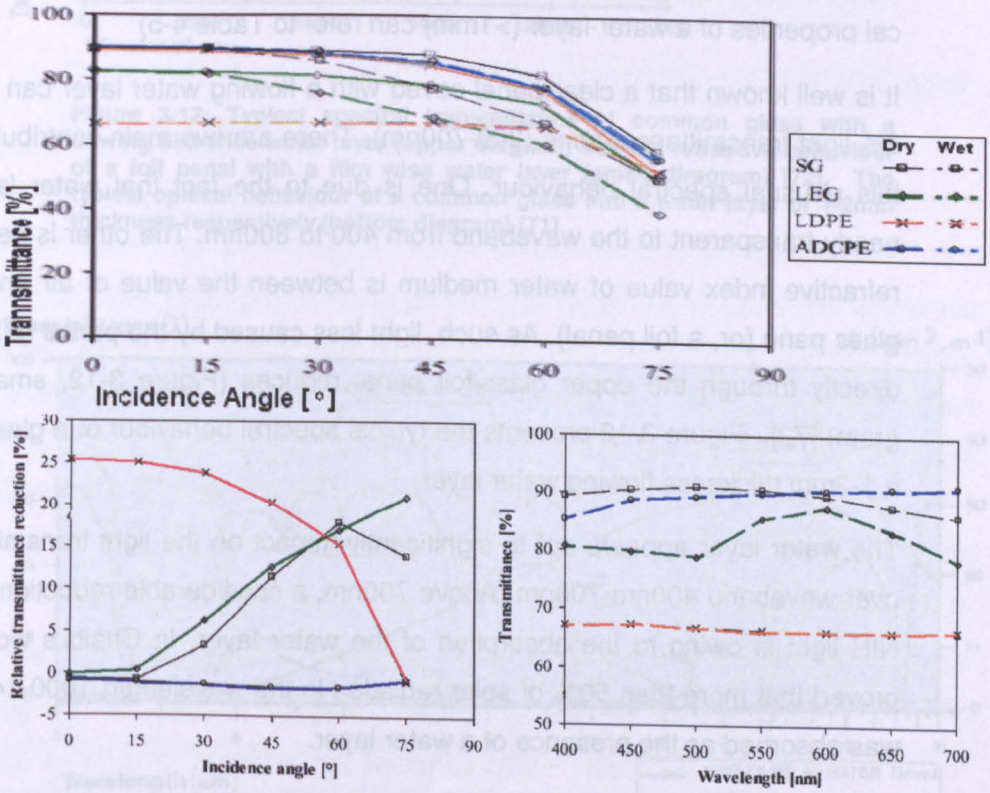

Figure 3-11: The opticcal performance of the selected cladding materials with and without water layer in the PAR waveband 400-700nm. [70] [NB: SG=single Glass; LEG=low emissivityion glass; LDPE=low density polyethylene; ADCPE=anti-drop condensation polyethylene. The data based on the research of Pollet, I.V. et al.] [Reproduced by author]

As mentioned in Section 3.2.1, except for ordinary PE films (LDPE film) most glazing materials are selective to transmit radiation, tending to have high transmittance over the solar radiation (short waveband) and various lower value in thermal radiation (Infrared wavelength). Once these cladding films are covered with a water film, the longwaver spectral transmittance reduces to nil because water is completely opaque to the far-infrared wavelength over 2.4 mm.

3.4.2.3 Effect of a running liquid film on the thermal-optical behaviour

Thin water film (1-2mm) is a perfect thermal medium for glazing as it is almost transparent to the visible radiation, translucent to the solar infrared and opaque to heat [71] (Figure 3-12, bottom chart). Within the spectral range of solar radiation, Chaibi pointed out that a typical glass covered with water flow layer had 2% increase in spectral transmittance between 300-700nm and 5% decrease in the NIR, between 700-1100nm [72] (Figure 3-12, upper chart). This behaviour was confirmed by Pollet, I. V. et al. [68]. (NB. The general optical properties of a water-layer (>1mm) can refer to Table 4-5)

It is well known that a clear penal coved with a flowing water layer can cause 2% light transmittance gains (300-700nm). There are two main contributors to this unusual spectral behaviour. One is due to the fact that water layer is nearly transparent to the waveband from 400 to 800nm. The other is because refractive index value of water medium is between the value of air and of a glass pane (or, a foil penal). As such, light loss caused by the partial reflection directly through the upper glass/foil penal reduces (Figure 3-12, small diagram) [72]. Figure 3-12 presents the typical spectral behaviour of a glass with a 1-2mm thickness flowing water layer.

The water layer appears not to significantly impact on the light transmittance over waveband 400nm-700nm. Above 700nm, a considerable reduction in the NIR light is owing to the absorption of the water layer. In Chaibi's work, he proved that more than 50% of solar radiation in the wavelength 1000-1400nm was absorbed as the presence of a water layer.

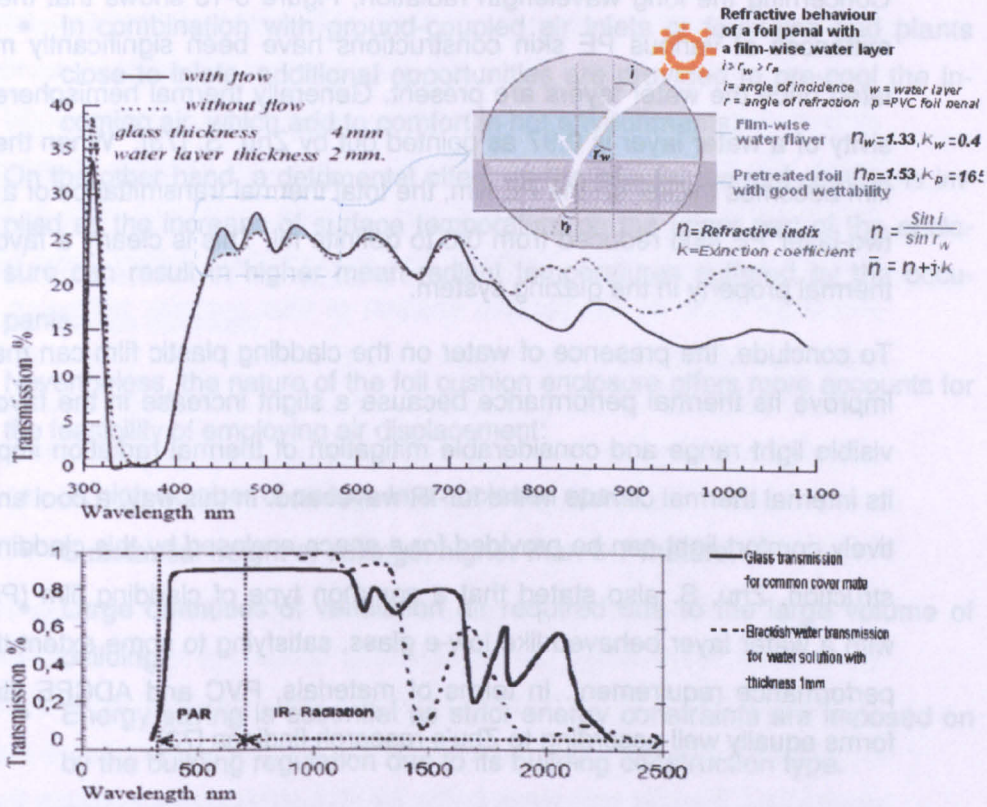

Figure 3-12: Typical spectral transmittance of common glass with a flowing film-wise water layer (upper diagram) and the refractive behaviour of a foil penal with a film wise water layer (small diragram) [72]. The typical optical behaviour of a common glass and a water layer of 1-2mm thickness respectively (bottom diagram) [71]

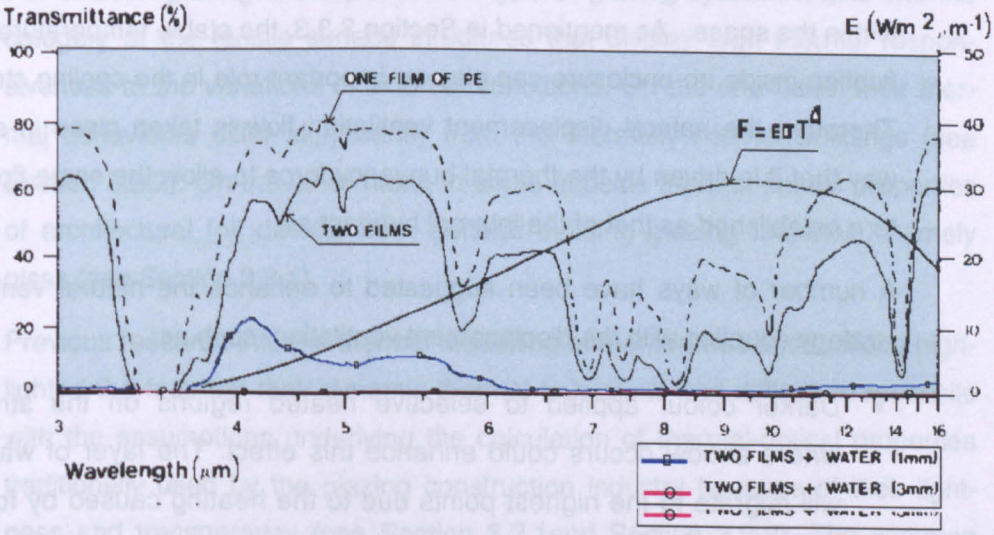

Figure 3-13: Typical thermal/ optical properites of various polyethylene (PE) cladding skin constructions with/without a water layer [74]

Concerning the long wavelength radiation, Figure 3-13 shows that the transmittances of various PE skin constructions have been significantly manipulated once the water layers are present. Generally thermal hemisphere emissivity of a water layer is 0.97 as pointed out by Zhu, S. [73]. When the water film becomes thicker on the PE film, the total thermal transmittance of a typical two-layer PE skin reduced from 0.6 to definite nil. This is clearly a favourable thermal property in the glazing system.

To conclude, the presence of water on the cladding plastic film can markedly improve its thermal performance because a slight increase in the favourable visible light range and considerable mitigation of thermal radiation impact on its internal thermal climate in the far-IR waveband. In this way, a cool and relatively comfort light can be provided for a space enclosed by this cladding construction. Zhu, S. also stated that a common type of cladding film (PE film) with a water layer behaved like low-e glass, satisfying to some extent thermal performance requirement. In terms of materials, PVC and ADCPE film performs equally well according to Zhu's research findings [73].

3.4.3 Ventilation strategies

Foil cushion clad buildings are classified as un-insulated buildings according to most building regulations. The ventilation strategy in the foil cushion enclosures should therefore take advantage of the natural ventilation and put the emphasis on the supply of out door air so as to remove the build-up of heat within the space. As mentioned in Section 3.3.3, the stable temperature stratification inside an enclosure can play an important role in the cooling strategy. Therefore the natural displacement ventilation flow is taken place in such a way that it is driven by the thermal buoyancy force to allow the same flow pattern established as that of the internal buoyant air.

A number of ways have been suggested to enhance the natural ventilation strategy coupling with the displacement ventilation, such as:

- Darker colour applied to selective heated regions on the structure where airflow occurs could enhance this effect. The layer of warm air will migrate to the highest points due to the heating caused by foil surfaces, heated by the solar radiation.

- In combination with ground-coupled air inlets or fountains and plants close to inlets, additional opportunities are provided to pre-cool the incoming air, which add to comfort in hot environments.

On the other hand, a detrimental effect on the internal thermal comfort is implied as the increase of surface temperature on the upper part of the enclosure can result in higher mean radiant temperatures suffered by the occupants.

Nevertheless, the nature of the foil cushion enclosure offers more accounts for the feasibility of employing air displacement:

- A high number of people in a enclosed space
- Substantial height of ceilings, higher than 6-7 meters.
- Large quantities of ventilation air required due to the large volume of building.
- Energy saving is essential as strict energy constraints are imposed on by the building regulation due to its building construction type.
- Contaminated environments might be the issue to deal with in the context of urbanization.

3.5 Conclusions and Summary

Foil cushion glazing envelop is a new type of glazing system. It falls into the category of the tensile surface structures that display high thermal responsiveness to the variations of external conditions. On the one hand, their thermal behaviours differ significantly from the thermally heavier buildings (see Section 3.2.2). On the other hand, in some aspects thermal-optical properties of architectural foil deviate from general building glazing materials, namely glass (see Section 3.2.1).

Previous research into the thermal modelling of membrane constructions highlighted the fact that their dynamic thermal behaviour was difficult to reconcile with the assumptions underlying the calculation of thermal-optical properties traditionally used by the glazing construction industry because of their lightness and transparency (see Section 3.2.1and Section 3.2.2). The common multi-layered construction and more complex geometry of a foil cushion have

aggravated the issues about the accurate assessment of thermal performance for a foil cushion envelop. Some authors suggested that the implementation of dynamic thermal modelling incorporating a spectral transmission model for foil layers with more detailed description on surface heat transfers be essential to evaluate the building performance and increase confidence in its application during the design stage. However, few attempts had yielded some bespoke simulation tools for the detailed analysis of their complex behaviour. Since scarce comprehensive information on the environmental properties of foil cushion constructions or no adequate analysis tool exists, the challenge of accurately assessing overheating control of alternative foil cushion constructions and then delivering energy performance optimised designs is a critical issue in the current context.

As stated in this chapter, the very nature of foil cushions conflicts with the conventional ways based on the control of conductive heat transmission for the thermal control in the glazing envelop. It was suggested in literatures that the effective strategies should count on the control of the radiative and convective heat transfer processes in the foil skin envelop to ameliorate the thermal environment inside the enclosure. Ventilated air cavity introduced into the foil cushion construction was therefore reported to be an efficient control method, which shift the heat transfer of external foil layer towards the external environment (see Section 3.2.2). The integration of chilling water process and a foil cushion can enhance the favourable process increasing the level of solar control and functioning at same time as a fluidized thermal glazing (see Section 3.4).

Influencing factors causing overheating in foil cushion enclosures are stated briefly in Section 3.3.1. Current strategies to improve the internal thermal environment in the enclosure focus on the natural displacement ventilation coupling the internal thermal driven buoyancy force. However due to the uncertainty on the thermal properties of foil material and its geometric form along with the dynamic thermal behaviours of foil cushion constructions, this passive cooling strategy utilizing vertical thermal stratification is not as reliable as expected. The foil cushion envelop incorporating chilling liquid process is assumed to be used as an alternative foil cushion glazing construction benefiting

the stabilization of thermal layering, thus to enhance the cooling effect of such natural ventilation.

The following chapter describes that a set of experiments on foil skin constructions have been carried out to investigate the extent of the impact that a pneumatic foil skin construction integrated with cooling fluid may have on the environment inside the space it encloses and relevant underlying parameters to enhance the effect.

PART II EVALUATION OF NOVEL CONSTRUCTIONS

| PARAMETER STUDY

| LABORATORY EXPERIMENTS

| ANALYTIC MODELLING

This part provides a detail account on the constructions of two full-scale experimental rigs. A parameter study was carried out to indentify the salient parameters affecting the thermal-optical behaviour of the novel constructions. Investigation on the overall thermal behaviour of the novel systems was performanced. The results have been evaluated and compared with outcomes from an analytical simulation tool, which is designated specifically to serve the research objectives.

CHAPTER 4
PARAMETER STUDY AND PRELIMINARY TESTS --- A NOVEL INFLATABLE FOIL SKIN ENCLOSURE

> *"Creativity is allowing yourself to make mistakes. Art is knowing which ones to keep"*
> --- **Scott Adams (1957–)**

4.1 Introduction

Chapter 2 (in Section 2.4) has proposed two types of foil cushion integration systems (concept model-A, and model-B) aimed at the improvement on the climate control of foil cushion constructions by innovatively integrating the cooling fluid with the foil cushion constructions. The existing knowledge of the thermal characteristics of architectural membranes and environment particularities of membrane skin enclosures has been reviewed in Chapter 3. These previous studies of thermal behaviours of foil cushion constructions implied the very compatibility of the evaporative cooling effect and the thin membrane skin envelope. However current researches have yet to explore such an integration with the foil cushion construction due to the reasons stated in Section 3.4.1. For these reasons, a set of preliminary studies on an integration system were carried out in the laboratory at the University of Nottingham. The preliminary tests are mainly relating to an experimental model: a dome-shaped, double skin inflatable clear PVC (UV-stabilized) foil skin envelope system. It is designed to be subject to the moderate and critical summer condition in the U.K.

As mentioned previously, Thaibault stressed the difficulties to accurately indentify the relationship between the environmental conditions and the thermal response of the multi-layer membrane skin due to the nature of the membrane materials. These difficulties might even deteriorate for the foil skin constructions with natural air flow or mechanical ventilation along with the evaporative cooling effect within the cavity. In order to derive great appreciation of the effect about an additional cooling liquid film along with various air-flow arrangements on the overall thermal performance of the constructions, an indoor full-scale foil cushion enclosure was designed to simulate a typical concept

model-A foil skin construction (refer to Section 2.4.2). The scale of the test rig was specified to fit inside a laboratory without directly exposing to the external weather variation, whereby a convenient comparative study of the thermal performance of the integration systems with different design arrangements in the cavity could be allowed.

This chapter provides a general description of the design specification, physical construction, equipment, and testing protocols of the test models set up at the Department of the Architecture and Built Environment, followed by the analysis of the test data for a series of tests.

4.2 Objectives

As a novel integration system, there has not been previous experimental assessment of the impact of the cooling liquid integration of the foil cushion correlated with thermal performance (particularly the overheating), nor the appropriate analytical tools available enabling researchers to explore the potential of such integration systems, especially for the control of internal thermal comfort and energy performance. Therefore a number of analytic testing were undertaken in this project. These studies were purposed to observe the following relevant issues:

- The characteristic thermal-optical behaviour of the foil skin samples with the cooling fluid process.
- The overall impression of the characteristic thermal behaviour of the experimental foil skin envelop when integrating the evaporative cooling effect.
- The relationship between the thermal behaviour of such an envelope and the effect of the involved cooling liquid process, and its impact on the internal temperature distribution, particularly on the vertical thermal stratification.
- The general heat transfer pattern in the glazing unit (the foil skin enclosure) when it incorporates the cooling fluid process, as well as the effects of various air-water flow arrangements.

Figure 4-1 details the relevant parameters underlying the thermal behaviour of the proposed pneumatic foil skin enclosure.

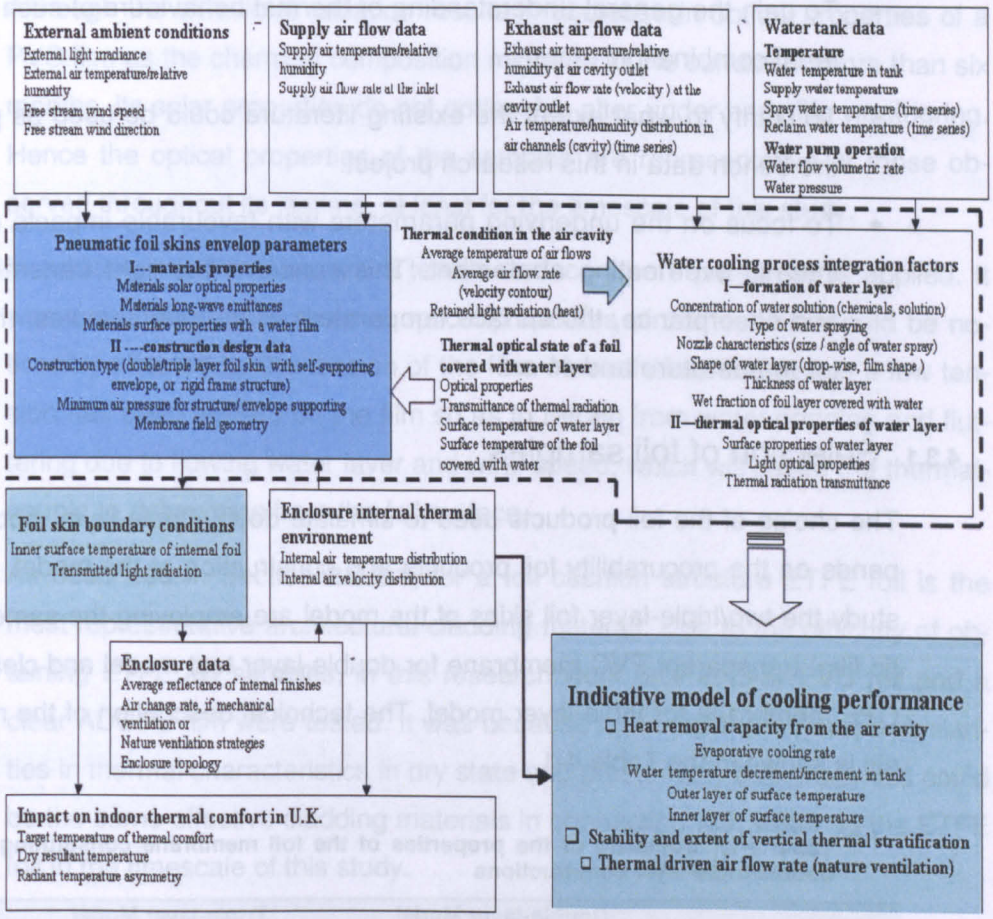

Figure 4-1: Schematic illustration of the relationship among the studied parameters in the experimental investigation

Finally, the above information gathered through the tests presented in this chapter are intended to establish a baseline for system design optimisation and benchmark data that would be required if an attempt was made to model thermal performance of such integration systems.

4.3 Preliminary Test on Double/Triple-layer Foil Skin Models

The model-A foil skin enclosure is a double-layer structure forming a channel from top to bottom, which provides space for air flow and water flow to be ducted for cooling purposes (see Section 2.4.2). The model-B foil skin construction is triple-layered. Because the information relating to thermal-optical properties of clear foil materials coupling with liquid cooling process is limited, some other research literature on these areas involving both materials are not straightforward for the purpose of this project. A min-test therefore is therefore designed to satisfy the three aims:

- To gain the general understanding of thermal behaviours of such a material combination.
- To clarify to what extent the existing literature could be used as part of the bench data in this research project.
- To focus on the underlying parameters with favourable impacts on the internal overheating abatement. This concerns the light transmittance and absorptance, the surface temperature of the test samples, the water temperature and so on.

4.3.1 Selection of foil samples

The choice of the foil products used to simulate double/triple-layer model depends on the procurability foil products and construction of the model. In this study the two/triple-layer foil skins of the model are employing the same plastic film: transparent PVC membrane for double-layer test model and clear AD-CPE membrane for triple-layer model. The technical description of the materials is shown in the Table 4-1.

Table 4-1: Summary of the properties of the foil membrane constituting the double/triple-layer constructions

	Double-layer Model	**Triple-layer Model**
	External layer/ Internal layer [a]	External layer/middle layer/Internal layer [b]
Membrane Product	IR-Blank Plastic Sheet / clear polythene (relevant information referring to right column)	SunMaster Clear Polythene (code: UV2793)
Manufacturer	Nanya Plastics Corporation	PLASTIKA KRITIS S.A.
Materials	**PVC** window material (clear)	**Polyethylene (PE)** clear anti-drip and anti-fog material
Thickness	0.5 mm	0.15mm
Weight	0.640kg/m^2@ density=1280kg/m^3	0.138kg/m^2@ density=920kg/m^3
Visible Light Transmittance	89.6%, up to 91% (400-800nm); 73.2%(800-2500nm)	89%, up to 91% (400-2500nm);
Visible Light Reflectance [a]	7% (400-800nm)	10% or 7% (400-800nm)
Thermal (longwave) Transmittance [c]	33% (or 16%, for reinforced foil type)	<63%
Thermal (longwave) Reflectance [c]	5%	5%
Position of Flowing water Layer	Flowing on the internal layer	Flowing on the cemtre layer

Notes:
a: the data in this column refers to both technical data sheet from Nanya Plastics Corporation [Appendix A.7] and Zhu, S. 1988 [73].
b: the data in this column is based on the technical data sheet from www.polytheneone.com and Zhu,S. 1988 [73].
c: the data derived from the Zhu, S. 1988 [73]. The spectral band is above 2.8um

Although the ultraviolet radiation results in decrease in optical properties of a PVC film as the chemical composition migrates to the surface in more than six months, its solar properties do not noticeably alter under early-life weathering. Hence the optical properties of the samples are representative of those observed throughout its lifetime, at least for the timescale of this study.

In addition, the foil skins are a tensile surface where pre-stress is applied. It was assumed that the thermal-optical properties of the test film would be noticeably affected by the tension of the film. Nevertheless in this test a low tension has been applied on the film so as to refrain from water ponding and fluttering due to flowing water layer and wind speed, which will cause the thermal-couple to delaminate from the foil surface.

As described in Section 2.2.2.1, for a foil cushion structure ETFE foil is the most representative architectural cladding material. Due to the difficulty of obtaining ETFE foil samples, in this research work only a clear PVC foil and a clear ADCPE film were tested. It was because that they shared some similarities in thermal characteristics in dry state and presumably both materials could be the same effective cladding materials in connection with water as the ETFE foil in the timescale of this study.

4.3.2 Assessment of the Water Source and Water Solution

The most convenient source of water in urban area must be tap water due to its good accessibility and liability. For cooling purposes, the tap water temperature, providing it is lower than dew point of the atmosphere air, can allow for an effective cooling for a system in operation.

In the asssement of the cooling ability of the water source, the tap water temperature can be calculated referring the soil temperature [33]. As the piping systems of tap water are buried under ground at the depth of 0.5m-1m, the water temperature will reach the same soil temperature at the same depth. This preliminary study is carried out particularly under the climate conditions of Nottingham, UK so that the typical cooling design parameters are presented and compared in Table 4-2.

The tap water temperature seems around 2℃ lower than the dew-point temperature of the ambient air, which allows the cooling liquid to achieve design expectation while raises however the risk of condensation in the test model. In fact, the observation of the real test cases indicated that the temperature of

tap water was higher than the dew-point because of piping system running through a building above ground and external weather variation, but the difference was within 5% [78].

Table 4-2: Summary of the water source applicability to the cooling purpose in building

Location: Nottingham, UK	**Cooling Design Temperature [℃]**	**Difference of Dry and Wet Bulb [℃]**
Dry Bulb [a]	24	5
Wet Bulb [a]	19	Difference of dry and wet bulb [℃]
Dew-point [a]	15.7	8.3
Relative Humidity [a]	62.2%	Difference of dry bulb and tap water [℃]
Mean Temperature of Tap Water [b]	13.8	10.2

Notes:
a: the cooling design temperature, such dry-bulb (DB), wet-bulb (WB), and dew-point (DP), are acquired from the CIBS guide A, 1999 [1]. The cooling design conditions are based on the wet-bulb temperature with extremes at 0.4% un-guaranteed frequency of occurrence.
b: The water temperature calculated derived from information of the under-ground temperature at the depth of 0.75m [77]. The mean water temperature is an average value in cooling seasons from May to September.

Table 4-3: Typical information for the water solution used in the test

	Relevant Information of Water Solution
Choice of the Product of Synthetic Surfactant Content [a]	Name: Fairy rinse aid, active drying power.
	Manufacturer: Procter & Gamble Co.
Chosen Concentration of the Mixed Water Solution [b]	1% (NB: photos of wettability performance shown as below, the right with 1% Fairy rinse acid comparing to the left without chemical)

Notes:
a: the relevant information refers to the appendix. And criteria of selection also concern the ecological impacts which appear non-adverse effects. [Appendix A.8]
b: 1.5% is suggested if the water flow rate is low and surface tension of the foil is high.

Concerning the formatin of the water layer, one could theoretically expect a good film-shape water layer on the selected sample due to the improved wettibility of material surface. It was found in the lab test that the desired spreading of a uniformly flowing film-wise water layer on the anti-drop surface of the foil samples could be impossible to achieve without further reducing the surface tension of water. A surfactant chemical is therefore suggested to add into

the water. The relevant information of the chosen product and water solution used in the test is shown in the Table 4-3.

It is to note that the synthetic surfactants are normally contained in the household detergent formulation. In consideration of not noticeably affecting the thermal-optical properties of the tested water solution, a low concentration of chemical is specified.

4.3.3 Method adopted and apparatus used

Pollet, I. et al. [79] had introduced comprehensive measuring techniques for the study of thermal-optical properties of clear cladding plastics coved with water. The resultant transmittance of such cladding material is defined as

$$\tau = 100\frac{\varnothing p}{\varnothing a}$$

$\varnothing p$ *The transmitted radiation flux in the presence of the test material [W.m^{-2}]*

$\varnothing a$ *The incident radiaiton flux in the absence of the test material [W.m^{-2}]*

Equation 4-1: The total transmittance of a glazing material

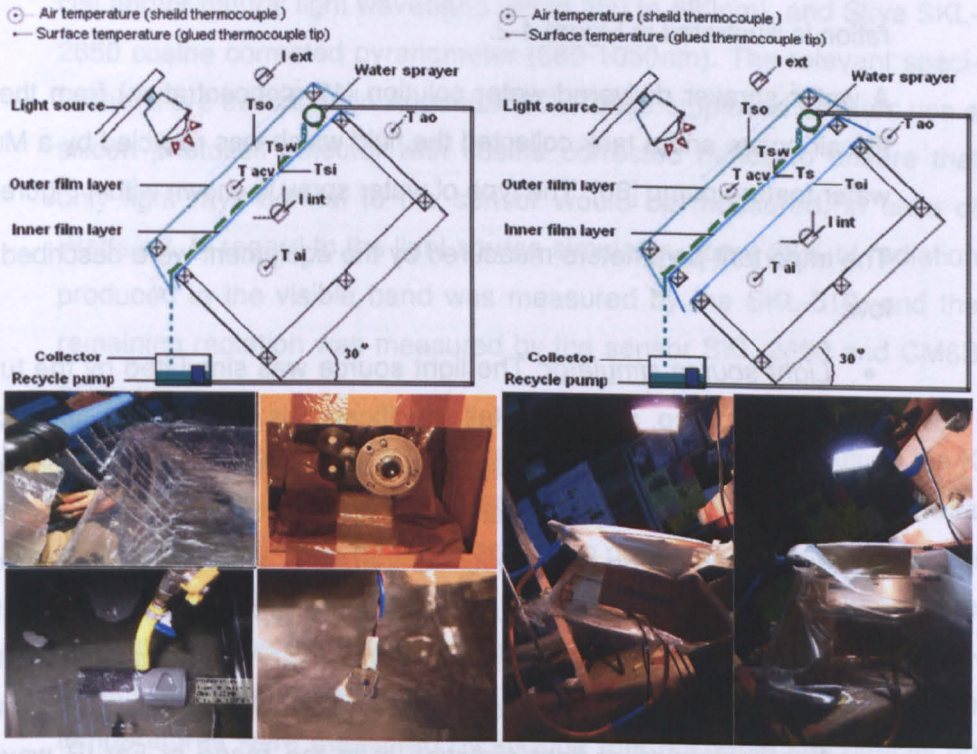

Figure 4-2: Ilustrations of the 2-layer(up left dragram) /3-layer (up right dragram) mini-test models for construcitons) with the the rig photos. [NB: Photos from left to righ depict 3-layer and 2-layer test rigs and the components including light sensors, shield thermocouple, sprayer, and small water pump]

Table 4-4: Table of temperature parameters measured on the test models

Sensor Symbol	Measured data
Surface temperatures	
T_{SO}	Outer layer surface temperature
T_{SI}	Inner layer surface temperature
T_{SW}	Water layer temperature on the surface of foil layer
Air temperatures	
T_{ao}	Outside air temperature
T_{aca}	Air cavity air temperature
T_{ai}	Internal air temperature

Notes:
The internal thermal environment can be indicated by a mean radiant temperature, which could be calculated theoretically based on the test data

Based on Pollet's research, a simpler form of a laboratory test was carried out to facilitate the aims to observe and evaluate the thermal state or optical performance of 2/3-layer foil skins with or without a flowing water layer.

Two layers of PVC plastic samples were mounted flatly on the rig. The two 220mm X 140mm clear PVC films were fully exposed to a light source, and normal to the direct light. The air space separating the two layers was 140mm deep while the distance from the top layer to the lamp was 600mm. The internal volume of the rig was fully sealed. The diagram of the test model configuration is illustrated in Figure 4-2.

A water sprayer delivered water solution (1% concentration) from the top of the air space and a tank collected the fluid which was recycled by a Multi 800 water feature pump [80]. The type of water spray is shown within Figure 4-2.

The important parameters measured by the equipment were described as below:

- *Light source simulator*: The light source was simulated by the tungsten halogen lamp, and the detail specification is described in Appendix A.3. Figure 4-3 illustrates the spectral output of a body is a function of temperature of an object (Wien's displacement law). For the selected light source simulator (the colour temperature around 3000°K), it is seen from the emission spectrum figure that of the total radiation emitted by the lamps, about 25% is within the near-infrared spectrum (0.8nm-1.1nm), 24% within the visible and 51% within the Far-IR (1.1nm-3nm). A large portion of light radiation is in the range of Far-IR waveband, nonetheless in the study the evolution of overheating in test rig is the essential condition to recreate and assess. For this reason, the moder-

ate level of external temperature condition was set between 21℃ and 25℃.

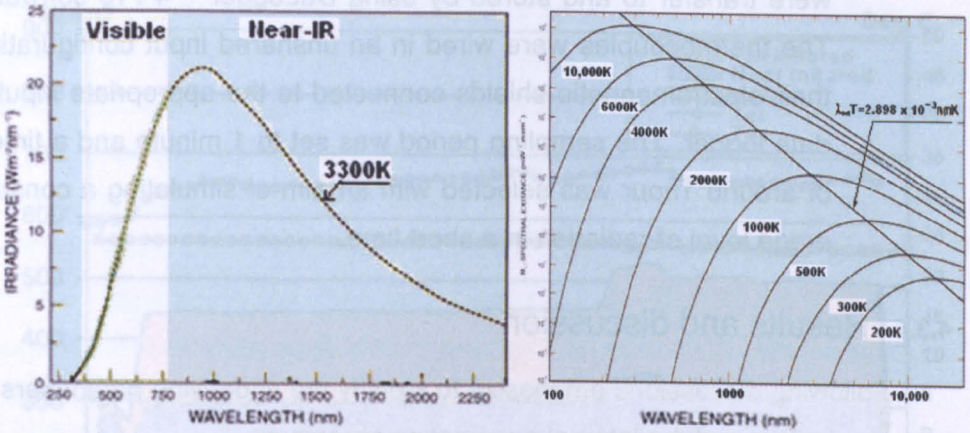

Figure 4-3: Emission spectrum of the tungsten halogen lamp for the colour temperature range: 3000℃K-3300℃K (left) and the peak emission spectrum in various black body as results of temperature (right). http://www.newport.com/store/genContent.aspx/Simulation-of-Solar-Irradiation/411986/1033 [Accessed Dec. 2010]

- *Pyranometers:* The light radiation was measured by three types of sensors: pyranometer global light sensor CM6B (305-2800nm), single channel cosine corrected energy sensors Skye SKL-510 (mixed artificial and/or natural light waveband within 380 to 680nm), and Skye SKL-2650 cosine corrected pyranometer (680-1050nm). The relevant specifications are described in Appendix A.2. These employed sensors use a silicon photocell detector with cosine corrected heads to ensure that only light rays normal to the sensor would be measured, in units of Watts/m². In regard to the light source simulator, about 28% of radiation produced in the visible band was measured by the SKL-510, and the remaining radiation was measured by the sensor SKL-2650 and CM6B accordingly.
- *Temperature sensors:* The temperatures were measured by using the K type thermocouple temperature sensors, and their technical data was listed in Appendix A.1. All the temperature parameters measured on the rig are tabulated in the Table 4-4. Moreover the air temperatures were measured by thermocouple sensors, whose tips were shielded in light-weight aluminium screens to exclude direct radiation effects. Surface temperatures were measured by sticking thermocouple tips directly on both sides of the test samples by adhesive reflective aluminium foil to avoid exposing direct heat from lamps.

- *Data logger:* These variables were measured continuously with a data-Taker DT500 [81] connected to a computer where the measured data were transfer to and stored by using DeLogger™ 4 Pro software [82]. The thermocouples were wired in an unshared input configuration and their electromagnetic shields connected to the appropriate input of the data logger. The sampling period was set to 1 minute and a time scale of around 1hour was selected with an aim of simulating a constant average level of radiation in a short time.

4.3.4 Results and discussion

Following discussions emphasize to identify the underlying parameters or factors in favour of the internal overheating abatement.

4.3.4.1 External condition measurements

One purpose of this study was to look into the impact of the presence of the water layer on the development of overheating. The setting of the external in UK climate was thus assumed to be around 22°C. The general external condition for this test model is visualised in Figure 4-4 as about 22°C and the average internal air temperatures were about and 31°C.

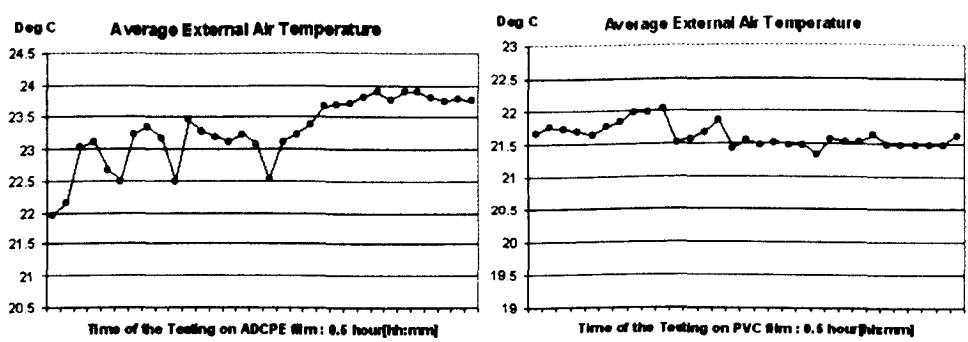

Figure 4-4: Examples of measured external temperature (Tao) for the test models covered with ADCPE and PVC film respectively

As shown in Figure 4-5 and Figure 4-6, the external intensity of the radiation was around 450 W/m^2 to 500 W/m^2, which was enough to develop high temperatures within the internal volume. The clear day average intensities are (from 1hour after sunrise to 1hour before sunset) about 590w/ m^2 in July at the location 50°N [83]. Compared to that, the average intensity of 500w/ m^2 apparently represents about 85% of the July conditions.

The general external ambient condtion of the laboratory test for the two sample foil has been visualized in the Figure 4-5 and Figure 4-6.

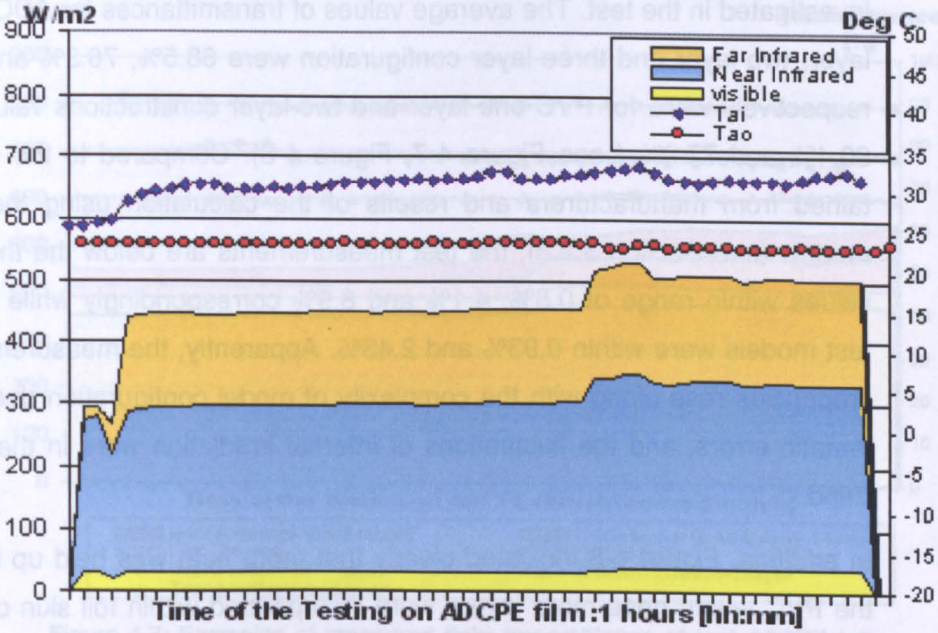

Figure 4-5: Examples of measured external irradiation intensity by radiation components without ADCPE film covered

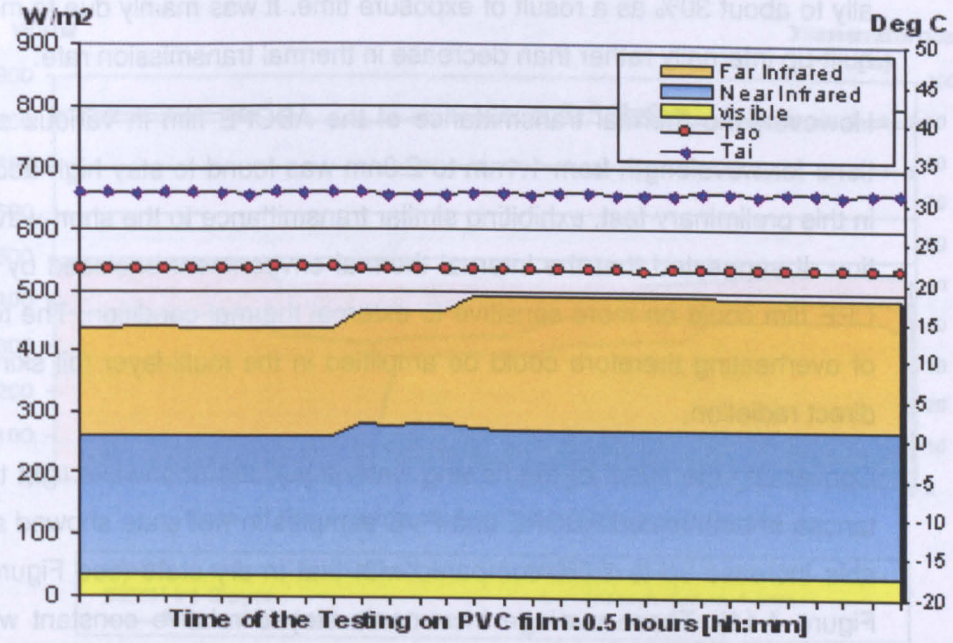

Figure 4-6: Examples of measured external irradiation intensity by radiation components without PVC film covered

NB. The specific data of the luminair from manufacturers is that: visible light output is 24%, Far-IR is 51%, and 25% is NIR. (Cf. Section 4.3.3) while based on the measurement, the results are 15% (visible), 50%(NIR), 40%(Far-IR).

4.3.4.2 Influence of a flowing water layer on spectral transmission

The light transmission of ADCPE samples in various constructions had been investigated in the test. The average values of transmittances for ADCPE one-layer, two-layer and three-layer configuration were 88.5%, 76.3% and 66.9% respectively while for PVC one-layer and two-layer constructions values were 90.4% and 77.9% (see Figure 4-7, Figure 4-8). Compared to the data obtained from manufacturers and results of the calculation using the optical models (see Section 3.2.3), the test measurements are below the theoretical values within range of 0.5%, 4.1% and 8.9% correspondingly while for PVC test models were within 0.93% and 2.43%. Apparently, the measurement discrepancies rose along with the complexity of model configuration due to systematic errors, and the fluctuations of internal irradiation were in the inverse trend.

In addition, Figure 4-8 indicated clearly that more heat was held up between the PVC layers once more layers were incorporated within foil skin construction. In comparison with the ADCPE film, the PVC film has been found that its thermal performance is better as more thermal radiation had been blocked out at an average rate of more than 60% initially, though the rate reduced gradually to about 30% as a result of exposure time. It was mainly due to more heat built-up internally rather than decrease in thermal transmission rate.

However, the thermal transmittance of the ADCPE film in various constructions for wavelength from 1.1nm to 2.8nm was found to stay high above 70% in this preliminary test, exhibiting similar transmittance to the short-wave radiation. It suggested that the internal thermal environment enclosed by the ADCPE film could be more sensitive to external thermal condition. The tendency of overheating therefore could be amplified in the multi-layer foil skins under direct radiation.

Concerning the effect of the flowing water layer, the shortwave light transmittances of both tested ADCPE and PVC samples in wet state showed a noticeable increase up to 2.5% compared with that in dry state (see Figure 4-9 to Figure 4-11). These average increments stayed relative constant when the test model configuration was altered from 1-layer to 2-layer. Similar to the optical behaviour in dry state, the light transmission rate tended to be lower when the model configuration incorporated with more layers.

The optical behaviours without water layer interference (dry–state of foil samples) have been illustrated in Figure 4-7 and Figure 4-8.

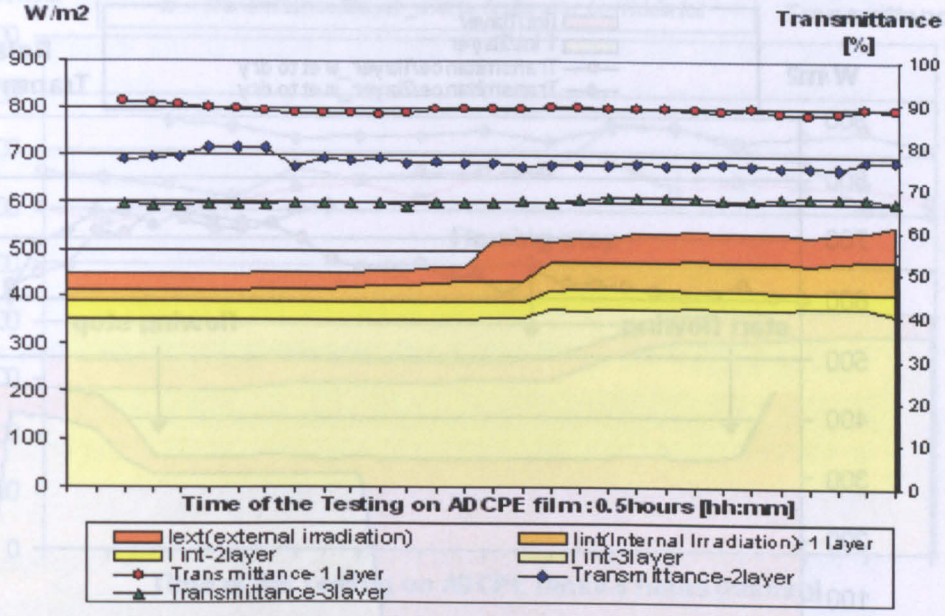

Figure 4-7: Examples of measured light trasnmittance of test ADCPE foil sample for dry-state in single/double/triple-layer configurations

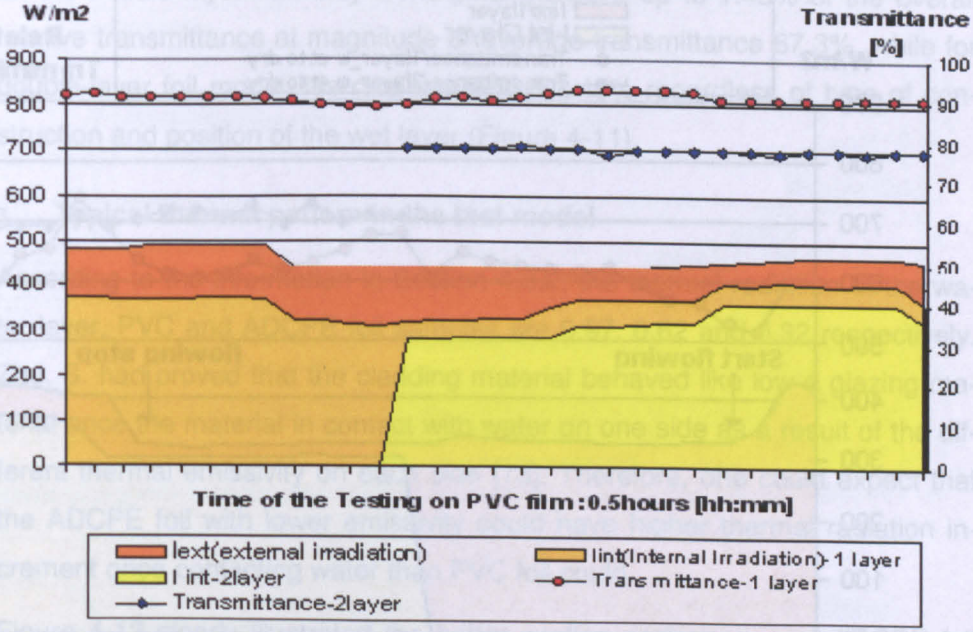

Figure 4-8: Examples of measured light trasnmittance of test PVC foil sample for dry-state in single/double/triple-layer configurations.

The optical behaviours with water layer interference (wet–state of foil samples) have been illustrated in Figure 4-9 and Figure 4-10.

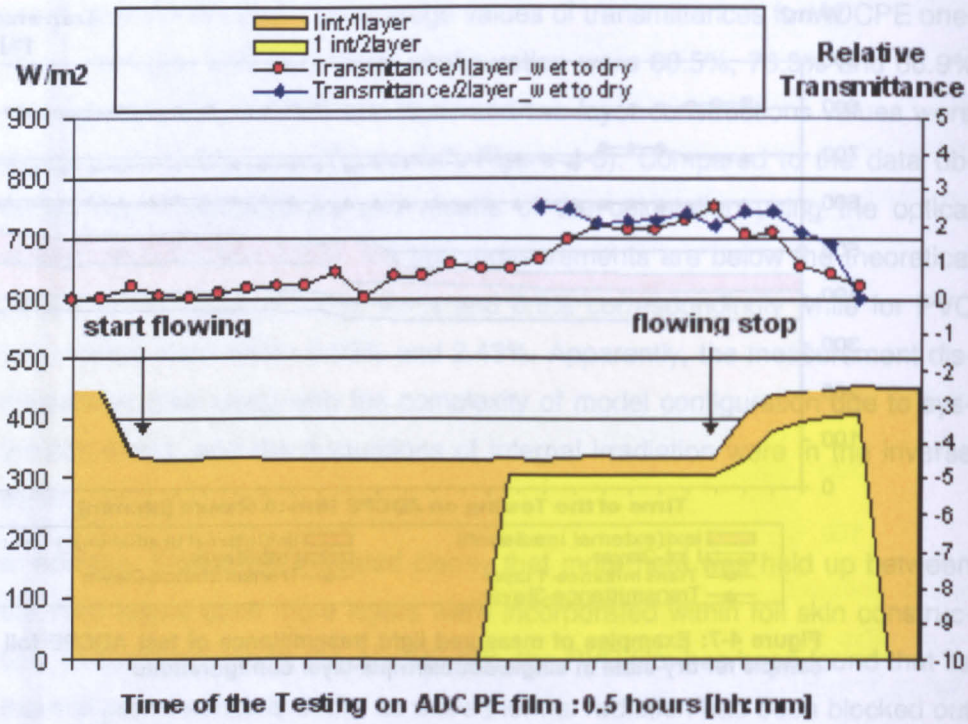

Figure 4-9: Examples of measured light trasnmittance of test ADCPE foil sample for wet- state in single/double-layer configurations

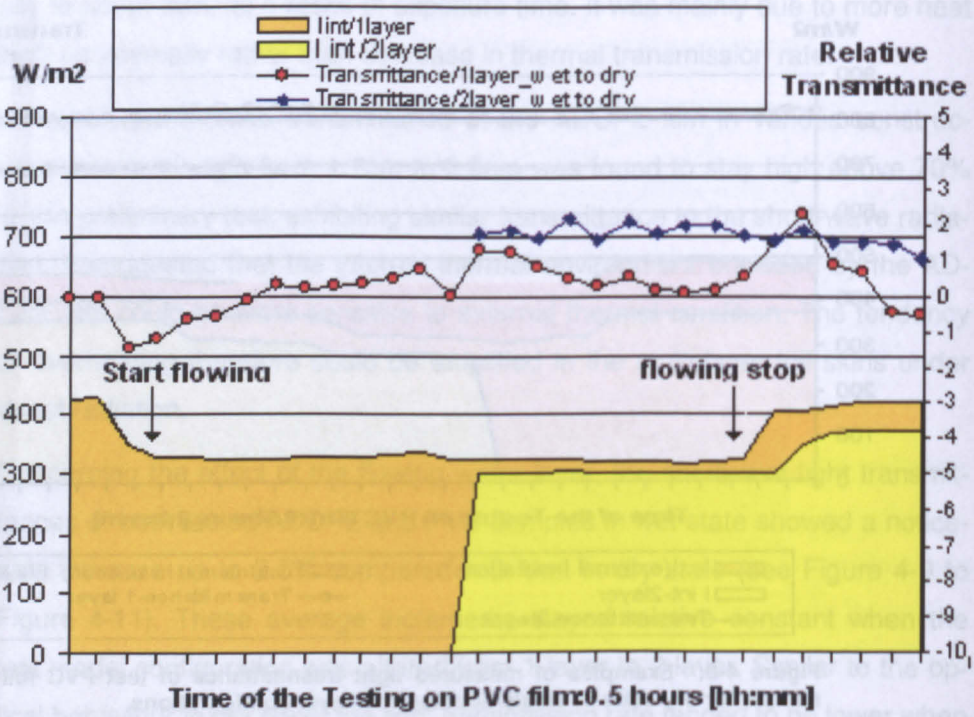

Figure 4-10: Examples of measured light trasnmittance of test PVC foil sample for wet-state in single/double-layer configurations.

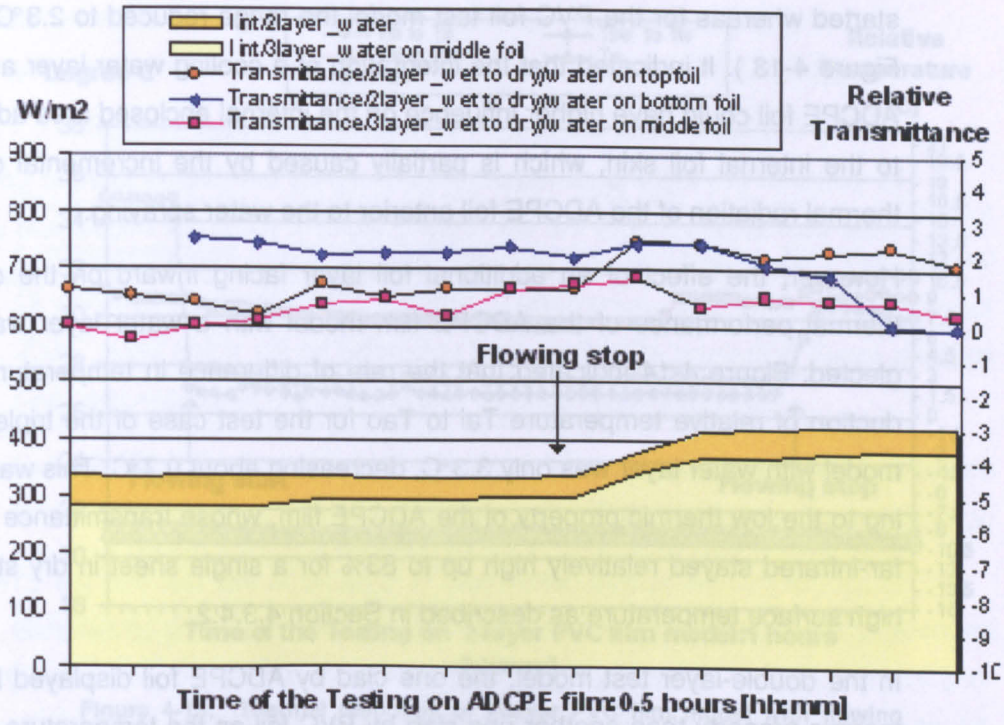

Figure 4-11: Examples of measured light trasnmittance of test ADCPE foil for dry and wet state in double/triple-layer configurations as water layer flowing on the different position

Meanwhile, the triple-layer foil construction model incorporating flowing water on the middle layer had only a marginal increase up to 1.45% of the overall relative transmittance at magnitude of average transmittance 67.3%, while for double-layer foil model this rate was about 2.45% regardless of type of construction and position of the wet layer (Figure 4-11).

4.3.4.3 Typical thermal pattern in the test model

According to the information in Section 4.3.2, the thermal radiation of the water-layer, PVC and ADCPE foil samples are 0.97, 0.62 and 0.32 respectively. Zhu, S. had proved that the cladding material behaved like low-e glazing material once the material in contact with water on one side as a result of the different thermal emissivity on each side [73]. Therefore, one could expect that the ADCPE foil with lower emissivity could have higher thermal radiation increment once contacting water than PVC foil could.

Figure 4-12 clearly illustrated the better cooling performance of ADCPE foil once incorporating with water in the case of double-layer test model. The temperature reduction of the relative temperature Tai to Tao for the test case using ADCPE foil was in the average range of 4℃ once the water spraying

started whereas for the PVC foil test model the range reduced to 2.3℃ (see Figure 4-13). It indicated that the integration of a cooling water layer and the ADCPE foil could have higher influence on the internal enclosed area adjacent to the internal foil skin, which is partially caused by the incremental overall thermal radiation of the ADCPE foil anterior to the water spraying.

However, the effect of an additional foil layer facing inward on the overall thermal performance of the ADCPE film model with a water layer was neglected. Figure 4-14 indicated that the rate of difference in temperatures reduction of relative temperature Tai to Tao for the test case of the triple-layer model with water layer was only 3.3℃, decreasing about 0.7℃. This was owing to the low thermic property of the ADCPE film, whose transmittance of the far-infrared stayed relatively high up to 83% for a single sheet in dry state at high surface temperature as described in Section 4.3.4.2.

In the double-layer test model, the one clad by ADCPE foil displayed higher thermic property than another one clad by PVC foil as the temperature difference between Tai and Tao or Tsi (Inner layer surface temperature) was up to 9.3 ℃ or 8.9 ℃ (Figure 4-12). However, this large temperature difference Tai to Tsi, (that is to say, a lower surface temperature directly adjacent to the internal air temperature), increased the risk of condensation.

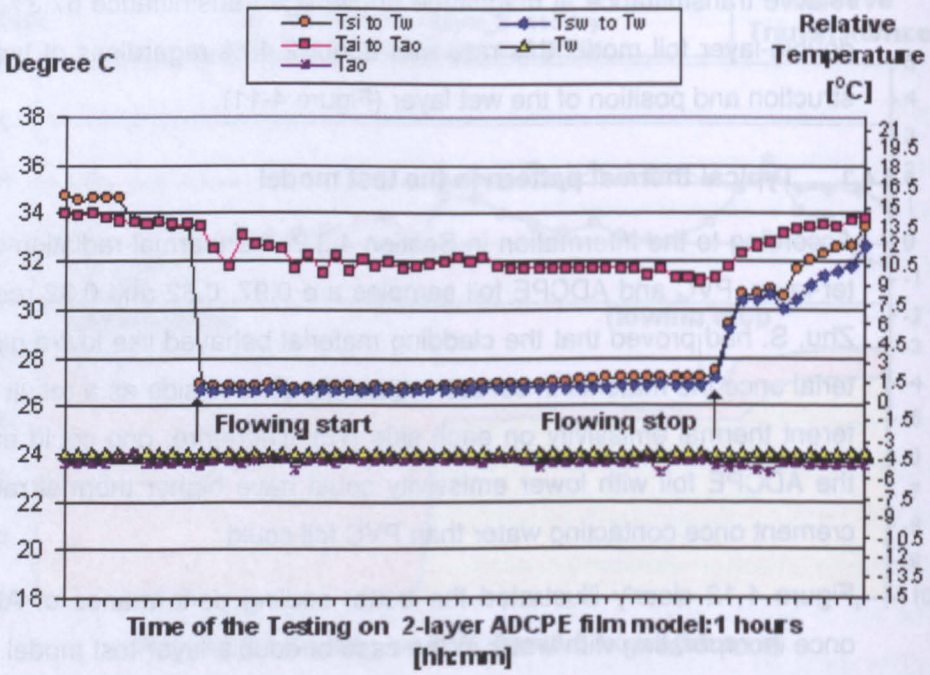

Figure 4-12: Thermal response of 2-layer ADCPEC film model with flowing water layer on the middle foil.

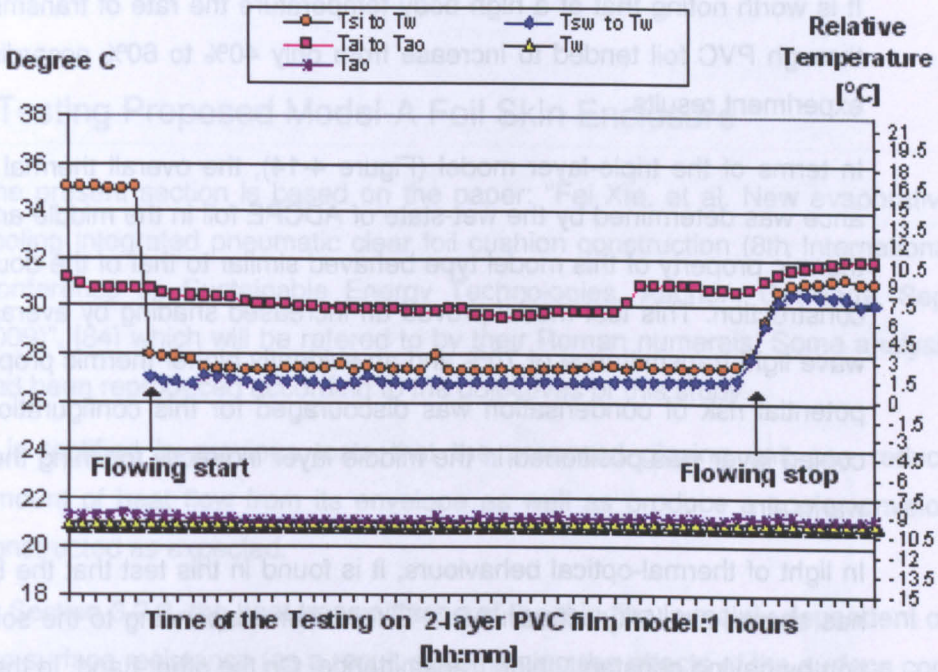

Figure 4-13: Thermal response of 2-layer PVC film model with flowing water layer on the middle foil

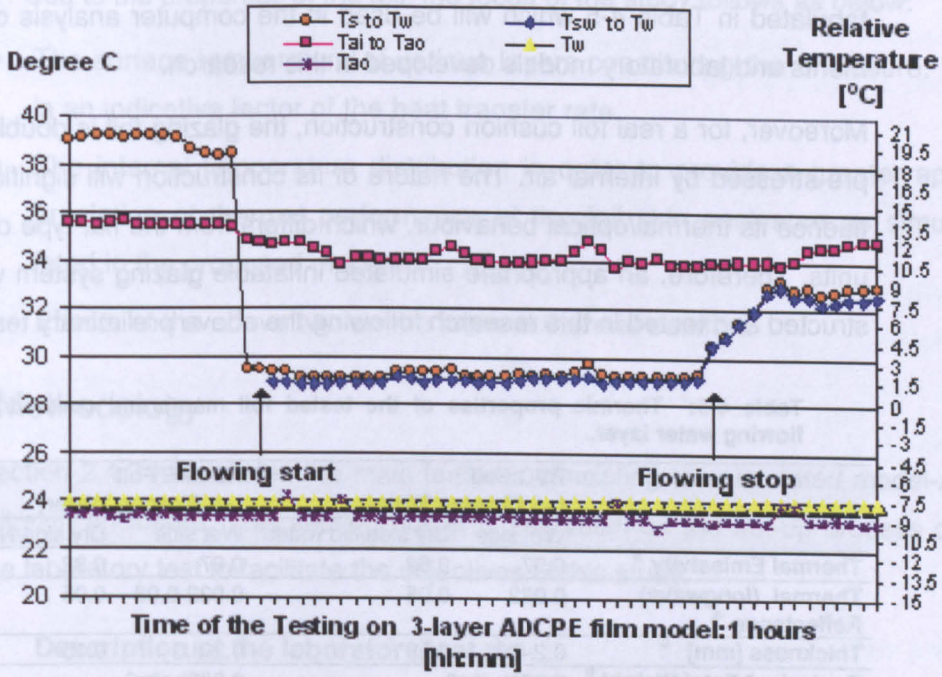

Figure 4-14: Thermal response of 3-layer ADCPE film model with flowing water layer on the middle foil.

To conclude, the test cladding material covered with flowing water behaves like low-e glazing material with better thermal properties than those without water covering.

It is worth noting that at a high body temperature the rate of transmitted heat through PVC foil tended to increase from only 40% to 60% according to the experiment results.

In terms of the triple-layer model (Figure 4-14), the overall thermal performance was determined by the wet-state of ADCPE foil in the middle and overall thermic property of this model type behaved similar to that of the double-layer construction. This test model proved an increased shading by average short-wave light transmittance of 70% and an evidently higher thermic property. The potential risk of condensation was discouraged for this configuration as the cooled layer was positioned in the middle layer indirectly touching the internal warm air.

In light of thermal-optical behaviours, it is found in this test that the ETFE foil has shared similarity with an ADCPE foil when responding to the solar radiation by having constantly high transmittance. On the other hand, to the thermal radiation above 3nm the ETFE foils behave more or less same as PVC foils.

The thermic properties of the test foil sample covered with flowing water are tabulated in Table 4-5 which will be used in the computer analysis of experiments and laboratory models developed in this research.

Moreover, for a real foil cushion construction, the glazing foil is double-curved pre-stressed by internal air. The nature of its construction will significantly influence its thermal/optical behaviour, which differs from the flat type of glazing units. Therefore, an appropriate simulated inflatable glazing system was constructed and tested in this research following the above preliminary test.

Table 4-5: Thermic properties of the tested foil mambrane covered with a flowing water layer.

	PVC Foil (+/- Flowing Water)		ADCPE Foil (+/- Flowing Water)	
	Wet side	Dry side/No water	Wet side	Dry side/No water
Thermal Emissivity [a]	0.97	0.62	0.97	0.32
Thermal (longwave) Reflectance [a]	0.022	0.05	0.022-0.03	0.05
Thickness [mm] [b]	0.2-0.3	0.55	0.2-0.3	0.15
Equivalent Total Weight [b]	0.890kg/m2		0.388kg/m2	
Equivalent Total Thermal Adsorption [b]	0.94		0.93	

Notes:
a: the data in this row refers to information from the Zhu, S. 1998 [73]. The Emissivity of a water layer (thickness>1mm) is 0.97, the overall transmittance for solar energy is over 0.95.
b: the data in this row were based on the information obtained from this experiment.

4.4 Testing Proposed Model-A Foil Skin Enclosure

The present section is based on the paper: "Fei Xie, et al. New evaporative cooling integrated pneumatic clear foil cushion construction (8th International Conference on Sustainable Energy Technologies, Aachen, Germany, Sept 2009)", [84] which will be refered to by their Roman numerals. Some analysis had been reproduced according to the objectives of this study.

It is testified in previous tests that the proposed glazing unit can reduce amount of heat flow from its envelope as well as produce a cooler envelop constructed as expected.

In Section 3.2.2, the heat transmittance of the thin film is mainly dependent on the surface resistance (as a result of combining the effects of the surface convective and radiative heat transfer). The foil cushion envelope is also an advanced glazing system having double-curve surfaces pre-stressed by internal air. Due to the properties of the foil, the focus of the study follows as below:

- The surface temperature of various layers constituting the enclosure. It is an indicative factor of the heat transfer rate.
- The internal temperature distribution in order to provide a greater appreciation of thermal performance of the foil skin enclosure as simulated in the proposed mode-A.
- Effects of the above two on the internal thermal comfort.

4.4.1 Methodology

Section 2.4.2 has briefed the main features consisting the simulated model-A foil skin enclosure. This section presents the detail on the set-up process of the laboratory test to facilitate the objectives of this study.

4.4.1.1 Description of the laboratory test rig

The core parts of the experimental facility are listed as below:

- Simulated double-layer foil skin enclosure: a inflatable PVC foil skin tent
- Incline supporting base
- Light source simulator

- Air supply units and auxiliary equipments
- Water supply units and spraying nozzles

Figure 4-15, Figure 4-16 and Figure 4-17 illustrates the major components consisting this experiment rig for varying air supply modes.

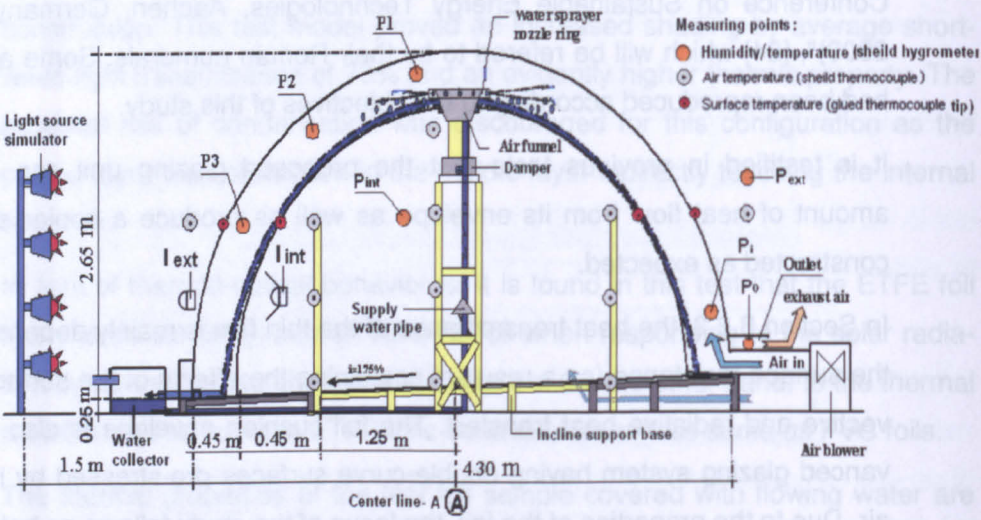

Figure 4-15: Experiment ficility: the cross section diagram (along center line -B) of the simulated enclosure for the air-blow-in-from-bottom mode

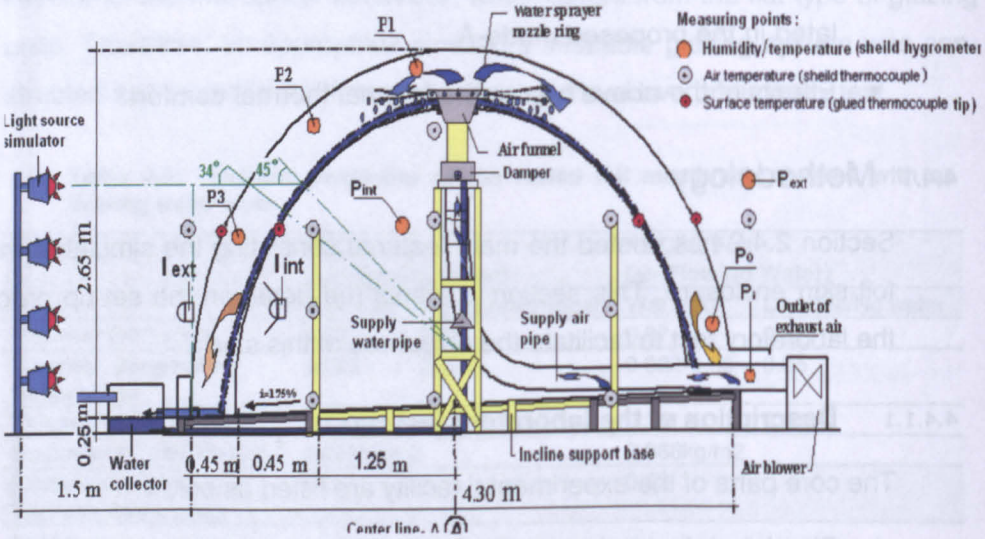

Figure 4-16: Experiment ficility: the cross section diagram (along center line -B) of the simulated enclosure for the air-blow-in-from-bottom mode

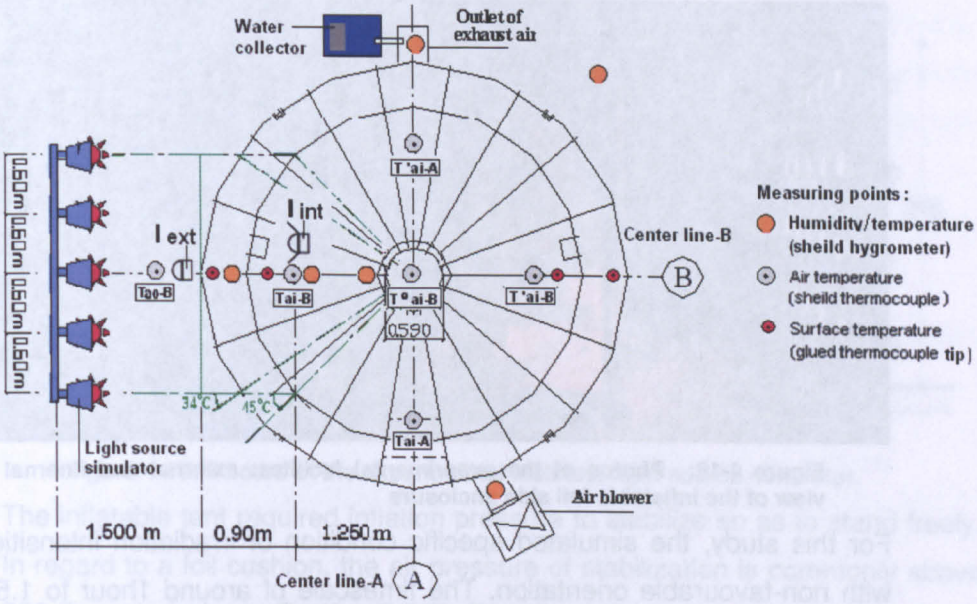

Figure 4-17: Experiment ficility: The plan of the simulated enclosure and the positions of the equipments.

The inflatable tent was constructed to simulate a double-layer foil cushion enclosure with an attempt to gain a general impression of the internal climate variations once the water cooling process was integrated into its construction. The foil material constituting the double-layer tent was PVC foil. The relevant information of its properties have been already described in the previous sections in this chapter.

This typical test tent favoured fully enclosed spaces, paticularly with a total height of 2.9 meters and about internal height of 2.4 metres. By this scale the internal thermal stratification could best be observed appropriately. Normally, the indoor temperature increase from 0.84 ℃ to 1.67 ℃ per metre in height [85]. Hereby there would be at least 2 ℃ difference along the internal height of the tent. A door was 1.58m high and 0.76m wide located along at one side and the main depth size of the cavity was kept to 450mm in all the cases. The very dimensions of the inflatable tent have been illustrated in Figure 4-15 to Figure 4-17.

A wooden inclined supporting base had served to produce a small slope and duct down the excess water to the collector (Figure 4-18). The average height of the base was 0.25m leaving the four sides of the basement open to the external enclosure to facilitate the ventilation design strategies for the system described in Section 3.4.3. Overall the size of the base was 2.5 X 2.5 m^2 supporting the border area of the tent with 2.24 X 2.24 m^2 empty in the centre.

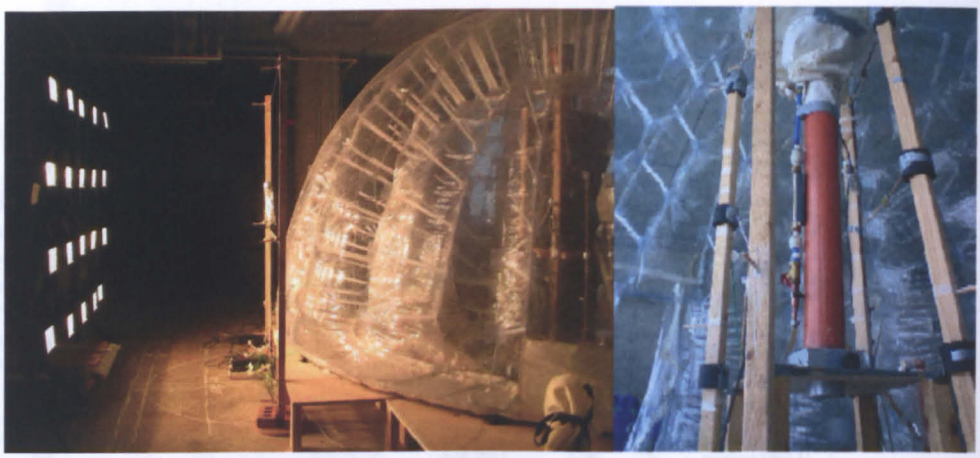

Figure 4-18: Photos of the experimental facilites: external and itnernal view of the inflatable foil skin enclosure

For this study, the simulated specific condition of irradiation intensities was with non-favourable orientation. The timescale of around 1hour to 1.5 hours was selected with an aim of simulating a constant average level of radiation in such a short period. The magnitude of irradiation intensity of about 600W/m² was set as constant on the top layer of the PVC sheet on the vertical plane. The intensity of the direct radiation was with a slight distribution over the surface, which was the result of the somewhat non-uniform lamp performance and the distance variation between the lamp rack and the double-curve membrane skin of the enclosure.

According to the weather data in CIBSE Guide for Environmental Design in the critical summer condition in location at 50°N, during short periods of time there were average values between 600 to 618 W/m² on the vertical surface on non favourable orientation and global radiation about 580 to 600 W/m² on horizontal plane [83]. Therefore, the selected setting of the typical testing condition was about 600W/m² of average irradiation intensity, assuming external temperature level between 21 and 25°C.

A light rack using 20 flood halogen lights, the same type of tungsten halogen lamps as that in the previous small test models (see Section 4.3.4), simulated the desired intensity of radiation. Figure 4-19 illustrated the location of the rack and lamps arrangement. The relevant specifications of the lamp and the quality of the light source has discussed in Section 4.3.4.

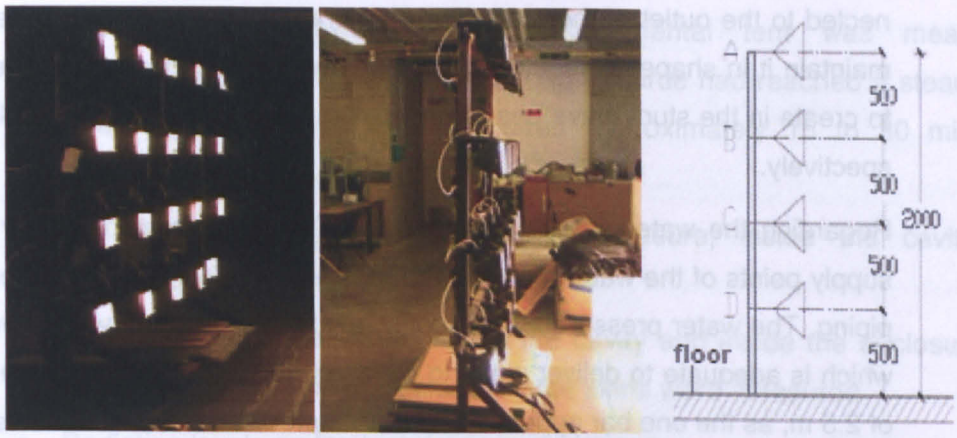

Figure 4-19: Photos of the experimental facilites: light source simulator.

The inflatable tent required inflation pressure to stabilize so as to stand freely. In regard to a foil cushion, the air pressure of stabilization is commonly above 200 Pascals (refer to Section 2.2.2). Based on the testing results indoors and the scale of the tent, maintaining air pressure of the tent indoor was generally around100 Pascals.

Figure 4-20 has shown the connection of three major components of the air supply system: centrifugal fan, motor and air ducting.

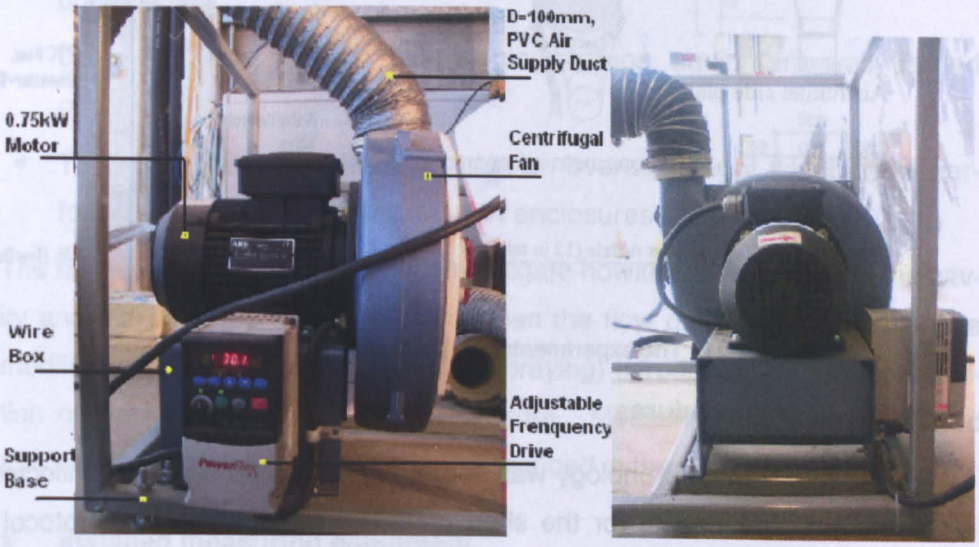

Figure 4-20: Photos of the experimental facilites: air supply power and components of the air supply units.

The inflation air pressure was supplied by a single inlet motor centrifugal fan, powered by a 3 phase AEG 0.75 kW motor [86]. The rotating speed of the motor was coupled with a 3 phase Allen-Bradley Powerflex 4 adjustable frequency drive (IP55) [87]. When the motor rotates in full power, the LCD digital panel displays 60 Hz. There was a diameter of 100mm PVC flexible duct con-

nected to the outlet of the motor fan, delivering the air to inflate the tent and maintain it in shape as required. The two modes of airflow pattern attempted to create in the study have been illustrated in Figure 4-15 and Figure 4-16 respectively.

Regarding the water spraying unit, sprayers were connected directly to the supply points of the water mains in the laboratory by ¼ inches diameter water piping. The water pressure at the supply point in the laboratory was two bars, which is adequate to deliver water to points of the spray nozzles at the height of 2.5 m, as the one bar approximates a 10 meter water column. Twelve spray nozzles in total were modulated along a bronze ring on the water tube in a subsequent angle of 30°. The unique orifice of spray nozzles was 0.5mm producing flat spray pattern in a 10° spray angle. The design of the nozzle ring and spraying supply units are illustrated in the Figure 4-21.

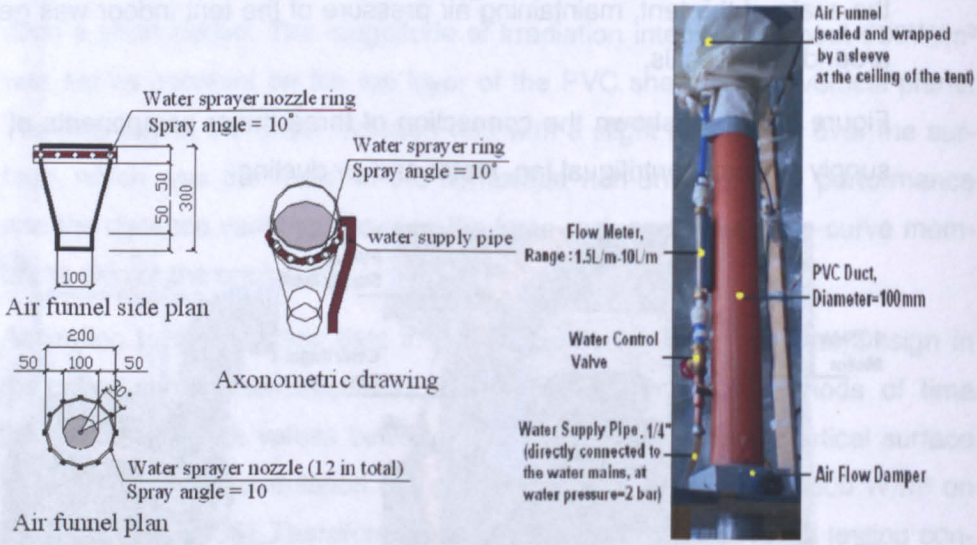

Figure 4-21: The experimental facilites: water spraying units.

4.4.1.2 Test procedures

The measuring chronology was set as 1.5 hours and data was collected at an interval of 1 minute for the short period of testing. The test protocol implemented for the tests using the simulated enclosure is as follows:

- The air blower was turned on and tent was inflated until a stable air pressure level was obtained, desired relative air pressure in the range of 100-103 Pascals.
- The artificial light source was turned on.

- The thermal behaviour of the experimental tent was measured for 1 hour 30 minutes after the light source had reached a steady level. The floodlights system required approximately 15 to 30 minutes to produce a steady luminous flow.
- Air temperature values outside the enclosure, inside the cavity, and inside the room were measured.
- Surface temperature values inside the cavity and inside the enclosure at the front and at the back closing inner skins were measured.
- Radiation levels on the test rig were measured.
- The air humidity values outside the enclosure, inside the cavity and internal enclosed space were measured.
- Cavity air pressure values were measured
- The water spraying system was turned on
- The above procedures were repeated.
- The rig was modified according to the parameters of tested structure of inflatable foil skin tent, air supplying models and dry or wet state of the tent.
- Data collection through data-logging/storage equipment was carried out.
- The results were assessed to gain an overall view of the thermal performance of the pneumatic foil skin enclosures.

The main aim of the testing was to investigate how the temperature of the cavity and the enclosed space behaved when the flow pattern in the cavity was modified and the cooling liquid (water spraying) introduced into the construction of the simulated foil cushion enclosure. Measuring equipment installed and detail of the installation has been described in the next section.

4.4.1.3 Installed measuring equipment

The instrumentation used to measure experimental condition in this test is listed in Table 4-6.

Table 4-6: Equipments used for experimental measuremnts

Number of Unit Used in the Test	Instrumentation
1	Data logger [Data sheet, DT500]
1	Data logger, CME (channel extension)
1	Pyranometers (Bandwidth 680-1050nm), SKL-2650 [Appendix A.2]
1	Visible light energy sensors (Bandwidth 380-680nm), SKL-510 [Appendix A.2]
7	HMP45A humidity/temperature probes [Appendix A.6].
22	K-type thermocouples: air temperature measurement—18units, Surface temperature measurement—4units.
2*	Glass mercury filled thermometers for measuring water temperature and air temperature in front of the tent.
1	Portable pitot tube multifunction anemometer for the cavity relative air pressure measurement [Appendix A.5]
1	Portable TA45 Thermal Anemometer for air flow measurement [Appendix A.4]
1	Delogger-Plus Software for recording and Monitoring. [82]
1	PC for data storage

Notes:
**: the mercury filled thermometer is 305mm in length and measuring range of temperature is 10℃ to 110℃. More details refer to website: http://uk.rs-online.com/*

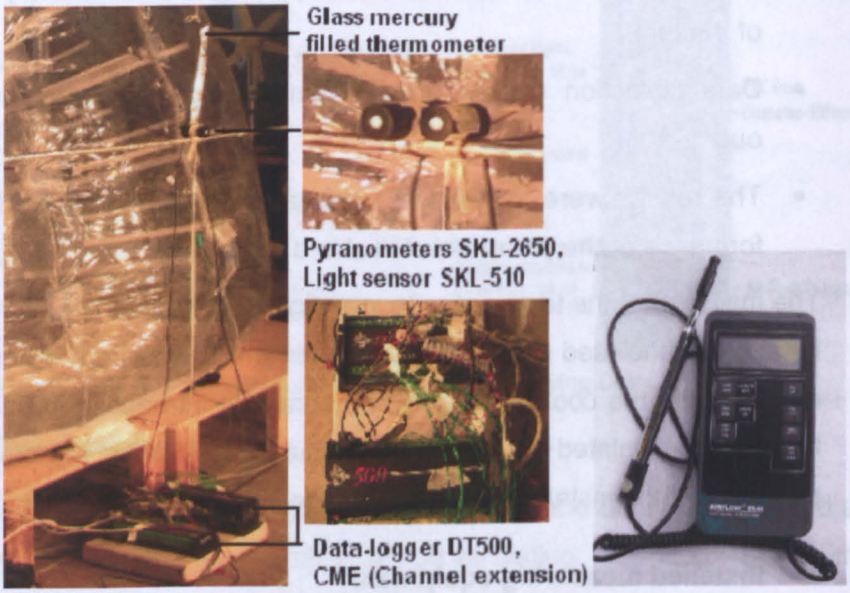

Figure 4-22: Photos of some intruments: the data-logger, pyranometers, mercury filled therometers and handheld thermal anenometer

The energy sensors Skye SKL-510 measures light energy within the waveband of 380 to 680nm, which represented about 28% of the light radiation produced by the light source simulator in this test. The pyranometer Skye SKL-2650 measures near-infrared light energy within the wavelength of 680nm to 1050 nm, which took up about 72% of the infrared radiation pro-

duced by the simulator. The radiation level measurements illustrated later section.

Air velocities were measured using a hand held thermal anemometer as shown in the Figure 4-22. The velocity meter was orientated to measure velocity magnitude on the airflow direction. The technical specifications and detailed descriptions of the instruments used in the experimental analysis can be found in Appendix A.4.

Surface temperature was measured by four K-type thermocouples fixed to the surface using silicone heat sink adhesive and shielded using 20mmx20mm aluminium screens placed against the light flow. The standard error of the thermocouples was ±0.5℃ or 4%. Due to the consideration of the enclosure scale and small area of the thermocouple installed, the manufacturer's error is reckoned as the implication of installation error [88]. For air temperatures, the thermocouples used were also shielded using aluminium screens to avoid being directly heated by the light source. The position of these shield thermocouple sensors is shown in Figure 4-15 to Figure 4-17. The full account of air and surface temperature parameters measured in this rig and their positions of installation is listed in Table 4-7.

Table 4-7: Position of the temperature sensors in the test-rig

	Distance to Central line-A of the Tent [m]: Towards the light simulator (+) Towards opposite way (-)			**Distance to Central line-B of the Tent [m]:** Towards the doorway (+) Towards opposite way (-)		
Air Temperatures	Sensor Symbol	Height [m]	Distance [m]	Sensor Symbol	Height [m]	Distance [m]
	T^0ai-B0	2.05	0	Tai-A1	1.45	1.25
	T^0ai -B1	1.45	0	Tai-A2	0.85	1.25
	T^0ai -B2	0.85	0	Tai-A3	0.25	1.25
	T^0ai -B3	0.25	0	T 'ai-A1	1.45	-1.25
	T^0ai -B1	1.45	1.25	T 'ai-A2	0.85	-1.25
	T^0ai -B2	0.85	1.25	T 'ai-A3	0.25	-1.25
	T^0ai -B3	0.25	1.25			
	T 'ai-B1	1.45	-1.25			
	T 'ai-B2	0.85	-1.25			
	T 'ai-B3	0.25	-1.25			
	T ao-B1	1.45	2.15			
	T 'ao-B1	1.45	-2.15			
Surface Temperature	Tsi-B1	1.45	1.6	**Subscript symbol**		
	Tso-B1	1.45	2.05	ai: internal air temperature		
	T 'si-B1	1.45	-1.6	ao: outside air temperature		
	T 'so-B1	1.45	-2.05	si: inner layer surface temperature		
				so: outer layer surface temperature		

Table 4-8: Summary of humidity parameters measured and installation position on the test-rig

Sensor Symbol	Measured Data	Height [m]
Cavity Humidity/Temperature		
P1/Tcav1	Humidity/temperature at the top	2.65
P2/Tcav2	Humidity /temperature at the middle	2.05
P3/Tcav3	Humidity /temperature at human height	1.45
Po/Tcavo	Humidity /temperature at the air outlet	0.25
Pi/Tcavi	Humidity /temperature at the air inlet	0.25
External / Internal Humidity		
P ext /Tao	External humidity /temperature	1.45
P Int/Tai	Internal humidity/temperature	1.45

Notes:
The photos of the hygrometers installed in the rig are shown as above.

Table 4-8 tabulates the humidity parameters measured in the rig.The relative humidities of the cavity, the internal and the external of the tent were measured using seven three-channel sensor HMP45A probes with temperature sensors. A radiation shield was used in order to avoid error readings from direct light sources. The specification of the equipment refers to Appendix A.6. The position of the probes is illustrated in Figure 4-15 to Figure 4-17.

The average air pressure of the cavity was measured by the Digitron multi-function anemometer by two measuring points, which are shown in the Figure 4-23. The meter connecting to the two measuring points at a height of 1.45m by Tygon pitot and Normaplastic straight / Y push-on acetal pipe connectors as shown in Figure 4-23. The measurements of the air pressure are detailed in a later section.

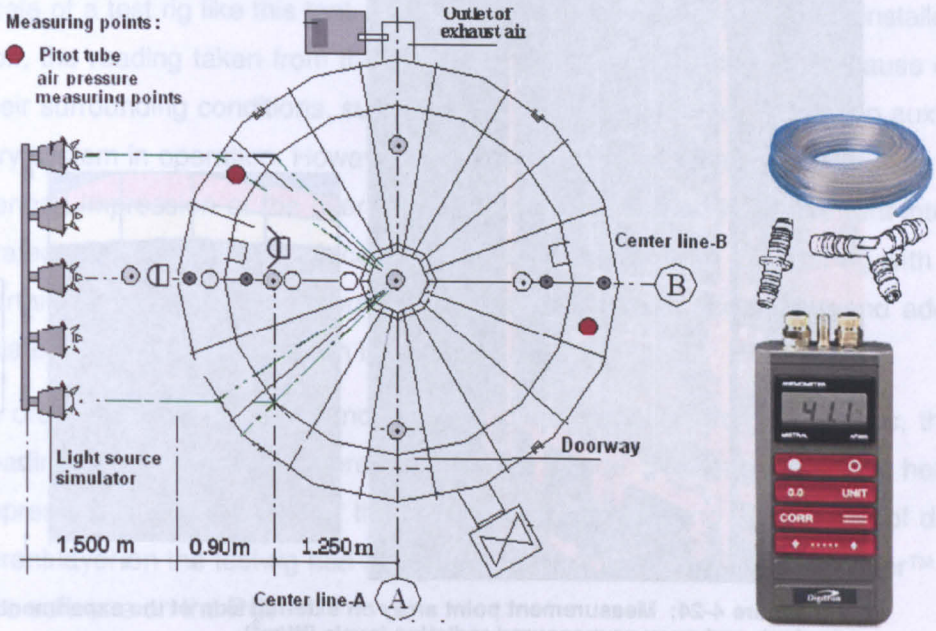

Figure 4-23: Position of the relative air pressure measured in air cavity of the tent by a pitot tube anemometer. [Photos of instrument components: Digitron anemomenter, acete conncetors and Tygon pitot tube]

4.4.2 Experimental measuring

4.4.2.1 Radiation measurement

The irradiance intensity on the front external skin of the tent had been measured on an assumed screen as shown in the Figure 4-24. Due to curvature of the skin of the tent and the size of the light rack, the screen was set as 2.4 meter in width and 2.1meter in height. An equal grid of 5 columns and 6 rows was used to divide the screen. The radiation level was measured at each intersection point. The distribution of irradiation on the screen is presented in Figure 4-24 that from row-1 at the height of 0.4m to row-5 at the height of 1.6m is almost uniform irradiation of above 600W/m^2. As indicated in Figure 4-17, the light incident angle for the scale of the 2.4m x 2.0m at the front of the tent was within 34° on the external layer from both the vertical cross view and plan view while on the internal layer the incident angle was 45°. In Section 3.4.2.2, Pollet's study showed that for normal plastic films in dry state, no significant influence on the transmitted radiation had been found when the incident angle of the radiation within 45°. Therefore, the irradiation intensity on the assumed screen was instead assumed as the irradiation distributed on the external skin of the tent.

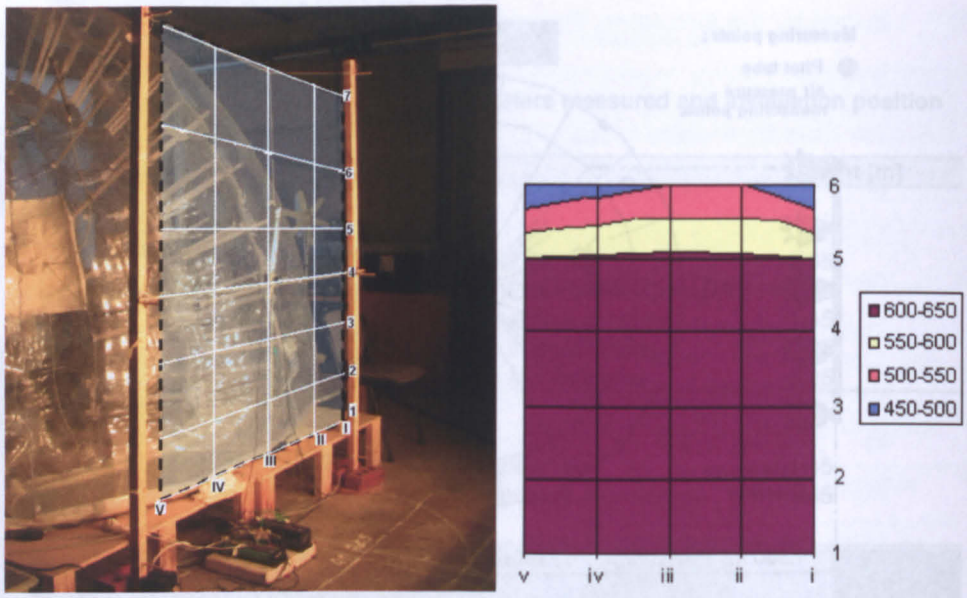

Figure 4-24: Measurement point array on external skin of the experimental tent and average measured radiation levels [W/m^2]

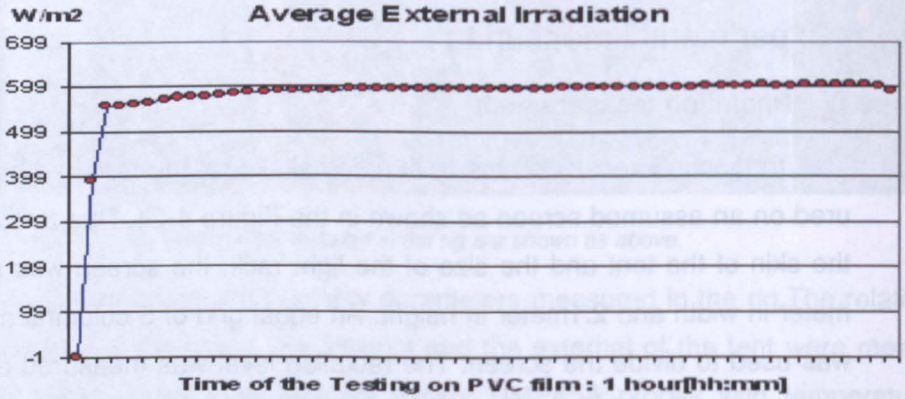

Figure 4-25: Examples of the total irradiation level measured at the centre of the front external skin of the tent.

The average irradiation intensity on the mid part of the external screen was 605.06 W/m² as shown in Figure 4-25 and the value decreased with the height over 1.6 meters. The average value was obtained around 20 minutes to 30 minutes ('warming up period' of the light source) after the lights were turned on.

4.4.2.2 Temperature measurements in the test rig

The experimental temperatures were measured over one hour period including around 30 minutes "warming-up period". Due to the size of the test tent, the test environment was hard to control strictly as required, especially creating a uniform external temperature in the laboratory surrounding the large

scale of a test rig like this tent. Therefore, according to the position of installation, the reading taken from the measuring equipment could vary because of their surrounding conditions, such as they were positioned closely to an auxiliary system in operation. However, this preliminary test targeted at obtaining a general impression of the overall thermal behaviour of an inflatable tent integrated with liquid cooling process. The data gathered from this test rig with a certain deviation on the external temperature set-up is acceptable and adequate for analytical discussion in later.

In order to avoid the direct incidence of direct radiation from the lamps, the readings of temperatures were taken in the shade. The graphic charts here representing temperatures of the internal, the external and the surface of different layer on the test rig had been generated directly from the DeLogger™ 4 Pro software on the PC.

In light of the surface temperature, one could expect a large variation of temperature between different areas of the foil skin roof resulting in a more heterogeneous internal thermal environment. One reason was that the topology of the structure and relatively high curvature of the enclosure roof caused the variation in tilt and effect of self-shaded areas on the roof, thus a greater contrast in surface temperatures was observed.

Figure 4-26 and Figure 4-27 indicated that the rapid effect of incident radiation on the surface temperature of the clear PVC films. About 7.1 ℃ temperature contrast between the front inner layer (Tsi) under direct radiation to the back with radiation in absence (T 'si) was observed. Meanwhile under the influence of the direct radiation the front outer and inner layers displays similar temperature as only less than 0.5 ℃ difference (Tso to Tsi) while about 4 ℃ deviation in surface temperature (T 'so to T 'si) for the layers at the rear two layers of the tent without direct radiation exposure.

This phenomenon confirmed further that in the absence of the short-wave radiation, the thermal balance of the outer foil skin was dominated by longwave radiation exchanges to the outside surrounding surface, such as the wall or ceiling in the laboratory. As a result of an additional inner layer separating the external layer by an air cavity, radiative heat gain of the external foil skin had been reduced largely from the internal space. A number of literatures (see Section 3.2.2 and Section 3.2.3) had reported this thermal behaviour

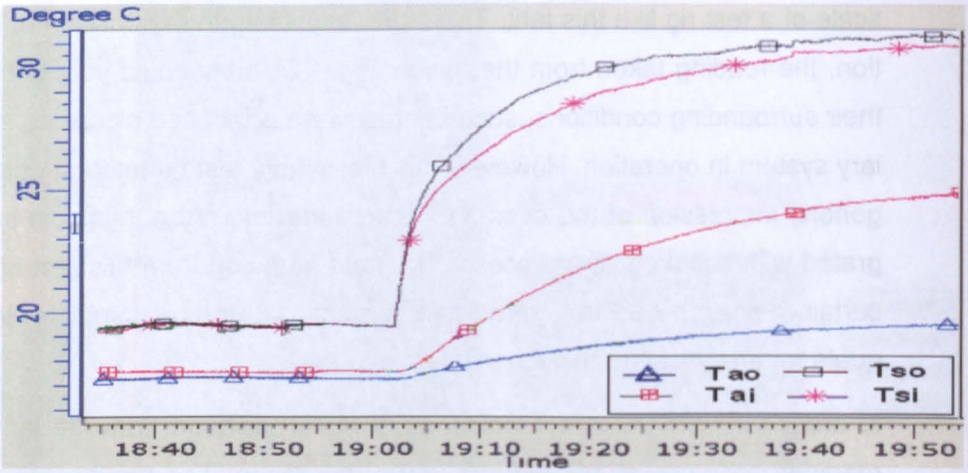

Figure 4-26: Examples of the measured the surface temperatures of the front skins (Tso, Tsi) and relevant internal and external air temepratures on the test rig. [NB. so=surface of outer layer, si=surface of inner layer]

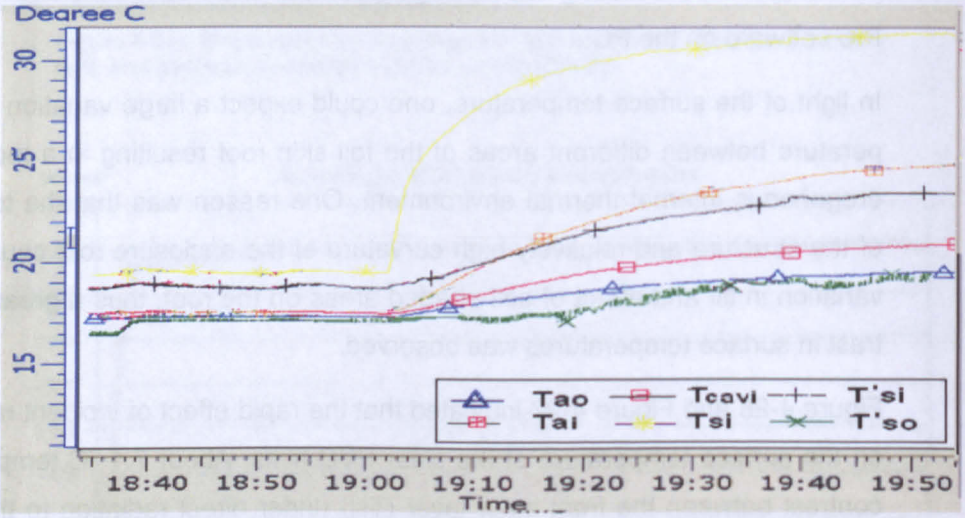

Figure 4-27: Examples of the measured the surface temperatures of the rear skins (T'so, T'si) and relevant internal and external air temepratures on the test rig.

The external temperature recorded by a thermometer in the foil shade next to the test rig in the testing time was around 19 ℃ while internal temperature was stable at 25 ℃.

The air temperature in the cavity was measured using 3 shielded HMP45 A probes along the vertical centre of the cavity. Figure 4-28 and Figure 4-29 exemplified the air temperature measured inside the cavity and average values for the test duration for two air supply modes. The air-blow-in-from-bottom mode is supplying air from a bottom sleeve at the external of the tent (Figure 4-15), and the air-blow-in-from-top mode supplies air from the ceiling sleeve from the internal of the tent (Figure 4-16).

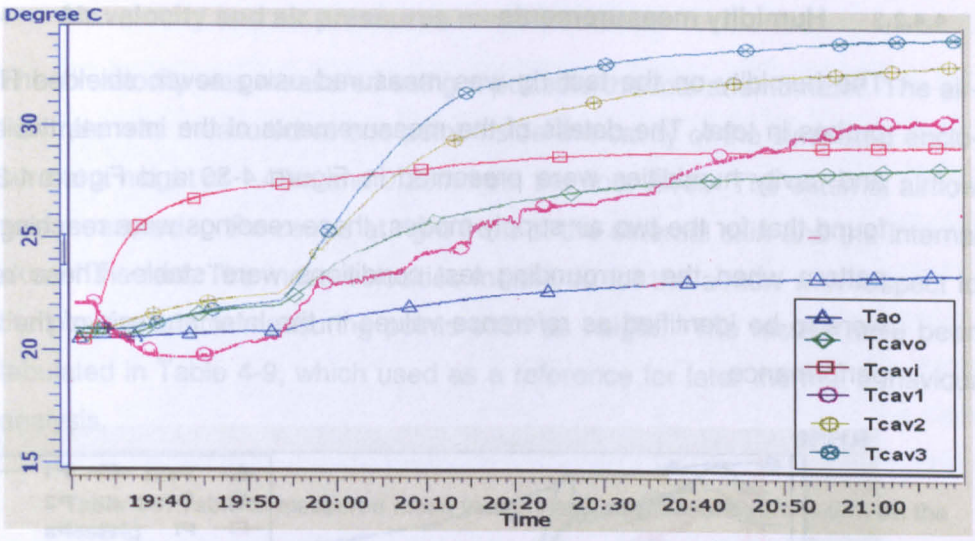

Figure 4-28: Examples of measured air tempeatures at the top, middle and bottom cavity (Tcav1, Tcav2, Tcav3) in the test rig using air blowing mode of air-blow-in-from-top. [NB. cavo=cavity outlet, cavi=cavity inlet, ao=air outside]

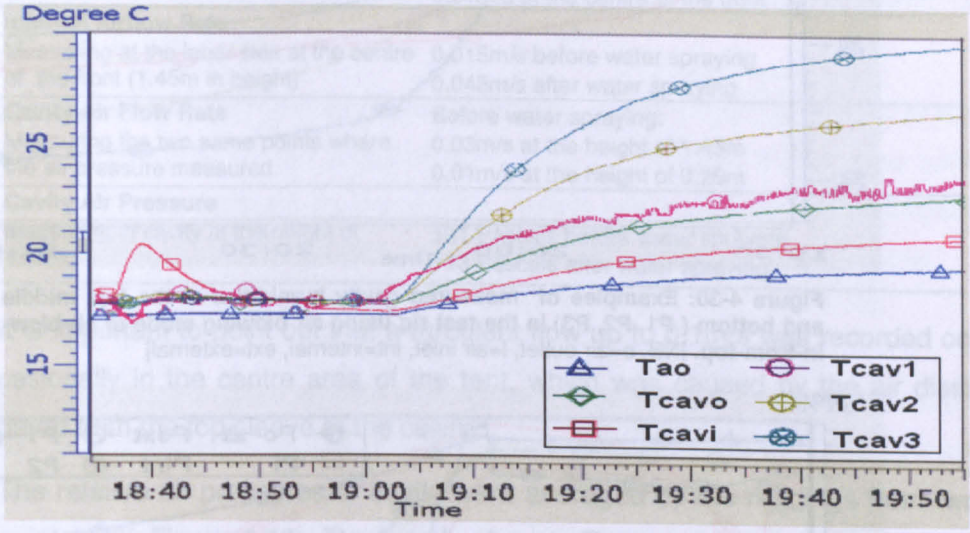

Figure 4-29: Examples of measured air tempeatures at the top, middle and bottom cavity (Tcav1, Tcav2, Tcav3) in the test rig using air blowing mode of air-blow-in-from-bottom

As seen in Figure 4-29 and Figure 4-29, the temperature readings from the measuring point (Tcav1) at the top of the cavity varied in the two cases accordingly. The adjustment in positions of the measuring points for Tcavi and Tcavo in these two air supply modes accounted for this discrepancy. To reiterate, the two types of the air supply were investigated with an intention to create different flow patterns and to observe their effect on the heat transfer process in the cavity of the foil skin envelope.

4.4.2.3 Humidity measurements

The humidity on the test rig was measured using seven shielded HMP45A probes in total. The details of the measurements of the internal, the external and cavity humidities were presented in Figure 4-30 and Figure 4-31. It is found that for the two air supply modes, these readings were reaching similar pattern when the surrounding test conditions were stable. These readings were to be identified as reference values in the later analysis of the thermal performance.

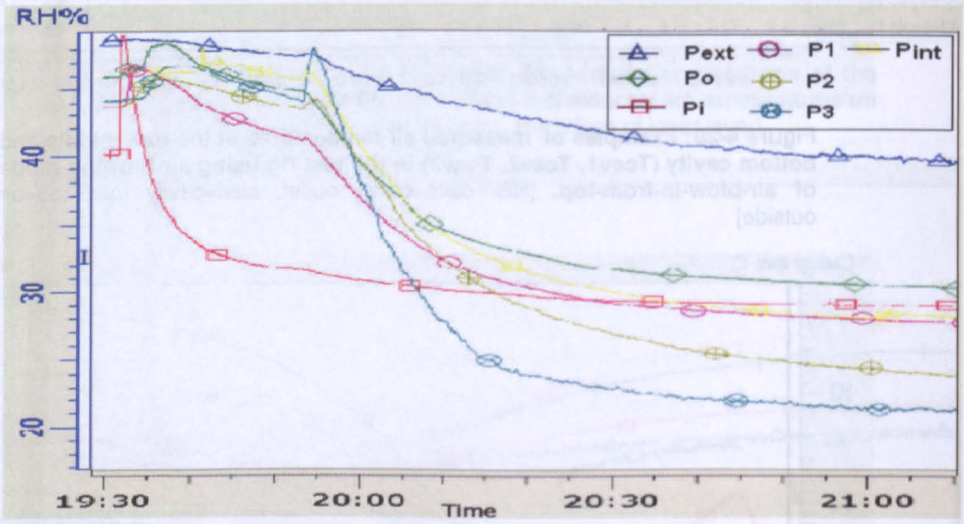

Figure 4-30: Examples of measured cavity humidities at the top, middle and bottom (P1, P2, P3) in the test rig using air blowing mode of air-blow-in-from-top. [NB. o=air outlet, i=air inlet, int=internal, ext=external]

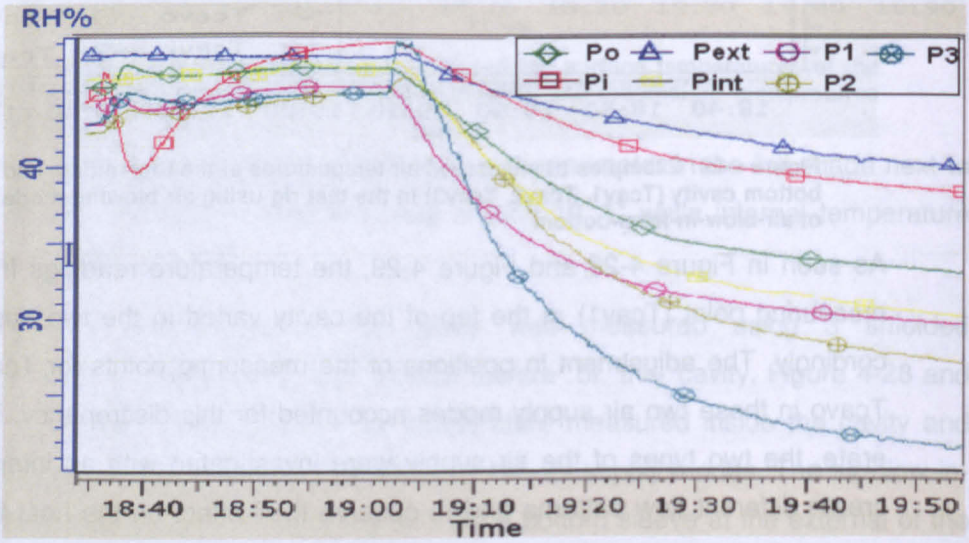

Figure 4-31: Examples of measured cavity humidities at the top, middle and bottom (P1, P2, P3) in the test rig using air blowing mode of air-blow-in-from-bottom

4.4.2.4 Air velocity and air pressures measurements

The air velocity was measured using a portable thermal anemometer. The airflow rate was measured at one point inside the cavity of the simulated enclosure at a height of 1.45m and 0.25m from the floor level. The external airflow was measured in the centre at right front of the external skin and the internal skin of the tent. The mean velocities measured for the airflow with respect to the position of the measuring points such as height. The results have been tabulated in Table 4-9, which used as a reference for later thermal behaviour analysis.

Table 4-9: Table of measured mean velocity and air pressure parameters on the test rig

Measured Data	Mean Values
External Airflow Rate	
Measuring at the outer skin at the height of 1.45m	0.033m/s at the centre of the back 0.01m/s at the centre of the front
Internal Airflow Rate	
Measuring at the inner skin at the centre of the front (1.45m in height)	0.015m/s before water spraying 0.045m/s after water spraying
Cavity Air Flow Rate	Before water spraying:
Measuring the two same points where the air pressure measured.	0.03m/s at the height of 1.45m 0.01m/s at the height of 0.25m
Cavity Air Pressure	
Measuring in cavity at the height of 1.45m	101 Pascals before water spraying 113 Pascals after water spraying

It is important to point out that a turbulent flow up to 0.1m/s was recorded occasionally in the centre area of the tent, which was caused by the air dissipated from the top sleeve of the ceiling.

The relative air pressures of cavity were averaged by the readings from two points (see Figure 4-23). The listed values in Table 4-9 were used as reference in this study.

4.5 Analysis of the Test Data and Discussion

The charts in this section represent measured temperature data smoothed using an average period of one minute. All numerical value given in a text format are based, however, on instant readings directly obtained from the Datalogger. The graphs were obtained from the Deloggoer software programme directly.

4.5.1 Overview of typical thermal behaviour patterns

4.5.1.1 Surface temperature

The surface temperature difference should be evaluated to identify the thermal function of the liquid cooling film in place. In Section 3.4 had argued that the addition of a water layer in a foil glazing system could enhance the heat transfer process on the external surface to shift towards the outside surroundings and then improve its thermal performance. Figure 4-32 and Figure 4-33 indicated the thermal impacts of a water layer on the foil skins.

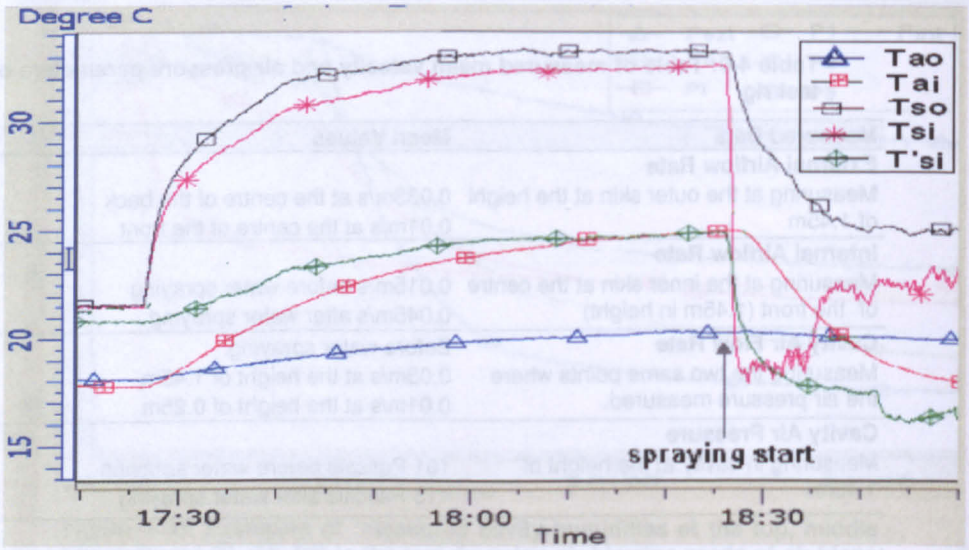

Figure 4-32: Examples of temperature behaviour of the tent at the front area (Tso, Tsi, Tai) before and after spraying in comparison. [NB: so=surface of outer layer, si=surface of inner layer]

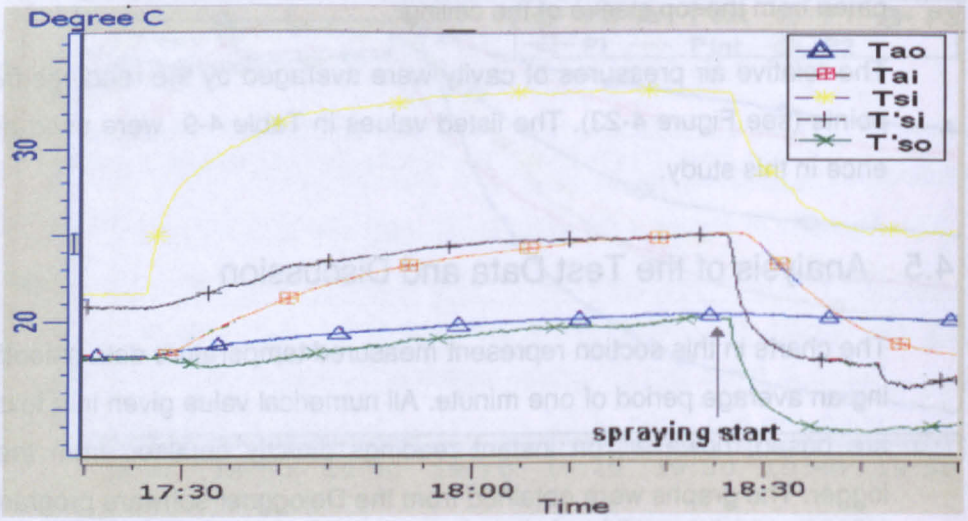

Figure 4-33: Examples of temperature behaviour of the tent at the rear area (T'so, T'si, Tai) before and after spraying in comparison

High thermal absorption of water coupling the PVC film could take on the heat from the surface without costing light penetration. Figure 4-32 shows that the internal surface temperature of the inner layer at the front (Tsi-B) rapidly responses to the water spreading and reaches the same 19 ℃ as that at the back (T 'si-B). Once the water layer reached a stable state, the Tsi gradually went up to average value of 22.5 ℃. As observed in the previous mini-test model, the light transmittance of the PVC film would be improved by a water-layer. The surface temperature (Tsi) therefore rose due to the increase of the radiation exposure. The finding was evident and further confirmed the high thermal responsiveness of the surface temperature of a foil skin to the radiative heat transfer in a high light irradiation condition.

It is important to note that the surface temperature variation between T si (internal surface temperature at the front of the tent) and T 'si (surface temperature at the back) was still large at an average of 4.5 ℃ after water spraying 15 minutes (Figure 4-32).

It was clear that both the surface temperature difference of Tso to Tsi at the front of tent (Figure 4-32) and that of T 'so to T 'si (Figure 4-33) at the back were relatively enlarged by introducing chilling water process, and therefore the internal climate was implicitly isolated from external condition variations.

4.5.1.2 Internal air temperature distribution

The temperature distribution in the simulated enclosure was of particular interest for the evaluation of the internal thermal comfort and, as a result, for the prediction of the energy required to maintain this specified level of occupant comfort. The temperature sensors were installed to investigate both the horizontal and vertical temperature stratification, which was identified as potentially having the greatest impact on the occupants' perception of the internal environment as well as the assessment of the environment design strategies implementation.

It was possible to identify two specific patterns in the thermal behaviour of the inflatable tent before and after water spraying, based on the same external radiation condition. One was the uniform internal temperature distribution; the other was the vertical thermal stratification pattern.

Once the water sprayer is in operation, the water droplet in contact the PVC film surface forms drop-wise or film-wise water coverate. The observation in

this test showed that the formation of the sprayed water on the film surface were largely drop shape as displayed in Figure 4-34.

Figure 4-34: Photos of the formation of water drops on the PVC foil surface.

The drop-wise water-layer provided adequate an amount of shading to the clear skin dome. The irradiation level behind the front internal skin was reduced by nearly 40%, at an average magnitude of 104 W/m^2, which was confirmed by previous literature. Under such reduced level of radiation, the foil skin enclosure thus demonstrated typically a stable internal thermal environment and relatively uniform temperature distribution.

Following water spraying, the membrane surface maintained a stable temperature, usually close to the average temperature of the water layer at about 16 °C. As a result of the reduced external solar heat gains into the enclosures and low surface temperatures of the foil skin, the vertical temperature stratification was weaker around the area closing to the internal enclosure skin through the test period, generating an almost uniform air temperature field (such as Tai-B and T 'ai-B). The typical thermal behaviour observed under reduced irradiation conditions and water spraying is illustrated in Figure 4-35.

During the period of exposing to high radiation such as before water spraying, large swings in the membrane surface temperature relative to surrounding air temperatures were observed (Figure 4-35, bottom diagram). The strong variations inside of the enclosure resulted in strong positive stratification, which is an asset for passive-cooled buildings (Cf. Section 3.3.2 and 3.3.3).

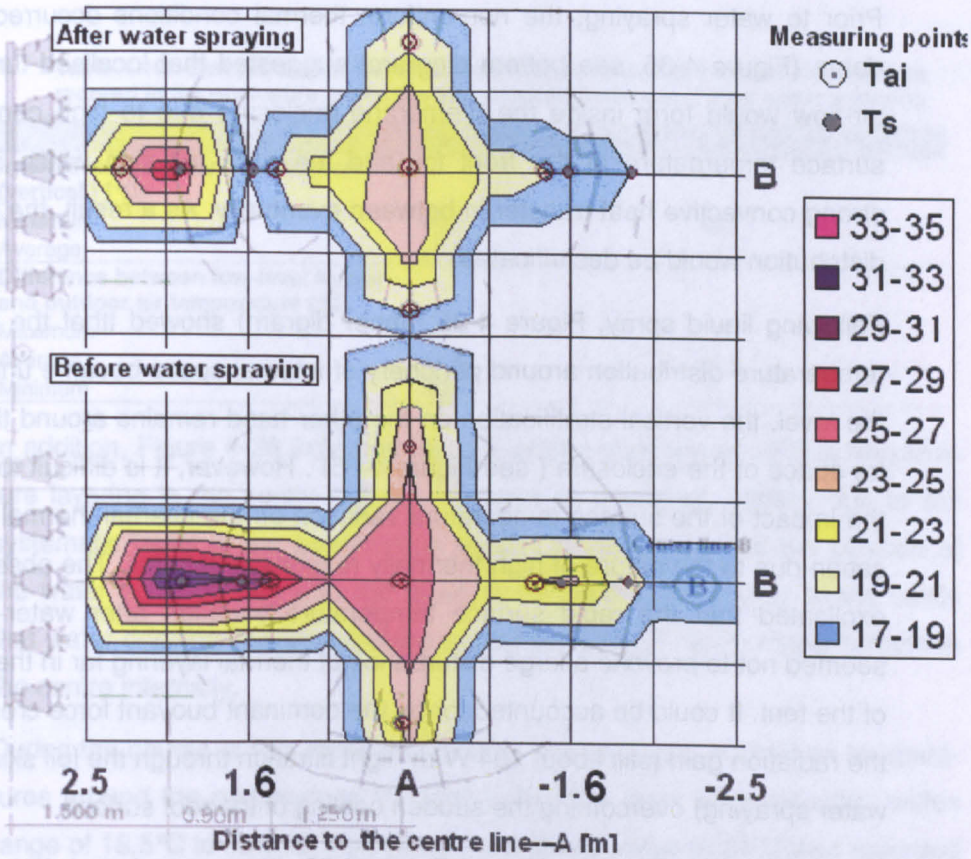

Figure 4-35: Internal temperature distribution before and after water spraying (measured at the vertical height of 1.45 m)

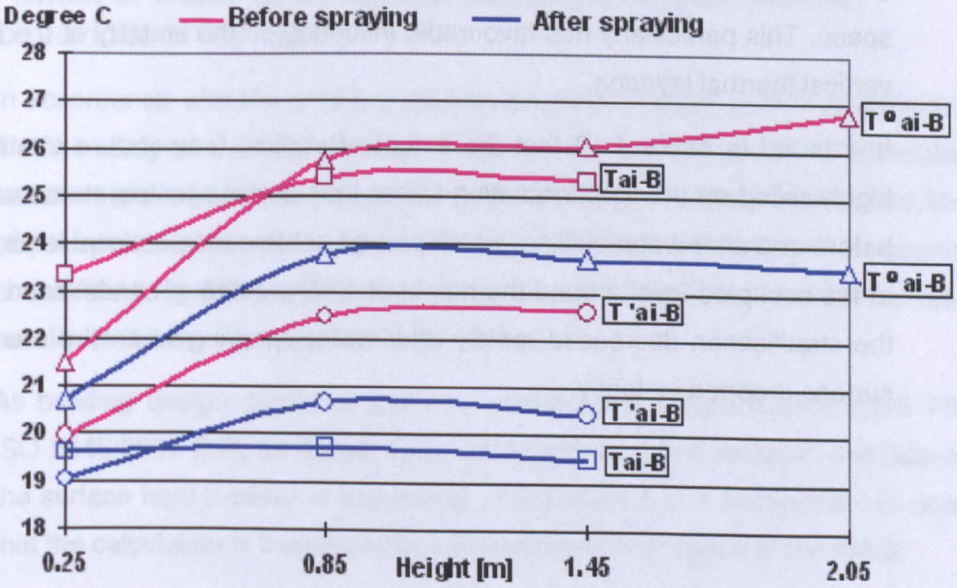

Figure 4-36: Evolution of the internal temperature stratification before and after water spraying. [NB. Air-temperature measured along the reference central line-B at the front, the centre and the back area in the tent: Tai, T^0ai, T'ai]

Prior to water spraying, the non-uniform thermal conditions occurred in the dome (Figure 4-35, see bottom diagram) suggested that localised turbulenct air-flow would form inside the membrane enclosure due to high contrasting surface temerpature at the front foil and the back foil skin which induced strong convective heat transfer in between eventually. As a result, the thermal distribution would be desitrificated.

Following liquid spray, Figure 4-35 (upper digram) showed tthat the internal temperature distribution around periphery of internal space became uniform at the level, the vertical stratification on the other hand remains around the centre space of the enclosure (see Figure 4-36) . However, it is difficult to isolate the impact of the surface temperature variation on the internal thermal stratification due to the nature of high thermally responsive thin foil. The observation explicated that the rapid surface temperature variation after water-cooling seemed not to provoke a large disturbance of thermal layering far in the centre of the tent. It could be accounted for by the dominant buoyant force created by the radiation gain (still about 104 W/m^2 light filtration through the foil skins after water spraying) overcoming the sudden cooling of the roof surface.

As seen in both Figure 4-35 and Figure 4-36, it was concluded that surface temperature contrast between the front and the back areas inside the enclosure had markedly been reduced and so had the thermal asymmetric and heterogeneous air temperature distribution in horizontal direction at the low-level space. This particularly has favourable influence on the stability of the internal vertical thermal layering.

It is found in Table 4-10 that the extent of vertical temperature stratification highly relied on the light irradiation rather than surface temperatures variation before and after water chilling, which proved not to cause noticeable air mixing at the occupied level around the height of 1.45m. Although it remained stable, the stratification decreased rapidly after water spraying when the membrane surface dropped instantly.

Table 4-10: Comparison of extreme stratification and relatie indoor temperature recored in the enclosure under the test condtion before and after water spraying

	Before water spraying	After water spraying
Internal temperature stratification (vertical) [℃]		
Maximum	+5.2	+3.2
Average	+3.5	+1.1
Difference between low-level indoor and outdoor air temperature [℃]		
Maximum	+5	+3
Average	+3.5	+1.5
Minimum	-0.5	-1

In addition, Figure 4-36 indicated that the strong variation of vertical temperature layering in the centre did not occurred as expected, patially due to the systematic faults of the construction design. It suggested that the position of the water spraying ring was too close to the central top ceiling in the cavity that water dripping had effected the air temperature (T^{0}ai-B) measurement in the centre internally.

During the course of two consecutive days, the averaged internal air temperatures around the periphery of the tent at the low level were recorded within range of 18.5℃ to 19.5℃. Meanwhile an average value of 23℃ was recorded in the centre area when external thermal condition were at an average temperature of 20.5℃ and average humidity of about 39.5% to 40%.

4.5.2 Effect of water spraying and airflow pattern on thermal behaviour of test rig

In accordance with the previous discussion (see Chapter 3), it is appropriate that the study on the heat transfer variation of the foil skin should focus on the radiation and convection force around the building boundary layers. The important parameters relating to this thermal behaviour analysis had measured and validated in the experiments and detailed in Table 4-11, to which the discussion in the later chapter could be referred.

As building design guide for wall/roof assessment, British Standard BS EN ISO 6946:2007 [89], an approximate treatment for a conservative analysis of the surface heat transfer is expressed as Equation 4-2. It is important to note that the calculation is based on the assumption of over cast sky condtions.

At external and internal surfaces, well-ventilated air layer

$h_{tot} = h_a + h_r$

$h_r = \varepsilon_j h_{r0}, \quad j=i, o$

$h_{r0} = 4\partial T_m^3$

$$h_a = h_{ai} \text{ or } h_{ao}, \text{ where } h_{ai} = \begin{cases} 5.0 & \text{if upwards heat flow} \\ 2.5 & \text{if horizontal heat flow} \\ 0.7 & \text{if downwards heat flow} \end{cases}$$

$$h_{ao} = 4 + 4v$$

At unventilated airspace (cavity space)

$h_{rca} = Eh_{r0}$

$$E = \frac{1}{\frac{1}{\varepsilon i} + \frac{1}{\varepsilon o} - 1}$$

$$h_{aca} = \begin{cases} 1.14 \times (\Delta T)^{1/3} & \text{if upwards heat flow} \\ 0.73 \times (\Delta T)^{1/3} & \text{if horizontal heat flow} \\ 0.09 \times (\Delta T)^{0.187} \times \theta^{-0.44} & \text{if downwards heat flow} \\ \text{or } \frac{0.025}{\theta}, & \theta \text{ is thickness of airspace} \end{cases}$$

ε	*Hemispherical emissivity of the surface*
h_r	*Radiative coefficient [W.m^{-2}·K^{-1}]*
h_a	*Convective coefficient [W.m^{-2}·K], o: external surface; i: internal surface*
T_m	*Mean thermodynamic temperature of the surface and of its surroundings air temperature [K]*
h_{r0}	*Radiative coefficient for a black-body [W.m^{-2}·K]*

Equation 4-2: Calculation of the surface heat transfer on the foil skins [89]

Table 4-11: Table of parameters in the heat transfer analysis

Symbol	Values
Surface Thermal Emissivity	
Water (0.2-0.3mm): ε_w	0.97
PVC layer (outer/inner,0.5mm): $\varepsilon_0 = \varepsilon_i$	0.62
Short-wave Optical Properties	
double-layer PVC (near normal) :	
τ @ the centre front of the external skin at the dry state	0.779
Measured Intensity of Irradiation	
I_0 @ the centre of outer skin at the front of the tent	608.9 W/m^2
I_i @ behind the centre of inner skin at the front	
• before water spraying	173.5 W/m^2
• after water spraying: $I_{i\text{-}w}$	*105.1 W/m^2
Measured Average Temperature	
Water : T_w @ the water tap	11.5 °C
T_w @ the water collector	16.5 °C

Notes:

**: This value was based on the assumption of 40% reduction in light irradiation according to the I. Pollet's research (Cf. Section 3.4.2.2).*

To be noted, the calculation is based on the assumption of over cast sky condition that the effect of the short-wave radiation has been ignored. It is a principle that the radiative heat exchange between two surfaces does not rely on an intermediate fluid and hence it is instantaneous and independent of any flow pattern generated in between.

The examples of calculation results are visualised in Figure 4-37 and Figure 4-38, which considering the effect of the airflow pattern on the surface heat transfer.

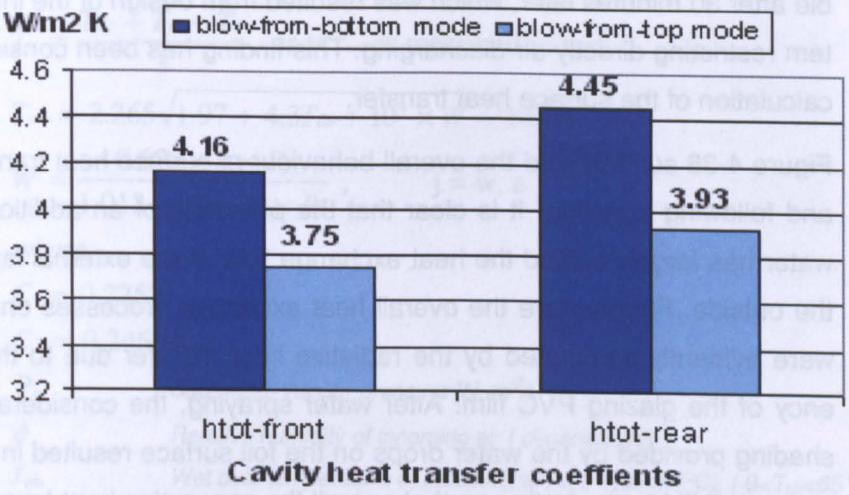

Figure 4-37: Total heat transfer level (h_{tot}) in the cavity of the foil skin enclosure

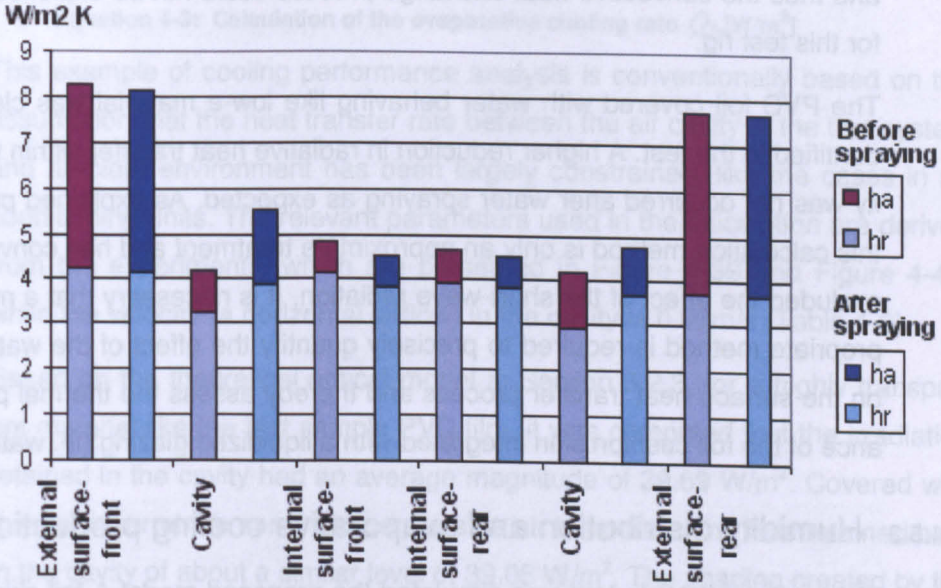

Figure 4-38: Overview of the surface heat tranfer evolution before and after water spraying for the air-blow-in-from-bottom mode

It was found in Figure 4-38 that the different air blowing modes creating airflow patterns seemed to affect the heat transfer rate more in the cold side cavity at the rear of the tent. And the upward air flow pattern generated by the air-blow-in-from-bottom mode marginally increased the surface heat exchange within the air space by more than 11% compared with the other air blow mode.

Based on the observation in airflow measuring position, the upwards air flow had formed steadily during the testing period. Whereas the downward air flow pattern changed to horizontal air flow once the experiment condition was stable after 30 minutes later, which was resulted from design of the inflatable system restricting directly air discharging. This finding has been considered in the calculation of the surface heat transfer.

Figure 4-38 summarized the overall behaviour of surface heat transfer prior to and following spraying. It is clear that the presence of an additional layer of water has largely shifted the heat exchange flow of the external layer towards the outside. Furthermore the overall heat exchange processes on the test rig were evidently dominated by the radiative heat transfer due to the transparency of the glazing PVC film. After water spraying, the considerable level of shading provided by the water drops on the foil surface resulted in decreasing amount of light penetration so that overall the convective heat transfer component had increased slightly, particularly in the front cavity. However due to the restriction of the system design, only about 0.03m/s airflow rate was reached and thus the convective heat exchange process could not be exploited further for this test rig.

The PVC foil covered with water behaving like low-e material was clearly indentified in the test. A higher reduction in radiative heat transfer within the cavity was not occurred after water spraying as expected. As explained previous, this calculation method is only an approximate treatment and has conveniently excluded the effect of the short-wave radiation. It is necessary that a more appropriate method is required to precisely quantify the effect of the water layer on the surface heat transfer process and thereby assess the thermal performance of the foil cushion skin integrated with a liquidized glazing (ie. water).

4.5.3 Humidity distribution and evaporative cooling production

The tested inflatable tent was simulated the proposed model-A foil skin enclosure using the direct evaporative cooling mechanism. The heat taken away by the evaporative cooling process in this test rig could be analysed by a conservative simplified method expressed as follows [90]:

$$Q_e = (C_1 + C_2 \times v_{ca})(P_w - \phi P_a)^{0.82}$$

$$P_w = 3385.5 \times e^{0.97608\sqrt{Tw+42.067}-8.0929}$$

$$P_a = 3385.5 \times e^{0.97608\sqrt{Tdb+42.067}-8.0929}$$

$$T_w = \frac{T_{wb} + T_{ai} + T_o}{3}, \text{ or } = T_{ws} \text{ as measured in test}$$

$$T_{wb} = 2.265\sqrt{1.97 + 4.3T_{db} + 10^4 \times W} - 14.85$$

$$W = \frac{0.622 \times \phi \times P_j}{1.013 \times 10^5 - \phi \times P_j}, \qquad j = w, a$$

where

$C_1 = 0.2253$

$C_2 = 0.24644$

P_j	*Saturated vapour pressure [N. m^{-2}]*
ϕ	*Relative humidity of incoming air [dimensionles]*
T_{wb}	*Wet bulb temperature of incoming air in a system [℃], (0<T_{ab}<65 ℃)*
T_{db} , T_o	*Air dry bulb temperature of incoming air and exhaust air [℃]*
T_{ai} , T_{ws}	*Indoor air-temperature behind inner skin, wet surface temperature [℃]*
Vca	*Air flow rate in cavity [m.s^{-1}]*
W	*Moisture content [Kg. Kg^{-1}]*

Equation 4-3: Calculation of the evaporative cooling rate Q_e [W/m^2]

This example of cooling performance analysis is conventionally based on the assumption that the heat transfer rate between the air cavity in the test system and ambient environment has been largely constrained, like the cases in air conditioning units. The relevant parameters used in the calculation are derived from the experiments, which are presented in Figure 4-39 and Figure 4-40, while the velocity (a horizontal airflow) in the cavity is 0.03m/s (Table 4-9).

Based on the theoretical optical model in Section 3.2.3, for a highly transparent material like the test sample PVC film, it was computed that the irradiation retained in the cavity had an average magnitude of 39.69 W/m^2. Covered with a water layer at the same temperature as air temperate, the foils retained heat in the cavity of about a similar level of 39.05 W/m^2. The shading created by the water droplets on the PVC foil was identified by the overall reflectance of this construction increasing from 10% to 30%. The resultant large reduction of the internal irradiation level of the enclosed place caused a noticible drop of internal air temperature (Tai from average 25 ℃ down to 21 ℃).

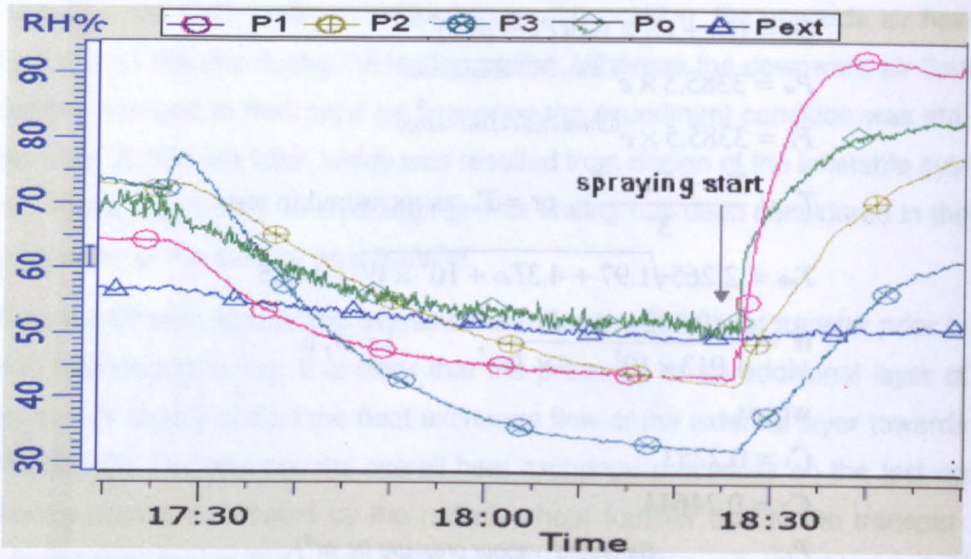

Figure 4-39: Measured humidity vertical distribution in cavity from the top, middle and bottom (P1, P2, P3) when spraying water

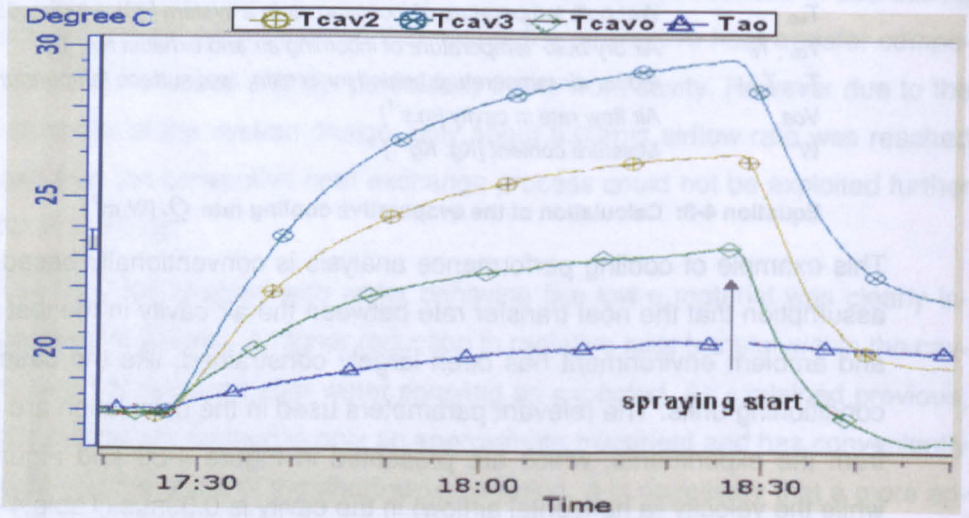

Figure 4-40: Measured vertical temperature distribution cavity from the middle and bottom (Tcav2, Tcav3) when spraying water

Table 4-12: Examples of calculation results of the propsed double-layer foil skin construction integrated evaporative cooling process.

Parameters	Cavity Inlet	Cavity Outlet Before spraying	Cavity Outlet After spraying
Temperature Tdb [℃]	20.5	23.4	17.1
Relative Humidity Ø [%]	50	51	83
Moisture Content W [Kg/Kg]	0.00720	0.00885	0.00976
Cooling Rate Q_e [W/m2] *	Q_e=51.962 @ retained heat flow rate in cavity with a water-layer=39.05M/m^2		

Notes:

**: This analysis was based on thermal condition after the water spraying:*
Vca (mean cavity velocity)=0.03m/s; Tai (measured behind the front inner skin)=21℃

Table 4-12 shows that the evaporative cooling rate is able not only to remove the retained heat in the envelope but also to extract heat from indoor splace under the measured testing conditions. However, it is important to note that the heat retained within the cavity is proportional to the received radiation intensity and ambient temperature whereas the evaporative cooling rate is in an inversely proportional relationship at the same air humidity (refers to Equation 4-3). Therefore, the evaporative cooling performance of this system at such low flow rate (0.03m/s) in the cavity is decreasing when the external environment is hotter, except for an increase in airflow rate. Tang, R. et al [90] pointed out that high air flow rate was a determiming factor for improving evaporative cooling performance on a free water surface (the similar case to the type of water layer genertated on this testrig), particularly more than 1.16 m/s at which a high forced evaporation is effectively developed. It is implied that the design of such a system should be considering the possibility of adjustable air velocity in the air space, which allowed the system to actively respond to the external energy input.

4.5.4 Surface condensation risk

As the relative humidity and temperature of the external and internal air were recorded in this test, it was possible to calculate the dew point of the indoor air, representing the temperature at which moisture would condense into liquid droplets. An empirical method was expressed as follows:

$$T_{dp} = 26.13722 + 16.988833 \times a + 1.04961 \times a^2$$

$$a = \ln(\phi \times P_a)$$

$$P_a = e^{0.97608\sqrt{Tdb+42.067}-8.0929}$$

P_a	*Saturation vapour pressure of the internal air [N/m²]*
ϕ	*Relative humidity of indoor air [dimensionles]*
T_{db}	*Air dry bulb temperature of indoor air [℃]*
T_{dp}	*Dew point temperature [℃]*

Equation 4-4: calculation of the dew point of the internal air [90]

If the surface temperature of the membrane roof drops below this dew point temperature T_{dp}, surface condensation would occur on the foil skin. Because the internal air temperature was observed high above outdoor air, and assuming the water content of the internal air was at least as high as that of the external air, simple psychrometric relationships indicated that the dew point of the internal air would be equal to or higher than that of the external air. This, in

turn, implicated that internal surface condensation would occur every time the foil surface temperature dropped below the dew point of the external air.

The average surface temperature of the test foil covered with water (directly from water mains, at 11.5℃) was recorded of16.5℃, which was lower than the dew-point temperature if internal air temperature is higher than 27℃ according to the calculation. The occurrence of the internal air temperature over 27℃ was recorded, particularly high in the internal front area under the light irradiation in this test (see Figure 4-35 and Figure 4-36). The high condensation occurrence of this double-layer foil skin construction was pronounced when low temperature water spraying process started.

It could be assumed that the risk decreased significantly following light source provision, as depicted in Figure 4-32, the surface temperature sharply increase from 17 ℃ to 22.5 ℃ when light exposure increased. However the scale of the enclosure and topology of the structure resulted in self-shading on a large area of the roof, which discouraged such risk decrement.

Although this simple analysis neglected a number of parameters in the evaluation of the surface condensation risk (such as moisture distribution in the enclosure and sensible heat losses/gains from the membrane during evaporation/condensation), it nevertheless highlights typical patterns of potential occurrence.

4.5.5 Impact on thermal comfort

The data measured during this test were compared with the original thermal comfort target of a dry resultant temperature at occupied level without artificial air conditioning: 13°C (for sports activities), or 18°C (for sedentary activities) for wintertime and 28°C (set to maxium 3°C above the outdoor air temperature, i.e.25 °C in this study) for summertime [91]. These target temperature based on a dry resultant termperature was set at the environmental design stage because the frequent experience of high internal surface temperature as well as surface temperature constract (Cf. Section 4.4.2.2 and Section 4.5.1) justified themal comfort estimation only relying on air temperature was inappropriate for this particular foil skin construction.

NB. A foil skin enclosure with large span is common built for multi-purpose centre or hall involving a large variation of activities. The target comfort temperature could be more influenced by the building users who tend to actively

adapt better to more extreme condition, hence the design condtions for such naturally ventilated buildings are often less rigid than for those that are fully air-conditioned.

As the dry resultant temperature conveniently combines air and mean radiant temperatures in a single index temperature, for engineering analysis ISO and ASHRAE standards have commonly adopted the dry resultant temperature as the operative temperature, a thermal index for moderate environments (low air velocity, no heat or cold stress). The index is defined as:

$$T_c = \frac{T_{ai}\sqrt{10v} + T_r}{1 + \sqrt{10v}}$$

T_{ai}	*Indoor mean air temperature [°C]*
T_r	*Mean radiant temperature [°C]*
V	*Air velocity [m.s^{-1}]*

Equation 4-5: Dry resultant temperature [76]

An approximate calculation on the dry-resultant temperature experienced in the centre tent of the occupied area could be made by assuming the airflow rate at this area below 0.1 m/s, the situation in this test for instance. In a realistic condition, this assumption considered the situation where no mechanical ventilation was installed and that the natural ventilation was likely to be maintained to a minimum during winter months. In these conditions, the simplified approximation of the dry-resultant temperature can be calculated as follows [76]:

$$T_c = 0.5T_{ai} + 0.5T_r$$
$$T_r = \sum_i V_{F_i} T_{S_i}$$

T_{ai}	*Internal air temperature at occupied area [°C]*
T_r	*Mean radiant temperature experienced at the centre of the tent [°C]*
V_{Fi}	*View factor of surface i [dimensionless]*
T_{si}	*Surface temperature of inner foil layer from in door [°C]*

Equation 4-6: Approximate calculation of dry-resultant temperature for low air velocities indoor and the estimated mean radiant temperature at the centre area

As expressed above, the mean radiant temperature can be derived from the view angle of internal surfaces and from their temperatures. It indicated that the effect of surface temperature contrast on the foil skin roof would be experienced by the occupants as a deviation of the mean radiant temperature from the air temperature. The calculation results are presented in Table 4-13:

Table 4-13: Examples of calcuation results of dry resutant temperature

Parameters	Values Before water spraying	Values After water spraying
Tai [℃]		
@ internal centre of the tent	25	23
T si [℃]		
@ internal front area At centre with V_F =35%	32.5	22.5
@ internal rear area At centre With V_F =61%	25	16.5
T r [℃]		
@ facing internal front area	28.12	21.2
@ facing internal rear area	25	19.03
T c [℃]		
@ internal centre of the tent	25.78	21.56

It has been agreed in literature that, for the high radiation as 600W/m^2, the target temperature 28℃ was systematically reached during most time of the exposure without any cooling input. Thermal discomfort may have been experienced most hours of the operation of the building, particularly early morning between 8am and 10am. Water spraying process as described above is an effective approach to improve rapidly the thermal comfort in the enclosed space.

4.5.5.1 Effect of foil skin temperature on thermal comfort of occupants

As previously discussed, the asymmetric radiant temperature was a fairly common experience in the thin foil skin enclosure (for instance referring to detail in Table 4-13). It is proved that the two typical characteristic of a foil skin enclosure accentuate the impact of surface temperatures on the mean radiant temperatures and thus the comfort level experienced by the occupants. One is the thermally "heavier" floor and intermediate structures which tend to stabilize the air temperature at the low level and reduce the effect of the surface temperature variation. The other is the relatively large view factor to the foil skin roof compared with conventional glazing building, which results in the internal dry resultant temperature more sensitive to the variation of surface temperature on the foil skin roof.

The air thermal layering was proven in this study to be largely influenced by the internal surface temperature contrast between the lightweight membrane skin and the thermally heavier internal surfaces of the enclosure. High solar radiation tends to enhance the thermal stratification in positive direction, which is a particular asset for cooling purpose. Internal buoyancy force driven by the

solar gain or other internal heat gain coinciding with the positive thermal layering provokes strong natural ventilation to remove internal excess heat.

Environmental design, CIBSE Guide A, recommends that less than 2.8℃ radiant temperature asymmetry could be in vertical direction while less than 5.56℃ would be for horizontal direction [76]. Thus, itl is implying that occupants would in general be more sensitive to a warm ceiling than to a cool wall.

Recorded data showed that the internal surface temperature was on average 7℃ above the low-level air temperatures, which was generally to be affected more directly by external air temperature. The surface temperature ranges measured in this thesis were limited to laboratory test, so that they are not necessarily representative of those experienced during real hot summer. This range however could be extrapolated using the numerical model which described in later chapter.

The irradiation from the solar simulator transmitted through the foil skin roof was measured in the region of 104W/m². Under such high exposure of radiation, the effect of radiative gains on occupants would therefore be dominated by transmitted solar radiation rather than by long-wave radiation from the warm membrane itself. Coupling with the high foil surface temperature, the sensation of discomfort experienced by the building users would however increase. Although, after the water spraying, the sharp drop of surface temperatures would not significantly affect air temperatures of the occupied space at low level to fall below the target temperature, the effect of the radiant cooling created by the water flow could compensate this potential discomfort by high radiation exposure experienced by the occupants to some extent.

4.5.6 Influences of air and water leakage on measurements

Neither air/water leakage nor devices operations could be precisely measured during the course of the testing period. It is however important to assess the potential effect these parameters may have had on the accuracy of the collected data.

The turbulent airflow generated by the mechanical fan was proved not affecting the external and internal condition based on the test recording. Considering the air leakage of the inflatable foil skin tent, these variables were considered unlikely to have a large impact on the internal air temperature measurements in comparison with the effect of the variation of external conditions.

It was possible to guess the operation of the air blower supplying air form the ceiling sleeve from inside dissipated a small part of the energy by convection through air duct. It was possible to identify the periods of operation from Tcav1 or T °ai-B, which was in the plume of warm air rising from the air funnel or right underneath of the water spraying. Under these circumstances, this temperature sensor was recording a temperature few degrees below or above the surrounding sensors.

As mentioned previously, the water spraying had effect the air temperature distribution as a mount of water leakage spilled on the floor of the tent. It could clearly be identified in the air temperature readings that internal air temperatures at the low level unexpected decrease in one or two degrees. But the high thermal mass of concrete floor had maintained a stable average temperature at the ground floor during the most course of the testing.

4.6 Conclusions and Recommendations

Besides a certain level of cooling provision, water cooling process integration would affect the thermal performance of a clear plastic foil glazing envelop in particular two ways (Cf. Chapter 3):

- To provide a higher quality of visible light at the cooler temperature. Some evidence of this aspect has been presented in this chapter.
- To promote internal natural ventilation driven by the buoyancy force.

As highlighted in Chapter 3, reducing the heat loads from the envelope and the cavity while promoting the heat removal from the enclosure were ideal measures to restrain the development of overheating under critical conditions. The water spraying integrated in the cavity of the foil cushion envelope was found to reduce the temperature of the cavity, perform the heat extraction from the internal space to some extent and consequently the quantity of heat gain that received by the enclosed space decreased. It has proved that coupled with the convective force in the cavity, the evaporative cooling can be an advantageous method to reduce overheating resources like a hot envelope, and perform heat extraction from the internal space. However due to the inherent restriction of the test rig tested in this chapter, the latter aspect has not been exploited further so that it is to be considered in the next test rig construction.

An effective reduction of internal air temperature was observed when water spraying was in operation combined with a constant air-flow inside the cavity, in particular on the periphery area close to the internal foil skin. As such, the internal air temperature distribution seemed to be more uniforom as surface temperature contrast of foils decreased in the vicinity of the internal foil layer, and so did subsequently the asymmetry of the radiant temperature and air temperature attenuated in horizontal direction at the occupied level. Therefore the sensation of thermal comfort was improved.

Under the critical radiation in this test, a strong vertical temperature stratification was expected to remain in the centre area following water spraying as the extent of this positive thermal stratification was mainly relying on direct solar radiation gain. The radiant temperature asymmetry in the test tent had been expounded to be weakened by the water cooling process. It implicated that the reduced magnitude of horizontal thermal heterogeneity provoked stabilization of the vertical temperature distribution in the centre of the occupied area. Natural ventilation driven by the buoyancy force therefore could be better formed to remove internal cumulative heat and improve internal thermal comfort.

This assessment has illustrated that some of the main characteristics concerning the thermal environment control of the novel foil cushion enclosure are as follows:

- Plastic cladding foil combined with a water layer behaves like low-e glazing material with better thermal properties.
- Thermal behaviour of triple-layer PE foil construction is mainly dependent on the property of the inter-layer covered with water, as the PE film is nearly transparent to the longwave thermal radiation.
- Under critical irradiation intensity (550-600W/m2), the radiation heat transfer process was dominant on the test rig. The internal radiative heat gain was found essentially from the short-wave radiation infiltration rather than the long-wave radiation from the warm foil skin itself. Hence the air temperature distribution was positively strengthened.
- Meanwhile it was found that the internal air temperature at low level was unlikely to be affected by such radiative heat gain and it was more influenced by the external air temperature.

- Internal thermal environment is heterogeneous, which remains positive and strong in vertical axis of the tent following spraying. It was enhanced further by high solar irradiation, by which the discomfort caused can be compensated by the radiant cooling provided by the cooled surface of the roof and natural ventilation driven by the buoyancy force or assisted by the displacement ventilation strategy. The thermal assessment for this typical environment adopted the dry resultant temperature as a thermal indiex.
- Thermal performance of the double-layer foil cushion envelope can be regulated effectively by water spraying, but the risk of the surface condensation has proved to be unacceptably high.

In light of the construction and design of the test rig, a recommendation based on findings from the preliminary study is pertaining to the improvement on the generation of controlled airflow both in the cavity of the envelope and internal environment. As a result, the effect of both evaporative cooling and buoyancy cooling could be exploited more efficiently.

It is concluded that the foil cushion construction integrating with the water cooling process has played an important role to stabilise the positive air thermal layering by reducing the asymmetry of the horizontal air temperature distribution at the low level. Coupled with the stabilization effect of the thermally inert floor, this integration system promises to enhance the vertical air temperature distribution and in turn the nature ventilation driven by the buoyancy effect. Due to the restrictions of a fully enclosed environment on this preliminary test rig, a further assessment on the impact of the buoyancy force and air displacement ventilation on the internal thermal behaviour is necessary.

The findings obtained from the series of experiments presented in this chapter are still too limited to provide information that can be extrapolated to a general case. Before proceeding the analytic modelling of the thermal behaviour of novel foil cushion envelopes, it was required that further investigation and improvement, considering some aspects highlighted above, into the thermal behaviour of a multi-skin such as triple-skin foil construction should be undertaken in a more controlled environment. The protocol and results of these experimental measurements are presented in the following chapter.

CHAPTER 5
NOVEL SYSTEM COMMISSIONING AND TESTING --- TRIPLE-LAYER FOIL CUSHION CONSTRUCTION

> *"Creativity is just connecting things...to connect experiences...and synthesize new things."*
> --- **Steve jobs (1955-2011)**

5.1 Introduction

Chapter 4 highlighted the facts that beneficial effects of the water cooling process on the internal thermal environment were observed inside the double layer foil cushion enclosure. In view of the heterogeneous air temperature distribution observed in the double-layer construction test rig with or without a water cooling process integration, it is necessary to further identify such effect invovling the triple layer foil skin construction may have had on the overall performance of the novel glazing system as followed the proposal in Section 2.4,

Because of the construction limitation of the double-layer foil skin enclosure, it was difficult to ascertain the relationship between the various airflow rate and its thermal improvement on the enclosed space once the water cooling process integrated. This relationship was further blurred by the shading provided by the drop-wise water coverage on the foil surface, which resulted in a sudden drop in the light irradiation and consequently the overall internal air temperature of the enclosure.

With consideration of above facts, an improved provision of air flow for surplus heat removal and better cooling production was contemplated particularly in the case of the concept model-B foil envelope (triple-layer model), with uniformly spread water film generated on the centre layer of the novel glazing system.

A test rig was constructed by an ADPE foil in the laboratory of the Department of Architecture and Built Environment to simulate the model-B foil cushion construction and test under similar simulated weather conditions to that in the preliminary tests in Chapter 4, for convenient comparative analysis later.

This chapter describes the design of the novel construction and testing protoco, followed by an experimental data analysis.

5.2 Objectives

The purpose of investigating the thermal behaviour of a typical triple-layer textile skin under laboratory controlled conditions was fourfold:

- To assess the effect of the novel triple foil construction with a water-film layer on the overall thermal performance of the proposed pneumatic foil glazing system.
- To ascertain the relationship between the temperatures of the novel envelop and various air flow in the cavity of the envelope, and in turn its cooling effect on the temperatures of the external and internal membrane surface.
- To identify the impact of varying air movement conditions/water flow rate on the thermal climate of the enclosed space for the purpose of overheat control
- To provide reference data for verification of the analytical model presented in Chapter 6

5.3 Test Rig Design and Methodology

The proposed model-B pneumatic foil glazing system is a triple-layer and two air-channel construction. The design of the test rig is based on the main features listed out in Section 2.4. Other than the investigation methodology, the characteristics of the test rig construction are detailed in the present section.

5.3.1 Simulated model-B foil cushion skin construction

Section 3.2.3 has listed out a number of environmental advantages for the common commercially available multi-layer foil skin construction. The nature of the multi-airspace in foil cushions gives a good account for the physical compatibility of the water cooling process and foil cushion construction. The proposal of the novel triple-layer pneumatic foil construction is aiming to apply an indirect evaporative cooling mechanism on a multi-layer foil cushion envelop. The scheme of a typical indirect evaporative cooling mode integrated with the triple foil skin construction is illustrated in the Figure 5-1.

In this scheme, the triple-layer foil construction become a counter-flow film heat exchanger consisting of a wet air and a dry air channel. Travelling down the dry channel, the supply air is cooled by the central foil layer, where the heat has been extracted as a result of both water chilling and the evaporation process in the wet channel. Finally a part of the product air is diverted into the wet channel as working air in a reverse direction to pick up heat and remove the saturated vapour, subsequently being discharged into the atmosphere.

For the counter flow arrangement, the higher cooling efficiency (saturation efficiency, see Section 2.3.1) can be achieved [1]. The wet surface of the central foil where water is evaporating forms a location of a heat "sink", lowering the temperature of the evaporating location, such as the central foil, remaining water and the wet air. A simple psychrometric chart (Figure 5-1) indicates the temperature evolution through the channels, for instance, T1>T2>Tsat (adiabatic saturation temperature, equal to wet bulb temperature Twb at a constant pressure).

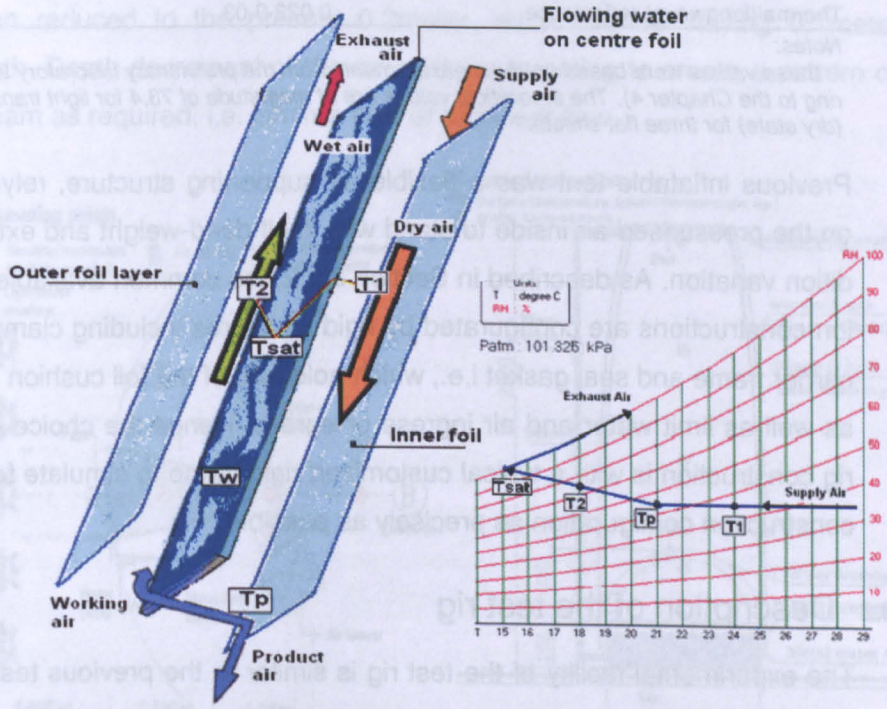

Figure 5-1: Schematic of a typical indirect evaporatic cooling mode integrated with the pneumatic triple foil glazing system (left), and the psychrometric chart (right)

The selected foil membrane used in the novel construction has been investigated for its thermal-optical properties in the preliminary test (see Chapter 4). Summary of the results is presented in Table 5-1.

Table 5-1: Table of properties of multiply ADCPE foil layer construction derived from preliminary tests

Parameters	Dry state	Wet state
Single ADCPE foil:		
Equivalent thickness [mm]	0.15	0.4@waterfilm=2.5mm
Equivalent weight [kg/m^2]	0.138	0.388@waterfilm=2.5mm
Visible transmittance (400-800nm) [%]	88.9	89.5*
Visible reflectance [%]	7	7@dryside, 2@wetside
Far-IR transmittance(1100-2800nm) [%]*	87.3	17.9
Thermal (longwave) transmittance [%]	63	-
Thermal (longwave) reflectance [%]	5	5@dryside, 2@wetside
Equivalent thermal absorption [%]	32	93.1
Triple ADCPE foil construction: *		
Shortwave transmittance (400-800nm) [%]	66.9	67.3
Far-IR transmittance (1100-2800nm)[%]	70.9	17.7
Air space thickness/single channel [mm]	100	100
Water layer:		
Thickness [mm]	2-3	
Weight [kg/m^2]	0.25	
Thermal (longwave) radiation	0.97	
Thermal(longwave) reflectance	0.022-0.03	

Notes:
**: these values were based on the measurements from the preliminary laboratory test. (referring to the Chapter 4). The theoretical values are at magnitude of 73.4 for light transmittance (dry state) for three flat sheets.*

Previous inflatable tent was a flexible air supporting structure, relying mainly on the pressurised air inside to stand with itself dead-weight and external condition variation. As described in Section 2.2.2, the common available foil cushion constructions are configurated by rigid structures including clamping plate, carrier frame and seal gasket i.e., which hold foils of the foil cushion in position as well as limit water and air ingress or egress. Hence the choice of the test rig construction is with a typical customized rigid frame to simulate foil cushion construction configuration as precisely as possible.

5.3.2 Description of the test rig

The experimental facility of the test rig is similar to the previous test comprising the following parts:

- Simulated inflatable ADCPE clear foil glazing unit
- Air supply units and auxiliary equipments
- Water cycling units and spraying nozzles
- Light source simulator

- Supporting base

The simulator of light source was continuously utilized in this test, to simulate the same climate as preliminary tests. Other experimental facilities used in the previous test were modified and developed to fit in the test objectives in this experiment. Details of the development in the facilities are presented in the following sections.

5.3.2.1 Design of experimental chamber

For convenient comparative analysis, the design of the triple-layer foil cushion construction is derived from the plan of the previous double-foil enclosure. In order to restrict impacts of external variation in the lab, the size of the test rig has been brought down to only a section (about 1/18) of the previous dome size, as shown in Figure 5-2 and Figure 5-3. This modification allows the foil cushion glazing system to cool down by the spraying water and the top ceiling to consist an opening for internal heat discharge. In comparison to the double-layer foil skin enclosure, the total depth of the airspace on this testrig had been reduced to the present 0.2meter, each channel having 0.1meter in depth. Depth decrement of the air cavity is targeting to create a pattern of air stream as required, i.e. laminar flow or turbulent flow.

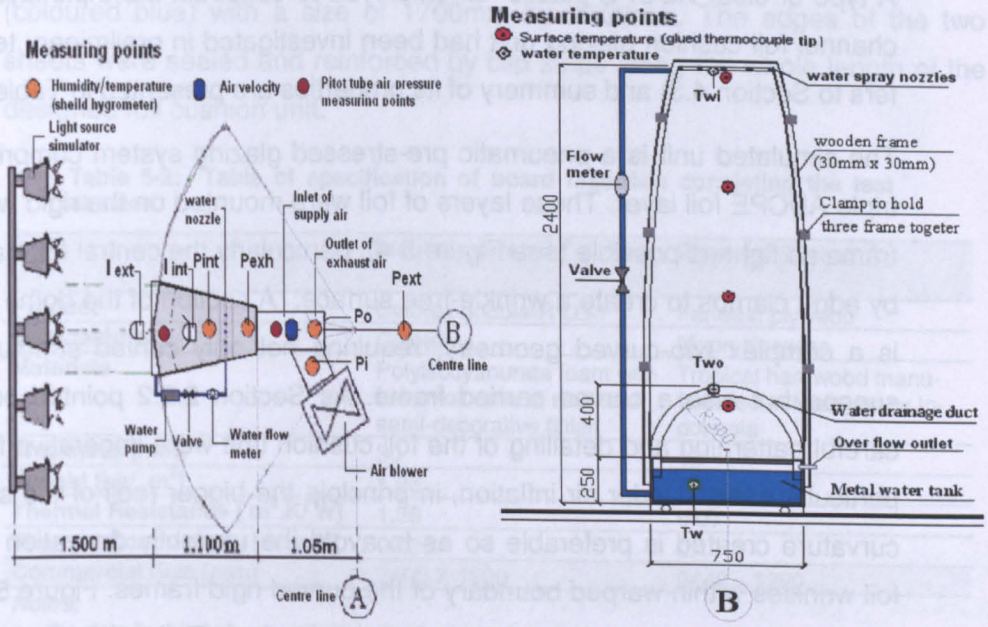

Figure 5-2: Experimental chamber: the plan (left) and front elevation diagram (right) of the chamber and positions of the measurment equipments, unit:mm

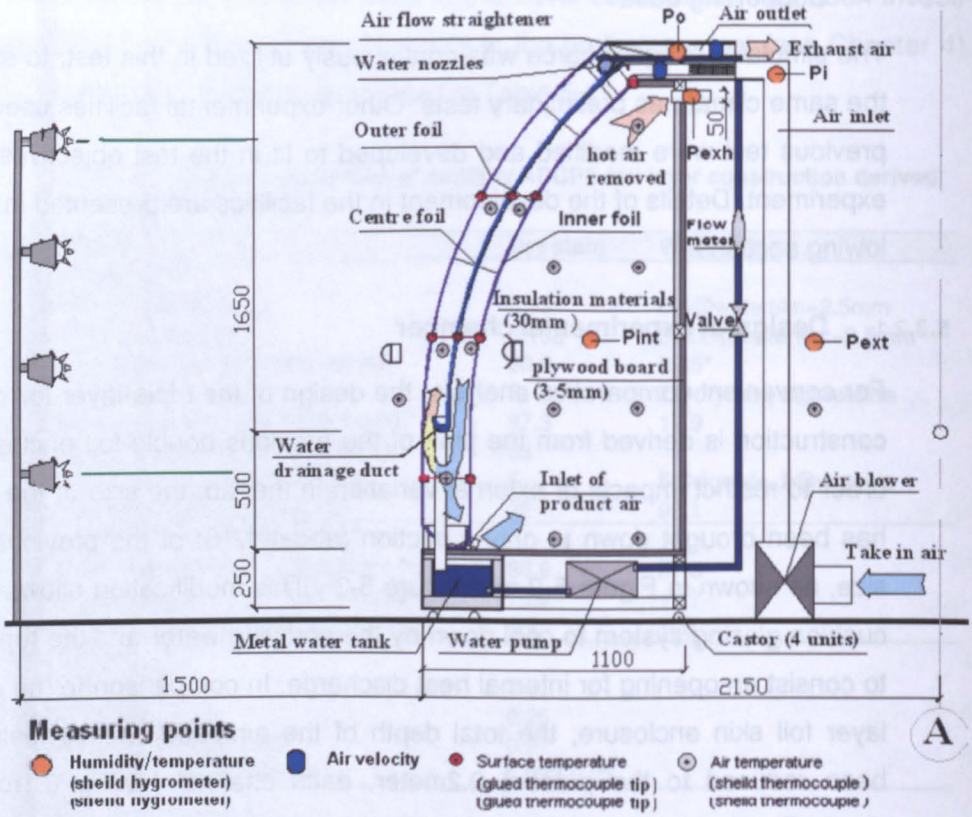

Figure 5-3: Experimental chamber: the section diagram of the chamber and positions of the measurment equipments, unit:mm

A type of clear ADCPE plastic foil employed to construct the triple-layer two-channel foil cushion glazing unit had been investigated in preliminary test (refers to Section 4.3) and summery of its properties are presented in Table 5-1.

The simulated unit is a pneumatic pre-stressed glazing system comprised of triple ADCPE foil layer. These layers of foil were mounted on the rigid wooden frame as tight as possible (see Figure 5-4), particularly the central foil clamped by edge clamps to create a wrinkle-free surface. A section of the dome shape is a complex two-curved geometry, requiring not only curved structures to support but also a curved carried frame. As Section 2.2.2 pointed out that careful patterning and detailing of the foil cushion unit were imperative for this particular case. Under air inflation, in principle the bigger radii of the surface curvature created is preferable so as to avoid the unsightly derivation of the foil wrinkles within warped boundary of the curved rigid frames. Figure 5-4 details the configuration of the foil cushion patterning. The main components constituting the foil cushion structure were the three elements: clamping strip/clamps, rigid carrier frame, supporting structure (wooden side-board).

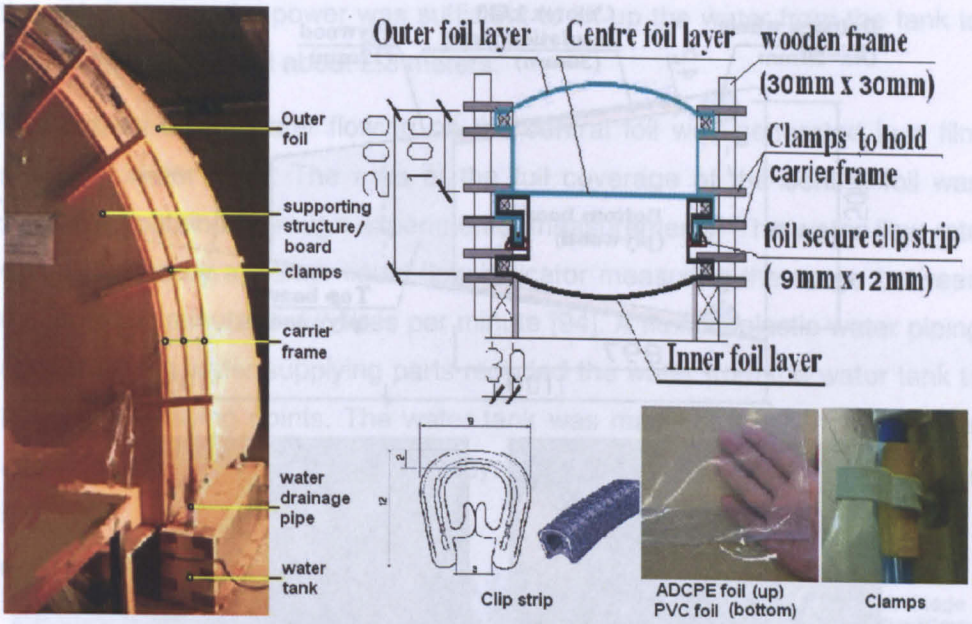

Figure 5-4: Diagram and photos of the triple-ADCPE foil cushion configuration, measurement unit:mm

In order to ensure air/ water tightness along the air ducting, the three-layer test rig actually employed two sheets wrapping around the carrier frame (a rigid tube, outer diameter=15mm) as illustrated in Figure 5-4 . The dry airchannel was shaped by a sheet (darkly coloured) at a size of 1100mm in width and 2900mm in length, while the wet airchannel was formed by a single sheet (coloured blue) with a size of 1700mm by 2900mm. The edges of the two sheets were sealed and reinforced by clip strips along the whole length of the designed foil cushion unit.

Table 5-2: Table of specification of board materials consisting the test chamer

	Insulation Panel [a]	Plywood Timber [b]
Product	Celotex double-R LG3	Far-east plywood
Manufacturer	Celotex	Nixon Knowles
Materials	Polyisocyanurate foam with low-e foil on one side and semi-decorative finish	Tropical hardwood manufactured in Malaysia or Indonesia
Thickness [mm]	30	12
Weight [kg/ m^2]	1.05	
Thermal Resistance [m^2.K/ W]	1.35	0.07
Thermal Conductivity [W/m.K]	0.022	0.17
Commercial Size [mm]	2400 X 1200	2440 x 1220

Notes:

a: the data in this column refers to the technical sheet from website: www.sigexpress.co.uk/.../Celotex%20Product%20Descriptions.pdf .

b: the data in this column obtained from product supplier: Nixon Knowles, Longwall Avenue, Nottingham, NG2 1LP

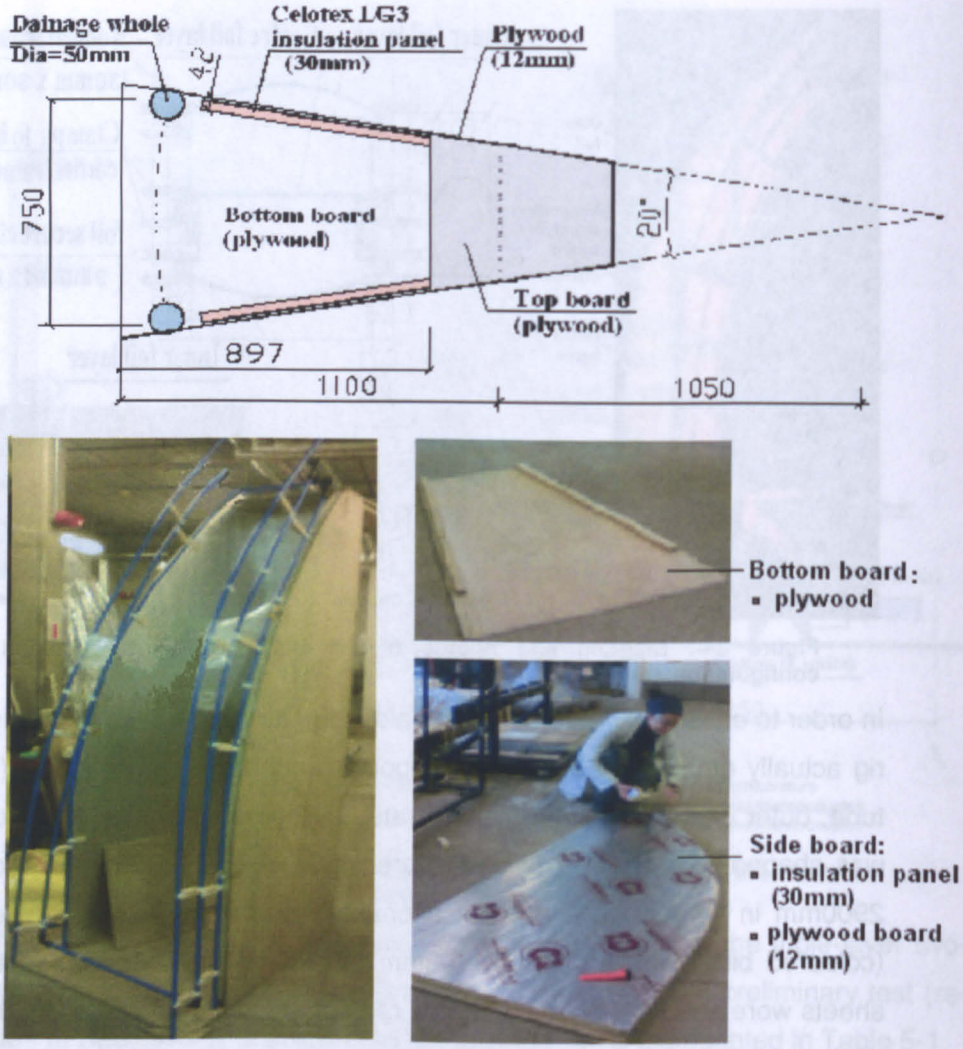

Figure 5-5: Diagram and photos of the chamber cosntruction, measurement unit: mm

Figure 5-5 illustrates the design dimension of the test chamber, at about a section size of a complete dome shape. The chamber consisted of two side-boards, a top board and a bottom board leaving the front open to fit with the foil cushion glazing unit.

Except for the bottom board, the rest three timber boards were clad with an insulating lining board facing interior, namely Celotex double-R LG3/30. The relevant technical information of the boards is listed in Table 5-2.

5.3.2.2 Water recycling system

In this experiment, the water supply system was powered by a magnetically coupled centrifugal pump, Totton-Pumps Nemp 40/4, by which the maximum water head can approach 4.4 meter high [93]. Considering the water head loss

through the pipe, the power was sufficient to lift up the water from the tank to the spray nozzle head about 2.3 meters.

The pattern of the water flowing on the central foil was generated in a film shape of water layer. The area of the full coverage of the central foil was 1.0516 m^2 obtained through experimental measurements. The water flow rate was indicated by a Parker liquid flow indicator measuring the range between 0.2 litres per minute and 2 litres per minute [94]. A flexible plastic water piping connected the water supplying parts recycled the water from the water tank to the water spraying points. The water tank was made of tough non-corrosive aluminium alloy. Photographs of the system components are shown in Figure 5-6.

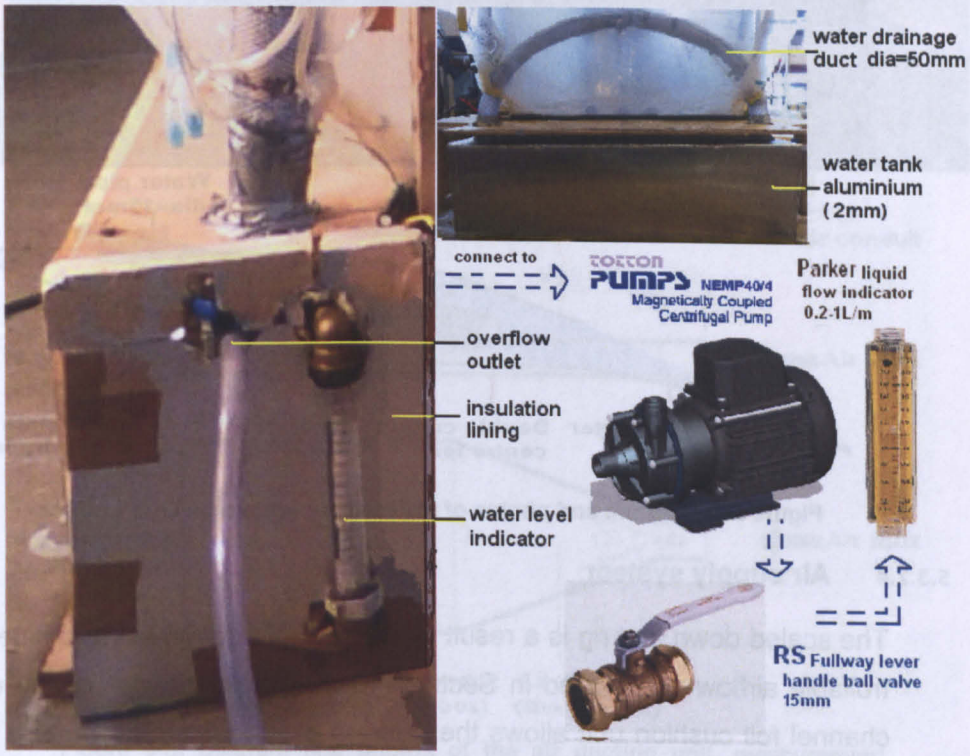

Figure 5-6: Diagram and photos of the chamber construction: components of water recycling system

5.3.2.3 Design of spraying nozzle tubes

Following the same principle as the preliminary mini-model test, the spraying water was supplied by low pressure water to create a steady running film-wise water layer on a relative flat foil surface and conserve energy. It is advantageous that the pattern of the "film-shape" water flow does not favour the creating of water droplets, which possibly drift from wet air-space to the dry side. Therefore for the configuration of wet/dry channels on the present test rig, the

generation of film-wise water flow pattern was appropriate to facilitate the design expectance and secure the quality of the product air.

The design of nozzles based on the mini-test model was modified to accommodate the present test rig. In order to reduce the possibility of generating drop-wise water spray, the control on the dynamic momentum of the spraying water is imperative. A type of overflow spraying was designed to meet the requirements, which are detailed in Figure 5-7.

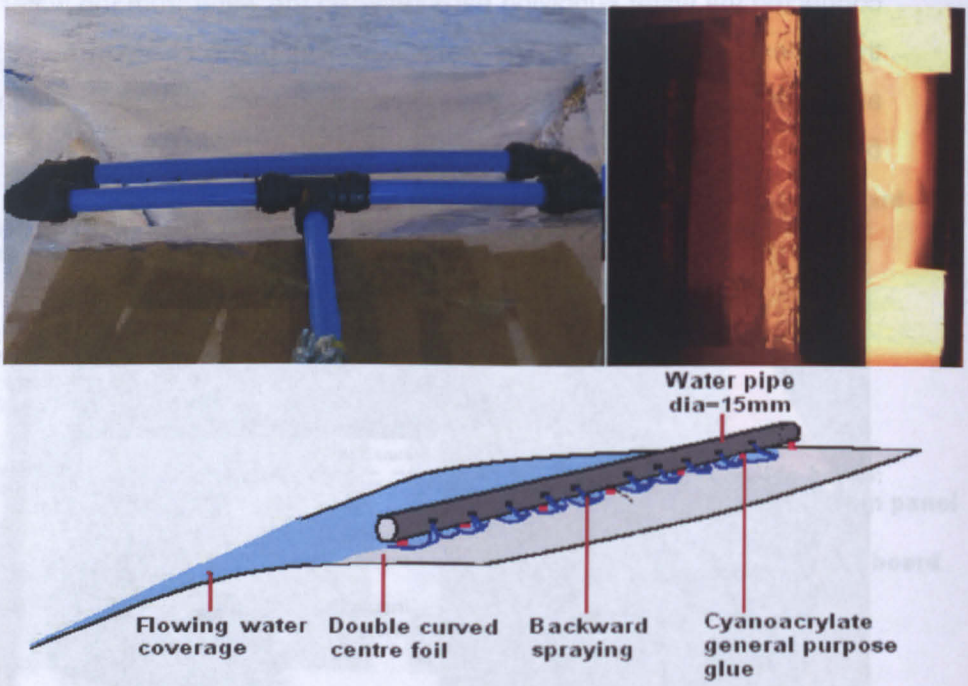

Figure 5-7: Diagram and photos of the spraying pattern design.

5.3.2.4 Air supply system

The scaled down test rig is a result of the design requirement to create a controllable airflow as outlined in Section 4.6 . The configuration of the double-channel foil cushion unit allows the creation of a counter-flow pattern around the surfaces of the central foil, which is assumed to achieve high cooling efficiency in terms of cooled air production.

In light of the heat transfer process, as described in Section 4.5.2, an upward air-flow in the air cavity could promotes the rate of high heat transfer on the boundary surfaces. In the air cavities of the foil cushion unit, both downward and upward air-flow patterns were created in the dry channel and wet channel respectively. It is thus expected that a higher magnitude of overall surface

heat transfer would be found in the wet channel, which contributes to enhanced water evaporation.

Precise modification to the design of the air supply system is shown in Figure 5-8. The main constituents of the typical system are three parts: an air blower unit (as discussed in Section 4.4.1), flexible PVC air ducting, and air ducting at the inlet ant outlet.

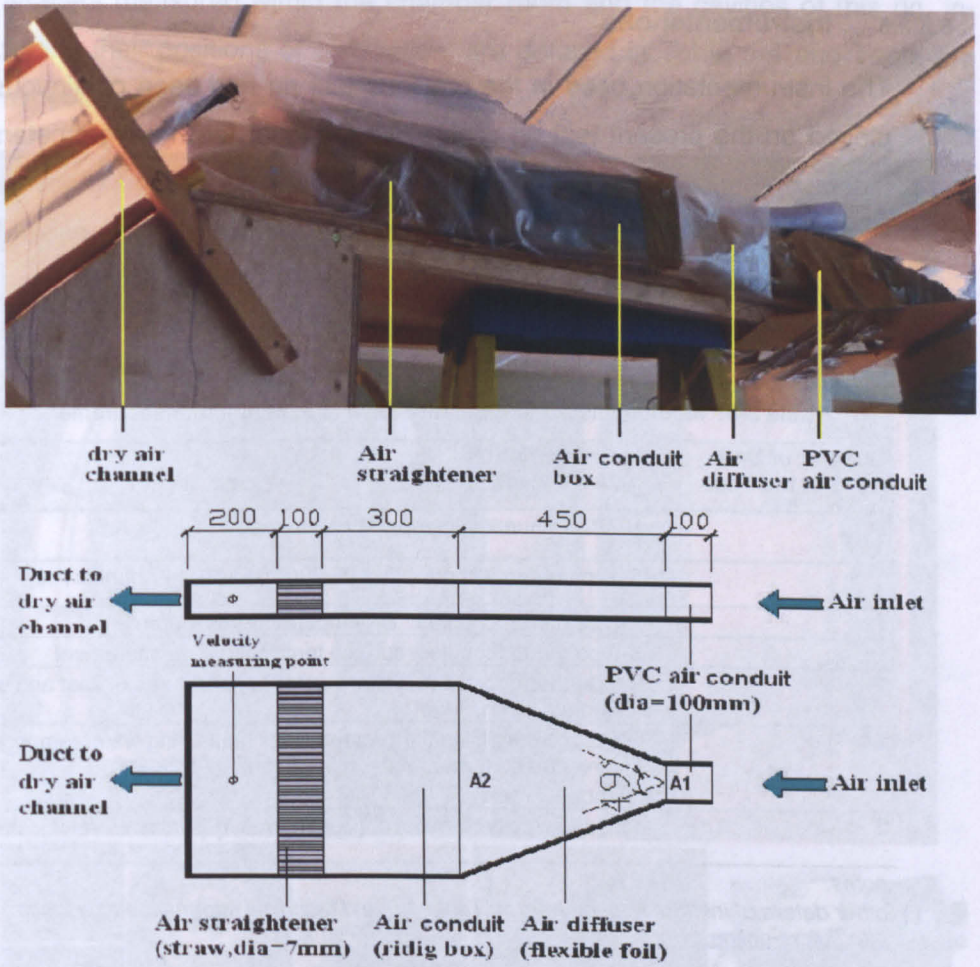

Figure 5-8: Diagram and photos of the air ducting unit, measurement unit:mm. [NB. A1=3.14x0.05^2(radium), A2=0.40(width) x 0.094 (height)]

The design of the ducting unit at the air inlet is derived from empirical principles as outlined in "fluid mechanics for engineers", particularly for airflow in non-circular ducts [95]. A honeycomb-like air straightener is located in the centre of the box with the intention to improve air distribution within the air duct. The honeycomb assembly comprises of a group of elements within a rectangular frame. Each element was 7mm in diameter and 100mm in length. Literature has presented that satisfactory results generally would be produced by

the ratio of length to diameter between 5 to 10 [96]. The measuring station was positioned 100 mm from the entrance of the dry air channel.

Furthermore, an airflow transducer was located at the centre of the circular duct, which was made from a 450mm long PVC tube with an outer diameter of 50mm and inner diameter of 40mm. The position of the velocity sensor head was 70 mm from the tube exit.

5.3.2.5 Instrumentations

The instrumentation used in the previous test rig had been continuously employed on the present test rig (Table 5-3), except for the hygrometers, thermocouple sensors and an increase in the number of measuring devices used to measure the velocity, which had been modified to obtain precise data for the later analysis. Table 5-3 lists the details of the modification of the instrumentation.

Table 5-3: Modified list of equipments used in experiment measurement

Number of Unit Used in the Test	Instrumentation
5	HMP45A humidity/temperature probes [Appendix A.6]
1	Pyranometers (Bandwidth 305-2800), CM6B [Appendix A.2]
12	K-type thermocouples: air temperature measurement
15	K-type thermocouples: surface temperature measurement
2	K-type thermocouples: instant water temperatures of inlet and outlet (symbols: T win, T wot)
2	Glass mercury filled thermometers for measuring water temperature in tank and air temperature in front of the tent. (symbols: T tank, T ext)
2	TSI, air velocity transducer [Appendix A.4] (symbols: Vel in, Vel out)

notes:
other details of instrumentation refer to Table 4-6 and technical information at website:
http://uk.rs-online.com/

Figure 5-9 displays the experimental facilities and some of the instruments used in the test rig. As shown in below figures, besides the energy sensor (Skye SKL-510) and the pyranometer (Skye SKL-2650) measuring light energy within the short waveband of 380 to1050 nm, a pyranometer (CM6B) was used in this test to measure the global radiation level produced by the soalr simulator.

Moreover, two velocity transducers (Figure 5-9) were used to measure airflow rates from the air inlet and outlet. Details of the commissioning for the air ducting are discussed in this later section. The experimental procedure is same as

that of the TA45 thermal anemometer (technical specifications are provided in Appendix A.4).

A group of K-type thermocouples were used, which were the same type as that in previous test measurements of the air and surface temperatures. The tips of the temperature sensors were shielded by 10mmx10mm aluminium screens against the direct light flow (see Figure 5-9). The temperature parameters measured within the chamber room and the cavities of this rig, including their positions of installation, are detailed in Table 5-4 and Table 5-5 respectively

Figure 5-9: photos of the experiment facility and some measurement equipments: temperature sensors, light energy sensors, velocity transducer (photos from left to right at bottom)

There were five HMP45A probes used in this test rig. The measuring methods followed the same principle as previous testing. Appendix A.6 describes the technical specification of these equipments. The details of their installation positions and the measured parameters are presented in Figure 5-9 and Table 5-6

In terms of air pressure, the measuring points were positioned at the air inlet, air outlet and transitional location between the dry-air channel and wet-air channel. The readings were taken from the Digitron anemometer. Technical description of the instrument can be found in Section 4.4.1.

Table 5-4: List of of the temperature sensors and their positions installed inside the room of the test chamber

	Distance from Central line-A (m): Towards the front (+)			*Distance from Central line-B (m)
Catergory	**Sensor Symbol**	**Height (m)**	**Distance (m)**	**Distance (m)**
Air Temperatures	T0ai0	2.05	1.25	
	T0ai1	1.45	1.25	
	T0ai2	0.85	1.25	
	T0ai3	0.30	1.25	
	Tai1	1.45	1.60	
	Tai2	0.85	1.60	
	Tai3	0.30	1.60	
Surface Temperatures	T si1	1.45	1.05	
	T si2	0.85	1.05	
	T si3	0.30	1.05	
	T si-sd1	1.45	1.25	0.22
	T 'si-sd1	1.45	1.25	-0.22

Subscript symbol
ai: internal air temperature; si: internal surface temperature
**: Towards the doorway(+); Towards opposite way(-)*

Table 5-5: List of the temperature sensors and their position installed in the cavity of the test rig

Sensor Symbol	Measured Data Description	Height (m)
Cavity Surface Temperature		
$T_{ca\text{-}so1}$		
$T_{ca\text{-}so2}$	Outer surface of outer foil	1.75
$T_{ca\text{-}so3}$	Outer surface of outer foil at human height	1.15
$T_{ca\text{-}sc1}$	Outer surface of outer foil at human height	0.55
$T_{ca\text{-}sc2}$	Inner surface of centre-foil	1.75
$T_{ca\text{-}sc3}$	Inner surface of centre-foil at human height	1.15
$T_{ca\text{-}si0}$	Inner surface of centre-foil at human height	0.55
$T_{ca\text{-}si1}$	Inner surface of inner foil at ceiling height	2.20
$T_{ca\text{-}si2}$	Inner surface of inner foil	1.75
$T_{ca\text{-}si3}$	Inner surface of inner foil at human height	1.15
	Inner surface of inner foil at human height	0.55
Cavity Air Temperature		
$T_{ca\text{-}ad1}$	Temperature in the dry channel	1.75
$T_{ca\text{-}ad2}$	Temperature in the dry channel	1.15
$T_{ca\text{-}ad3}$	Temperature in the dry channel	0.45
$T_{ca\text{-}aw1}$	Temperature in the wet channel	1.75
$T_{ca\text{-}aw2}$	Temperature in the wet channel	1.15

Notes:
The diagram of the sensors installed in the rig is illustrated in Figure 5-2 and Figure 5-3

Table 5-6: List of hygrometers and their positons installed on the testrig

Sensor Symbol	Measured Data	Height [m]
Cavity Humidity/ Temperature		
P_o/T_{cavo}	Humidity /temperature at the air outlet	2.25
P_i/T_{cavi}	Humidity /temperature at the air inlet	2.35
External /Internal Humidity		
P_{ext}/T_{ao}	External humidity /temperature	1.15
P_{int}/T_{ai}	Internal humidity/temperature	1.15
P_{exh}/T_{exh}	Internal exhaust humidity/ exhaust air temperature	2.10

Notes:

The diagram of the hygrometers installed in the rig is shown in Figure 5-2 and Figure 5-3

5.3.3 Test process

The test protocol follows the same procedure as that in preliminary tests. The following highlights the simulated conditions in the present test rig:

- The measuring chronology is set over sufficient amount of time: 1.5 hours (up to 2 hours). The data was sampled at an interval of 1 minute for each test, using a data logger (TD500) connected to a PC.
- An average level of radiation at 600 W/m^2 created on the vertical assumed screen following 30 minutes exposure of artificial lights on the entire test rig.
- A moderate level of external temperature on the test rig is maintained between 21and 25°C.
- The thermal comfort targets of the internal environment are designated the dry resultant temperature range of 15.6°C (for sedatory activities or 13°C for sport acivities) and 28°C (Cf. sectin 4.5.5), taken as around 0.6m or 1.1m above the floor for a seated person or a standing one respectively.

5.4 Commissioning Results

Before proceeding with experiments on the entire novel foil cushion system, an investigation on the performance of essential components of the novel glazing system is necessary in order to explore the appropriate testing methods and establish reference line on which the later testing on the novel glazing assembly can be based. The results of the commissioning on the significant elements are presented in this section.

5.4.1 Velocity in the simulated air ducting

The simulated triple-layer foil cushion envelop was clad by a typical ADCPE plastic clear foil. Thus, air channels constituting the envelope appeared like inflatable air ducting system. As a result of of the test-rig geometry (refer to Figure 5-3), the shape of the air channels in the simulated model can be analogous to a big air diffuser with a taper angle at 20°. For this typology, it is explicit that the highest airflow rate in the air channel can merely be recoreded right at inlet of the diverge section in such a diffuse analogue. In principle, the diffuser efficiency is inversely proportion to the diverge angle [95]. Furthermore literature indicates that the optimal diverge angle is below 15° in order to constrain the air pressure loss in a closed conduit to an acceptable level [95].

With concern to the characteristics of the inflatable air-duct construction and the objectives of investigation in this test, a rigid box-shape air conduit was comprised in the assembly of air ducting in front of its inlet with intention to depress the duct fatigue caused by foil flapping. The box made by cardboard facilitates the installation of velocity transducers to measure precisely the airflow rate at the measuring stations. The size of the box is 400mm (width) by 94mm (height) by 600mm (length).

In light of velocity measurement in the rectangular duct, Log-Tchebycheff method is recommended by the ASHRAE 1997 Fundamental Handbook to minimise the positive error due to fail to account for the pressure loss at the duct wall. However, for such a small cross-sectional area of 0.0376 m^2, Klassen and House [97] has argued that equal area method is sufficient to accurately measure the airflow in the duct. Hence, a comparative testing has carried out to find out an appropriate one for the velocity measurement on this test rig. Figure 5-10 shows the distribution of measuring points on the cross-section of the duct corresponding to the mentioned two methods.

The results indicate that for such a small duct area the velocity differentials using varying testing methods are marginal. Typically, the measuring results acquired by using simplified version of the Log-Tchebycheff method (denoted in the 5 green dots) displayed slight deviation from the other two methods and the variation was though within the acceptable range rising from 0.84% to 5.86% along with the fan power increase. It is also found that the correlation between the velocity readings taken from the centroid of the duct traverse and mean values using the Log-Tchebycheff method seems relative linear.

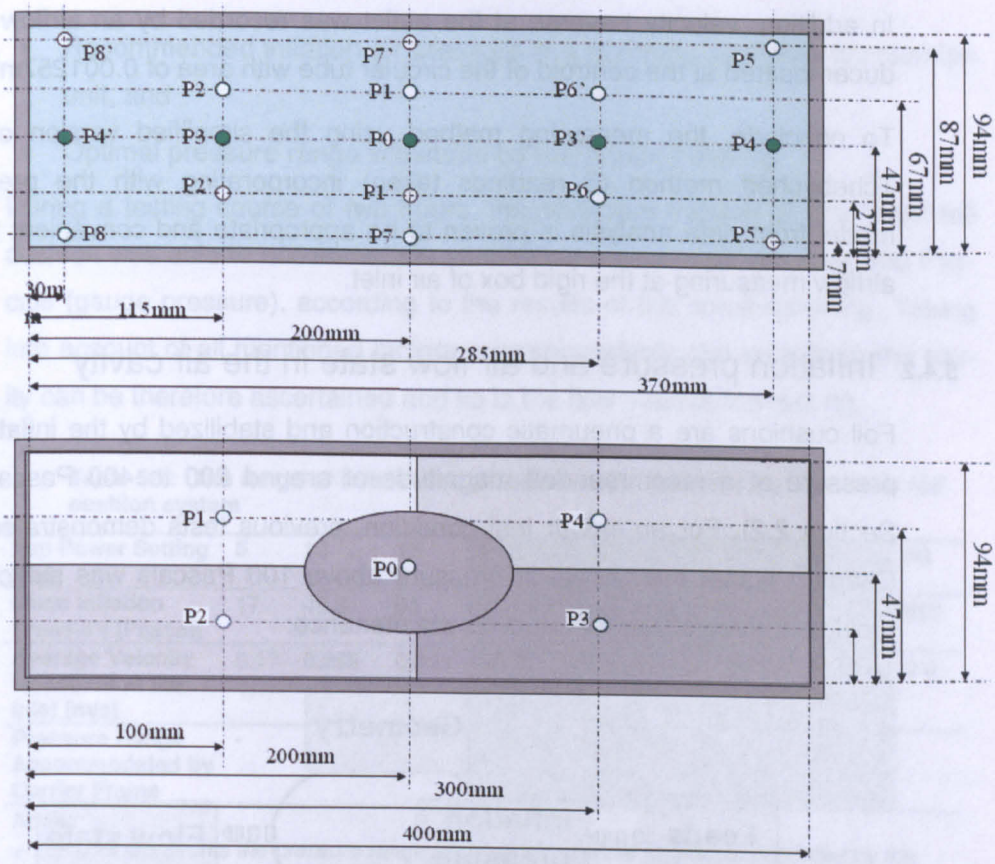

Figure 5-10: Methods of velocity measurement and measuring points. Log-Tchebycheff method (up diagram), Equal area method (bottom diagram)

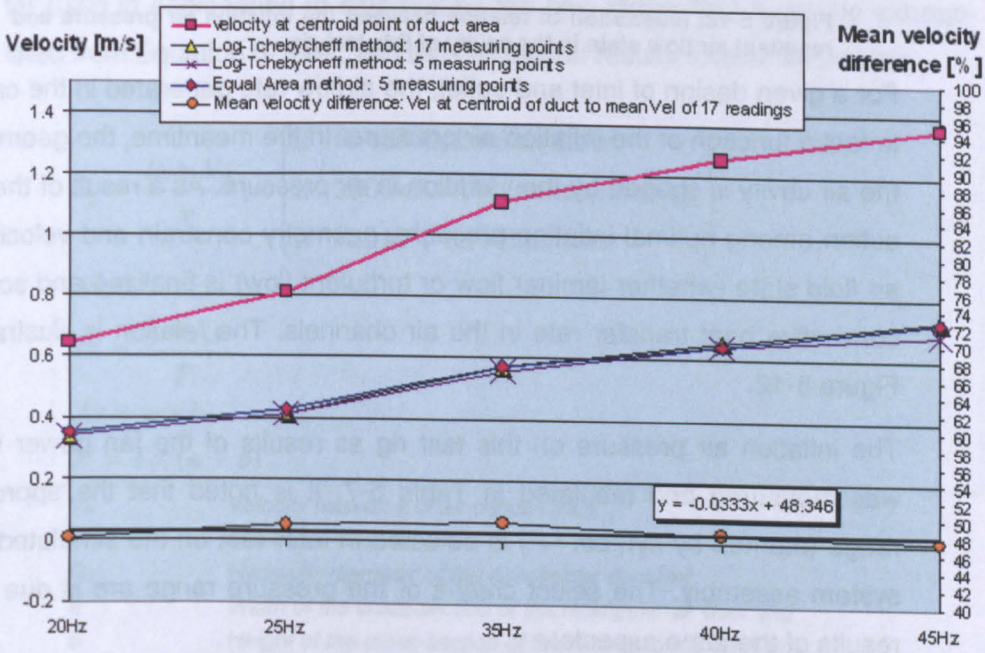

Figure 5-11: Results comparison of various methods and variation between the velocity at the centroid and mean velocity of 17 readings for different fan power settings

In addition, velocity traverse at the outlet was recorded by an airflow transducer located at the centroid of the circular tube with area of 0.001257m^2.

To conclude, the measuring method using the simplified version of Log-Tchebycheff method (5 readings taken) incorporating with the prediction model from data analysis is proven to be appropriate and convenient for the airflow measuring at the rigid box of air inlet.

5.4.2 Inflation pressure and air flow state in the air cavity

Foil cushions are a pneumatic construction and stabilized by the inflation air pressure at a recommended magnitude of around 200 to 400 Pascals (Cf. Section 2.2). For an indoor test condition, previous tests demonstrated (see Chapter 4) that the gauge air pressure above 100 Pascals was sufficient to provide surface stress for structure maintenance.

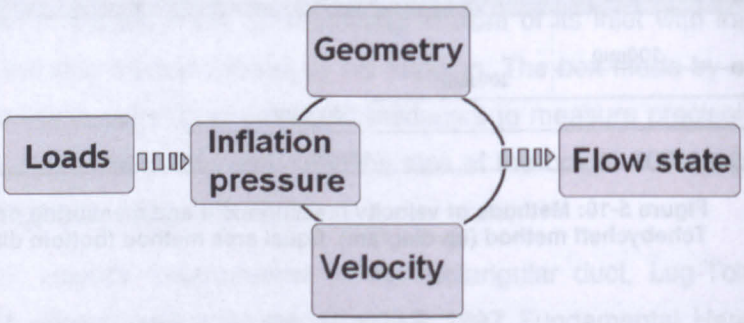

Figure 5-12: Illustration of relation between the inflation air pressure and resultant air flow state in the cavity of this test rig.

For a given design of inlet and outlet, the airflow rate generated in the cavity is in fact a function of the inflation air pressure. In the meantime, the geometry of the air cavity is shaped by the variation in air pressure. As a result of the interaction among optimal inflation pressure, geometry constrain and velocity, the air fluid state (whether laminar flow or turbulent flow) is finalized and so is the convective heat transfer rate in the air channels. The relation is illustrated in Figure 5-12.

The inflation air pressure on this test rig as results of the fan power setting was measured and tabulated in Table 5-7. It is noted that the appropriate range (marked by symbol "+") is selected in later test on the simulated novel system assembly. The select criteria of the pressure range are is due to the results of the three aspects:

- Experimental observation from previous laboratory test,

- Recommended inflation air pressure in a common available foil cushion unit, and
- Optimal pressure range withstood by the present test rig.

During a testing course of two hours, the perimeter framing of this novel foil cushion was able to accommodate an inflation pressure of less than 300 Pascals (gauge pressure), according to the results of the commissioning. Taking into account of all mentioned factors comprehensively, the velocity in the cavity can be therefore ascertained and so is the flow state in the test rig.

Table 5-7: The range of inflation air pressure accommodated by the novel foil cushion system

Fan Power Setting [Hz]	5	10	12	15	18	20	22	25	30
Mean Inflation Pressure [Pascal]	17	48.3	64	98.3	134	166.3	195	252.7	362
Average Velocity Measured at the Inlet [m/s]	0.17	0.285	0.311	0.368	0.485	0.525	0.591	0.672	0.8
Pressure Range Accommodated by Carrier Frame	-	-	-	+	+	+	+	+	-

Notes:

+ : symbol represents the pressure range which is appropriate and accommodated by the typical carrier frame on the novel foil cushion rig.

- : the pressure range is not appropriate.

For forced convection in closed conduits, Reynolds' number (Re) is a parameter used in engineering to differentiate the flow states that it can be extrapolated from Equation 5-1[99], and the calculation results follows afterwards.

$$R_e = \frac{D_e \times V_m}{v}, \quad \begin{cases} \text{if } R_e<2300, \text{ laminar flow} \\ \text{if } 2300<R_e<10^4, \text{ transition stage} \\ \text{if } R_e>10^4, \text{ turbulent flow} \end{cases}$$

where

$$D_e = \frac{4 \times As}{P}$$

$$As = a \times b$$

$$P = 2 \times (a + b)$$

V_m	*Velocity trasverse of air conduit [m.s^{-1}]*
v	*Kinematic viscosity [m^2.s^{-1}]*
D_e	*Hydraulic diameter of the noncircular duct [m]*
a	*Width of the cross-section of the retangular air duct [m]*
b	*Height of the cross-section of the retangular air duct [m]*

Equation 5-1: Calculation of Reynolds number in the noncircular air ducts.

Table 5-8: Results of the flow state determing in the air cavity

Selected fan power setting [Hz]	15	18	20	22	25	30
V_m [m/s]	0.368	0.485	0.525	0.591	0.672	0.8
De@ inlet duct [m]	0.15233	0.15233	0.15233	0.15233	0.15233	0.15233
Critical Re number *	3610.95	4758.89	5144.1	5796.09	6593.37	8031.91

Notes:
**: $v = 15.53 \times 10^{-6}$ @ air temperature=25℃.*
ADCPE film: its face to face coefficient of friction is in the range of 0.3-0.5

Moreover, considering the typical double-curve geometry of the air channels, these bends in air passages can superimpose turbulence along the flow boundary on the internal surface of the air duct, which is though beneficial to the heat exchange process. Therefore, the velocity profile in the air channel can be distorted meanwhile coupling with centrifugal force, a secondary flow is produced. The impact of the bends on the convective heat exchange rate is indicated by the following correction factor of conduit bends:

$$\varepsilon_r = 1 + 1.77\frac{d}{r}$$

d — *Dameter of the air conduit [m]*
r — *Radius of carrier framing curvature [m]*

Equation 5-2: Correction factor due to effects of air conduit bends [99]

In this particular case of the test rig, the correction factor is as low as 1.0843. It can be concluded that the flow state at transition stage is predominated in the air channels of this test rig for these selected fan power settings, and it is resulted from combination effects of the geometry and inflation air pressure.

5.4.3 Foil surface wettability

The impact of the flowing water film on thermal behaviour of the ADCPE film has been discussed briefly in Section 3.4.2 and Section 4.3. It is necessary to generate an evenly distribution of a film-wise water layer on the foil surface when an investigation on the thermal performance of the novel foil cushion system is carried out. In comparison to flat surfaces, the double curvature of the foil surface in this test rig is not in favour of uniform spread of film-wise water flow. Some literature suggested that an equivalent surface coverage factor of water (φ) could be used to describe the wet fraction of the surface [73]. In this way, the thermal transmittance (τ_{rw}) and emissivity (ε_{mw}) of the partially wet foil surface can be expressed as weighted mean values:

$$\tau_{rw} = (1-\varphi)\times\tau_r$$

$$\varepsilon_{mw} = (1-\varphi)\times\varepsilon_m + \varphi\times\varepsilon_w$$

where

$$\varphi = K\times\frac{V_w}{V_{w\,\max}}$$

$$\frac{1}{K} = \frac{\theta_{wf}}{\theta_{wf\,\max}}$$

V_w	*Volumetric supply water flow rate [L .m^{-3}]*
θ_{wf}	*Equivalent flowing water film thickness [mm]*
ε_m	*Thermal emissivity of the foil membrane*
ε_w	*Thermal emissivity of the water film*
τ_r	*Thermal transmittance of the foil membrane*

Equation 5-3: Calculation of Reynolds number in the noncircular air ducts.

Both maximum water flow rate and thickness of the flowing water film were only determined through experiments. In the computation, the equivalent thickness of a water film spread for is estimated according to a given supply water flow rate, based on the different wet states of the foil. The results of the estimation on the wet fraction of the surface (φ) and the equivalent thickness of a water film (θ_{wf}) in comparison to commissioning results has shown in Table 5-9.

Table 5-9: Results of the estimation and commissioning on the surface wetability of the simulated clear ADCPE foil cushion test rig

Estimation Results	Ideal Maximum Values		Estimated Maximum Values		Estimated Minimum Values	
Coverage Area of Wet Surface : A [m^2]	1.17		0.994		0.92	
Wet Fraction of Surface: φ [%] [a]	100		85		78.7	
Water Flowrate [L/m]@water film thickness=1mm [b]	11.70		9.94		9.20	
Commisoning Results						
Tested Water Flow rate: V_w [L/m]	0.5	0.6	0.7	0.8	0.9	1.0
Measured Wet Fraction: φ [%]	60	70	75-80	80	85	85
Equivalent Water Film Thickness: θ_{wf} [mm]	0.07 1	0.079	0.1	0.11	0.11	0.12

Notes:

a: the estimated (maximum and minimum) values were computed according to the data obtained from the experiment.

b: estimated water flow rate is computed when the timing of the water flowing from the sprayers to the drainage is set as 5-6 seconds, which is based the measurements through experiments.

Table 5-9 has explicated that for the selected range of the water flow rate, and there is no direct correlation between the water flow and wet coverage (φ). In

addition, Table 5-9 also shows that the thickness increment of the water film is negligible with increase of the water flow. The values highlighted in shade in the table indicate that the flow rates of supply water have met the minimum fraction of wet coverage in the tested system, no less than 78.7% coverage area of water film. Furthermore, the equivalent thickness of water film appeared relatively small as shown in Table 5-9, similar to the thickness of the ADCPE foil itself (0.15mm). The results suggested in all that a good surface wettability as a determinant factor for cooling production could be achieved at supply water flow rate of 0.7l/m, without significant dead weight of water imposed on the central foil of the envelop.

The chemical concentration in the water solution was chosen as 1%, using the Fairy rinse aid to reduce the surface tension of water on the test plastic foil. Combining the anti-drip surface treatment of the foil and the careful design of the spraying nozzle, the surface wettability of the double curved central foil was relative satisfactory, reaching up to 85% wet coverage at low supply water rate.

5.4.4 Air/water leakage control issues

It is evident that the control of air/water vapour leakage is imperative in the design of foil cushion constructions in spite of its constructional beneficialness insitu. For this typical design of the test rig, an assessment is necessary to carry out to indentify the issues of leakage (results illustrated in Figure 5-13).

Constructional characteristics (air tightness and pneumatic pre-stress) of conventional foil cushions pose a special consideration to condensation. Common foil cushion units hence have air dryers in conjunction with the air inflation system to minimize the humidity in the foil cushions. The built-in channels then filter out the condensated water at the cushion connections. However high humidity in the airspace of the proposed cushion system is not a big concern as a forced ventilation is in place collaborating with water chilling process. It is believed that the surface condensation occurrence inside cushion diminishes when high air movement is present.

At the design stage of the test rig, the special considerations had given to the design of the water drainage units, which should allow for flexible shapes conforming to double-curve membrane structure and a provision of non-obstacle passage for the dry air to wet air transition in the air cavity. It was contem-

plated in the first place that the leakage control could be complicated by such a sophisticated design on this water recycling system. Therefore, it had driven special attention in the leakage assessments.

Following careful study on the materials compatibility of the foil and imbedded drainage gutter as well as the nature of the foil cushion construction, a practical solution of a water-collecting device has been provided for this test rig to facilitate the above considerations. The design details of the drainage unit have been illustrated in Figure 5-13. Its performance was evaluated by using smoke test. The test results showed that an amount of inflation air had escaped from the drainage unit, leakage locations on which are highlight in dark red in Figure 5-13.

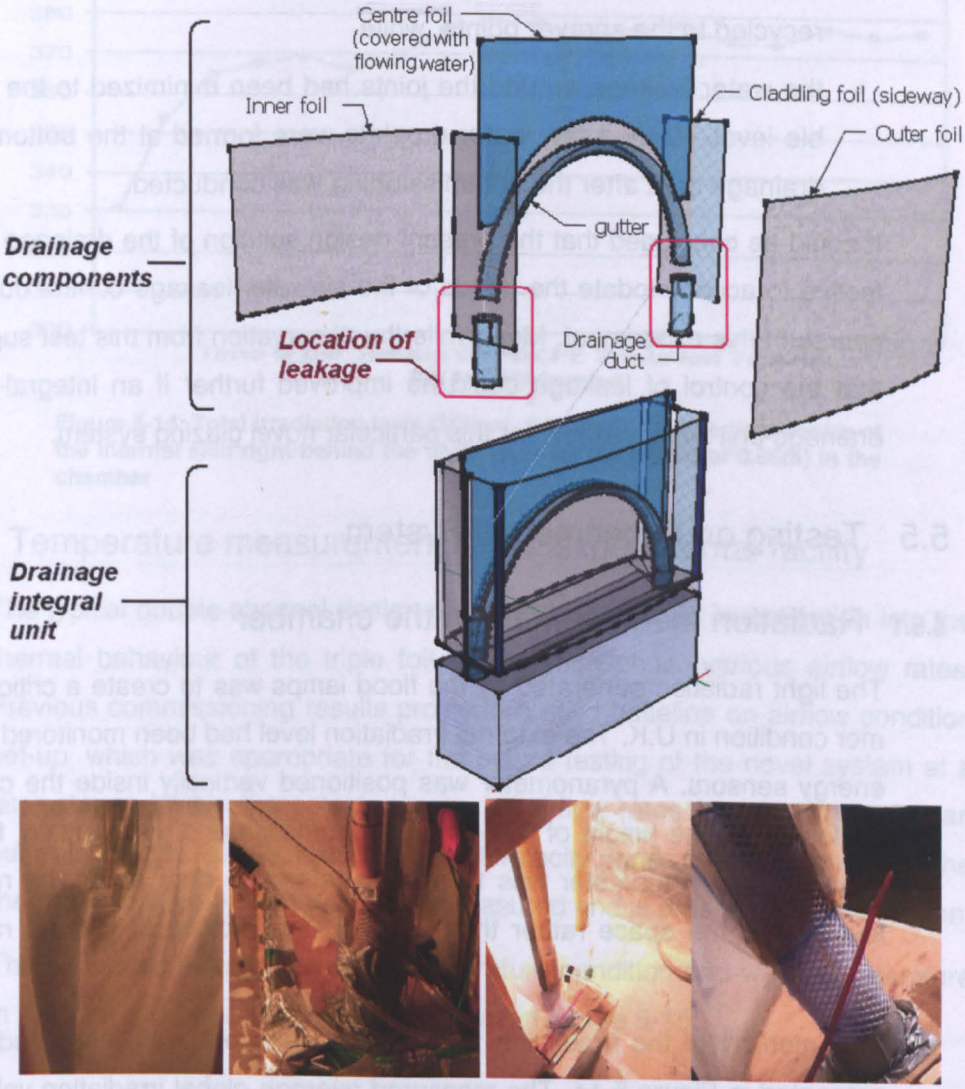

Figure 5-13: Illustration of air /water leakage in the test rig and photos of the water gutter, the drainage parts, smoke-test of leakage and the location of the leakage (from bottom left to right)

The assessment indicated that the vulnerability of the present water collecting design to air/ water leakage essentially linked to the two factors:

- The non-integral design of drainage unit creates clandestine air/water 'exits', although water-proof tapes and glue had been applied along with every joints and seams.
- The unfavourable pressurized environment inside the cushion fosters the presence of imperceptible gaps and provokes the evolution of the crevices adjacent to the joints or foil seams.

On the other hand, the test presented some positive results on water leakage control when this design solution was adopted:

- the flowing water on the central foil had been effectively collected and recycled to the sprayer points, while
- the water leakage around the joints had been minimized to the negligible level. Only a few water droplets were formed at the bottom of the drainage duct after the commissioning was conducted.

It could be concluded that the present design solution of the drainage was effective to accommodate the needs of the air/water leakage control during the course of this experiment. Meanwhile the observation from this test suggested that the control of leakage could be improved further if an integral-forming drainage unit was available for this particular novel glazing system.

5.5 Testing on Experimental System

5.5.1 Radiation measurement in the chamber

The light radiation generated by the flood lamps was to create a critical summer condition in U.K. The external irradiation level had been monitored by light energy sensors. A pyranometer was positioned vertically inside the chamber enclosure, at the height of 0.85 meter from the ground. Here again, the purpose of this pyranometer was to provide reference data about the radiation level inside the space rather than an accurate tracking of internal radiation condition.

The intensity of the irradiation through the triple foils was measured and is presented in Figure 5-14. The measured average global irradiation value was 376.6 w/m^2 in the spectral range from 400nm to 2800nm, with 570 W/m^2 of ex-

ternal light radiation condition in the spectrum of 400nm to 1100nm. As highlighted in previous chapters, the thermal-optical properties of the ADCPE foil were not 'blind' to the thermal radiation. There was a significant amount of longwave radiation penetrated through the triple-foil envelop at average magnitude of 152.7 W/m^2. In the testing time scale of half hour, the measured average transmittance of thermal radiation (1100nm to 2800nm) was as high as 0.54 of triple-layer construction, in comparison to 0.63 of single sheet. It could be assumed that such high thermal transparency of PE foil could aggravate the risk of over-heating within the space enclosed by this type of foil when solar exposure is high.

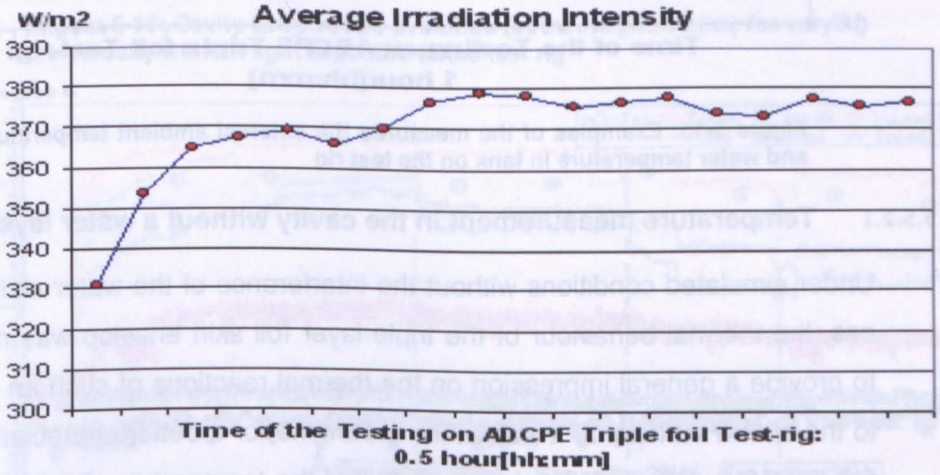

Figure 5-14: Total irradiation level (380nm -2800nm) at the vertical centre of the internal skin right behind the triple-layer (at the height of 0.85m) in the chamber

5.5.2 Temperature measurement in the experimental facility

The typical double-channel design of the test rig allowed investigation into the thermal behaviour of the triple foil construction under various airflow rates. Previous commissioning results provided a solid baseline on airflow condition set-up, which was appropriate for the hybrid testing of the novel system at a later stager. Within the selected range of airflow rates (generated by the fan set from15Hz to 25 Hz), the influence of velocity generated in the cavity on the thermal condition of the test rig was measured and is presented in this section.

The simulated external ambient temperature condition and water temperature in the tank are generalised and presented in Figure 5-15.

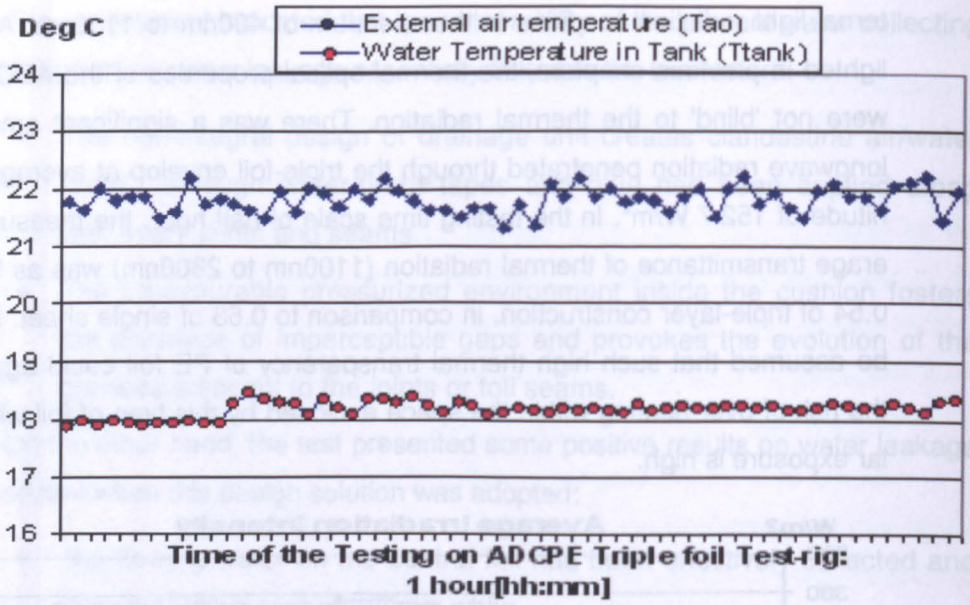

Figure 5-15: Examples of the measured the external ambient temperature and water temperature in tank on the test rig

5.5.2.1 Temperature measurement in the cavity without a water layer

Under simulated conditions without the interference of the water chilling process, the thermal behaviour of the triple-layer foil skin envelop was monitored to provide a general impression on the thermal reactions of such an envelope to the airflow variations. It was at the meantime for a better appreciation of the possible correlation of the airflow rates and the temperature distribution in the two air channels (illustrated in Figure 5-16 and Figure 5-17).

The results show that the amount of retained heat in the cavity has been removed when the high airflow rate (higher than 0.6m/s in the air inlet) is generated and cavity air temperatures can be reduced to average 40℃ under light exposure (Figure 5-17). The constant high surface temperature in the cavity regardless of varying airflow rates attests that radiative heat transfer has a greater influence on the surface temperature than convective transfer, which coincides the conclusions from the previous test (Cf. secton 4.6). It is implied that to only rely on airflow generated in the cavity of this particular foil cushioln construction is not sufficient to decrease the evenlope temperature and remove accumulative heat in cavity (as the surface temperature of inner foil generally stayed above 39℃). It thus necessitates the integration of appropriate chilling measures (i.e. evaporative cooling) in a foil cushion construction to cool down the surface temperature of the envelope effectively.

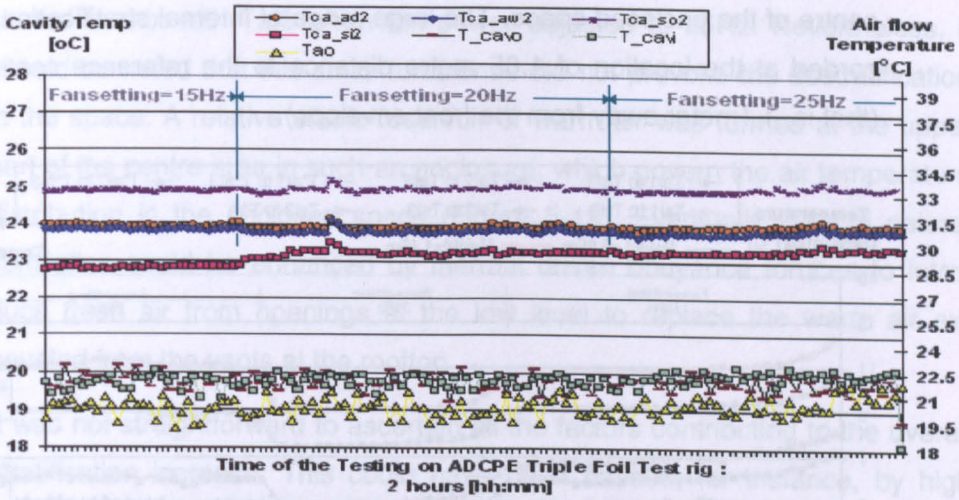

Figure 5-16: Cavity temperature evolution (at the height=1.15m) for varying air velocity without light exposure in the test rig

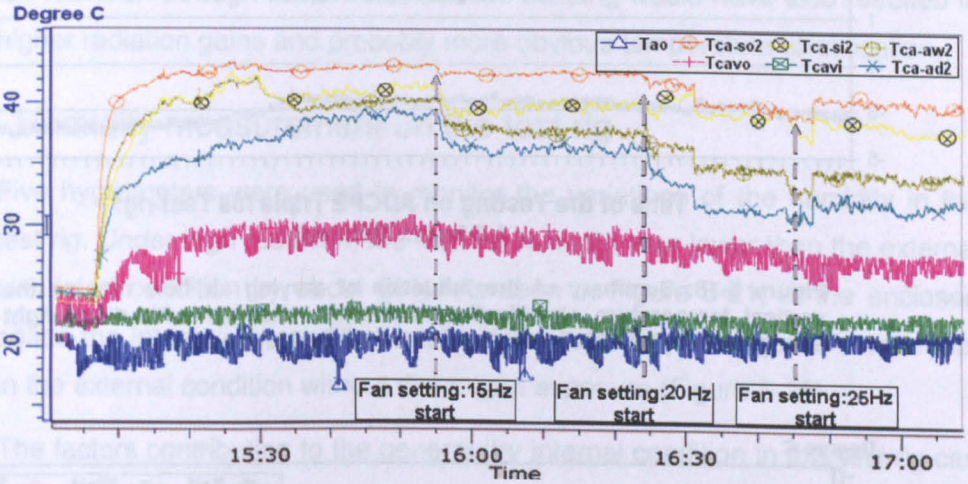

Figure 5-17: Cavity temperature evolution (at the height=1.15m) for varying air velocity under light exposure in the test rig

5.5.2.2 Air temperature distribution in the chamber without water chilling

The air temperatures inside the chamber under direct beam radiation prior to water chilling process were measured by using three sets of shielded thermo-couples along the vertical space (the locations of the sensors are refered to in Table 5-4). Each set of temperature sensors (for instance, Tai1/2/3, T^0ai0/1/2/3, and Tsi1/2/3) were positioned away from the reference centre line-A at 1.6 meters, 1.25 meters and 1.05 meters respectively for varying heights, i.e. Tai3 at height of 0.3m, Tai2 at 0.85m and Tai1 at 1.45m.

Figure 5-18 summed up the statistical analysis of the temperature stratification indoor without water chilling. It can be seen in Figure 5-18 that cooling effect of the higher airflow rate (fan setting higher than 20Hz) in the envelope can promote the extent of the temperature stratification in the place close to the

centre of the enclosed space. The large range of internal stratification was recorded at the location of 1.05 metre distance to the reference centre line-A (that is, 1.1meter away from the front envelope).

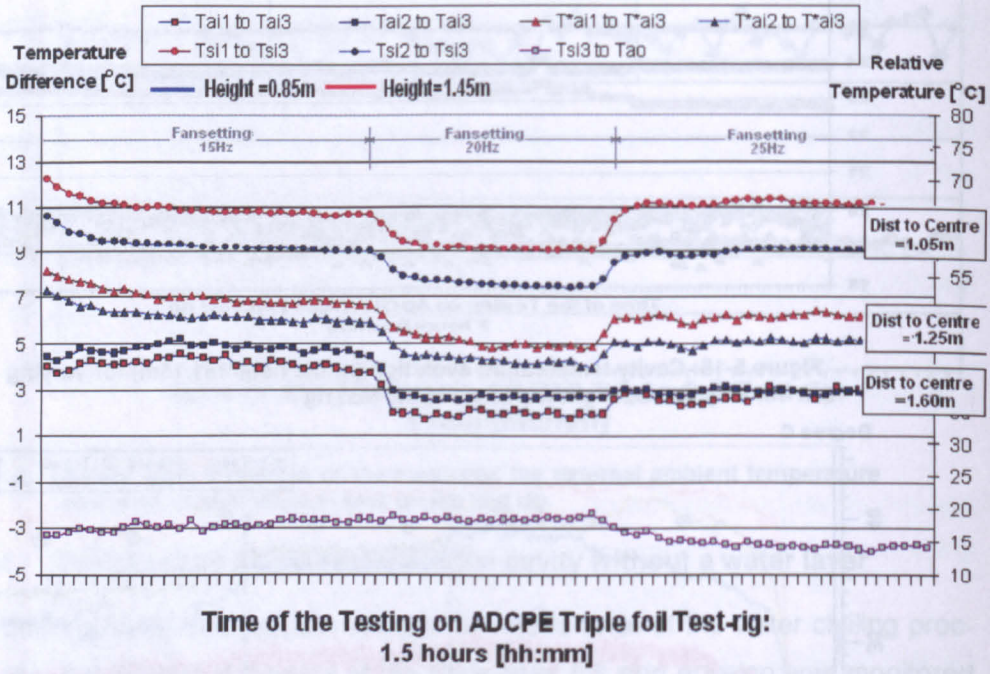

Figure 5-18: Summary of the influence of varying air flow rate on the vertical temperature stratification inside the chamber with direct light exposure (for various distances to the reference centre line-A)

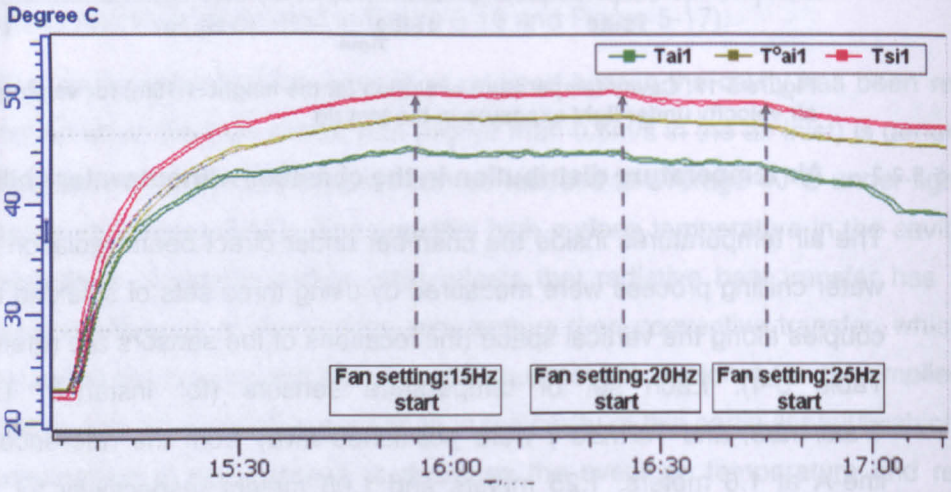

Figure 5-19: Influence of the air flow rate on the internal temperature distribution (at the height=1.45m) inside the chamber

The cooling effect generated by the continuous operation of the air blower and increasing airflow rate in the air channels of the cavity can be identified from mixing of the warm air layer at the upper level near the vicinity of the envelope and that in the occupied areas. For instance, Tai1 decreased up to 2°C and

started to mix with Tai2 when fan power adjusted to 25Hz. Nevertheless, it should be noted that this small turbulence did not provoke the destratification in the space. A relative stable reservoir of warm air was formed at the upper part of the centre area in such an enclosure, which govern the air temperature distribution in the enclosed space (Figure 5-19). Eventually internal natural ventilation could be enhanced by thermal driven bouyance foruces to introduce fresh air from openings at the low level to replace the warm air exhausted from the vents at the rooftop.

It was not straightforward to ascertain all the factors contributing to the overall stratification increase. This could have been caused, for instance, by high transparency of such a foil envelop, and the significant amount of the transmitted radiation through the envelope of the building would have also resulted in higher radiation gains and probably more obvious temperature stratification.

5.5.3 Humidity measurement on the test rig

Five hygrometers were used to monitor the variations of the humidity in the test rig. Under high radiation, the internal humidity was lower than the external simulated condition by about 30%. As seen in Figure 5-21, in the enclosed space the internal air condition was relatively drier by average 10% than that in the external condition without direct light exposure (Figure 5-20).

The factors contributing to the general dry internal condition in this test rig can be indentified as the high thermal transmittance of the foil envelop, and the internal space is fully enclosed without vents allowing fresh air in.

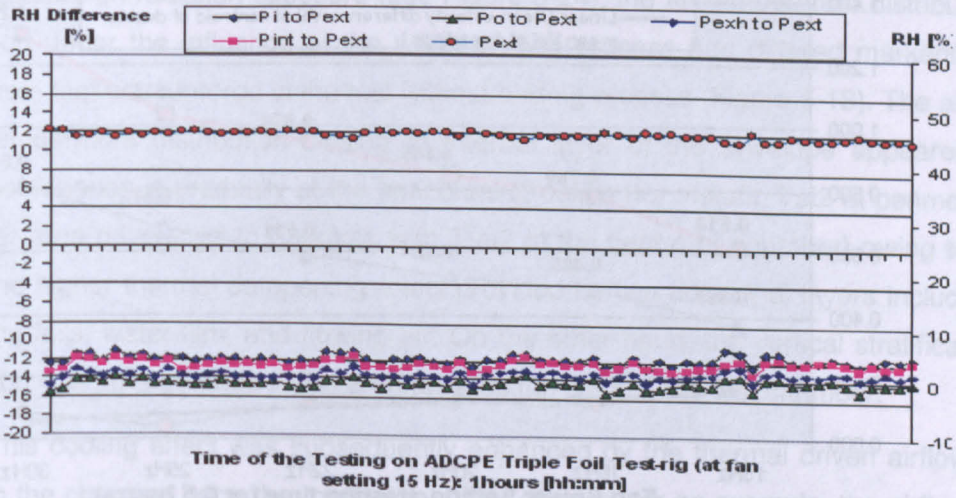

Figure 5-20: Examples of the humidity ditribution without light exposure on the test rig. [NB. o=air-outlet, i=air-inlet, int=internal, exh=exhaust, ext=external]

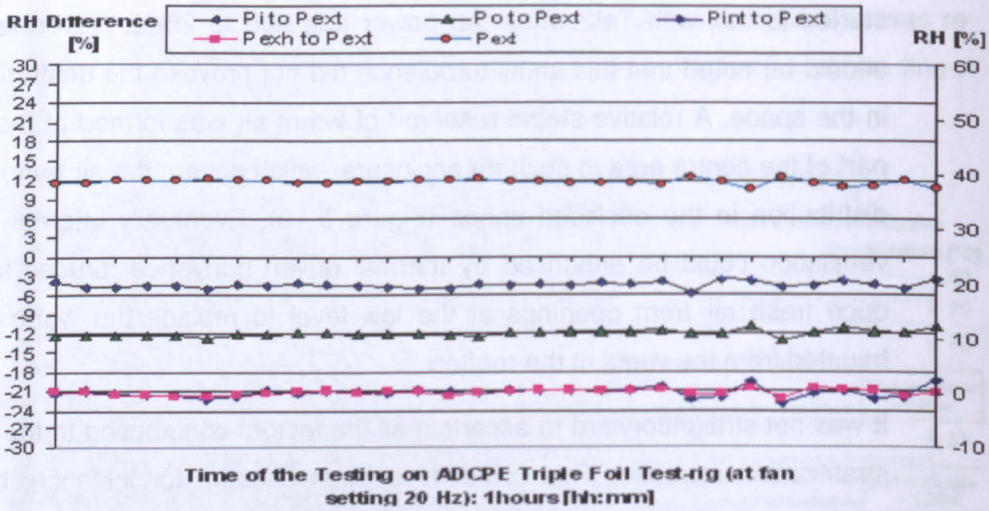

Figure 5-21: Examples of the humidity ditribution with light exposure on the test rig.

5.5.4 Air pressure and velocity measurement in the cavity

Section 5.4.1 explained that measuring method of the velocity could adopt Log-Tchebycheff method (5 readings taken) for convenience against the single sampling value taken at the centroid of the duct of the inlet. The summary of the measuring results of velocity for a range of fan power settings is illustrated in Figure 5-22. The measurements was undertaken when the entire novel system was in operation, where the situation was simulated as close as to the final testing condition. (NB. The information is used as reference data for the analysis on the convective heat transfer in the novle envelope.)

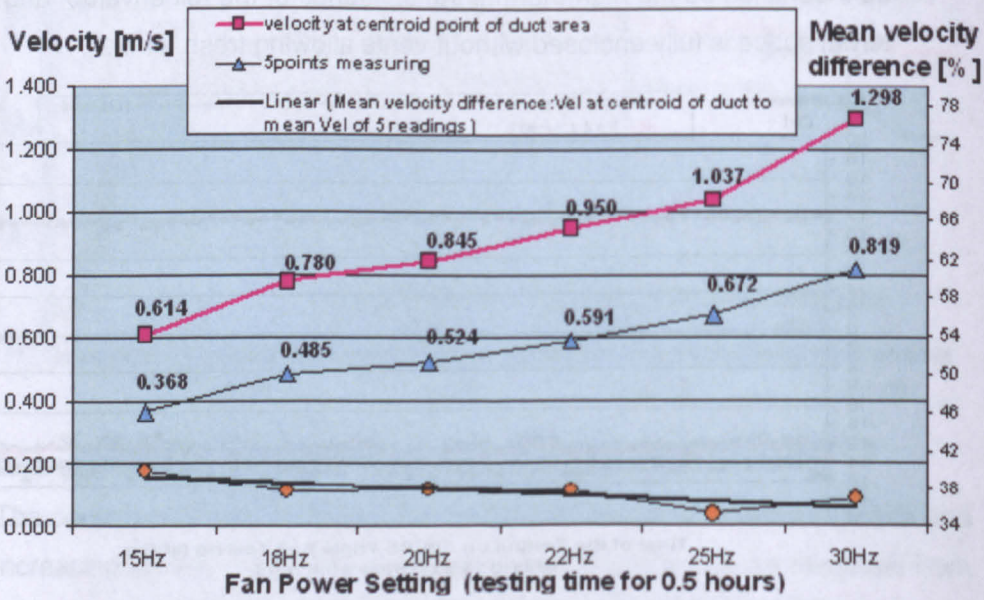

Figure 5-22: Results of the measured velocity at the centroid and mean velocity of 5 reading under different fan power settings.

5.6 Experimental Analysis and Discussion

In this section, the thermal behaviour of the envelope has been investigated for the condition, which incorporated the the water chilling process on the test rig. In line with the testing conditions without water cooling process, two typical thermal regimes were assessed: one is the test rig under direct beam radiation and the other is tested at a low level of radiation (that is, test rig is in shade).

5.6.1 Typical thermal behaviour patterns

For the external condition without direct light exposure, the influencing factor of simulated solar radiation can been reduced to minimum value. In Figure 5-23, a stable internal temperature distribution was recorded and it indicated that variations in the external air conditions did not appear to have a significant impact on the condition of the internal air temperature. At the meantime, the extent of the thermal laying was relatively weak, around average 1.5℃ difference between air temperature at the height level (i.e. Tai1, T^0ai1 and Tsi1) at hight of 1.45m and low level at the height of 0.3m (Tsi3).

As seen in Figure 5-23, the warm air at a high level inside the chamber had become more homogeneous when velocity at the inlet of cavity channel approached at 0.6m/s (fan-power set as 22 Hz). This suggests that the cooling effect provided by the airflow rate and water film is beneficial to the stability of the vertical air temperature stratification, which to some extent enhances the affect of buoyancy force inside this foil skin enclosure.

Under high radiation exposure (see Figure 5-24), the air temperature distribution under the influence of the water chilling process has differed markedly from that encountered in the test without chilling process (Figure 5-18). The air temperature distribution closing to internal layer of the envelope appeared homogeneous gradually at the horizontal direction (for instant, Tai2 at perimeter area developed to entangle with T^0ai2 at the centre of chamber) owing to the higher thermal dampening effect provided by two additional layers including foils, water film, and flowing air. On the other hand, the vertical stratification was strengthened in the area towards the back of the test chamber.

This cooling effect was subsequently enhanced by the thermal driven airflow in the chamber once the rooftop vent was opened, for an example, the airflow reading at the low level suddenly increased from average 0.1m/s to 0.18m/s.

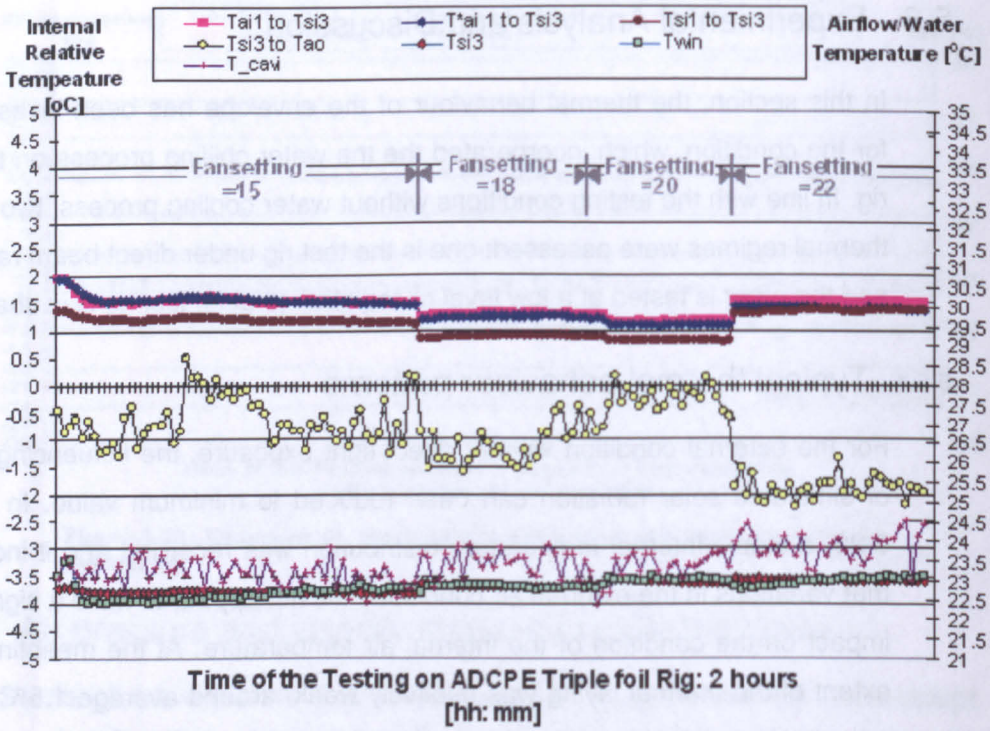

Figure 5-23: The typical indoor temperature stratification behaviour under influence of the air flow and water temperature fluctuation without direct beam radiation at WFR=0.7L/m

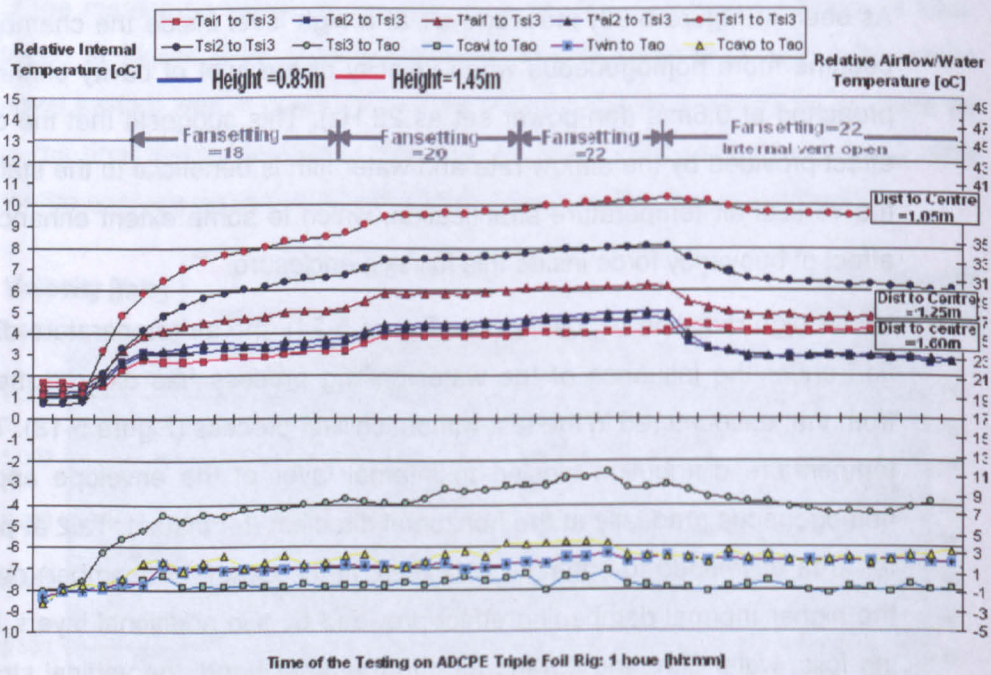

Figure 5-24: The typical indoor temperature stratification behaviour under influence of the air flow and water temperature fluctuation with direct bean radiation exposure at WFR=0.7L/m

At the specific height (i.e. 0.85m) Tai2, T^0ai2 and Tsi2 reduced by 2 ℃ in 5 minutes while the Tai1 started closing to T^0ai1 and the temperature gradient at height level (such as Tsi1) remained relatively same. Subsequently the tem-

perature difference between the high level and occupied zone was increased and "stack effect "was strengthened further.

It is shown in Figure 5-24 that the enclosed single volume of the chamber has been naturally subdivided into four thermal zones:

- *occupied zone*, which is driven by thermally-heavier-floor, at vertical range of 0.3m to 0.85m in this test case
- mid level zone, at the height from 0.85m to 1.45m
- *roof level zone*, where internal accumulative heat gathers up and is highly responsive to the transmitted magnitude of the thermal radiation, at the height above 1.45m up to 2.05m
- *envelope perimeter zone*, which is affected by the envelope condition with thermal homogeneous tendency, where temperature readings denoted as Tai1/2/3 corresponding to varying height.

Furthermore, the high contrast in surface temperatures of the inner foil at the envelop roof level seemed to beiflatten to some extent by the combination effect of the two cooling process (cool water spread and forced airflow induced convective condition in the cavity). The tendency of local turbulence commonly created by the high surface temperature difference was hence constrained. Figure 5-25 indicated the shading effect of the additional water film on the internal temperature variation. It was found that the wet fraction of the central foil surface varying from 75% to 85% (that is, water flow rate from 0.7 L/m to 0.9 L/m) seemed making a week impact on the overall temperature reduction.

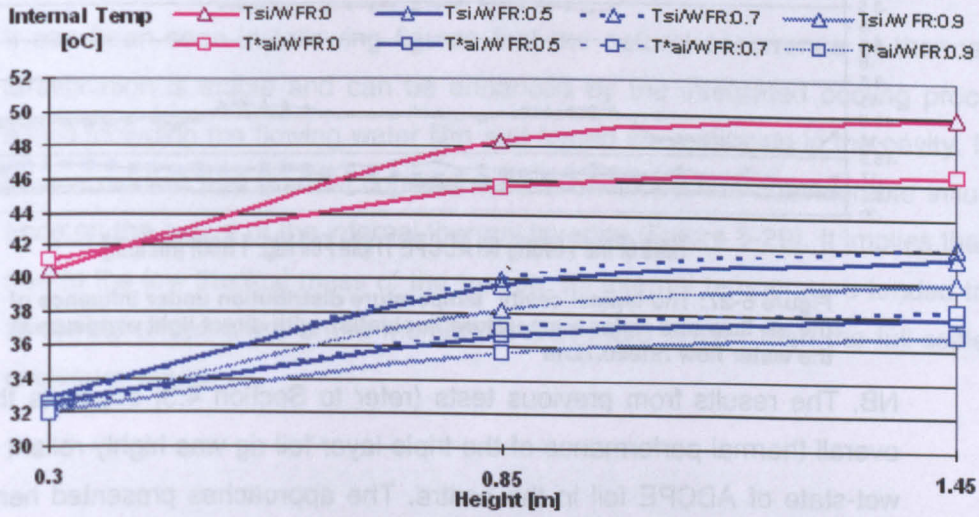

Figure 5-25: The typical indoor temperature stratification behaviour under influence of the wet coverage variation with direct light exposure.

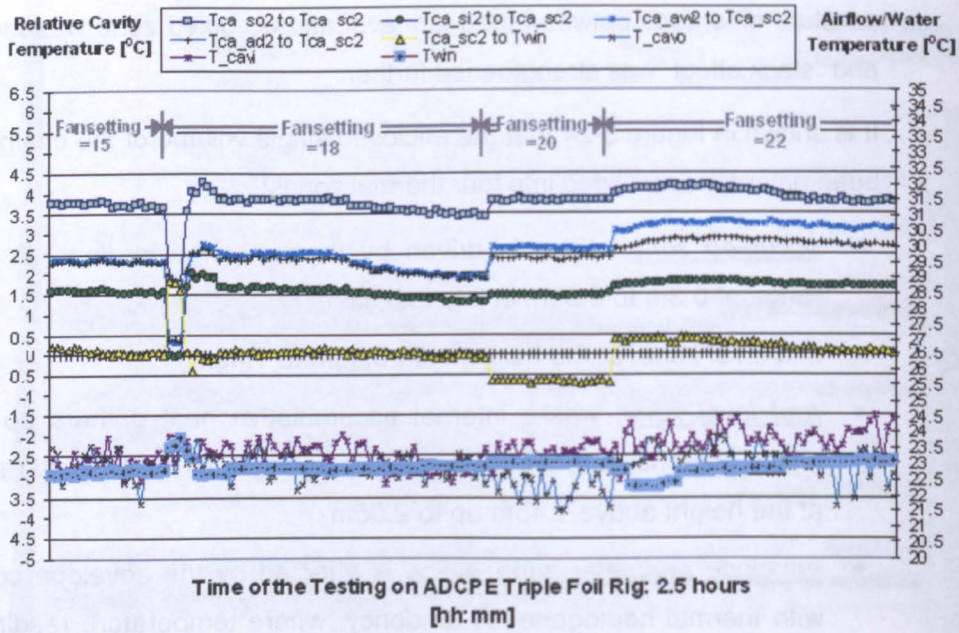

Figure 5-26: The typical cavity temperature distribution under influence of the air flow and water temperature fluctuation without light exposure at the water flow rate=0.7L/m. [NB. ca=cavity, o/i= outlet/inlet, sc=surface of centre-layer, ad=air in dry-channel, aw=air in wet-channel, win=water-inlet]

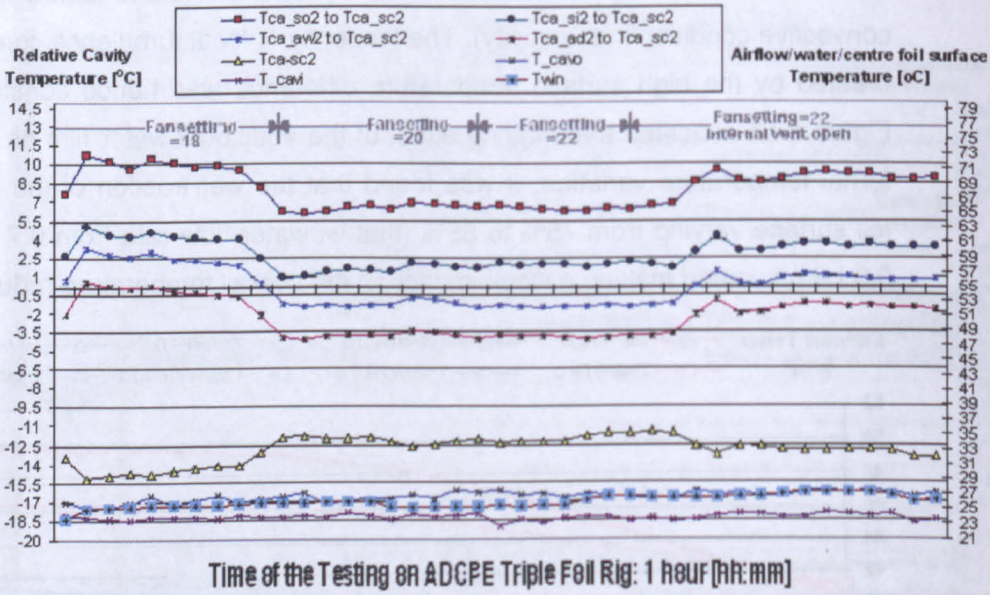

Figure 5-27: The typical cavity temperature distribution under influence of the air flow and water temperature fluctuation with direct light exposure at the water flow rate=0.7L/m

NB. The results from previous tests (refer to Section 4.3) suggests that the overall thermal performance of the triple-layer foil rig was highly reliant on the wet-state of ADCPE foil in the centre. The approaches presented here thus concerning the thermal behaviour to that of the centre foil.

Figure 5-26 displays that the air temperatures fluctuation in the two air channels has a dominant impact on the cavity temperature progress comparing with the temperature variation of supply water.

It can be seen in Figure 5-26 that surface temperature of central foil appeared relatively close to that of flowing water film with less than 0.5℃ difference once no direct light radiation involved. At the same time, the surface temperature gradient of outer foil and inner foil coincided with the trend of air temperature progress in the cavity, which was a result of the combination effect of the evaporative cooling and air-cooling due to high flow rate.

With high light radiation, there is a pronounced thermal shading effect due to the additional layer of water film results in up to a 6℃ surface temperature difference between the outer foil and inner foil (Figure 5-27). For the cavity under dominant convective condition without the influence of the radiation, the magnitude of surface temperature difference was less than 2℃ (Figure 5-26). Moreover, up to 2℃ difference between the air temperature in dry channel and wet channel proved the effective thermic property of the additional water layer on the central foil. As mentioned in Chapter 4, the thermal transmittance (for the wavelength of 1100nm to 2800nm) of the triple foils (ADCPE film) reduced from 78% without water layer to 17.7% with water layer.

Figure 5-28 and Figure 5-29 visualizes the overall typical thermal behaviour pattern mentioned as above for the typical test setting-up: fansetting is 20Hz (which is 0.524m/s at the inlet of the air channel); water flow rate is 0.7L/m (the temperature of supply water at the inlet is from 23 ℃ to 25 ℃).

It can been seen in following figures that the natural occurrence of thermal stratification is stable and can be enhanced by the integrated cooling processes including the flowing water film and forced air ventilation in the cavity. It is also evident that thermal condition of the envelope has considerable influence on the extent of the internal thermal layering (Figure 5-29). It implies that due to the low thermal mass of the test rig, its internal temperature tended to follow the temperature of the membrane skin more closely than the full-scale enclosure would.

Thermal behaviour of test rig under convective condition in the cavity without cooling water layer involved:

- A greater influence of radiative heat transfers on the surface temperature than convective transfers in the cavity. The airflow generation in the cavity is found not sufficient to decrease the surface temperature of the envelope and the integration of appropriate chilling measures for a foil cushion construction is necessitated
- Strong internal thermal stratification and high contrasting surface temperature of rooftop level

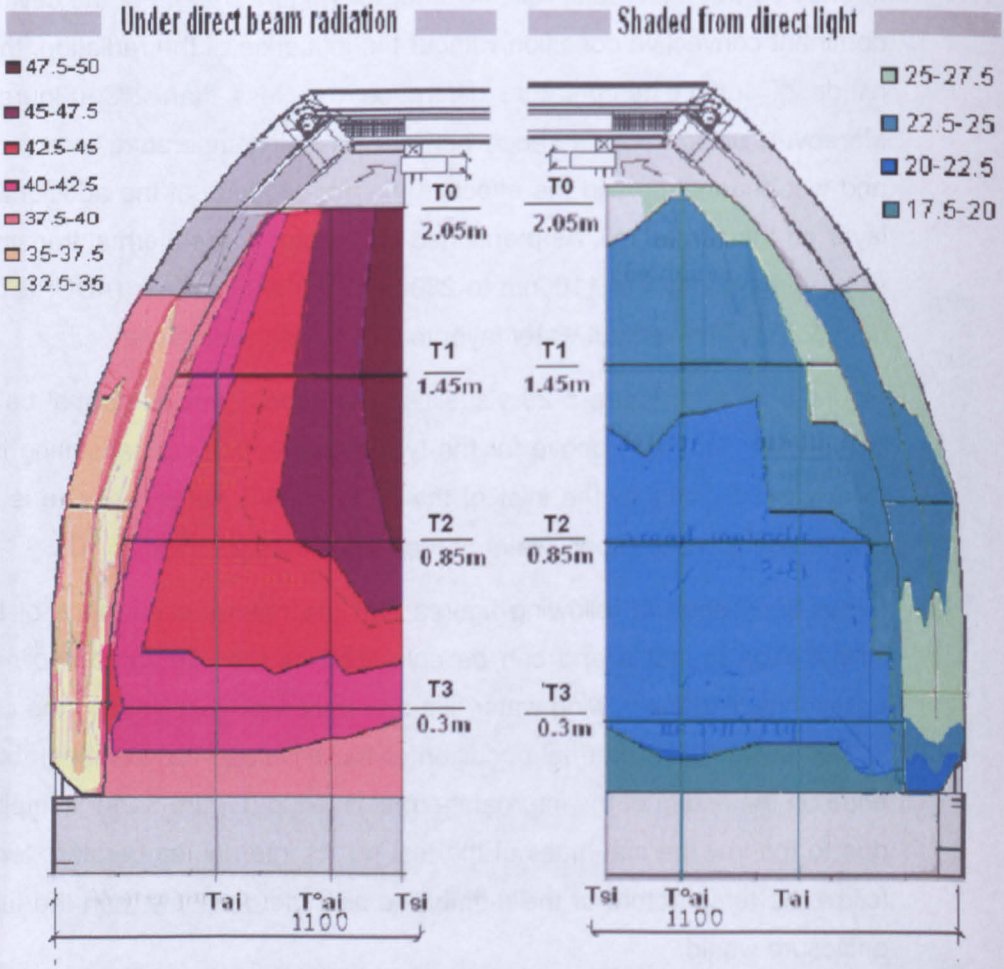

Figure 5-28: The typical temperature distribution on the test rig without flowing water layer in the cavity for various external radiation conditions at the Fansetting=20Hz

Thermal behaviour of the test rig under the combination affect of the airflow and additional cooling water layer in the cavity:

- High contrasting surface temperatures at the roof level being flatten. Reduced envelope temperature in favour of the stability of the vertical air temperature stratification and consequently enhancing the affect of buoyancy force in the chamber.

- Four thermal subdivisions naturally formed in the chamber and the tnermall zone around envelope perimeter following a close relationshiop to the envelope condition and having thermal homogeneous tendency

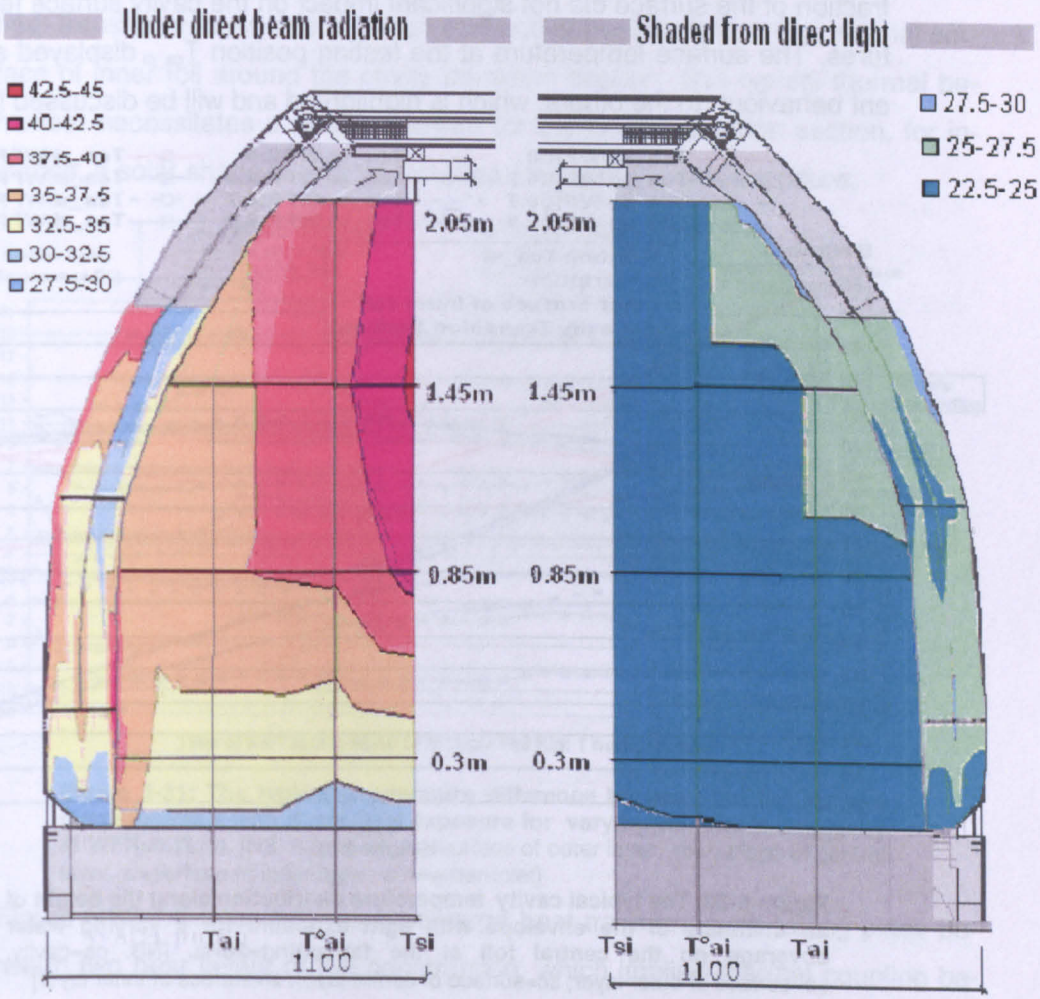

Figure 5-29: The typical temperature distribution on the test rig with flowing water layer in the cavity for varying exteran radiation condition at the WFR (water flow rate)=0.7L/m and Fansetting=20Hz

5.6.2 Relationship between the surface temperatures of the triple foil layers and thermal behaviour

For a series of airflow rates and water flow rates, the correlation between these surface temperature measurements and simulated test condition was investigated in order to assess the thermal improvement that the novel envelope system could be provided.

Figure 5-30 illustrates the typical surface temperature evolution along the height of the cavity for a varying water flow rates (from zero to 0.9L/m) in the presence of light radiation. Except for the outer foil layer, the cooling effect provided by the flowing water layer on the overall surface temperature of the cavity performed similar to that on the internal temperature: the increasing wet fraction of the surface did not significant impact on the cavity surface temperatures. The surface temperature at the testing position T_{ca_si} displayed a different behaviour to the others, which is highlighted and will be discussed later.

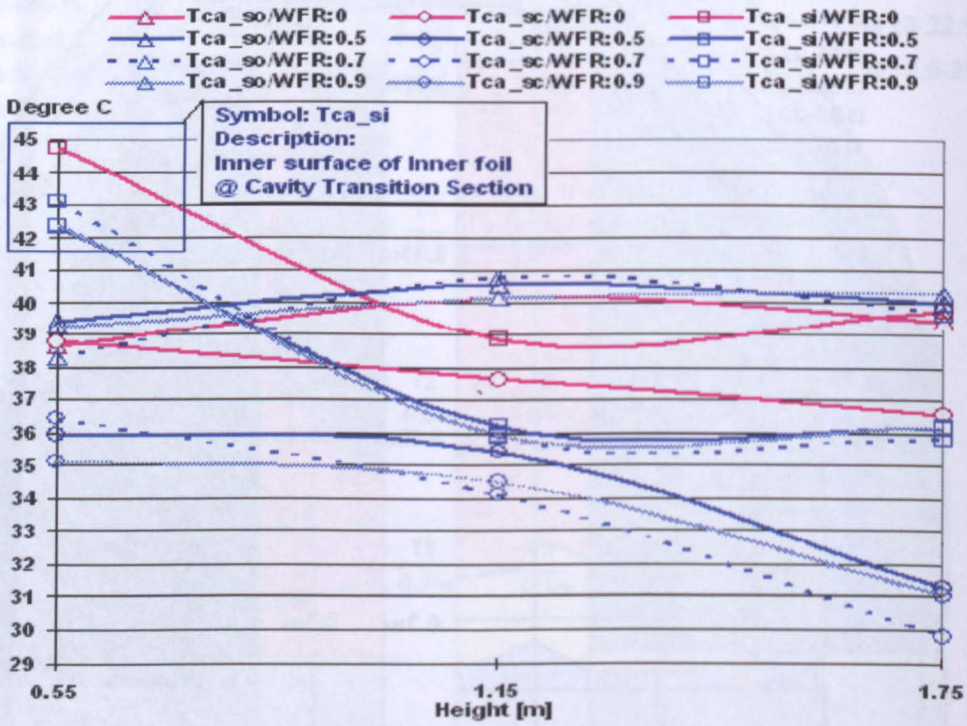

Figure 5-30: The typical cavity temperature distribution along the height of air channels of the envelope with light exposure for a varying water coverage on the central foil at the fansetting=20Hz. [NB. ca=cavity, so=surface of outer layer, sc=surface of centre layer, si=surface of inner layer]

Figure 5-31 illustrates the effect of external radiative heat transfer on the deviation of the foil surface temperatures from a theoretical median temperature, which expressed as the average temperature between external and internal

air temperatures (i.e. T_{med}). The median temperature approach assumed that the foil layers were under pure convective heat transfers. It is worth notting that the deviation is only representative of the effect of radiation exchanges on the foil thermal state and this approximation however does not account for the asymmetric convective heat transfers on opposite sides of the membranes. In case of the central foil, the results deduced from the real median temperature (T_{conv_sc2}) displayed slightly different behaviour from that from the theoretical temperature (T_{med}).

In Figure 5-31, it can be seen that unlike other surface temperature on inner skin area, the inner surface at the transition section displayed a distinct thermal responsiveness to radiative transfer variation. Under direct beam exposure, the temperature difference ($T_{ca\text{-}si3}$ to T_{med}) indicated a strong radiative heat transfer process and a limited convective transfer rate at the internal surface of inner foil around the cavity transition section. This typical thermal behaviour necessitates a detailed design for the cavity transition section, for instance, a solar shade to pretect this area from direct beam exposure.

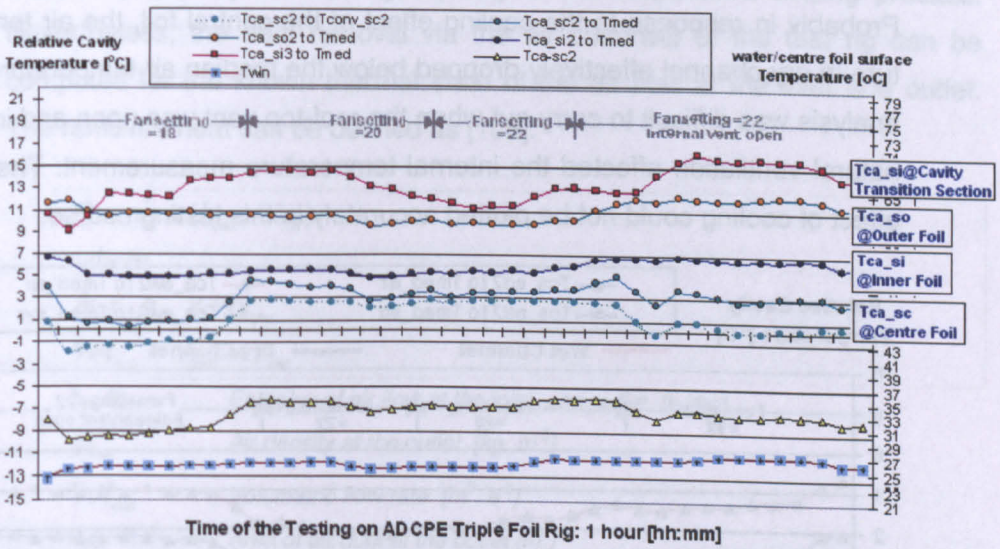

Figure 5-31: The typical temperature difference between the foil surface temperatures a with direct light exposure for varying velocity in the cavity at WFR=0.7L/m. [NB. ca=cavity, so=surface of outer layer, sc=surface of central layer, si=surface of inner layer, win=water-inlet]

Figure 5-32 indicates that relatively large heat transfers were taking place between two near layers of the construction, which implied thermal coupling between them. Two theoretical temperatures were used to compare between the air temperatures in the two channels (dry channel and wet channel) of the cavity in order to distinguish between convective and radiative exchanges:

- *Tmed_air*: The median temperature between the outdoor and indoor air temperature.
- *Tmed_s* (w: wet channel, d: dry channel): The median temperature between the surface temperatures of the two adjacent foils surrounding the channel (either wet or dry channel) of the cavity.

The value of the cavity air temperature in the wet channel relative to the median air temperature appeared high during the hours of light exposure (see Figure 5-32, red curves). On the other hand, in the dry air channel this value remained constantly low, indicating reduced influence of radiative transfer. Moreover regardless of the air channel, both median surface temperatures deviated markedly from the corresponding channel air temperatures implying equally weak influence of convective transfer (Figure 5-32, red/blue curves with dot markers). It could therefore be assumed that radiative heat transfer process was predominant particularly in the wet air channel and a thermal coupling would be expected to take place between the two surrounding foil surfaces.

Probably in response to the cooling effect of the central foil, the air temperature in dry channel effectively dropped below the median air temperature. The analysis was difficult to carry out when the roof-top vent was open and internal natural ventilation affected the internal temperature measurement. There the effect of cooling could not be plotted accurately in this testing course.

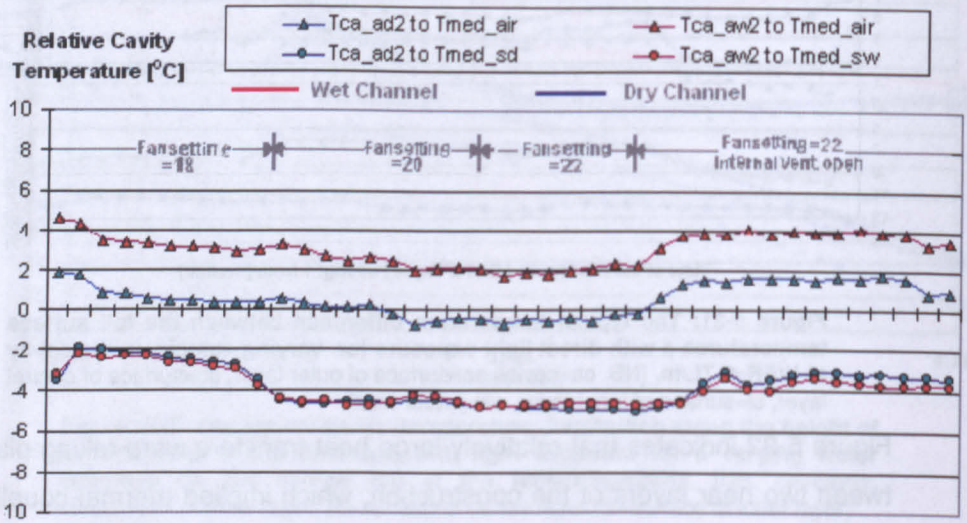

Figure 5-32: The typical temperature difference between the foil surface temperatures and the internal air temperature with direct light exposure for varying velocity in the cavity at WFR=0.7L/m. [NB. ca=cavity, ad=air in dry-channel, aw=air in wet-channel]

Figure 5-32 indicated that convection did not dominate the heat transfer tooking place in the dry air channel, as it would have cause closer relationship between the air temperature and the surrounding surface temperatures.

It is because that the ADCPE foil is not opaque to long-wave radiation, that is to say, it was not possible to isolate clearly the effect of convection and long-wave radiation exchanges between the foil skins. Hence due to all difficulties in experiments as mentioned above, quantitative analysis poses a demanding on a detailed theoretical description of the heat transfers governing their thermal balance in order to better assess these heat transfer processes.

5.6.3 Cooling performance

5.6.3.1 Cooling production

Unlike that in a commercially available evaporative cooler, the evaporative cooling process in the air channels of the novel foil cushion construction involves radiative exchanges through its transparent skin. Thus it is difficult to accurately quantify the cooling capacity of the evaporative cooling process. Nevertheless, the heat removal via the air channels of the test rig can be computed for the known thermal state of the air flow at the inlet and outlet. The removed heat can be defined as [103]:

$$Q = \dot{m} \times (h_{out} - h_{in})$$

where

$$\dot{m} = \rho_{out} \times Vol_{out}$$

$$Vol_{out} = A_{out} \times v_{out}$$

h_{in}, h_{out}	*Enthalpy of air flow at the inlet and outlet [kJ/kg]*
ρ_{out}	*Air density at the outlet [kg. m^{-3}]*
Vol_{out}	*Volumetric flow rate [m^3. s^{-1}]*
A_{out}	*Area of air duct at the outlet [m^2]*
V_{out}	*Velocity at the outlet [m. s^{-1}]*

Equation 5-4: Calculation of the removed heat from the envelope cavity

For known humidities (i.e. Po, Pi) in the two air-ducts and the temperatures (i.e.Tcavo, Tcavi), the corresponding enthalpy (i.e. h_{in}, h_{out}) can be obtained from a psychrometric chart. The results are presented in Table 5-10.

Table 5-10: Examples of calculation results of the novel foil cushion construction integrated evaporatie cooling process

Parameters	Fansetting=18 Hz	Fansetting=20Hz	Fansetting=22 Hz
Area of Air-duct [m2]: Aout	0.001257	0.001257	0.001257
Velocity [m/s]: Vout	12.14	13.82	15.24
Enthalpy [Kg/Kg]:			
hin,	35.96	36.34	36.09
hout *	40.59	40.38	40.46
Heat Removal [W]:			
Q	82.64	81.86	97.48

Notes:
The initial water temperature for the course of the test is 23.3 degree C.
The test condition was set as water flow rate at 0.7L/m
** : hout is calculated the working air enthalpy at the outlet of the air cavity.*

It is found in the above table that the total removed heat increased significantly when fan power was set higher. R. Tang and his fellows elaborated that the water evaporation rate for a water free smooth surface (like the case in this test) was much higher than the common porous wetted surface when the air flow crossing the wet surface was more than 1.16 m/s [90]. In the case of this test rig, the maximum velocity of the air channel was measured as 0.6m/s at the inlet of the air passage for fan-setting at 22 Hz. The average velocity in the diffuser-shape air channel made up 55% of the inlet velocity according to computation results. It suggested that the cooling performance of the test rig was far below the optimal level. In order to reach an average 1m/s in the air channel, the inflation pressure in this test system would need to double the magnitude of 360 Pascals gauge pressure, which is above the pressure limited accommodated by this test rig. The interaction between the inflation pressure and air flow state has been illustrated in Figure 5-12.

5.6.3.2 Risk of surface condensation

As discussed in Section 4.5.4, the general risk of surface condensation is generally low when the foil cushion glazing system is under high light radiation. Because the foil cushion enclosure is classified as a naturally ventilated building with low occupancy, the analysis of the condensation risk tends to use the external air as a more stable reference. Figure 5-33 displays the typical range of deviation of the foil surface temperature from the external air. For such a small thickness of flowing water film (around 0.11mm), the central fiol surface temperatature seems responsive to the external radiation rapidly as its variation wang bwteenn 5℃ and 11℃ higher than the external sir. Or the in-

ner fiol surface, the range of the deviation was up to 14℃ because of tis complicate heat exchanges with the airflow and flowing wate film in the cavity.

Nonetheless, when the test rig was shielded from the direct light source, the thermal state of the inner foil surface was relatively close to the chilling water temperture, with a maximum 2 ℃ difference. Based on the water assessment in Section 4.3.3 , the occurrence of surface condensation of this type of foil cushion construction can be assumed as minimum of the smulated critical summer weather in the UK.

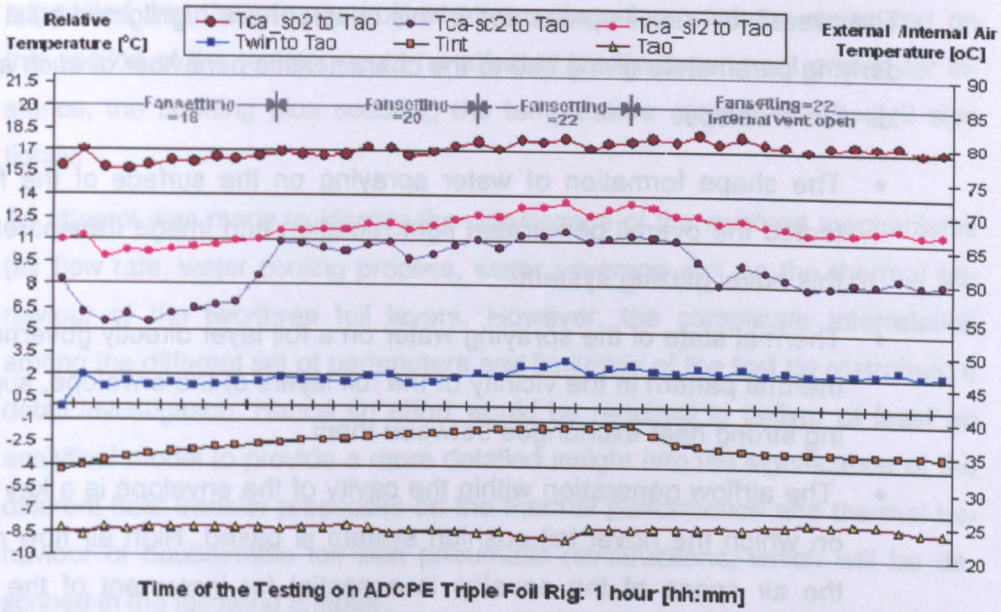

Figure 5-33: The typical temperature difference between the foil surface temperatures and the external air temperature with direct light exposure for varying velocity in the cavity at WFR=0.7L/m

5.7 Conclusions and Suggestions

The experiment of a typical triple-layer foil skin pneumatic construction incorporating a water cooling process was presented in this chapter. The observation of its thermal behaviour was considered as a consecutive part of Chapter 4 to investigate the interrelation between the different sets of parameters to identify a clear relationship among the thermal behaviour of the multiple foil layers under the influence of the water cooling process. Their correlation with the external and internal air temperature would further elucidate the influence of the membrane surface temperature variation on the thermal behaviour of the space it encloses, in particular on the extent of stability of the vertical tem-

perature stratification (which tends to develop naturally in such a typle of enclosure with large single internal volume).

Two air channels constituting the envelope of the novel construction were ventilated by a centrifugal fan. The selected ADCPE foil was used to create the prototype of a typical ETFE triple-layer foil cushion construction integrated with a water cooling process. The thermal effect of an additional water film flowing on the central layer is the focus of the assessment in order to clarify to what extent the over-heating control in foil cushion enclosures could be enhanced by the proposed envelope construction.

The overall test results presented in this chapter have highlighted a list of underlying parameters giving rise to the characteristic behaviour of such a novel foil skin envelope:

- The shape formation of water spraying on the surface of the foil affected the overall penetrated light radiation and image transparency of this novel glazing system.
- Thermal state of the spraying water on a foil layer directly governed the thermal pattern in the vicinity of the foil layers of the envelope, suggesting strong heat exchanges between them.
- The airflow generation within the cavity of the envelope is a key factor on which the novel foil cushion system is based. High air flow rate in the air space of the envelop is essential for increment of the water evaporation rate and heat removal from the cavity of this type of envelop.

It was found that the radiative exchanges were dominant in the two air channels of the novel construction and further shifted towards outside owing to the additional water layer. Thanks to the thermal dampening effect of the central foil with a cooled water layer as well as airflow in the cavity, the inner foil experienced smaller temperature swings than the outer layer foil.

In terms of the internal thermal environment of the test chamber, the analysis of the test results showed that under the combination of effects from the airflow and water layer the internal thermal zoning appeared as four subdivisions (occupied zone, mid level zone, roof level zone, and envelope perimeter zone). Unlike common thermal pattern in a foil skin enclosure, the perimeter zone had the tendency towards thermal homogeneity without high contrasting

surface temperature along the vertical height. This behaviour implied the reduced possibility of local turbulence around the inner skin and thus the desirable vertical thermal stratification could be stabilized.

Following water spraying, the surface temperature reduction of the central foil was observed to be much smaller than that in the previous small test mode (refer to Section 4.3.4) and so was the inner foil. It might be the results of the relative thin water layer formation on the surface of the central foil by around 0.11mm compared with 1 to 2 mm thickness of water layer in the small model, whereby only a small thermal inertia was added into this system. It is also suggested that the accuracy of extreme surface temperatures measured on this section of the test rig would be affected by the experiment errors, for instance, the bonding glue securing the temperature sensors on the foil skin tightly.

An attempt was made to identify the significance of the involved mechanisms (air flow rate, water cooling process, water coverage etc) on the thermal behaviour of the two/three foil layers. However, the complicate interrelation among the different set of parameters and limitation of the test rig restrained a detail investigation. Hence an effort would be required to deliver at least an analytical model to provide a more detailed insight into the significance of the different heat transfer processes on the thermal performance and thermal behaviour of double/triple foil skin pneumatic constructions, which will be described in the following chapter.

CHAPTER 6
ANALYTIC MODELLING OF THERMAL BEHAVIOUR OF THE EXPERIMENTAL FOIL SKIN CONSTRUCTIONS

> *"Sharp tools make good work." ("工欲善其事，必先利其器。")*
> --- **Confucius**

6.1 Introduction

The thermal behaviour of the foil skin pneumatic construction incorporating a water cooling film had been studied and results were discussed in Chapter 4 and Chapter 5 in accordance with both indoor full-scale structures and small test models in more controlled conditions. In the presence of the water layer coupled with airflow in the cavity of the envelope, the internal thermal environment of the enclosed space has been meliorated according to the experimental data:

- The large variation in internal surface temperatures had flattened out and it followed a close thermal relationship with that of the foil with a water layer and airflow within the cavity. This thermal phenomenon discourages the recurrence of local turbulence developed at the low level of the internal enclosure, which is generally originating from a large contrasting surface temperature of the foil skin roof.
- A large reduction in infer-red radiation penetration through the envelope resulted in up to 10 ℃ drop at the occupied zone of the foil skin enclosure while the transmittance of the desirable short wave radiation remains high.
- A strong thermal stratification has been enhanced in the central area of the enclosure as the thermal sub-homogeneous zone developed around the perimeter of internal skin by the cooling water process. The envelope perimeter zone is functioning as a natural homogeneous thermal buffer zone so that the influence of the external thermal varia-

tion on the internal thermal condition can be constrained to some extent.

- For the triple-layer foil skin construction, the better control of surface condensation has been achieved at large than that of the double-layer construction.

In the pool of knowledge currently available to the design community, this novel type of envelope has provided limited tools in the prediction of the thermal behaviour of the foil skin pneumatic envelope itself due to the complexity of the heat transfer processes involved and thermal phenomenon highlighted as above.

In the commercially available analysis packages for building environment designs, the field of Computational Fluid Dynamics is generally applied to the analysis of relatively small-scale enclosures in the building industry. However as the facts highlighted in Chapter 3, early approaches adopted for predicting the thermal behaviour of tensile membrane structures based on U-values, and shading coefficients have proved inappropriate. It was proposed that more accurate description of their thermal behaviour would be offered to account for their surface heat transfer at any instant and their characteristic thermal-optical properties.

Some alternative approaches used to inform design processes have been explored by early researchers. Three popular mathematical methods of the dynamic modelling of membrane skins were applied to an air-supported enclosure: the finite difference method (developed by ABACUS at Strathclyde University), the response factor implemented by Granlund (UK) and the admittance method, developed by CIBSE (UK) [1]. However, it was reported that they were based on the detailed modelling by using a built-in model (empirical combined heat transfer coefficients), which were originally designed for thermally heavier constructions.

Another attempt carried out by Hart et al. was to develop a model using a modified version of the DOE-2.1 that the membrane skin roofs had been treated as window glazing panes. U value and solar shading coefficients were only accepted to define the heat flux through the glazing panes. The impacts of various internal loads had been accounted by the use of alternative combined heat transfer coefficients in this approach. But the validity of this model

was complicate and "*more field data and experimental should be obtained*" [105].

The preliminary study on both the thermal and optical performance simulation of ETFE foil cushions carried out by Harris Poirazis, *et al.* [13] was about to assess the impact of external longwave radiative exchanges on their resulting thermal performance. *A* three-layer ETFE cushion element had been modelled by a dynamic thermal model for the scenario of a warm sunny summer day and treated as an advanced glazing element allowing for long wave transmission. Its non-opacity to long wave radiation was evaluated while the fritted interlayer in the cushion was opaque to the longwave. The main outputs of the simplified model were the ETFE layer surface temperatures and heat fluxes via the cushion element.

The simulation results obtained from the model indicated an insignificant impact due to the long wave transmission behaviour on the resulting thermal performance of the foil cushion when exposed to solar radiation condition. The only possible contributor to the increase of long wave heat transmission was due to the optical nature of ETFE, the longwave transmittance, which was arbitrary set as 0.2.

Nevertheless previous literature reported a strong effect of thermal coupling existing between the layers owing to the high emissivity of membrane skin, which resulted in similar surface temperature of the layers in the heat transfer balance (Cf. Section 3.2.2). This specific thermal behaviour of the membrane skins augmented the long wave radiative heat exchange between the cushion roof and the internal environment. But ignoring of this factor caused a considerable underestimation of the longwave transmission. Moreover another contribution to such under-estimation in the Harris' method could be the simple use of one air temperature defining the internal and external thermal condition in the model, which may also result in an under-prediction of the natural convective heat transfer on the cushion and an unrealistic description of internal air temperature distribution.

Nevertheless, a significant improvement of Harris' study was that the emphasis of the thermal analysis moved away from the conductive process in the membrane construction and looked into the dynamic radiative and convective heat transfers between the membrane skin and its environment (see Section 3.2.2.1). The validation of the model is difficult because *"this output is purely*

indicative" and *"Tentative models did not provide confidence in the applicability of the tool for the different boundary conditions and further work is required."* [13] .

Early attempts on the dynamic modelling of membrane skins were either based on the assumption of uniform internal air temperature distribution or regardless of the impacts of variations in the high internal thermal condition.

An important effort made by Harvie, was to develop a dynamic detailed thermal model (refer to Section 3.2.2.1), which focused on the surface heat transfer process on the membrane surface. The convective heat transfer between the membrane skin and the enclosed space was modelled separately (by a commercial airflow analysis package FLOVENT, based on a number of empirical models). Most characteristics conditions were encountered during his test cell monitoring, including a stratified configuration was considered. The two main outputs were the predicted surface temperatures of each layer and the prediction of heat fluxes through the roof element.

The internal stratification corresponding to hotter clear days was reported to be under-predicted in this model. Due to the limitations of the available CFD analysis code (only allowing for relatively coarse meshing to be achieved and consequently having the difficulty of implementing passive buoyancy driven flows) and neglecting the importance of external thermal radiation in the prediction of buoyant airflow in the enclosure, as highlighted in recent research work [106].

Following Harvie's study, Thaibault developed the sensitivity of the model and extended it to evaluate the thermal performance of double-layered membrane constructions. Some conclusions from his modeling work have been regarded as a referenced basis in the analytic modelling of this research (refer to Section 3.2.2) on grounds of the relevant findings reaffirmed in the experiments of this research project.

In comparison to the numerical model developed by Thaibault for typical textile membrane skin buildings, this analytical model involves more intricate processes in the novel foil cushion construction, and thus required more customised specification and particular expansion for the case of triple-layered foil construction in order to fulfil the research objectives in this chapter.

Last but not least, because of the high thermal responsiveness of foil skin to the surrounding environmental variation, an accurate prediction of surface temperature of the internal foil layer is fundamental for the reliable estimation of the level of thermal comfort experienced by the occupants.

This chapter describes the implementation of an analytical model on the basis of Harris', Harvie's and Thaibault's work for the simulation of thermal behaviour of a double/triple-layer foil skin pneumatic envelop with an additional water layer and the evaluation of the impacts this behaviour may have on the thermal environment of the space they enclose. The main outcomes are the surface temperatures of each modelled foil layer and heat fluxes through its roof units of the foil skin model.

6.2 Objectives

The aims of the analytic modelling presented in this chapter were the following:

- To predict the thermal behaviour of double/triple-layer foil skin pneumatic constructions based on their surrounding environmental conditions
- To indicate the impact of the additional water layer on the overall thermal performance of the foil skin construction in more detail.
- To develop a tentative tool from which a bespoke numerical modelling can be initiated for this particular construction case to serve the purpose of delivering confident information for a design process.
- To provide informative boundary condition so as to assist in the prediction of the internal thermal environemnt of enclosures clad by this novel foil cushion system.

6.3 Approach Adopted in the Thermal Behaviour Prediction

6.3.1 General description

Due to the limitation of current commercial fluid simulation packages, Harvie and Thaibault suggested and developed an alternative approach which coupled with external boundary and flow models, allowing both models to operate and develop independently, and exchang data with each other in a predefined

way. This proven method laid a ground for the thermal behaviour simulation processes presented in this chapter.

The general approaches adopted in the analytic modelling process are described by the three major parts:

- the proposed format of the analytical model, which is illustrated schematically in Figure 6-1
- constituted modularity, and
- comparative study

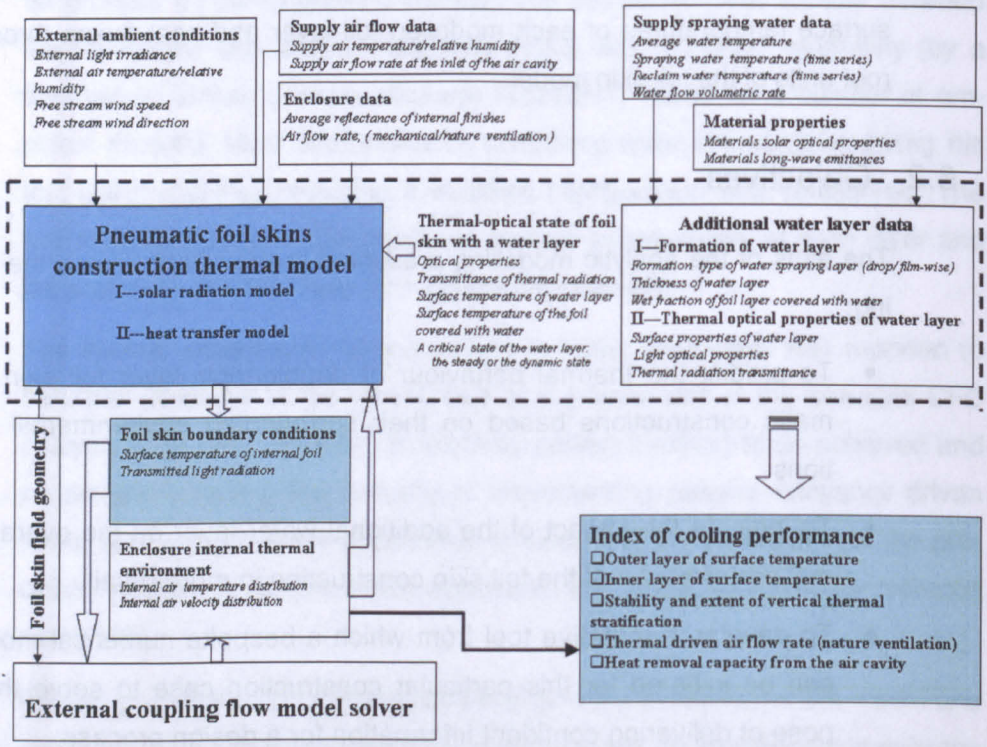

Figure 6-1: Suggested data flow between the thermal model of the proposed foil skin construction and other components in the analytical thermal model

The analytical model is developed based on the model suggested by Harvie. The thermal state of an additional water layer has been incoporated in the data base of the thermal model for this foil skin construction, including imperative parameters regarding the water layer investigated during the course of this research.

The analytical model is implemented in a spreadsheet format followed the suggestions from Thaibault. It is advantageous that this format allows a reasonable trade-off between usability, expandability and computational performance to accommodate further developments in a bespoke model for this novel

type of buildings. In addition, the considerable computational overhead incurred by this programme can greatly simplify the alteration and testing processes of the model for the current development stage without requiring in-depth knowledge of the programme language. In brief, the implementation of this chosen model format is to provide a user-friendly method, which allows a quick visual display of the calculation output and statistical analysis of the involved data.

Modularity is one major characteristic of the analytic modelling. It is reiterated that the aim of this analytical model is only to serve as the purpose of assisting the assessment of the impacts of varying energy transfer processes, which are affected by an additional water layer and forced airflow within the envelope, on the overall internal thermal environment of an enclosure. A modular system constructed in this process could provide the desirable means on assessing the sensitivity of the computation evaluation for every participating heat transfer process in the thermal equilibrium of the foil penal individually. It thus could assist to identify the contribution of the different heat exchange for the different configuration of foil cushion construction as well as the relevance of various modelling assumptions on its accuracy.

Finally, the surface temperatures generated from the analytical thermal models were compared with the test results obtained in the course of this research. The analytic modelling were checked against the data from the experiments of double-layer foil skin enclosure (refer to Chapter 4) and triple-layer foil skin test rig (refer to Chapter 5) respectively. Moreover, a set of parameters used in this model was at same time verified against the data from the small scale tests (see Chapter 4).

The results of the comparative analysis are presented in Section 6.5.

6.3.2 Assumption on the thermal behaviour of the foil skin envelope with a water layer

This analytical model was developed to predict the surface temperature of an internal foil penal and assess its thermal contribution on the internal environment of the space enclosed by this novel envelope. There were considerably complex heat transfer processes involved in thermal prediction, as described in previous section. As a result, a series of assumptions and constraints were incorporated into the model to simplify the modelling process in the light of the

current knowledge ragarding the thermal performance of the foil cushion construction and the the experiment results obtained during the course of this research. The assumptions are listed as follows:

- The geometry field of foil skin was broken down into a series of finite element (discrete panels), each of them with uniform material properties and independent thermal behaviour to the adjacent panels, assumed the thermal behaviour of foil skin panels is discrete.
- High responsiveness to energy exchange process was accounted for in the heat balance for each element of the pneumatic foil skins construction. It was proved during Thaibault's monitoring project the that the thin foil panel could quickly reach its thermal temperature equilibrium due to its negligible thermal mass and the small cross section of the foil panel.
- Insignificance of the thermal capacity of foil membranes on their thermal behaviour was assumed (Cf. Section 3.2.2). The temperature gradient cross the section of foil panels was therefore taken as nil. It is taken into consideration that the temperature-changing rate between the foil surfaces and the surrounding materials (i.e. fluid, including air or liquid) entirely relies on the fluid boundary layers.
- Temperature gradient across the core of the combining material (water covered foil layer penal) is approximate to a negligible level at the thermal equibilium of a given foil penal (less than 1 ℃).
- Thermal conditions on the adjacent area of the surface boundary of the internal foil was considered as a thermal sub-homogeneous condition predefined by one internal air temperature or alternative empirical values derived from corresponding experiments. This assumption based on the observation from this research project suggests that the errors which occurred in the prediction of internal convective exchanges could be reduced, as the extent of internal thermal heterogeneous is estimated to decrease in the vicinity of the envelop perimeter. The depression of the convective transfer rate on the boundary of the internal foil layer could be assumed according to this method.

NB. Throughout the description of the thermal modelling process, the sign of the heat exchange rates q was designated as positive if the heat flow took place towards the surface (heat gain to the surface).

6.4 Fundamentals of Thermal Behaviour Modelling

6.4.1 Introduction

The thermal behaviour model of the novel foil skin penal includes two parts:

- short-wave radiation model, and
- heat transfer model

On the basis of the set-up procedure of laboratory experiments (see chapter 4, chapter 5), the intensity of light radiation incident upon the outer skin was simulated to the experimental ambient condition by average 600W/m^2 as a critical summer scenario of a warm sunny day in UK. In addition, the varying intensities of light radiation incident on the double curvature foil skin envelopes would be computed by this part of the model accordingly. Subsequently, the following simulation steps enabled the two processes, i.e. the shortwave energy transmission and the resultant longwave radiation exchange, to initiate respectively.

Despite the fact that the shortwave energy transmission is dominant in a warm summer condition, the longwave radiation exchange is affecting the resulting heat flow distribution which at large depending on the temperature differences between the various foil layers (which may include fritted and thus absorbing layers), the internal surfaces of the enclosure, the sky and any surrounding buildings.

The heat transfer model considered the heat balance for each of the component foil layers on gounds of the low capacity of the foil membrane. The heat balance included the radiative and convective heat transfer. The calculation results from the net heat transfer between the foil layer and its surroundings were subsequently participating in the prediction of its equilibrium surface temperature. At the thermal equilibrium of the foil panel, it was neither losing nor gaining heat to its surrounding, and the internal surface temperature of the internal foil panel could be computated. The equilibrium temperature was tracked in the heat flow model over simulation timesteps, and a good approximation of its transient thermal behaviour could be found.

Regarding the additional water layer, it was acting as a functional coating on the attached foil penal (see Chapter 3) in the short-wave radiation model. It is proven to maniplate overall shortwave transmittance of a foil penal depending

on the formation type of water layer, i.e. film-wise or drop-wise, which have been compiled in the database of material properties.

For the heat transfer model, the water layer affected the thermal behaviour of the envelope in two critical states:

- *The dynamic state*, at which a portion of the heat gains in the foil skin penal is absorbed by the cooling water layer and participates the evaporation and air convection process at the meantime when the thermal condition in the air cavity is under favourable low humidity and airflow rate. The surface emissivity of the foil penal is modified and radiative heat transfer is enchanced. Meanwhile the thermal state of the water layer evenly spreading on the foil surface, particularly a constant flowing water film generated in the triple-layer model, affects the water convective transfer rate and the heat exchange between the foil layer and water layer. In the double-layer model, merely evaporation process is considered as only a drop-wise water layer is formed. The water drop layer is designated to stay in the same shape and detain on the foil surface until complete evaporation. At its transient heat balance moment, a rational low equilibrium surface temperature of the combined material of waterlayer and foil can be attained. The maximum drop of the equilibrium surface temperature could be verified by experimental observation.
- *The steady state*, at which the evaporation process is depressed due to the high humid and not-well-ventilated condition in the air spaces of the novel envelope, in the meantime the waterlayer is detained over on the foil surface with a uniform spread. It occurred after a period of time whe the water spraying was operating at low water flow rate. This experimental observation indicated a threshold value of evaporation rate in a typical designed novel envelope. The value is defined by its interrelation with heat gains of the cavity, water flow rate and air flow rate. At this state, the equilibrium surface temperature of the studied water/foil panel is obtained while the water layer is mainly functioning as a coating to alter the surface emissivity of the foil penal.

In the following sections, the specific methods adopted in each modelling stage are elucidated in more detail.

6.4.2 Description of the short-wave radiation model

The existing source of the short-wave modelling has proved a vast list of the empirical models to solve the specific requirements of these fields. The analytical model of the short-wave radiation presented in the section has considered different circumstances of the existing empirical models and selected the most appropriate simulation techniques for the objectives of this study. The primary processes involved in this modelling aimed to determine the light irradiance on the external and internal surfaces of the foil panel at a given orientation. The simulation procedure follows the steps detailed as below:

6.4.2.1 Angle of incidence

The amount of light radiation reaching external surface of a foil panel depends on the position of the light source relative to the foil panel surfaces. The position of the solar simulator in the external space is determined in terms of *Altitude* of the solar simulator (α_s) and *Azimuth* of the solar simulator (α_z). When the azimuth of the foil panel (β_z) and inclination (β) are known, the angle of incidence (i) of direct light radiation incident on the external surface of the foil panel can be computed from [107]:

$$i_{sp} = \cos^{-1}\left[\cos(\alpha_s)\sin(\beta)\cos(\omega_{sp}) + \sin(\alpha_s)\cos(\beta)\right]$$

$$\omega_{sp} = |\alpha_z - \beta_z|$$

i_{sp}	*Angle of incidence between solar simulator and foil panel normal [degrees]*
α_s	*Solar simulator altitude [degrees]*
α_z	*Solar simulator azimuth [degrees]*
β	*Inclination of foil panel (tilt from horizontal) [degrees]*
β_z	*Panel azimuth [degrees]*
ω_{sp}	*Foil panel solar simulator azimuth [degrees]*

Equation 6-1: Angle of incidence of direct beam light on foil panel

NB. This angle of incidence of greater than 90° suggests that the external surface of the membrane is shaded and direct beam radiation received is null.

6.4.2.2 Intensity of shortwave radiation

The irradiation level in front of the foil skin enclosure is predefined as average 600w/m^2 (see Chapter 4). For a laboratory test, the external ambient condition is rationally treated as not being interfered by the attenuation affect of the at-

mosphere with large particles. The external light insolation is therefore seen as only direct beam (I_d), no diffuse component involved in the simulation.

6.4.2.3 Incident shrotwave radiation on the external foil surface

On the external surfaces, the overall short-wave irradiation is comprised of the following tow parts, such as intensity of ambient diffuse light radiation, and intensity of direct beam light radiation. Generally the diffuse light radiation simulation should account for the amount of the radiation reflected from the surrounding objects (such as ground, obstruction surfaces), which are simply defined by the relative view angle (view factor) that the foil membrane has to those surfaces. In this modelling procedure, the diffuse light part could be neglected because the specific laboratory set-up only had the direct beam light radiation simulated.

In the case of this research, the composition of the light radiation incident on the external surface of arbitrary tilt and azimuth is only consisted of the direct beam light radiation and its ground (or obstruction in the surroundings) reflected radiation. Considering the solar simulator in the experiments casting light rays approximately paralleling the ground level, the amount of radiation reflection from the ground is therefore seen as insignificant to the overall irradiance while the simplified model is of analytical purpose.

Because of the known angle of incidence and the position of the space geometry of the solar simulator, the incident direct beam of the incoming solar radiation can be found from [109] :

$$I_{direct} = I_d \cos i_{sp} / \sin \alpha_s$$

where

$$\alpha_s = 90^\circ$$

I_{direct}	*Direct beam radiation on panel [W.m^{-2}]*
i_{sp}	*Direct beam light angle of incidence on panel [degrees]*
α_s	*Solar simulator altitude [degrees]*

Equation 6-2: Direct beam irradiance incident on the membrane skin

6.4.2.4 Typical simplifying methods adopted in the simulation process

Considering the difficulties in the simulation of optical behaviour of the entire envelope, due to the innate complex curvatures of foil skin surfaces, an simplifying approach ws adopted by Harvie. It was that an approximate flat envelop panel of equivalent area was used to be representative of the average

optical behaviour of the double-curved foil panel as a whole. For a foil cushion enclosure, this approximation is rational because of the overall symmetric topology of a common foil skin envelope and the overall low angular optical selectivity of a foil cushion roof element so that the curvatures of a foil cushion envelope tend to balance out the variation of the overall light penetration. For a given light source the incident angle is generally varying on the curved foil surface, diffuse optical properties were therefore designated to this approximate flat foil panel.

Due to both the complex nature of the double-curved foil membrane and the scarcity of detailed optical information for the foil sample, a mathematical representation of the angular light optical properties was developed by Harvie [110]:

- Namely, the approximations of the angular light optical properties (or called generic angular light optical profile)

The diffuse light optical properties of the foil materials can be calculated knowing these properties, although technical information is also available from manufacturers. Following this operation, the predicted generic angular factors τi, ρi and αi with corresponding light incidence angle *isp* of the direct beam could be conveniently incorporated into the theoretical modelling process.

Finally, the penetrating light radiation through outer foil layer can be found from:

$$I^0 = \tau^k_{(i_{sp})o} \times \tau_{(0)o} \times I_{direct}$$

$\tau_{(0)o}$	*Near normal direct light transmittance of outer membrane layer*
τ^k	*Generic angular solar transmittance factor*
i_{sp}	*Direct light incidence angle on a foil penal [degrees]*
I_{direct}	*Direct irradiance incident on external surface of membrane skin [W.m^{-2}]*

Equation 6-3: Direct ligth irradiance penetrating the membrane construction [109]

6.4.2.5 Shortwave energy distribution within the foil skin construction

NB. The values and method used here are not the same as that used to predict the optical behaviour of the test cells (small-scale models), which were calculated based on actual foil orientations and angular properties.

In the case of the multiple-layer foil skin construction, the shortwave radiation is redistributed within the air spaces of the envelope depending on their optical

properties, and the thermal behaviour of the envelope has been influenced consequently.

As discussed previously, the curved nature of foil skin envelopes tends to even out the variation of the light radiation penetration by their inherent symmetry. Followed Harvie's simplified approach, a representative flat foil panel of equivalent area is defined to represent the average behaviour of the entire curved foil membrane panel. The representative foil panel is only considered to be with diffuse light optical properties.

The incident light radiation on the external surfaces either transmits into the envelope construction or is reflected back to the atmosphere. This part of transmitted radiation energy follows a journey undergoing successive reflections between the foil layers and between the foil skin and the internal surfaces of the interior until the remaining light energy is progressively absorbed by the encountering objects during the journey and reduced to a minimum level. The successive reflections are simulated with consideration to the above suggestions, and the model is clarified and illustrated in Figure 6-2.

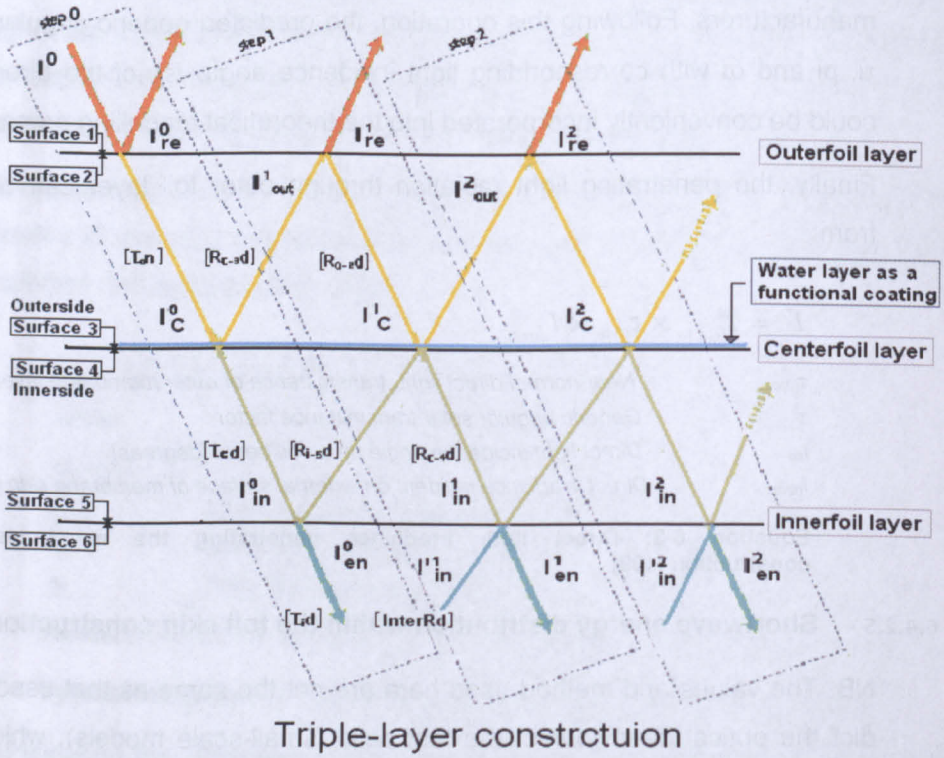

Figure 6-2: Schematic model of the optical system of the multiple foil skin construction. [NB. Rd: diffuse reflectance; Td: diffuse transmittance; Tn: near normal transmittance]

With a comprehensive consideration of all mentioned suggestions, a number of assumptions were made to simplify the simulation process of the multiple reflections:

- The double curved foil panels were represented by infinite parallel planes in all directions
- The internal surfaces within the enclosure were parallel to the representative flat panels.
- The penetrating light radiation and the reflection within the envelope and enclosure are assumed as diffused
- The reflections between the external foil with its surrounding surfaces were assumed to be insignificant.
- The additional water layer is functioning as solar control coating, manipulating the overall transmittance of the studied foil penal.

The total incident light radiation of different surfaces constituting the envelope was computed by an iterative method until the residual energy was negligible. In terms of the double-layer construction, the inner layer can be substituted by a virtual air layer with 100% transparency. This model could automatically adapt the optical properties data of the every construction input by the user.

6.4.2.6 Irradiance incident on the internal surface of the enclosure

Based on the Harvie's suggestion, the light irradiance on the internal surfaces of the envelope is a function of the transmitted light radiation through a representative flat envelop panel of equivalent area as a whole.

At the first step of the iterative method, the overall optical properties of the enclosure should be calculated based on the diffuse properties of the foil panel *i* as expressed in Equation 6-4.

These calculated optical properties of the enclosure are seen as constant values used in the following simulation process.

Consequently, the overall penetrating irradiance initially incident on the internal surfaces within the enclosure before occurrence of any internal reflection can be calculated by the following Equation 6-5:

$$\bar{\tau} = \frac{\sum_{i=1}^{N} A_i \tau_{(f)}^{i}}{\sum_{i=1}^{N} A_i}$$

where for each panel i,

If in double-layer foil construction

$$\tau_{(f)} = \frac{\tau_{(f)o}\tau_{(f)i}}{1 - \rho_{(f)o}\rho_{(f)i}}$$

If in triple-layer foil construction

$$\tau_{(f)} = \frac{\tau_{(f)o}\tau_{(f)c}\tau_{(f)i}}{(1 - \rho_{(f)o}\rho_{(f)c})(1 - \rho_{(f)c}\rho_{(f)i}) - \tau_{(f)c}^{2}\rho_{(f)o}\rho_{(f)i}}$$

τ_f	*Diffuse light transmittance of panel i*
A_i	*Area of panel i*
$\tau_{(f)o}, \tau_{(f)c}, \tau_{(f)i}$	*Diffuse light transmittance of outer, central and inner foil layer respectively*
$\rho_{(f)o}, \rho_{(f)c}, \rho_{(f)i}$	*Diffuse light reflectance of outer, central and inner foil layer respectively*

Equation 6-4: Total light transmittance of enclosure [58]

$$I_{en}^{0} = \bar{\tau} I_{direct}$$

I_{direct}	*Direct beam irradiance incident on the representative foil panel [W.m^{-2}]*

Equation 6-5: Light irradiance incident on the enclosure's internal surfaces before any internal reflection takes place

6.4.2.7 Irradiance incident on the internal foil surface

The light irradiance incident on the internal surface of a foil panel is composited of the sum of the diffuse light reflected multiply from the internal surfaces within the enclosure field and the internal surfaces of the foil skin roof field weighted by their respective view factors. The view factor of each of these regions is defined as a portion of a hemisphere facing towards the internal surface of the panel, in other words, the elevation angle of surrounding surfaces can be actually 'seen' by the foil panel.

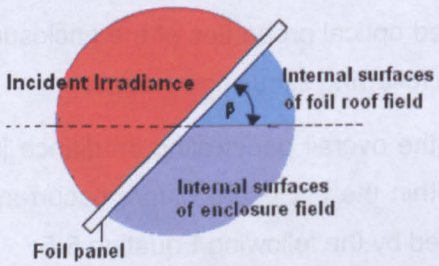

Figure 6-3: Simplified calculation of view factors between the foil skin construction and the surrounding surfaces

However it is impractical to accurately calculate the view factors between the foil surfaces and surrounding surfaces. So the simplified estimation of view factor suggested by Harvie [111] is illustrated in Figure 6-3.

If the view factors of the enclosure and foil roof field surfaces are known in the case of this project, the overall reflectance of the internal surfaces of the enclosure can be approximated as follow:

$$\rho_{inter} = \rho_{mi} \times V_{Fm} + \rho_{si} \times V_{Fe}$$

where

$$V_{Fm} = \frac{\beta}{180}$$

$$V_{Fe} = 1 - V_{Fm}$$

V_{Fm}	*View factor of the roof foil field*
V_{Fe}	*View factor of the enclosure surfaces*
β	*Tilt of the considered membrane panel, horizontal is null [degrees]*
P_{mi}	*Diffuse light reflectance of the internal surface of inner foil layer.*
P_{si}	*Aaverage diffuse light reflectance of the internal finishes in the enclosure.*

Equation 6-6: Overall reflectance of the interanl surfaces of the enclosure

Subsequently the average diffuse light reflectance of the internal surfaces (ρ_{inter}) of the enclosure can be calculated by summing the average light reflectance of the internal finishes in the enclosure and that of the downside of the foil skin construction weighted by their view factors from the considered panel. Following the first internal reflection from the internal surfaces of the enclosure, the irradiance incident on the internal surface of the studied foil panel can be predicted from:

$$I_{in}^{1} = \rho_{inter} I_{en}^{0}$$

Equation 6-7: Irradiance incident on the internal surfaces of the foil panel after initial internal reflection in the enclosure [W/m^2]

6.4.2.8 Iterative model on successive internal reflections

Following the initial step as explained in previous sections, the multiple internal reflections at the arbitrary recursive step n can be simulated based on the diffuse properties of the foil panel as follows:

In the case of triple - layer foil construction :

$$I'^{n}_{out} = \rho_{i-3} I^{n-1}_{c} + \tau_c I'^{n-1}_{c} \qquad with\ I'^{0}_{out} = 0$$

$$I^{n}_{c} = \rho_{c-2} I'^{n}_{out} \qquad with\ I^{0}_{c} = \tau_o I^{0}$$

$$I'^{n}_{c} = \rho_{i-5} I^{n-1}_{in} + \tau_i I'^{n-1}_{in} \qquad with\ I'^{0}_{c} = 0$$

$$I^{n}_{in} = \rho_{c-4} I'^{n}_{c} + \tau_c I^{n}_{c} \qquad with\ I^{0}_{in} = \tau_c I^{0}_{c}$$

$$I'^{n}_{in} = \rho_{inter} I^{n-1}_{en} \qquad with\ I'^{0}_{in} = 0$$

$$I^{n}_{en} = \tau_i I^{n}_{in} + \rho_{i-6} I'^{n}_{in} \qquad with\ I^{0}_{en} = \bar{\tau} I_{direct}$$

$$I^{n}_{re} = \tau_o I'^{n}_{out} \qquad with\ I^{0}_{re} = \rho^{k}_{o-1}(i_{sp}) \times \rho_{o-1} \times I_{direct}$$

I'^{n}_{out}	*Incident irradiance on inner surface of outer foil layer [W.m^{-2}]*
I'^{n}_{c}, I'^{n}_{in}	*Incident irradiance on outer surface of center / inner foil layer [W.m^{-2}]*
I^{n}_{c}, I^{n}_{in}	*Incident irradiance on inner surface of center / inner foil layer [W.m^{-2}]*
I^{n}_{en}	*Incident irradiance on the internal surfaces of the enclosure [W.m^{-2}]*
I^{n}_{re}	*Radiation rejected outside the enclosure at step n [W.m^{-2}]*
ρ^{k}	*Generic angular solar reflectance factor*

Equation 6-8: Incident light energy at step n. [NB. Subscript number: o=outer layer, c=center layer, i=inner layer. 1,2,3, 4, 5, 6, specifies each surface of a foil in the sequence constituting the triple-layer construction. respectively]

The remaining light energy as a result of successive reflection at the step n can then be computed from the sum of the light irradiance incident on the different surfaces of the studied construction. The iterative computation is designated to halt when the amount of the remaining energy is less than an acceptable threshold value ($R^n \varepsilon$), such as the default set to 0.001W/m^2 in this research. It is generally found that for a typical double/triple layer foil skin construction the residual energy reaches a insignificant level after about 20 iterations. More recursions might be required where low emissivity surfaces are present. The iterative method to compute the total light energy incident on every surface is schematically illustrated in Figure 6-2.

The total shortwave energy gain of the each foil layer is calculated in the iterative simulation of a triple-layer foil skin model as expressed in Equation 6-9.

It is to note that the heat exchages rates q, the output of this model, were specified as positive when there are the heat gains to the surfaces. Knowing its solar optical properties, the total incident light radiation on every surface of the considered construction panel and those rejected to the atmosphere can be determined. In the case of the double-layer construction, the algorithm described can be modified by substituting the inner layer with a virtual layer of air possessing a transparency of 100%. This model could automatically adapt the optical properties data of the every construction input by the user.

In the case of triple - layer foil construction

If $R_{\varepsilon}^{n} \leq 0.001\text{W/m2}$; where $R_{\varepsilon}^{n} = I_{out}^{'n} + I_{c}^{n} + I_{c}^{'n} + I_{in}^{n} + I_{in}^{'n} + I_{en}^{n}$

then

$$I_{out}^{'} = \sum_{n=0}^{\infty} I_{out}^{'n} \quad ; \qquad I_{c} = \sum_{n=0}^{\infty} \left\{ I_{c}^{n} + I_{c}^{'n} \right\}$$

$$I_{re} = \sum_{n=1}^{\infty} I_{re}^{n} \quad ; \qquad I_{in} = \sum_{n=0}^{\infty} \left\{ I_{in}^{n} + I_{in}^{'n} \right\}$$

$$I_{en} = \sum_{n=0}^{\infty} I_{en}^{n}$$

finally, the total shortwave light gains of foil layers are found from :

$$q_{Slo} = \alpha_{o} \left(I_{out}^{'} + \alpha_{o-1}^{k}(i_{S}) \times I_{direct} \right)$$

$$q_{Sli} = \alpha_{c} I_{c}$$

$$q_{Sli} = \alpha_{i} I_{in}$$

I'_{out}	*Total incident irradiance on inner surface of outer membrane layer [W/m²]*
I_{in}, I_c	*Total incident irradiance on center and inner foil layer respectively [W/m²]*
I_{en}	*Total irradiance transmitted into the enclosure [W/m²]*
I_{re}	*Total shortwave light energy rejected outside the enclosure [W/m²]*
q_{Slo}, q_{Slc}, q_{Sli}	*Total shortwave light gains to outer, centre and inner foil layer respectively*

Equation 6-9: Total incident light energy and shortwave energy gains.

After all, the output of this model, i.e. the total transmitted light radiation through such an envelope, is subsequently incorporated in an informative part of a boundary model to interface with any external coupling flow analysis software for the analysis of the internal thermal environment. The total shortwave radiative gains to the different foil layers are then output to the heat transfer model, used to determine the surface temperature of the foil membrane considered as described as following sections.

6.4.3 Description of the heat transfer model

The main heat fluxes on a typical multi-layer glass glazing system typical foil skin construction have been clarified in Section 3.2.4. It highlights the major contributors to the thermal loads in an envelope construction and the factors to restrain the development of overheating in the enclosure.

Originated from the Harvie's heat transfer model (refer to Section 3.2.2), a dynamic model of a foil skin penal with a water layer is developed and presented in Figure 6-4.

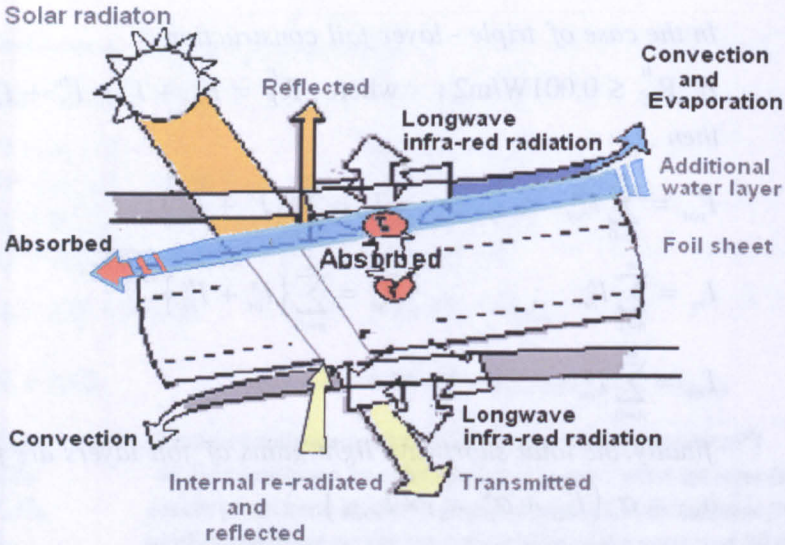

Figure 6-4: The dynamic model of the thermal behaviour for a foil skin with an additional water layer

This heat transfer model for a foil panel mainly includes:

- *long wave infrared radiation heat exchanges*, which involve the modelling on the longwave infrared radiation heat transfer on the external and internal surface of a given foil layer in a studied foil skin construction
- *convection heat exchanges*, on the external / internal surface of each foil layer and their respective surroundings, along with the short wave radiation gains of its core material
- *cooling water layer incorporation*, which interferes the above heat exchange processes. A rational low equilibrium surface temperature of the water/layer combined material is reached either at the dynamic state of the water layer, or at its steady state.

6.4.3.1 Longwave radiation exchange at the external/internal surface of the foil skin constructions

Section 3.2.2 briefed the particularities of the thermal behaviour regarding the foil membrane constructions. A simplified model has been developed for the novel double-layer foil skin construction system (refer to Section 4.5.2). With a comprehensive consideration of all mentioned knowledge input, work has been carried out to develop a model via a comparatively more detailed modelling in order to gain more confidence in the information. Some Roman numeral are used to refer to the previous simple model and important equations would be rewritten for the purpose of this study.

According to the findings from the experiments presented in this study and the theoretical frame work of the tentative model, the assumptions and constraints incorporated into the analytic model are made as follows:

- The model deals with key external conditions of irradiation level similar to the experiment set-up, a typical summer condition in UK.
- The layers of the double foil construction have a longwave transmittance of zero (or 0.3) and thermal emissivity of 1 while for the triple layer construction, the longwave optical properties of the layers are with reflectance of zero, emissivity of 0.4, and transmittance of 0.6.
- The foil layer with a water-layer is 'blind' to long wave infrared radiation.
- All penetrated and reflected longwave radiation in the enclosure is diffuse.
- The fluid media in the air space of the multilayer construction is single phase airflow and is assumed not to be involved in the radiant exchanges.
- All surfaces are deemed as diffuse grey body emitters.
- Calculations of the view factors between the foil surfaces and their surrounding surfaces are in a similar fashion to that for predicting reflected short-wave radiation shown in Section 6.4.2.4.

For this model, the net long wave radiation exchanges between the considered surface i and surface j can be described as [100]:

The net long - wave radiative exchange
if between two infinite parallel surfaces

$$q_i = \frac{\sigma(T_j^4 - T_i^4)}{\frac{1}{\varepsilon_i} + \frac{1}{\varepsilon_j} - 1}$$

if between a convex surface i fully enclosed in a surface j

$$q_i = \varepsilon_i \sigma(T_j^4 - T_i^4)$$

q_i	*Net long-wave infrared radiative heat gain to surface i [W.m^{-2}]*
$\varepsilon_i, \varepsilon_j$	*Emittances of surface i and j respectively*
σ	*Stefan-Boltzmann constant [5.6697x10^{-8} W.m^{-2}.K^{4}]*
T_i, T_j	*Absolute temperatures of surface i and j respectively [K]*

Equation 6-10: Net long-wave infrared radiative exchange between two surfaces

In this modelling, a simplified method is adopted to represent the surface temperature of surrounding objects to the external surfaces by an equivalent temperature *Tsout*. Hence, the net long-wave radiation exchange at a given foil panel i can be found by [109]:

$$q_{LWout} = \varepsilon_o \sigma (T_{sout}{}^4 - T_{SO}{}^4)$$

where

$$T^4{}_{so} = V_{F_{se}} (T_{se})^4 + V_{F_g} (T_g)^4$$

ε_o	*Emittance of the external surface of the outer membrane skin*
T_{SO}	*Surface temperature of the outer membrane skin [K]*
V_{Fse}, V_{Fg}	*View factors of the surroudings and ground respectively*
T_{se}, T_g	*Approximate temperature of the surroudings and ground respectively [K]*

Equation 6-11: Net longwave radiative exchange on the external surface of the foil skin construction (W/m²)

NB. The temperatures of the surroundings and ground in the above computation are imput by user according to the experimental measuremnts.

The computation of net radiant exchange at the inner surface of the foil skin construction follows a similar manner as described above. The temperature of the internal surroundings is represented by an equivalent hemispherical temperature (*Tsinf*) 'enclosing' the internal surface of the given foil panel i, so that the net radiant exchange at the internal surface is [109]:

$$q_{LWin} = \varepsilon_i \sigma (T_{\sin t}{}^4 - T_{s\,i}{}^4)$$

where

$$T^4{}_{\sin t} = V_{F_e} (T_{en})^4 + V_{F_m} (T_m)^4$$

ε_i	*Emittance of the external surface of the outer foil skin*
T_{si}	*Surface temperature of the inner foil skin [K]*
V_{Fe}, V_{Fm}	*View factors of the surroudings and ground respectively*
T_{en}, T_m	*Approximate temperature of the enclosure flied and membrane field respectively [K]*

Equation 6-12: Net longwave radiative exchange on the internal surface of the foil skin construction [W/m²]

According to the findings in the experiments, the typical foil skin construction with a flowing water layer appeared a better thermal behaviour (as described in Chapter 4 and Chapter 5). The observed temperature changes at the envelop construction at the peripheral and floor area was comparatively low. Therefore it is reasonable to assume that the average surface temperature of the internal surfaces of the enclosure field could be close to the indoor air temperature at the occupied space. In addition, the average temperature of

the foil field is obtained form the previous recursive simulation step. The initial input value used is set as a theoretical median temperature (as described in Section 5.6.2).

6.4.3.2 Radiant exchange at the layers of the foil skin construction

For a common multilayer foil skin construction, the layers tend to be separated by air spaces so that the two adjacent layers are asumed to be completely exposed to each other and thus could be represented by two infinite parallel surfaces. In the case of the one air space configuration, the longwave radiation exchange between the two parallel surfaces surrounding the air space could thus be described by Equation 6-10.

The net infrared radiant exchange at the foil layers constituting a typical multilayer construction could be expressed as follows:

If in the case of a double - layer foil skin construction

$$q_{LW\,o} = q_{LWout} + q'_{LWca}$$

$$q_{LW\,i} = q'_{LWin} + q_{LWca}$$

If in the case of a triple - layer construction

$$q_{LW\,o} = q_{LWout} + q'_{LWca1}$$

$$q_{LW\,c} = q_{LWca1} + q'_{LWca2}$$

$$q_{LW\,i} = q_{LWin} + q_{LWca2}$$

$q_{LWo}, q_{LWc}, q_{LWi}$ *Net long-wave radiative exchange of outer, centre and inner foil layer*

q_{LWca} *Net radiant exchange at the surfaces facing to the air space*

Equation 6-13: Net long-wave radiative exchange of the inner and outer membrane layers of a double-skin construction [W/m²] [NB. Symbol ' =downward-facing surface. ca1 = facing the topside cavity, ca2= faving the downside cavity]

6.4.3.3 Convective heat exchanges of air flow at the external surface

The convective heat exchange at the external surface of a given foil panel depend the thermal state of the foil surface and the characteristics of its adjacent well-ventilated air layer. For a typical foil membrane structure with non-standard double curved geometry, the reliable wind design code is still absent. Considering the complex process of determining the convective heat transfer coefficient and the specified experimental conditions in this research, the following empirical equations presented by Clarke [108] to describe the convective heat transfer of a wind driven airflow moving parallel to a surface, such as a smooth copper plate, at a reference temperature of 21.1 °C is used.

$$h_{ao} = 5.678\left[0.99 + 0.21 \times \frac{294.26V'}{0.3048T_{ao}}\right]$$

where

if a free stream wind is present

$V' = 0.5$, *panel surface situated at windward*

$V' = 0.33$, *panel surface situated at leeward*

otherwise,

$V' = 0$

V'	*Reference air velocity parallel to the surface [m.s^{-1}]*
T_{ao}	*Outdoor air temperature [K]*

Equation 6-14: Convective heat transfer coefficient of air flow at the external surface of the membrane panel

This empirical relationship derived from experimental observation under realistic external conditions was originally used for vertical surfaces. For `he indoor test condition in this research, it might be more practical to evaluate the convective coefficient h_{ao} to 5.0 W/m^2, as only upward heat flow presented in the vicinity of the studied surface was experienced in the experimental observation (relevant analysis refer to Section 4.5.2).

Hence, the net convective heat gain can be extrapolated by:

$$q_{ao} = h_{ao}(T_{ao} - T_{so})$$

h_{ao}	*Convective heat transfer coefficient on outer foil panel [W.m^{-2}.K^{-1}]*
T_{ao}	*Outdoor air temperature [K]*
T_{so}	*External surface temperature of outer foil panel [K]*

Equation 6-15: Net convective heat gain of air flow at the external surface of the outer foil layer.

6.4.3.4 Internal surface convection

The common internal natural convection condition is thermal driven due to different air densities at different air temperature, which tends to produce vertical thermal stratification in an enclosed space with large volume. The force of the thermal driven, buoyant force, generally results in either from the total heat gain from internal heat sources in the enclosure or in the air-to-surface temperature differences(Cf. Section 3.3). For the conventional building surfaces, the three basic categories of internal surface natural convention heat transfer are shown as [112]:

Wall, buoyant conditions:

$$h_{ai} = \left\{ \left[1.5 \left(\frac{\Delta T}{L} \right)^{\frac{1}{4}} \right]^6 + \left(1.23 \times \Delta T^{\frac{1}{3}} \right)^6 \right\}^{\frac{1}{6}}$$

Ceiling, buoyant conditions:

$$h_{ai} = \left\{ \left[1.4 \left(\frac{\Delta T}{D_e} \right)^{\frac{1}{4}} \right]^6 + \left(1.63 \times \Delta T^{\frac{1}{3}} \right)^6 \right\}^{\frac{1}{6}}$$

Ceiling, stably stratified conditions:

$$h_{ai} = 0.6 \left(\frac{\Delta T}{D_e^2} \right)^{\frac{1}{5}}$$

ΔT	*Surface-to-air temperature difference [°C]*
D_e	*Hydraulic diameter of horizontal surface [m]*
L	*Height of vertical surface [m]*

Equation 6-16: Convection heat transfer coefficients for natural flows

The above equations were found to be difficult to apply to the double curved and complex topology of the foil skin construction, as its foil surface was hard to clearly categorise as vertical or horizontal. In order to account for surface inclination at tilt angle β, a model suggested by Fishendem determined the convective coefficient of an inclined surface:

$$h_{ai(\beta)} = \frac{[(\beta \times h_{ai(v)}) + [(90 - \beta) \times h_{ai(h)}]}{90}$$

β	*Tilt angle of the foil surface [°C]*
hai(v), hai(h)	*Convective coefficient of vertical and horizontal surface respectively [W.m^{-2}.K^{-1}]*

Equation 6-17: Convection heat transfer coefficients for inclined surfaces [112]

The applicability of the above equations to the internal surface of a common foil skin construction generally raised a number of problems because the estimation of surface-to-air temperature difference was based on the assumption of the internal thermal sub-homogeneous condition. However, the environment particularities of a common enclosure are of high contrasting surface temperature and non-uniform air temperature distribution in the warm or sunny days (Cf. Section 3.3.1). It had been discussed that this unrealistic estimation of the surface-to-air temperature incured unacceptable inaccuracy against test rigs data in the thermal modelling of a sunny day scenario. Therefore, the above estimation model is more appropriate for the situations, where the internal stratification is weak and the measurements of internal air temperature close to the internal surface.

For the particular case of the foil cushion with a water layer, the above assumption was nevertheless applicable and proved in a series of experiments presented in this work (Cf. Section 6.3.2). It suggested that such a decision would be positively adequate to produce a realistic estimation of the convective heat gain for the case of the novel foil skin construction. As a result, the convective heat gain at surfaces facing the interior of the enclosure is computed from:

$$q_{ai} = h_{ai(\beta)}(T_{ai} - T_{si})$$

Equation 6-18: Net convective heat transfers of air flow at surfaces facing the interior of the enclosure [W/m^2]

6.4.3.5 Surface convection between the foil layers

In the light of the construction configuration of the foil cushion and experimental observation in this project, the air low within the cavity was generally pressurized and driven by:

- *The thermal buoyancy force*, a natural convection created by surface-to-air temperature difference in the double-layer construction case. Or
- *The forced air flow*, a low velocity (at a measured average speed of generally less than 0.7m/s) generated by the fan power in the triple-layer construction, which tends to mix with the strong nature convection in the cavity of the triple-layer case (for detailed information refer to Section 4.5.2 and Section 5.4.2).

For the double-layer case, the assumption made was based on the condition that the air space was not well ventilated due to the structure configuration constain allowing for small ventilation openings. The surface temperature variation had therefore larger impact on the air movement in the cavity.

For the triple-layer case, the prediction model for the forced convection assumed a turbulent flow regime at the large foil surface.

Generally, the selection of an appropriate convective coefficient h_{aca} is based both on the orientation of the considered surface (whether it is upward-facing of the inner foil, or downward-facing of the external foil panel) and on the surface-to-air temperature difference, whereby to consider its assisting or opposing buoyancy effects.

As a result, the surface convective coefficient h_{acv} can be estimated from [113]:

In the case of double - layer construction

Vertical plate :

$h_{aca} = 1.33(\Delta T)^{0.25}$

Horizontal plate (upward - facing when heated, downward when cooled) :

$h_{aca} = 1.52(\Delta T)^{0.33}$

Horizontal plate (downward - facing when heated, upward when cooled) :

$h_{aca} = 0.7(\Delta T)^{0.33}$

In the case of triple - layer construction

$$h_{aca} = \frac{(3.76 - 0.00497t)V^{0.8}}{D^{0.2}}$$

where

$D = D_e$, *for the horizontal surface*

$D = L$, *for the vertical surface*

ΔT	*Surface-to-air temperature difference [°C]*
t	*Temperature of incoming air flow rate [0 to 200°C]*
V	*Air velocity parallel to the surface [m.s^{-1}]*

Equation 6-19: Convection heat transfer coefficients of air flow

Following the same manner as Equation 6-18 to calculate the convection coefficient ($h_{acv(\beta)}$)for a panel of arbitrary tilt β , the net convective heat transfers occurring at the intra-construction surfaces are found by:

$$q_{aca} = h_{aca(\beta)}(T_{aca} - T_{spca})$$

Equation 6-20: Net convective heat transfers of air flow at surfaces facing the cavity [W/m^2]

6.4.4 Net heat balances of the foil layers

The modelling approach used to define total heat transfer on any studied foil layer at its balanced state is to calculate its equilibrium temperature, at which the sum of all its individual heat transfer is approximate to nil. This calculation follows a recursive process, which halts when the remaining total energy $R\varepsilon$ at iterative step n reaches the acceptable threshold value, which is evaluated using the default 0.0001w/m2, in this case. The recursive calculation is programmed by using the spreadsheet-imbedded application, namely Visual Basic Application, in the similar procedure to Thaibault's [114].

NB. The equilibrium temperature of the central layer foil with a water layer is to be computed by treating the two layers separately with no airspace in between.

In the case of the double - layer construction

$$q_{neto} = q_{Slo} + q_{LWo} + q_{ao} + q'_{aca}$$

$$q_{neti} = q_{Sli} + q_{LWi} + q_{ai} + q_{aac}$$

$$R_{\varepsilon} = |q_{neto}| + |q_{neti}|$$

In the case of the triple - layer construction

$$q_{neto} = q_{Slo} + q_{LWo} + q_{ao} + q'_{aca1}$$

$$q_{netc} = q_{Slc} + q_{LWc} + q_{aca1} + q'_{aca2}$$

$$q_{neti} = q_{Sli} + q_{LWi} + q_{ai} + q_{aca2}$$

$$R_{\varepsilon} = |q_{neto}| + |q_{netc}| + |q_{neti}|$$

Equation 6-21: Thermal equilibrium of the membrane skins and total energy residual [W/m^2]

6.5 Results and Comparative Analysis

The analytical model is to serve the assessment of the impact of the additional water layer covered on one of the component layers to the overall thermal performance of the foil cushion construction. The internal surface temperature of the foil skin is of the significance in this thermal assessment because its significant influence on the internal thermal comfort level and the risk control of the condensation (Cf. Section 4.5.3 and Section 4.5.4). The main output of the analytical model was the foil layer temperature and heat fluxes of each layer.

In order to simplify the overall modelling process, only the steady state of the water layer has been accounted for most parts of the analyis. A modified model assessing the dynamic state of the water layer is presented in the later section for the purpose of comparsion. A simple comparative study is carried out against the experimental data from this research to ascertain the extent of the reliability of the information provided by this modelling. In addition, the heat transfer process was modelled based on the assumptions that air flow in the cavity was single-phase, and not participating the overall radiative exchanges between the components of the fiol cushion construction and their surroundings.

The overall results responding to the different simulated conditions of a test rig are analysed and presented in the following sections.

6.5.1 Double-layer model

6.5.1.1 Thermal behaviour modelling

A list of relevant input parameters used in the implementation of the analytical tool for the double-layer is described in the following tables.

Table 6-1: Spectral properties of the clading material in the double-layer model

Cladding Material	Beam Light Radiation (near normal)	Diffuse Light Radiation	Longwave (thermal) Radiation
PVC foil			
Transmittance	0.896	0.81	0.33
Reflectance	0.07	0.09	0.05
Emissivity			0.62
PVC foil +water-layer	Film-layer	Droplet-layer	
Transmittance	0.92	0.50	0
Reflectance	0.05``	0.40	0.03@ wet side
Emissivity			0.97@ wet side
Water layer			
Transmittance	1	1	0
Reflectance			0.03
Emissivity			0.097

Notes:
All data is the summery of the properties used and discussed in the previous chapters.
The listed test foil sample is of 0.5mm thickness and the thickness of water layer is 0.2mm

Table 6-2: Parameters for the thermal modelling of the doulbe-laery foil cushion construction monitored in the experiment.

Parameters	Values
External light irradiance	600 W/m^2
External ambient air temperature (Tao)	25°C
Beam light-panel incident angel (isp)	8.3°
Panel Area	1.07 m^2
Panel azimuth	0° (due south)
Construction	Double layer
Outer layer material	PVC foil
Inner layer material	PVC foil
Overall translucency of the envelop	66.15% (dry state)
Average reflectance internal surfaces	20%

The external thermal condition in this modelling was set to the same indoor experimental condition as that for the double-layer test rig. The summary of the parameters used in the modelling process was tabulated in Table 6-2

6.5.1.2 Typical foil surface temperature

Figure 6-5 presents the simulation results of the surface temperature compared to the experimental records of the double-layer foil skin enclosure.

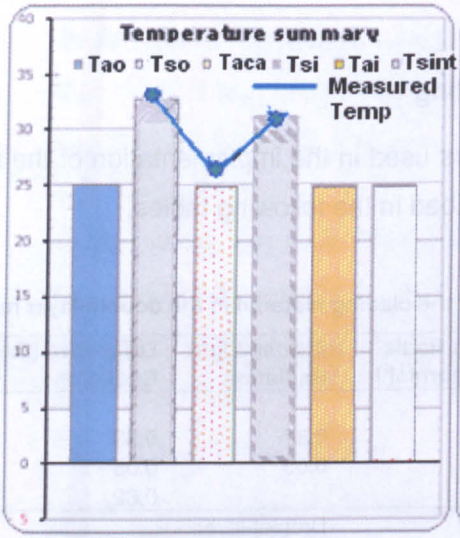

Double-layer model without water layer

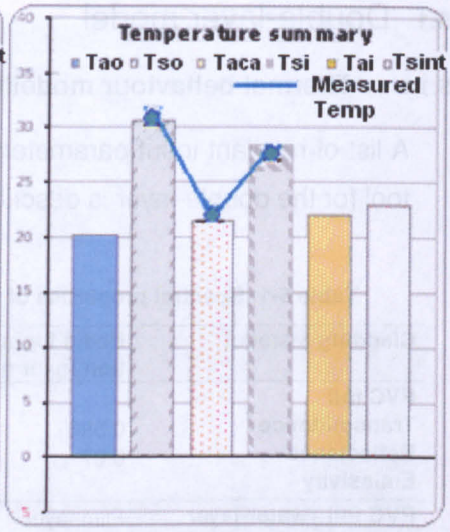

Double-layer model with water layer

Temperature(°C)	Tso	Taca	Tsi
Predicted Vales	**32.71**	**24.9**	**31.2**
Measured Values	33.1	26.5	30.782

Temperature(°C)	Tso	Taca	Tsi
Predicted Vales	**30.69**	**21.5**	**28.4**
Measured Values	31.5	22	28

Figure 6-5: Comparison of the predicted values and the measured in experiments.

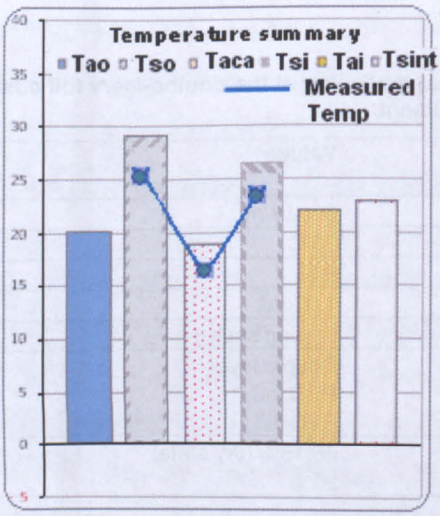

Results of 2-layer model for simulation condition with water layer at dynamic state

Temperature(°C)	Tso	Taca	Tsi
Predicted Vales	**29.2**	**18.85**	**26.55**
Measured Values	25.5	16.5	22.5
Difference(°C)	3.7	2.3	4.1
Deviation (%)	14.5	14.2	18

Figure 6-6: Comparison of results between simulation and experiment for the surface temperature in the 2-layer model with a dynamic-state water layer on the inner layer

The situations with and without the presence of a water layer on the inner foil layer were simulated. The estimated surface temperatures of the outer and inner foil panels matched the corresponding values measured in the experimental condition with maximum deviation 5%. It implied that in the case of the typical double PVC foil layer model, the output could be reliable for further thermal analysis. However, these experimental values were obtained only when the

drop-wise water layer evenly covered the surface of the inner foil layer at the steady state that water layer was stayed over the foil surface and evaporation was depressed.

For the moment of the water layer at the dynamic state, the computation model exhibited the incapability of producing a good approximation of the thermal behaviour of the studied foil panel at its heat balance (Figure 6-6).

In the dynamic process, evaporation in a favourable thermal condition consistently transferred heat flow from the drop-wise water-spread to the airflow of the cavity. The presented analytical tool in disregard of this dynamic state (see Section 6.4.1) resulted in the unacceptable erros.

According to the experimental observation in the double-layer foil skin enclosure, the full cycle of the drop-wise water layer on a foil panel comprised of three main stages: formation of water drop on the foil surface, spread-out and detaining in water-drop shape at steady state before complete evaporation. The outcome of the simulation implied that the water layer at the third stage was appropriately modelled and this analytical tool could give a reliable insight into the thermal process governing their thermal behaviour.

6.5.1.3 Heat fluxes of the component layers

Based on the temperature measurement, the distinct importance of each process on the overall heat transfer process was difficult to pinpoint. Nevertheless the developed simulation tool allowed the assumed heat transfer processes participating in the thermal equilibrium of the foil skins to be quantified individually. This break-down allowed the contribution of different heat exchanges to be identified for different configurations of foil skin constructions that were tested in the course of this research.

For an external light irradiance of 600w/m^2, the average transmittance of 66.15% for the double-layer model was calculated and the predicted heat fluxes to each foil layer are illustrated in detail in Figure 6-7 and Figure 6-8.

It is found that the high incident light energy was on the inner layer due to the external foil of high direct light transmission. In the presence of the water layer, the average shortwave energy penetrating the envelop was only 67% of that without water layer, and the rejected part of the overall incident energy increased 222%, apparently due to the drop-wise water layer. The average en-

closure light transmittance fell to 42.01%, giving a good account for the average internal temperature drop of 4 ℃.

On the other hand, both convection and radiation heat transfers were very strong on the internal foil layer, concerning the high incident light, this implies that a relatively high temperature difference between the internal foil surface and internal space enclosed by this foil skin.

It is evident that the heat transfer process on the external foil shifted toward the outside when the water layer appeared on the inner foil. The external radiative heat exchange of the outer foil increased from 4 W/m^2 to 9 W/m^2, at the same time, the convective transfer rose from 19.9 W/m^2 to 21.7 W/m^2.

In all, the results depict that the thermal-optical properties of the foil appears to significant influence on the thermal behaviour of the internal foil layer.

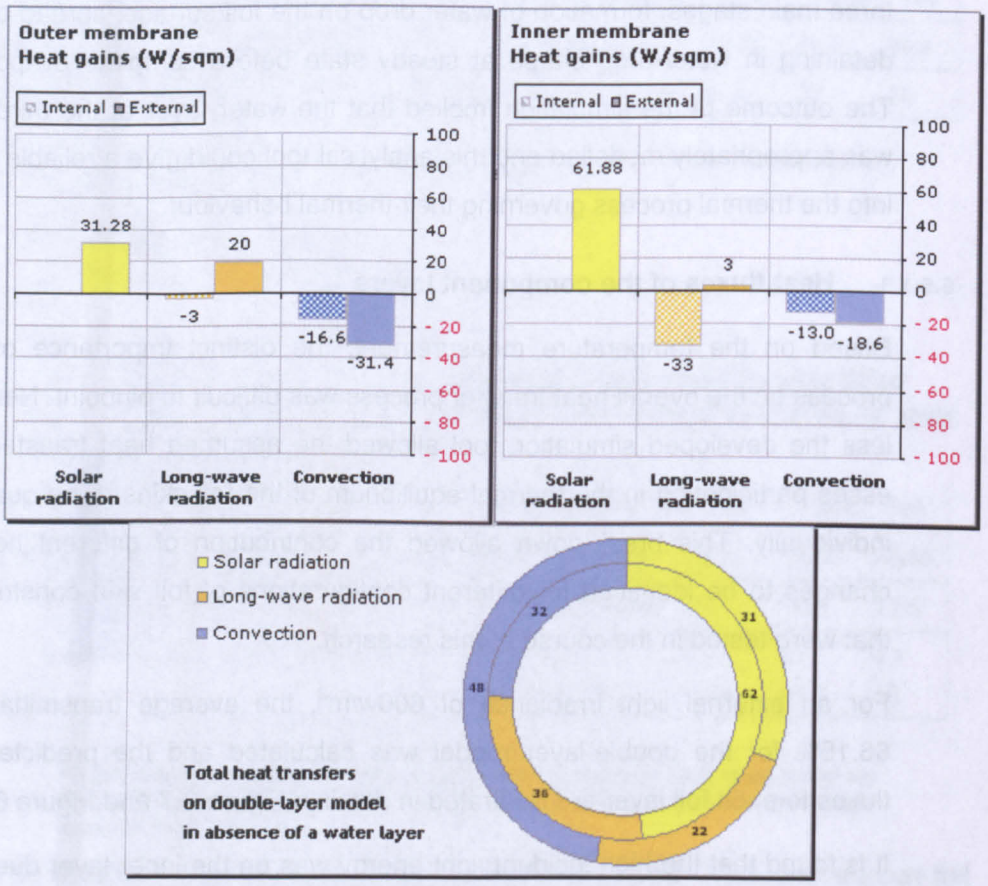

Figure 6-7: Output of the overall heat transfer break down in the 2-layer model without a water layer on the inner layer

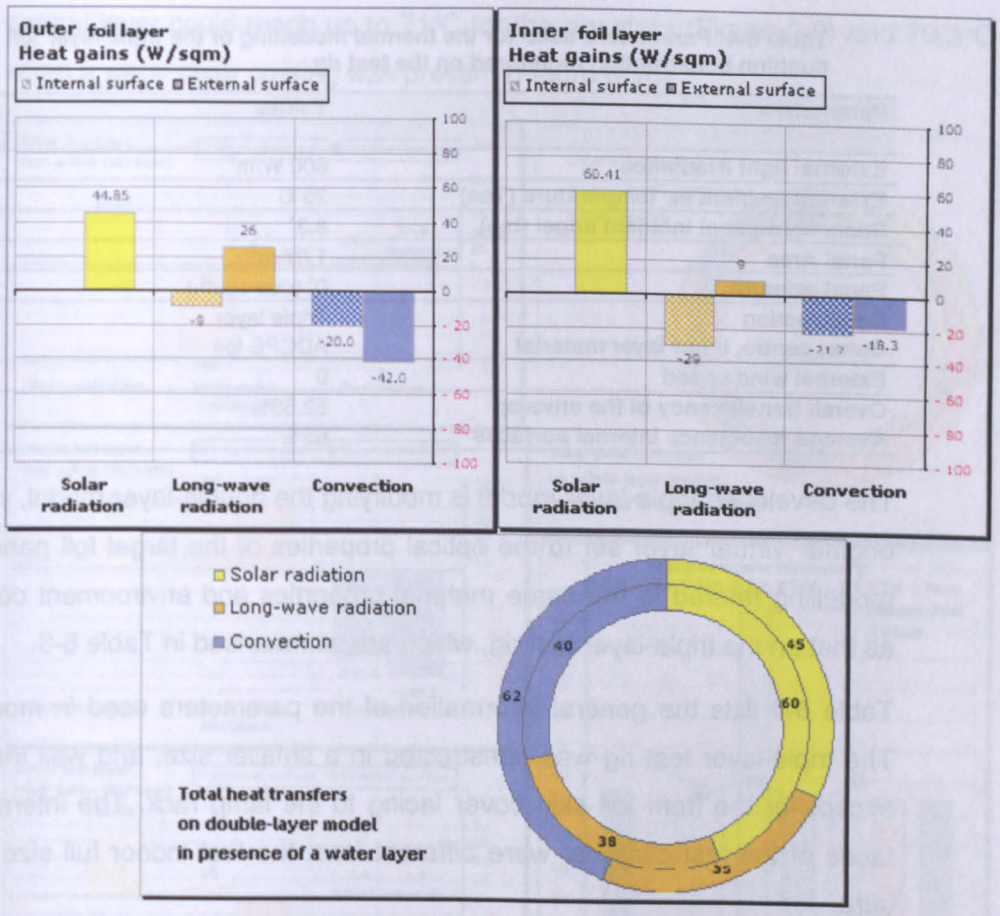

Figure 6-8: Output of the overall heat transfer break down in the 2-layer model with a steady-state water layer on the inner layer.

6.5.2 Triple-layer model

6.5.2.1 Thermal behaviour modelling

NB. the triple-layer model simulated to the experimental condtions of the standard testing setting at: fanpower setting =20Hz, water flow rate =0.7L/m.

Table 6-3: Spectral properties of the clading material in the triple-layer model

Cladding Material	Beam Light Radiation (near normal)	Diffuse Light Radiation	Longwave Radiation
ADCPE foil			
Transmittance	0.89	0.80	0.62
Reflectance	0.07	0.10	0.05
Emissivity			0.33
ADCPE foil +water	Water Film-layer	Water Film	
Transmittance	0.91	0.81	0
Reflectance	0.05	0.10	0.03@ wet side
Emissivity			0.97@ wet side

Notes:
All data is the summery of the properties used and discussed in the previous chapters.
The test foil sample is of thickness about 0.5mm, and thickness of water layer is 0.2mm

Table 6-4: Parameters used for the thermal modelling of the triple-layer foil cushion construction monitored on the test rig

Parameters	Values
External light irradiance	600 W/m^2
External ambient air temperature (Tao)	25°C
Beam light-panel incident angel (Isp)	8.3°
Panel Area	1.07 m^2
Panel azimuth	0° (due south)
Construction Outer, centre, inner layer material	Triple layer ADCPE foil
External wind speed	0
Overall translucency of the envelop Average reflectance internal surfaces	52.58% 65%

The developed triple-layer model is modifying the double-layer model, with the original 'virtual' layer set to the optical properties of the target foil panel. The modelling refered to the same material properties and environment condition as that on the triple-layer test rig, which are summarised in Table 6-3.

Table 6-4 lists the general information of the parameters used in modelling. The triple-layer test rig was constructed in a smaller size, and well insulated except for the front foil skin cover facing to the lamp rack. The internal surfaces of the test chamber were different from the first indoor full size enclosure.

6.5.2.2 Typical foil surface temperature and heat fluxes

Figure 6-9 has visualised the general thermal behaviour of the triple-layer model responding to the high light exposure. The outcome of the calculation showed that the surface temperature prediction of the triple-layer model at its dry state was up to 7℃ deviation, particularly for the internal foil panel. The underlying factors causing such big discrepancy in the triple-layer mode are that the analytic modelling unrealistically presumed all the studied foil to be opaque to the longwave radiation. In fact, the material sample used in the experiments was of thermal translucence at the magnitude of 63%. Therefore the influence of longwave radiation exchange is required to be accounted for in this mode, otherwise the inaccuracy occurred as displayed as shown in Figure 6-9. More discussion on this aspect will be presented in a later section.

However, concerning the purpose of the this research, these results give a good impression of an overheating situation in a multi-layer construction with a longwave 'blind' cladding foil, which is common for most architectural membranes. In the transient heat balance moment, the surface temperature of the

central layer could reach up to 71℃ for the dry state (Figure 6-9) and 79.3℃ when a water layer coating was present (Figure 6-10).

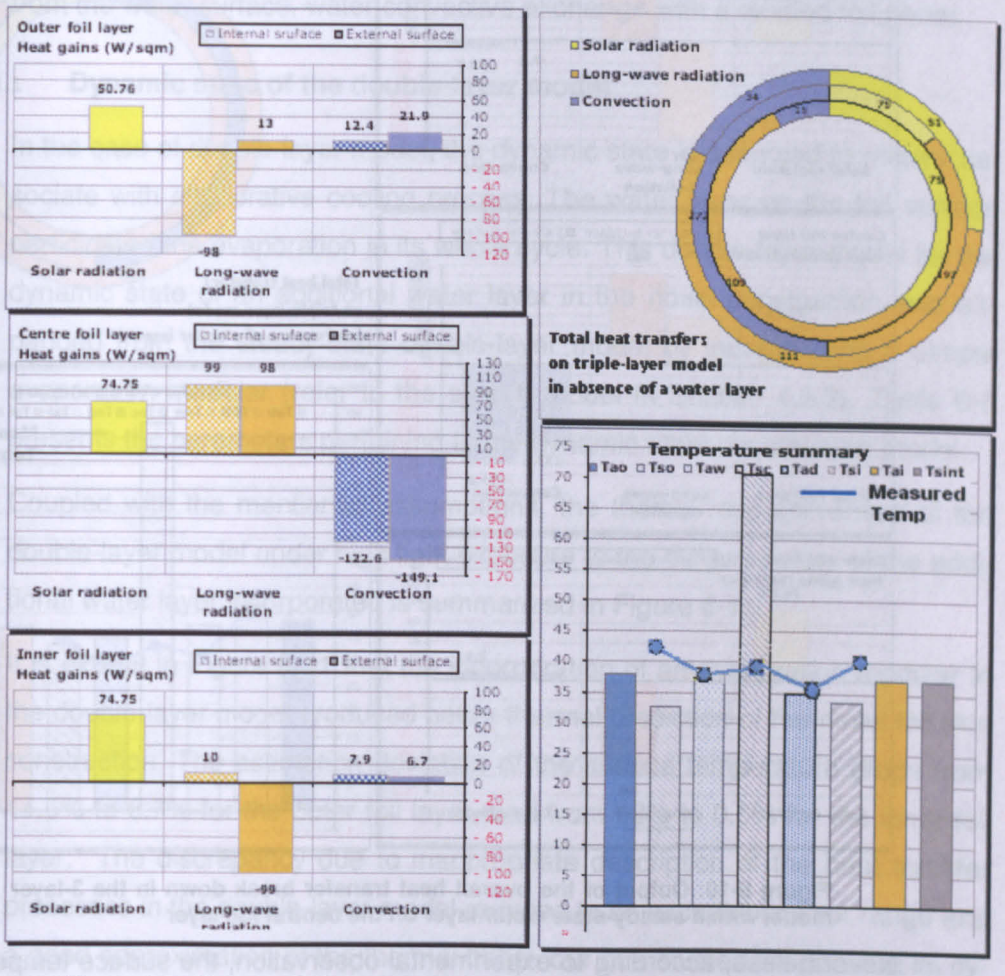

Figure 6-9: Output of the overall heat transfer break down in the 3-layer model without a water layer on the central foil layer

In terms of the simulation for the water layer in presence (Figure 6-10), the results of surface temperature prediction for outler and inner layer displayed are relatively coincident with the data measured in the experiments. This is because the presence of the water layer altered the thermal/optical property of the intermediate layer from thermal translucence to the thermal blind. The impact of longwave radiation on the thermal behaviour of the inner foil was reduced and temperature difference between the external foil and internal foil was augmented from 2℃ at the dry state to 7.9℃ for a water layer.

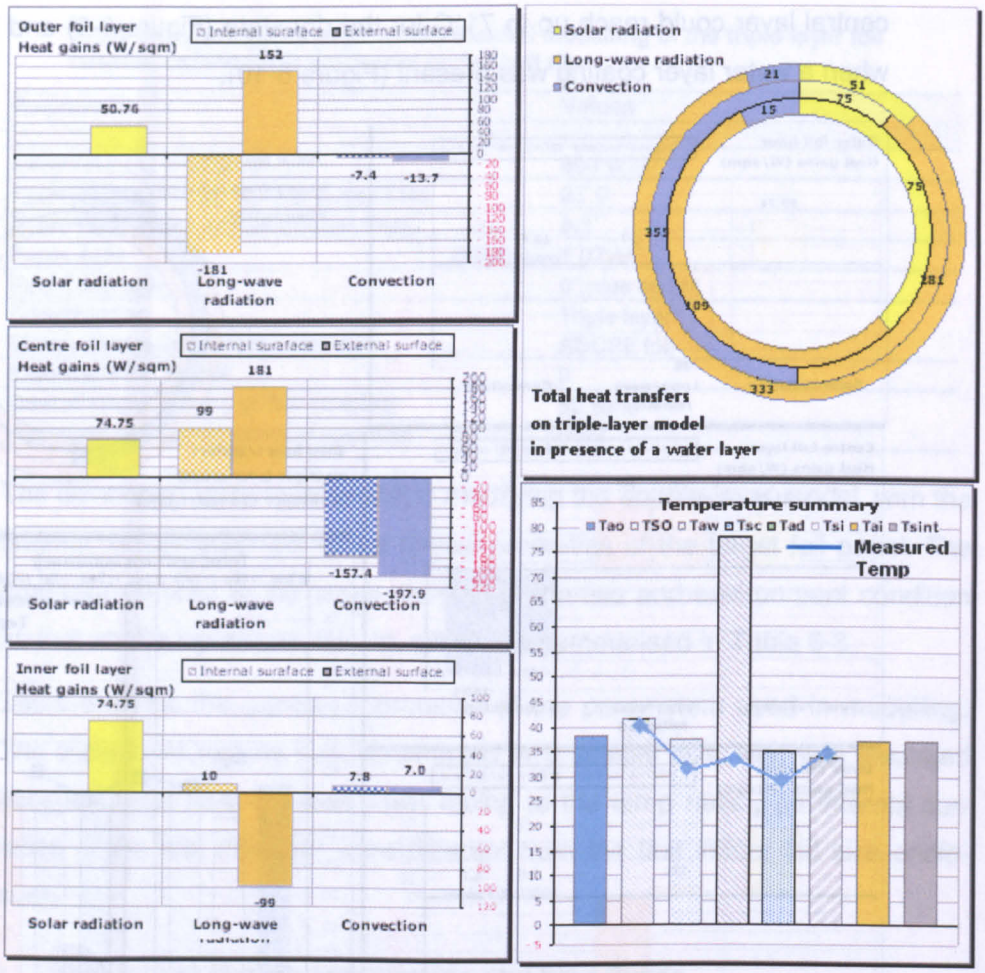

Figure 6-10: Output of the overall heat transfer break down in the 3-layer model with a steady-state water layer on the central foil layer

Nevertheless, according to experimental observation, the surface temperature of the central layer maintained around 34℃ as a result of the airflow, water flow and evaporation process consistently taking away residual heat from the surface. The temperature difference of 45℃ between the predicted and measured value could be indicative to appreciate cooling performance of a running water layer on the central layer. The displayed model was modelling the non-flowing waterlayer on the central layer where evaporation was de-pressed.

6.5.3 Tentative modelling of the dynamic state of a water layer incorporation

Section 6.4.1 briefed the dynamic state of a water layer in the novel foil skin constructions and explained the intricate heat transfer processes involved in the evaluated constructions. Therefore, a tentative model presented in this

sectin is in effort to assess the extent of cooling affect produced by the additional water layer at its dynamic state, i.e. active evaporative heat transfer from the water surface, water convective exchange with a studied foil penal.

6.5.3.1 Dynamic state of the double-layer model

In the case of double-layer model, the dynamic state is assumed to merely associate with evaporative cooling process. The water layer on the foil surface participated the evaporation in its whole cycle. This double-layer model for the dynamic state of an additional water layer in the novel construction was expanded from the steady-state double-layer model by incorporating a simple evaporation modular (refer to the simple model in Section 4.5.3). Table 6-5 presents the parameters pertaining to the dynamic-state double-layer model.

Coupled with the mentioned assumptions, the themal responsiveness of the double-layer model under high light exposure to the dynamic state of the additional water layer incorporated is summarized in Figure 6-11.

It is explicit in Figure 6-11 that the incorporation of an evaporation modular in the double-layer model produced better thermal prediction of the novel foil skin construction. The estimation deviation of the surface temperature drops from 14.5% to 6.7% for the outer foil layer, and from 18% to 0.6% for the inner foil layer. The discrepancy due to inappropriate description of the heat transfer processes in the double-layer model reduced to an acceptable error range and a good approximation of the thermal behaviour of a studied foil panel at its dynamic state is provided by this improved model.

Table 6-5: Parameters and calculation examples in the evaporation modular relating to the dynamic-state modelling of the double-layer construction

Parameters	Air @Cavity inlet	Air @Cavity outlet	Air @ Enclosure
Temperature [°C]: **Tdb** **Twb**	 20.5 (Ti/Tcavi) 14.02	 17.1(To/Tcavo)	 21(Tai)
Relative Humidity Ø [%]	50	83	52
Velocity in Cavity [m/s]	0.03	---	0.015
Water Surface Temperature Tw [°C]	=(14.02+17.1+21)/3=17.2		
Cooling Rate Q_e [W/m2] *	Q_e=51.962 @ retained heat flow rate in cavity with a water-layer=39.05M/m^2		

Notes:

**: This analysis was based on the evaporation model expressed as Equation 4-3 in Section 4.5.3*

Temperature [°C]	Tso	Taca	Tsi
Predicted	27.2	18.9	22.6
Measured	25.5	16.5	22.5
Difference	1.7	2.4	0.1
Deviation [%]	6.7	14.2	0.6

Figure 6-11: Output summary of the thermal responsiveness in the double-layer model with a dynamic-sate water layer

To be noted, as a dynamic state water-layer was recorded in the experiment, the measured values therefore varied along the evaporation progressing in the cavity. But a general view of the evaporation impacts process is proveded.

6.5.3.2 Dynamic state of the triple-layer model

In the case of the triple-layer model, the dynamic model is necessary to account for two cooling processes (Cf. Section 6.4.1):

- Evaporation from the film-wise waterlayer
- Convection of the water flow on the studied foil penal, where the water flow is uniformly speading on the foil surface and creating a consistently flowing water layer in film-wise shape.

The modelling process of the formal one is in a similar fashion to the dynamic state of the double-layer model. Table 6-6 lists the relevant parameters used in the evaporation modular.

Table 6-6: Parameters examples in the evaporation modular for the dynamic-state modelling of the double-layer construction

Parameters	Air @dry channel	Air@ wet channel	Surface @ centre foil
Temperature [°C]: T	30(Tad/Tdb)	33.1(Taw)/26.6(Twb)	33.7(Tsc)
Relative Humidity Ø [%]	30		---
Air Velocity in Cavity [m/s]	0.4755 (relative air velocity to water flow)		
Cooling Rate Q_e [W/ m²] *	Q_e =268.72 @ Tw=(Tad+Taw+Tsc)/3=32.2°C (Water Surface Temperature)		

Notes:

**: This analysis was based on the evaporation model expressed as Equation 4-3 in Section 4.5.3 where the Tw is approximate to the measured Tsc.*

For a given foil penal, the simple approximation of water-flow heat transfer is expressed in a fluid convection modular as Equation 6-22.

For a given length of a smooth plate (L)

Mean water flow heat transfer coefficient is exp*ressed by* :

$$\overline{h_{wca}} = 0.664 \frac{\lambda \times \mathrm{Pr}^{1/3} \times \mathrm{Re}^{1/2}}{L}$$

where

$$R_e = \frac{L \times V_w}{v}$$

V_w	*Velocity trasverse of air conduit [m. s⁻¹]*
v	*Kinematic viscosity at a given temperature [m².s⁻¹]*
L	*Length of the plate covered with flowing water [m]*
λ	*Thermal conductivity of a water layer at a given temperature [W.m⁻¹k⁻¹]*
Re	*Reynolds number of water flow layer on the foil surface [dimensionless]*
Pr	*Prandtl number of water flow layer a given temperature [dimensionless]*

Equation 6-22: Convection heat transfer coefficients of a flowing water layer [101]

Table 6-7: Calculation results from the water flow convection modular in the dynamic-state modelling of the double-layer construction layer construction

Parameters	Air @dry cavity	Air@ wet cavity	Surface @ centre foil
Temperature T [℃]	30(Tad)	33.1(Taw)/26.6(Twb)	33.7(Tsc)
Relative Humidity Ø [%]	30	---	---
Water Velocity in Cavity V_w [m/s]	0.233	Temperature [℃] Tw	32.24
Water/Foil Mean Temperature Tm [℃]	33	Reynolds Number	452569.77
Water Convective Coefficien hw [W/ $m^2 \cdot K$]	46	Water Convection Rate Q_w [W/m2]*	=ΔT x hw=65.8

Notes:

**: The resulats were obtained when the thermal conductivity of the waterlayer (λ), Prandtl numbe (Pr), and kinematic viscosity (v) are 0.0623[W.m^{-1}k^{-1}], 5.1, and 0.76 [m^2/s] respectively, which are directly found in the thermal properties table of water at the Water/Foil Mean Temperature of 33℃. [102]. The given length of the smooth plate is 0.712m*

Table 6-7 presents calculation results of the water-flow heat transfer prediction. The output summary of the the dynamic state triple-layer model is visulised in Figure 6-12

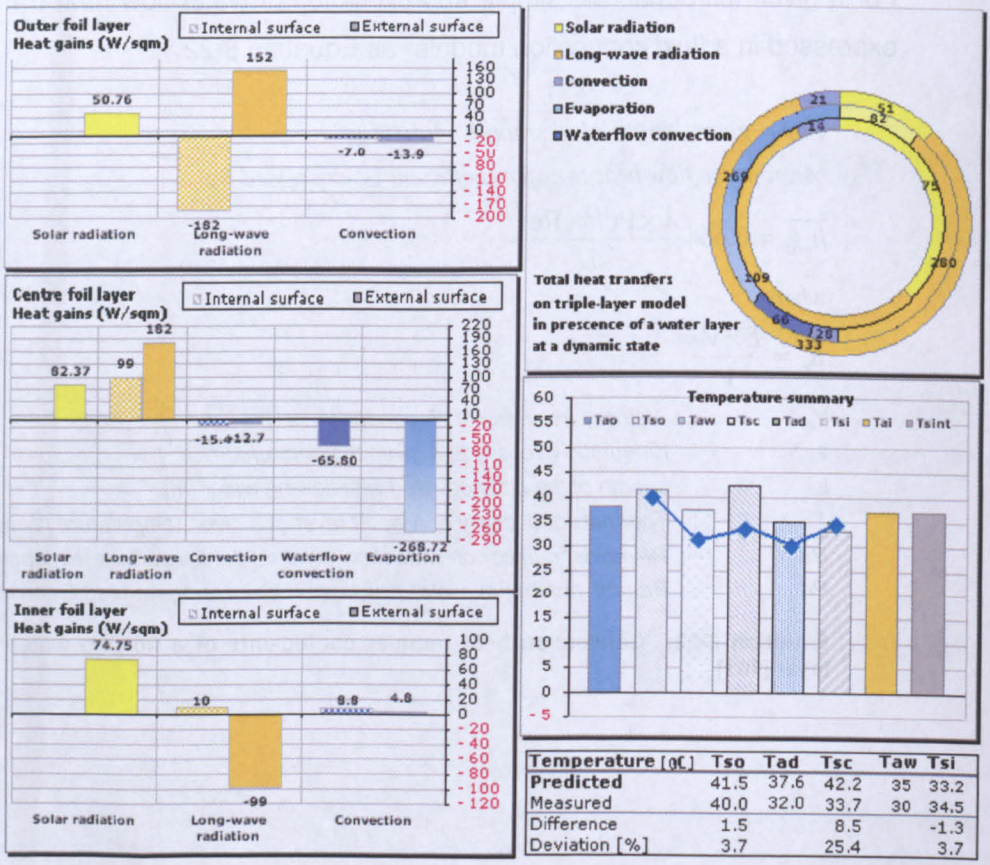

Temperature [℃]	Tso	Tad	Tsc	Taw	Tsi
Predicted	41.5	37.6	42.2	35	33.2
Measured	40.0	32.0	33.7	30	34.5
Difference	1.5		8.5		-1.3
Deviation [%]	3.7		25.4		3.7

Figure 6-12: Output summary of the thermal responsiveness in the triple-layer model with a dynamic-state water layer

It is seen in Figure 6-12 that the thermal output is more approximate to the experimental records as a result of integrating both evaporation modular and wa-

ter-flow convection modular in the triple-layer model. The resulting discrepancy between the prediction and measument for the surface temperature of central foil is found to decrease from 45.3℃ to current 8.5℃ in comparison to the steady-state model (refer to Figure 6-10). However the deviatin from this result comparison was 25.4%, which fell outside of the acceptable error range (i.e. less than 10%). The factors incurring such errors will discuss in a later section. It is worth noting that the results compared to that from the steady-state model gives a good account for to what extent of the cooling impact of an additional water layer on the overheating control of multi-layer foil skin constructions, causing about 37℃ reduction on the central layer at its transient heat balance moment. Meanwhile the internal convective heat transfer is found to generally account for less than 10% of the overall heat exchange on the inner foil penal, which was testified by the experimental observation as a low airflow was recorded in vicinity of the inner foil layer.

6.5.4 Discussion on results

It has been stressed previously that the present tool was aming to provide tentative methods to assist the investigation ofthe thermal performance of the novel foil cushion construction. For such a novel foil skin envelope, it is found that it was intricate to precisely model it's complex heat transfer processes involving forced airflow transfer, evaporation, convection of flowing water, dynamic surface heat transfer and dynamic longwave radiation coupling with its thermal translucence. A list of assumptions was made initially in order to simplify the modelling process. However, calculation results displayed the importance of longwave transmission on the overall assessment of thermal performance, particularly for the case of the multiple layer construction clad with thermally translucent material. Although the predictions from the triple-layer model were not satisfactory to the experimental results, some qualitative study still can be performed according to the information gothered in this analytical tool.

6.5.4.1 General impact of an additional water layer on thermal prediction

It has been highlighted in a number of literatures that the contribution of the membrane envelope to the thermal behaviour of the space it encloses was primarily the result of the solar radiation transmission into the space. Under high light irradiance, the presence of additional foil layer, ventilated air gap etc

in the foil skin construction served to shift the heat transfer from the external foil layer to the outside of the enclosure. An additional water layer to the foil skin construction was expected to further shift the heat transfer process and thus reduce the resultant light radiation gains of the enclosure.

Both simulation and experimentation have proved the cooling effect of the addition water layer within the foil cushion construction. The surface temperature of internal foil panel could be reduced up to 3℃ and 4℃ for the double-layer and triple-layer foil skin construction respectively, when the water cover was at its steady stage (refer to Chapter 4 and Chapter 5). The principles accounting for the temperature reduction however is different for those two analysis tools. Concerning the assessment results from the simulation tool, the significance of the presence of the water layer at a steady state was as results of the incremental thermal emissivity of the foil panel covered by a uniform water spead. For the experimental simulation, the cooling more likely links to the dynamic cooling state of the flowing water layer, mainly due to the evaporation proves. This could explain the large temperature reduction experienced in laboratory when the water spraying in operation.

As the water layer interferes the overall thermal performance of the construction at variable states by different mechanism, it is hard to generalis a simple rule to indentify the relationships among them.

6.5.4.2 Double-layer foil skin construction

The double-layer foil skin enclosure was constructed by PVC foil sheet with low longwave transmission property (up to 33%). Based on the simulation results, the decision of ignoring the thermal translucence for this particular test rig case did not effect the estimation accuracy of the surface temperature of the considered foil panel. It implies to some extent that the cladding materials with thermal translucence at a certain low range could not significantly influence the overall thermal performance of the construction as expected. This argument has also been put forward by Harris Poirazis et.al in his research on the ETFE foil cushion [13].

Thaibault also mentioned that this simulation tool could give a good approximation to the surface temperature of a membrane panel, generally with thermal emissivity higher than 82% to 85%. It is therefore unlikely that a noticeable error was induced by the above extrapolation used in the analytical model

that the thermal/optical properties of a foil penal was substituted by the common standard nature of the membrane materials with longwave radiation opaqueness.

As an additional water layer altered the surface emissivity of the given foil panel to nil, the overall double-layer model was more approximate to the assumed steady-state condition in this simulation tool. Therefore, it is not surprised that results from dynamic-state model, which was extended from the steady-state one, fall within the acceptable range of accuracy in comparison with experimental measurements. This analytical model is capable of assisting the thermal environment design of such a novel system by providing a good insight into its overall thermal performance, either in the steady-state and dynamic-state model.

6.5.4.3 Triple-layer foil skin construction

In the case of the triple-layer model, the cladding material of ADCPE foil has a high longwave translucence of 62%. The analytical model displayed an inability to produce an acceptable errors for the surface temperature prediction, in particular on the intermediate layer. The underlying reasons causing the deviation of the prediction from that measured, can categorised by two aspects:

- Firstly, the analytic modelling deemed all the considered foil panel to be longwave radiation blind. Whereas the high longwave transmittance of a studied foil penal could not be neglected as in the triple-layer case. Ignoring the impact of its thermal properties caused markedly inaccurate predictions.
- Secondly, the general trend of underestimation to the longwave radiation exchange observed in this model further deviated the calculation.
- Finally, the unrealistic description of the water layer condition in the triple-layer model excluding the flowing water-film convection and active evaporation process, both taking place on the surface of the central layer. These two processes were particularly aggrandised by means of specifying the configuration of the novel construction to provoke better air flow generation and consistently flowing water in the cavities (Cf. Section 5.4).

It is seen in Figure 6-10 Figure 6-12 that the inability of this tool for the simulation of buildings clad with a high thermal translucent foil material. Although the

presence of the water layer could minize the deviation of the estimation from the realistic condition to a certain degree, the prediction results from both the stead-state model and the dynamic-state still fell far outside of the acceptable range, set to 10%. It is a critical case for the estimation of the surface temperature of the central foil.

It is somehow confirmed by this analytical model qualitatively at least that the overheating control is a critical case for a foil cushion construction incorporating more layers. In comparison with the measured surface temperature of the central layer at an average of 33℃, the prediction was close to 80℃. In view of overheating issues in foil cushion constructions, these results indicate the significant cooling effect the water layer could bring out.

To conclude, a thermal modelling process accounting for the longwave transmission is required for foil skin constructions, particularly incorporating more layers with relative high heat translucence.

6.5.5 Discussions on the thermal modelling process

The general trend of an underestimation in the surface temperature of the critical inner layer was proved more relating to the constant heat transfer process including long-wave radiation and convective exchanges of airflow and waterflow. Thus a discussion is presented to identify specific source of systematic errors in the model.

6.5.5.1 Short-wave radiative processes

As the model simulated the indoor test condition with a steady light source created by a lamp rack, there no identifiable systematic calculation error relating to the short-wave radiation in general.

Although the angular selectivity of direct beam light of the studied foil panel was extrapolated based on an approximation approach, which generally adopted for the material with low diffuse light transmittance, this value was only applied to the external foil. Other parts of the calculation process only involve the optical properties of diffuse light.

6.5.5.2 Long-wave radiation processes

It has been pointed out that most of the extrapolation used for the estimation of the thermal properties of the membrane tested in this study were primarily

suitable for the foil products with the hemispherical long-wave emittance in the range of 84 to 88%.

With regards to the external long-wave radiation exchange, a large amount of heat generated by the lamps (see Chapter 4), had been underestimated which contributed to errors of estimation of the external surface temperature. Meanwhile, because the solar simulator had a large view angle as seen by the studied foil panel, the calculation of external mean radiant temperature became a non-trivial task.

In terms of the internal long-wave radiation exchange, the surface temperatures inside the enclosure were the most likely to deviate from low-level air temperatures during a strong insolation period, thus errors could be offset by the decreased significance of internal long-wave processes under high light exposure. However, the surface temperature was proved to be markedly different from the air temperature. It is better to explicitly measure temperature of these surfaces in the test rig.

6.5.5.3 Convective processes

In the current context, the estimation of the convective heat transfer coefficient for the geometrically complex foil cushion should now most probably remain in the form of empirical relationship, and its determination is out of the scope of this research. The two convective processes pertained to the simulation are airflow convection and waterflow convection on the central layer.

In light of the airflow convection, the approximated internal convective heat transfer coefficients used in the model were essentially a function of the temperature difference between the membrane surface and the surrounding air, and of the air velocity in the vicinity of the surface.

In the case of a mechanically ventilated envelope, the forces driving the air flow in the air channel are explicitly linked to the ventilation system specifications and the approximation of air velocities close to the foil skin is required to be more reliably predicted.

Generally, internal convective heat transfer was found to account for 30% of the total surface heat exchange for the double-layer model with a steady state water layer. Once the dynamic-state water layer was present, the percentage reduced to around 10% for the double-layer model and triple-layer model. Small inaccuracies in the estimation of internal convective heat transfer coeffi-

cients did not generally influence the accuracy of the surface temperature prediction. In the triple-layer model, the mixed airflow generated by the fanpower and buoyancy force resulted in intricate modelling processes and underestimation of this heat transfer further.

Unlike internal airflows, the estimation of convection coefficient at the external surface of the membrane could not be necessarily dependent of the thermal state of the membrane skin itself if the wind-induced forced flow dominates over buoyancy forces that may develop at the surface of the foil. At this moment, the convection coefficient may be considered to be entirely a function of the air velocity at the boundary layer of the membrane surface. Ideally, the appropriate factors specifically for the non-Cartesian, double-curved geometry of foil cushion enclosures can be derived based on data from wind-tunnel test or from CFD wind pressure analysis.

As the calculation of these air velocities is not straightforward, empirical factors according to building forms and configurations typically encountered in the built environment were used. It was found, however, in this model that the variation in external convective heat transfer was actually a function of the temperature difference between the external air and the membrane surface, which were the controlled parameters. Therefore, the calculation of the external convective heat exchange could be considered insensitive to these modelling simplifications and the effect of the suggested improvements on the overall accuracy of the model would only be limited.

In terms of the waterflow convection, the presented prediction was results of the largely simplified approximations. As the evaluatd construction is newly developed, the bespoke empirical relationship for this modelling process to follow is not yet available. Therefore the results require further verified by academics who are interesting in this field to improve the current analytical model whereby a more confident informantion could be provided.

6.5.5.4 Evaporation processes

It is worth noting that the evaporation has actually participate all the heat transfer process. But the simplified method of modelling for the steady state presumed that the evaporation process was depressed and waterflow convection was not involved in the meantime. It is found that this assumption is true for the double-layer model at a certain stage of testing course. As the cavity

thermal condition was highly humid and the waterlayer detained on the foil surface in drop-wise shape. While the triple-layer model had improved ventilation and water spreading behaviour in air cavities, the evaporation were largely enhanced as indicated in Table 6-6 in comparison to the results listed in Table 6-5.

Nonetheless, the evaporation modular incorporated in the simulation tool has disregarded the facts that external and internal thermal conditions have involved its heat transfer process. An empirical theoretical model for evaporation processes specified for this novel construction is necessary. The current format is functioning as a tentative tool to give a general view of cooling performance of the additional water layer that the novel construction system might expect.

6.6 Conclusions

In view of the incompatibilities of conventional thermal modelling techniques with the characteristics of membrane skins, an analytical model was developed based on the previous research suggestions, in order to gain more insight into the underlying salient parameters influencing the overall thermal performance of the double-layer and triple-layer foil skins constructed with an additional water layer.

This analytical model was designed to be an informative boundary model for flow-modelling packages. The extreme thinness of foil and complex geometry of the surface have been accounted for in this model. The results of the analytic modelling were compared with the corresponding measurements from the full-scale indoor enclosure and test rig data presented in Chapter 4 and Chapter 5.

The preliminary comparative study showed that the predicted surface temperature for a double-layer foil skin satisfied the experimental results, with an absolute average error up to 0.9ºC for the case of the steady state water layer in presence.

The simulation was then extended to a typical triple layer foil construction. The surface temperature predictions displayed a large discrepancy to the test rig data, in particular, the surface temperature of the interlayer panel. It was found that a comparative satisfactory prediction of the internal surface temperature

appeared when the condition of the water layer was simulated. However, these simulation results were not stable, varying largely from one case to another. It suggested somehow unreliability of the data from this triple-layer model. The source of these errors was identified as follows:

- the inherent systematic errors of the modelling: its tendency of the underestimation to the long-wave radiation exchanges, and
- unrealistic description of the thermal-optical properties to the considered foil type with high thermal translucence: presuming the simulated thin film to be longwave radiation blind.
- the unrealistic description of the water layer condition in the triple-layer model excluded the flowing water-film convection and active evaporation process (Cf. Section 5.4).

Although the data predicted from the triple-layer model was not satisfactory, the breakdown of the heat transfer processes from this tool provided indicative information of their relative significance in the overall thermal behaviour of the foil skin construction.

This tentative tool gave an account of the radiative exchanges, which had generally dominant influence on the component layers in the case of the clear foil cushion construction.

The significance of a water layer integrated in the foil skin construction was studied by the analytical tool. It appeared in the simulations that internal radiant exchanges around double than that without an incorporated water layer, while convective heat exchanges were up to average 8% increment. It transpired that the external coupling of this boundary model would not introduce a significant error in the subsequent flow analysis once the construction incorporated a water layer. This finding coincides with the experimental observation that the impact of internal convection on the area adjacent to the internal skin of the envelope was limited due to the thermal sub-homogeneous zone created by the process incorporating a cooling water-layer in the envelope cavity (Cf. Section 4.5.1 and Section 5.6)

The following chapter will sum up the findings of this research and will discuss their consequences on the environmental design of tensile membrane enclosures.

PART III DISCUSSION AND CONCLUSIONS

The idiosyncrasies of the thermal performance of the novel systems are summarised in this part. The research findings presented in this thesis support the idea that the additional water layer film in the cavity of envelop plays an important role in the cooling load reduction of this building and on the thermal comfort of its occupants during the critical summer condition. The overheating control of the foil cushion buildings is enhanced by such holistic eco-friendly means.

CHAPTER 7
DISCUSSION AND CONCLUSIONS

> *"The only Zen you find on the tops of mountains is the Zen you bring up there."*
> --- **Zen proverb**

Building envelope construction plays an important role in the overall thermal balance of any building. Foil cushion envelope now is a popular alternative to a large fully glass glazing system due to reduced U-value and the light weight offered by this type of envelope. However, the typical thermal-optical properties of the cladding materials, the configuration of this type of envelope, and the thermal environmental condition when it exposes to high light irradiation, are argued to be underlying factors leading to overheating. This research proposed a novel thermal control concept to incorporate an additional water layer into the foil cushion construction. A series of experimental assessments of the thermal behaviour of foil cushion constructions are designed on the basis of this concept and a tentative model simulating to the thermal behaviour of these laboratory tests built at the University of Nottingham have been presented in this thesis.

7.1 Discussion of Findings

7.1.1 Thermal behaviour of foil panels covered with a water layer

In view of the thermal-optical properties of foil membrane, it is claimed that the integration of an additional water layer to the foil skin construction conformed to the critical nature of the foil materials and was particularly effective and environmentally sustainable measure for solar control as well as favouring cooled air production. This hypothesis was made based on a review of the existing body of knowledge on inherent thermal characteristics of architectural foil sheet. In particular, the following thermal behaviour were revealed to be salient;

- The thermal resistance of the core of coated woven membranes plays a negligible role in their thermal behaviour

- Thermal behaviour depends entirely on convection and radiation heat exchanges, both of which vary significantly with surrounding conditions and with the thermal state of the membrane skin itself
- The extremely low thermal mass of the membrane materials causes their thermal state to be highly variable in response to fluctuation of energy input

A number of preliminary studies were carried out in the timescale of this research to investigate the thermal-optical properties and consequent thermal behaviour of foil skin construction with a water layer. Experimental results identified the improved thermal properties of such a foil skin construction as follows (refer to Chapter 4):

- The visible light transmission was increased 2% for a ilm-shape water layer and showed a 40% reduction for drop-shape water layer.
- A rapid reduction of the residual heat accumulated on the considered foil panel was at a magnitude order of 50%.
- A rise in thermal quality of a foil sheet covered with a water layer was evident. Its thermal response was behaving similar to low-e glass causing the air temperature deviation between the internal and external about surfaces to be 4℃ bigger than that without a water layer.

The physical mechanisms contributing to the above thermal amelioration can be generalized into two categories:

- The modification of the foil surface's emissivity and reflectance by the water-layer coating enhanced the shifting of the radiative exchanges on the internal foil layer towards outside the enclosed space, coupled with the incremental magnitude of convective heat transfer inside the cavity of a foil cushion driven by thermal natural force or mechanical force.
- The rapid cooling effect of the active state water layer took place due to convective heat exchanges between the cooling water body and its surrounding, as well as the evaporative cooling processes involved.

7.1.2 Thermal performance of the novel foil skin constructions

Overheating on foil cushions in places because of high solar gains was mainly linked to the following factors:

- overall transmitted solar radiation,

- the thermal radiative heat flow from the overheated envelope. and
- dry resultant temperature of the occupied space.

The balance between these factors is critical to control overheating and the subsequent thermal discomfort experienced by the building users. The addition of a water layer to the construction could restrain these two or even three factors to some extent at the same time according to the evaluation work presented in the thesis.

It was stressed out in the experimental observation that the rate of convective heat transfer was of equal or higher significance than radiative heat transfer for the heat removal in the cavity of the envelope. The forced ventilation mixed with thermal-driven natural convection in the cavity benefited the temperature drop of the internal foil layer and the temperature field in the users' spaces next to the envelope. In the meantime, the additional cooling water layer in presence can enhance this cooling process as observed in the experiments.

To identify a clear relationship between the surface temperatures of the varying component foil penals once a water layer incorporated is a non-trivial task. The physical state of the water layer involves three essential stages:

- formation of the water layer in shape of drop-wise, film-wise, (which manipulates the thermal-optical properties of the foil penal)
- water layer spreading, either at a steady state, or at a dynamic state, and
- water-layer detaining after water spraying stopped.

One or two of the water layer conditions could govern and interfere overall temperature relationship. It was found that the highest cooling effect was achieved when the water layer was evenly spreading on the foil surface, for instance, in the experimental case of a double-layer construction, showing about an average 9℃ to 10 ℃ drop of the surface temperature. However, the risk of the internal surface condensation was proved unacceptably high.

In light of triple-layer constructions, the addition of a foil layer and air channels in the foil skin construction evidently advocated to reduce the risk of internal surface condensation in the envelope. Generally, the recorded internal surface temperature was about average 1℃ to 1.5 ℃ higher than the average internal air temperature when a water layer appeared on the interlayer foil (see Chap-

ter 5). About 5℃ decrease in the surface temperature of the inner layer was found in the experiments as results of a flowing water layer is in presence.

7.1.3 Internal thermal environment of the enclosure

The combined effect of the airflow cooling and cooling water in the foil skin construction favoured a better performance of the thermal zone at the low level next to the perimeter of the envelope. Both fullscale laboratory test rigs had proved that the internal air temperature distribution was seemed to be more homogeneous next to the envelope regardless of the existing high contrasting surface temperature on the foil skin roof once the water layer in presence.

Natural thermal zoning appeared in the enclosed space into four subdivisions:

- Occupied zone: a thermally heavier area, whose temperature field most likely is influenced by the air temperature at the floor level and the external air temperature.
- Mid level zone,
- Roof level zone: a low thermal mass area under high light exposure, where high contrasting surface temperature is experienced, is highly responsive to fluctuation of external thermal radiation.
- Envelope perimeter zone: a thermal sub-homogeneous area, where the behaviour of this temperature field was likely governed by the overall thermal behaviour of the adjacent envelope. This naturally generated thermal stable field is particularly significant in the overall thermal performance of the building by applying natural ventilation strategies.

Unlike characteristics of the thermal boundary commonly occurring in a foil skin enclosure, the perimeter zone had the tendency towards thermal homogeneity. This behaviour implied the reduced possibility of local turbulence around the inner skin, which is also in line with the results from the analytical model in Section 6.5. Hence a desirable vertical thermal stratification could be stabilized to some extent and reliable to be exploited for the buoyancy-induced nature ventilation to remove cumulative internal residual heat and improve internal thermal comfort level.

In addition, it was observed that the internal thermal asymmetry in the tested enclosure in the horizontal direction was limited to a lower level than than that

in the triple-layer test rig. It was largely because of the shading created by the drop-wise water layer covering the inner foil layer.

It is concluded that the foil cushion construction integrated with the water-cooling and airflow-cooling process played a critical role to stabilise the positive air thermal layering by reducing the asymmetry of the horizontal air temperature distribution at the low level. Coupling with the stabilization effect of the thermally inert floor, this integration system optimistically enhances the vertical air temperature distribution and the desirable natural ventilation driven by the buoyancy effect. The extent of the internal stratification can be further expanded by high solar irradiation while the caused discomfort could be compensated by the cooling provision owing to the radiant cooling by the cooled surface of the roof and natural ventilation driven by the buoyancy force or assisted by the displacement ventilation strategy.

7.2 Possible Improvements to the Adopted Methods in This Project

7.2.1 Experimental simulation programme

The overall experiments were carried out indoors. The overheating condition was created by a rack of tungsten lamps, which produced more heat than that from a real solar light source. The excess heat penetrating the thermally translucent foil skin envelope caused an unnecessary high internal air temperature, which might not be the case when it exposes to the real solar light source at the same irradiation level. It might be result of the overestimation of the overheating on those test rigs. Higher light efficiency luminaries were preferrable in order to give a realistic simulation to real thermal condition.

Internal and external equivalent mean radiant surface temperature are important parameters used to assess the effect of the radiant heat to the thermal comfort level. In particular, the comparatively large scale of the PVC foil skin enclosure tends to experience large temperature variation in the internal surfaces and foil penals at roof level. It is better to explicitly measure by appropriate devices rather than to estimate by using a number of empirical factors. The inaccuracy of the equivalent surface temperature prediction could result in underestimation of the long-wave radiation exchange, and consequently the surface temperature prediction of the studied foil panel.

7.2.2 Analytical modelling process

Dynamic modelling with consideration to the longwave radiation process is required particularly for the thermal translucent glazing materials like an ADPE foil penal. Along with the increasing complexity of the foil cushion construction, i.e. incorporating more foil layers, the effect of the long wave radiation exchange on the surface temperature and heat fluxes estimation was more evident. The current available simulation tools have been generally ignorant of this effect as most thin membrane products are longwave radiation blind. But it is not true to a foil sheet. Unrealistic thermal-optical discription can result in a certain leve of discrepancy in the prediction, for instance, as the analytical model showed in this thesis.

Although the presented modelling results for the double-layer model with low longwave transmittance was relative satisfied, the flexibility of the model for thermal analysis applying on other type of foil products allowing high heat transmission was limited.

In all, the heat transfer model specified for the thin membrane structure is necessary to include the dynamic thermal radiation simulation components in order to give a good approximation to its thermal behaviour and widen its applicability.

Concerning the simulation of the dynamic state of the additional water layer, the case of the novel construction necessitates the development of an empirical theoretical model, which is specifically tailored for the evaporation process in the cavities of the construction. It was indicated in the thermal modelling that the evaporation process made up about 40% of the overall heat exchanges on the suface of the foil coved with a cooling water layer (Cf. Section 6.5.3.). A good approximation to this process is therefore critical for the overall thermal performance assessment of the novel foil skin construction.

Compared to the complicated thermal behaviour modelling, the external coupling flow analysis could be markedly simplified according to the experimental observation and modelling results presented in this research. As the existence of a thermally sub-homogeneous zone: envelope perimeter zone, the boundary condition of the evaluated envelope could be defined by a limited number of air temperatures close to the foil panel surface. Meanwhile the Internal air velocity close to the surface of the internal foil panel could be considered to be negligible as the internal convective transfer on the inner foil penal is compu-

lated as less than 10% of its overall heat exchanges. Consequently, a simplified boundary model could better interface with the external coupling airflow analysis software. As a result, the interactive steps between the two applications for data feedback into each other could reduce.

7.2.3 Cooling production

One purpose of this proposed system is to produce cooled air from the air cavity of the foil cushion. It is testified in this research that this purpose is infeasible for such an envelope to be exposed to high direct beam radiation. The large volume of airflow functioned to remove heat away from the cavity of the envelope, acting similar to that in a solar chimney.

The sources of the cooling in the presented foil cushion systems can be identified as below:

- The airflow generated either by the mechanical fan, or by nature buoyancy force.
- Relatively low surface temperature of the water layer, the thermal inertial of water adding to the thin foil panel and its modified surface properties due to the water layer.
- A big shading level provided by the drop-wise of the water layer.
- Evaporation process and water convective exchanges on the foil penal with an uniform water spread
- The enhancement on the extent of internal thermal stratification, and then on the desirable buoyancy-induced natural ventilation in the enclosed space

However because a foil cushion unit is structurally stabilised by internal inflation pressure, the flexibility to adjust the airflow rate to higher rate is not practical. The trinity of the velocity in the cavity, inflation pressure, and geometry of the envelope needs to carefully consider when a high velocity is targeted.

To create a uniform water-spread on the designated foil layer is a critical case in the novel construction. The doubly curved surface of the foil skin and complex geometry of a foil cushion result in a negative effect on the water spread generation. According to the comminssioning results (see Section 5.4.3), the thin water layer is preferred that a low water flow rate is required and a minimal amount of thermal mass is imposed on the novel foil cushion construction.

In terms of water sources to provide low water surface temperature, it is possible to use underground water on site, which had been assessed in Section 4.3. Nevertheless, this part of water cooling effect was not investigated in the full-scale enclosure.

In order to create better cooling performance, designers should carefully balance all the above factors when applying this novel glazing system to building applications.

7.2.4 Design implications

It was observed that the foil cushion with a water layer improved its thermal quality if the cladding foil material had a high heat transmittance. But the selection of the material has to balance its thermal performance in dry state and in wet state. Generally, the longwave radiation transmittance below 20% could not produce noticeable modification on its thermal-optical quality, which is verified by the experimental observation and modelling results besides a number of pevious literatures. But the implication of a building clad with such foil products needs a detailed assessement in each particular case in order to reduce the unnecessary heat gains in a warm day when no waterlayer in presence.

The position of the foil cushion unit with a water layer should pay a special attention in order to encourage the cooling performance as required. It had better to locate the foil skin penal with a water layer at the low level close to occupied zone while the roof top area could be clad with the high transparent cushion units without water spraying devices.

As indicated previously, for each cushion unit the transition area of airflow and water collecting outlet requires a careful design to avoid direct exposure to the solar radiation. Moreover, the water-tightness and air tightness were always the issue to the novel foil cushion constructions. The connection components of the construction should be better moulded integrally to prevent vapour and water ingress or egress (Cf. Section 5.4.4).

To sum up, the factors, including solar irradiation, climate condition, building location, orientation, construction design, material selection, user thermal comfort, and building regulations etc, should be comprehensively considered at the design stage in order to bring it into bioclimate strategies to run buildings passively.

7.3 Conclusions and Future Work

The main sources of the rapid overheating in foil cushion enclosures are identified as follows:

- High average solar transmittance of the foil cushion envelope
- Insufficient removal of the heat accumulated in the envelope's construction.
- Inappropriate design to incorporate multiple foil layers with high solar absorption fritted surfaces into foil cushion units

The investigation presented here has proved that the presence of a water layer in the foil cushion envelop coupled with a certain air flow rate could eradicate the impact of the second heat source, mitigate the thermal radiation influence as well as result in no significant drop in the visible light level.

7.3.1 Original contribution to knowledge

Integrating a water layer into a foil cushion construction as an environment friendly means to control the overheating of foil cushion enclosures is put forth by this research for the first time. The evaluation work on the thermal perfomance of the novel construction has produced a number of benchmarks for its later devepment.

- The compatibility of the novel concept and foil cushion constructions has been succefully attested through out this research work.
- Two prototypes of full-scale foil skin constructions based on the novel concept were constructed and satisfied the original design expectations
- A series of preliminary test for the parameter study were carried out to identify the salient parameters underlying the thermal behaviour of the novel constructions. It has proved that the radiative heat transfer has a more dominant role than the airflow convective exchanges on the surface thermal behaviour of the inner foil layer, (which in the meantime follows a close relationship to the state of water layer in presence).
- The varying state of the additional water layer was investigated in the two full-scale test prototypes to establish a set of reference data on the extent of its influence on the overall thermal behaviour of the novel construction.

- Desirable internal themal zoning was evident according to experimental observation. A thermally sub-homogeneous zone around the perimeter envelope was developed and favoured the stablization of the internal posivitive thermal stratification and advocated buoyancy force for internal natural ventilation. The conventional simplified boundary flow model using a limited number of air temperatures to define the internal thermal condtion is testified to be feasible in the external coupling analysis software for this particular construction without raising a concern on the acceptable inaccuracy
- An analytical model is established particularly for this case of construction to facilitate the thermal performance assessment for its intial design stage and provides a startpoint for later devepment.

7.3.2 Suggestions for future work

The foil cushion construction incorporated a cooling water layer is a novel glazing system, and more research input is required to improve its functionality and efficiency. For the moment, this glazing system is only possible to serve as an alternative glazing system with dynamic thermal control functions, running in an environment friendly manner.

Further work is required to produce a design guide for this particular construction.

This analytical simulation tool to predict thermal performance of this typical construction is in a preliminary stage. In future studies one can develop a bespoke numerical model to produce more confident information. The datasets in this thesis could be used to validate the future numerical model as a reliable tool in the thermal environment design. It is hoped that the future development of the thermal simulation tool could assist designers to better appreciate its environmental performance and extend its building applications.

> *"The journey is the reward."*
>
> --- **Chinese proverb**
>
> This PhD study is the toughest journey I have accomplished, and certainly the first of many. The road ahead is long, I will keep going and not settle.
>
> --- Author

REFERENCES

[1] **Krewinkel, H.W**
Glass Buildings: Material, Structure and Detail
1st ed. 1998, Basel: Birkhäuser.

[2] **Schittich C. et al**
Glass construction manual
2nd rev. and expanded ed. Basel: Birkhäuser, 2007. pp73

[3] **Vector Foiltec**
ETFE U values (based the tested on Texlon thermo.)
http://www.vector-foiltec.com/etfe-insulated-structures.html [Accessed on July 2010]

[4] **Architen Landrell**
ETFE foil: a guide to design
http://www.architen.com/technical/articles/etfe-foil-a-guide-to-design [accessed July 2010]

[5] **Robinson L. A.**
Structural Opportunities of ETFE (ethylene tetra fluoro ethylene),
Master Dissertation, Department of Mechanical Engineering, Massachusetts Institute of Technology. June 2005. pp22-23

[6] **G.James Group**
Glass Handbook
1st edition, pp8, http://www.gjames.com.au/brochure/glasshandbook.pdf,

[7] **Wigginton M. and Harris J.**
Intelligent Skins
2002, Oxford: Architectural Press

[8] **Kragh M.**
Building Envelopes and Environmental Systems: Modern Façades of Office Buildings
2000. The Netherlands: Delft Technical University.

[9] **Uuttu S.**
Study of Current Structures in Double Skin Facades
Department of Civil and Environmental Engineering, 2001, Helsinki University of Technology: Helsinki, Finland

[10] **Velazquez R., et al**
Case study of outdoor climatic comfort: The Palenque at Expo'92
Proceedings of the Ninth International PLEA Conference: Architecture and Urban Space, Seville, Spain, September 24-27, 1991. London: Kluwer Academic Publishers, pp. 203-208.

[11] **Harvie G. N.**
An investigation into the thermal behaviour of spaces enclosed by fabric membranes.
PhD Thesis, Cardiff University of Wales, 1995

[12] **Devulder T.**
The thermal response of textile membrane
PhD Thesis, School of the Built Environment, The University of Nottingham, 2005.

[13] **Poirazis H., et al**
Energy modelling of ETFE membranes in building applications
Eleventh International IBPSA Conference, Glasgow, Scotland July, 2009. pp. 696-703

[14] **Thomas Hofmann**
FoilGlass - an innovative glazing. From concept to reality
Centrosolarglas GmbH & Co. KG, Gerhard Reisinger, Research Centre Jülich GmbH

[15] **Beukers A., Van Hinte E.**
Lightness
3rd Edition, preface by WIJERS, G. J. Rotterdam: 010 Publishers, 2001, p. 5

[16] **Rice P.**
Lightweight structures: Introduction
The Arup Journal, Vol. 15, No. 3, October 1980, p.2..

[17] **Robinson G., et al**
ETFE foil cushions in roofs and atria
Construction and Building Materials. Vol.15, Feb. 2001, pp.3 2 3 -32

[18] **Kaltenbach, F. (ed.)**
Translucent Materials: Glass Plastic Metals
Munich: Architecktur-Dokumentation GmbH & Co.KG, 2004. pp.64-69

[19] **Vandenberg M.**
Soft Canopies, Detail in Building
Singapore: Academy Editions, 1996, p.9

[20] **Erger H.**
Light structures, structures of light. The art and engineering of tensile architecture
Basel: Birkhauser-Verlag fur Architektur, 1996, p.32

[21] **Stephen Tanno**
ETFE foil cushions as an alternative to glass for atriums and roof-lights
ICBEST 97 conference proceedings, 1997, p. 357

[22] **Popovic Larsen O., Tyas A**
Conceptual Structural Design: Bridging the gap between architects and engineers
London: Thomas Telford, 2003, pp.107-123

[23] **Forster B., Mollaert M**
The European Design Guide for Tensile Surface Structures
2004, Tensinet, Brussels, pp. 51

[24] **Klaus-Michael Koch, et al**
Membrane structures: innovative building with film and fabric
Munich; London: Prestel, c2004. pp. 115-116

[25] Ibid. Klaus-Michael Koch, et al, Membrane structures ..., pp. 58-59

[26] **Hegger M., et al**
Construction Materials Manual
Basel : Birkhäuser, c2006. pp. 93-95 and pp. 129-130

[27] **Herzog T.**
Pneumatic Structures: A Handbook of Inflatable Architecture
Oxford University Press, p. 142

[28] **Seidel M.**
Tensile Surface Structures: A Practical Guide to Cable and Membrane Construction
1st edition, Wiley-VCH, August 12, 2009, p.35

[29] **Santamouris M. and Asimakopoulos D., (eds)**
Passive Cooling of Buildings
London: James & James Science Publishers Ltd. 1996

[30] **Zhao X., et al**
Numerical study of a novel counter-flow heat and mass exchanger for dew point evaporative cooling
Applied Thermal Engineering, Volume 28, Issues 14-15, October 2008, pp. 1942-1951

[31] **Guillermo Z., et al**
Watergy project: Towards a rational use of water in greenhouse agriculture and sustainable architecture.
Desalination, Volume 211, Issues 1-3, Ninth Environmental Science and Technology Symposium - September 1-3, 2005, Rhodes, Greece, 10 June 2007, pp. 296-303

[32] **Nelson R.**
Liquid solar technologies
http://www.solaroof.org/wiki/SolaRoof/LiquidSolarTech. [access Jun 2010]

[33] **Zhao X. et al**
Feasibility study of the dew point evaporative cooling system for UK & EU building air conditioning
the 7th International Conference on Sustain-able Energy Technologies, Soul, Korea, August 2008, pp. 921-926.

[34] **Sujoy Pal et al.**
Heat transfer modelling on windows and glazing under the exposure of solar radiation,
Energy and Buildings, Volume 41, Issue 6, June 2009

[35] **Compagno A.**
Intelligent Glass Facades
5th revised and updated ed. 2002, Basel, Boston, Berlin: Birkhäuser

[36] **Wu H., et al**
The Stratification in fabric roof structures a strategy of energy conservation and system design
International Symposium on Architectural Fabric Structures, AFSF, 1984, pp. 192-196

[37] **The Nature of Radiation**
The nature of radiation
2009 http://www.physicalgeography.net/fundamentals/6f.html [accessed July 2010]

[38] **Lienhard J. IV et al**
A heat transfer textbook, 3rd ed.
Phlogiston press.2004, p.529

[39] Ibid. Lienhard J. IV et al, A heat transfer... p. 30

[40] Ibid. Lienhard J. IV et al, A heat transfer... p. 534

[41] **Giacomelli G., Roberts, W.**
Greenhouse covering system
Rutgers University Cook College, http:/bettergreenhouses.com/ GreenhouseGlazing.pdf [accessed December 2010]

[42] **Nan Ya plastic corporation**
Thermal-Optical properties of typical Nan Ya flexible PVC sheeting
Plastics 1st Division, [received via E-mail communication, Dec, 2009.] Appendix:A7

[43] **Reisinger G., et al**
Glass Foil – A New "Glazing" Possibility
FLABEG Solarglas GmbH & Co. KG. Library Article . website: http://www.glassfiles.com/library/ [Retrieved at 27th Jun 2010]

[44] **Hightex**
ETFE Transparent or translucent ETFE membranes
Highexworld, http://www.hightexworld.com/technical/materials/efte-foil [accessed Aug. 2010

[45] **Hanson, K, J**
The Radiative Effectiveness of Plastic Films for Greenhouses
U. S. Weather Bureau, Washington, D. C., December 1963. website: http:// journals.ametsoc.org [accessed December 2010]

[46] **Devulder T.**
The thermal response of textile membrane constructions
PhD Thesis, School of the Built Environment, The University of Nottingham, 2005, pp.6-73

[47] **Nicholls R.**
Low energy design
Action Energy (programme), Interface Publishing, 2002. p.19

[48] **Thermal transmission through buildings**
Thermal transmission through buildings, at website:
http://personal.cityu.edu.hk/~bsapplec/newpage218.htm [accessed July2010]

[49] **Schittich C. et al.**
Glass construction manual
2nd rev. and expanded ed. 2007, Basel: Birkhäuser,. p. 60

[50] **Goodfellow**
Polymer thermal property
www.goodfellow.com [accessed July 2010]

[51] **BS EN ISO 10077**
Thermal performance of windows, doors and shutters---Calculation of thermal transmittance
British Standards Institution, 2006. p. 15

[52] **Hirokazu M., Kiyotaka K.**
Thermal property of coated fabrics
International Symposium on Architectural Fabric Structures: The Design Process, 1984, pp. 66–69.

[53] **Devulder T. , et al.**
The thermal behaviour of buildings incorporating single skin tensile membrane structures
International Journal of Low Carbon Technologies 2/2, 2007, pp200

[54] **El-Asfouri S., et al**
Effect of various factors on the shading coefficient of different types of glazing
Building and Environment, Volume 23, Issue 1, 1988, pp. 45-55

[55] **Ieremia L.**
Client communication letter to Carisbrook Stadium Trust,
June 2008. at website: http://www.dunedin.govt.nz [accessed July 2010]

[56] **Larsson L**
Heat insulation of air-supported structures
International Symposium on Air Supported Structures, 1977, pp. 202- 219

[57] **Croome D., Moseley P.**
Environmental design of air-houses
Proceedings of conference "The design of air-supported structures", Bristol, the Institution of Structural Engineers, London, 1984, pp. 213-222

[58] **CIBSE Guide A**
Environmental design
page Bros. (Norwich) Ltd., Norwich, UK, 1999, pp5:80-5:81.

[59] **Forster B., Mollaert M**
The European Design Guide for Tensile Surface Structures
2004, Tensinet, Brussels, pp.104-106

[60] Ibid. Forster B et al, The European ... p.110

[61] **Faggembauu D.**
Heat transfer and fluid-dynamics in double and single skin facades
PhD Thesis, Departament de Màquines i Motors Tèrmics, Universitat Politècnica de Catalunya, 2006, pp. 82-84

[62] **Hoar C.**
An overview of advanced glazing technology.
the Proceedings of Symposium on Glass in Buildingsh,1999, the University of Bath,pp. 165.

[63] **Baker N. , Steemers K.**
Energy and Environment in Architecture. 2nd ed.
2005,Oxon, UK: Taylor and Francis. P. 224

[64] **Kessling W., et al**
Innovative Design Concept for the New Bangkok International Airport, NBIA
Proceedings of Symposium on Improving Building Systems in Hot and Humid Climates, 2004, Dallas

[65] **Hegger M.**
Construction Materials Manual,
Basel : Birkhäuser, c2006. pp.97-145

[66] **Pieters, J. G. et al**
Light transmission through condensation on glass and polyethylene
Agricultural and Forest Meteorology, Volume 85, Issues 1-2, June 1997, pp 51-62

[67] **Cemek B, et al**
Testing of the condensation characteristics and light transmissions of different plastic film covering materials
Polymer Testing, Volume 24, Issue 3, May 2005, pp 284-289

[68] **Pollet I. V., et at**
Condensation and Radiation Transmittance of Greenhouse Cladding Materials, Part 2: Results for a Complete Condensation Cycle
Journal of Agricultural Engineering Research, Volume 75, Issue 1, January 2000, pp.65-72.

[69] **Pieters, J. G. et al**
Light transmission through condensation on glass and polyethylene
Agricultural and Forest Meteorology, Volume 85, Issues 1-2, June 1997, pp 51-62

[70] **Pollet, I.V. et al**
PAR transmittances of dry and condensate covered glass and plastic greenhouse cladding
Agricultural and Forest Meteorology, Volume 110, Issue 4, 28 February 2002, pp. 285-298,

[71] **Chaibi M.T., et al**
Effects of a Solar Desalination Module integrated in a Greenhouse Roof on Light Transmission and Crop Growth
Bio-systems Engineering, Volume 90, Issues 3, 2005, pp319–330,

[72] **Chaibi M.T.**
Greenhouse Systems with Integrated Water Desalination for Arid Areas Based on solar Energy
PhD Thesis, Department of Agricultural Bio-systems and Technology, Swedish University of Agricultural Sciences, Swedish University of Agricultural Sciences, Alnarp 2003, pp14

[73] **Zhu, S. et al**
Modelling the thermal characteristics of greenhouse pond systems
Aquacultural Engineering, Volume 18, Issue 3, September 1998, pp201-217.

[74] **Nijskens, J, et al**
Heat transfer through covering materials of greenhouses
Agricultural and Forest Meteorology, Volume 33, Issues 2-3, December 1984, pp193-214

[75] **Environmental Design: CIBSE Guide A**
Chartered Institution of Building Services Engineers
CIBSE 1999, pp2:27-2:38

[76] Ibid. Environmental Design: CIBSE Guide A... pp. 1:6-1:12

[77] **Chang J.**
Ground Temperature
Volume II, Harvard University, Blue Hill Meteorological Observatory, Milton Massachusetts, June 1958, pp111-169

[78] **Mori H.**
Enhancement of heat transfer for ground source heat pump systems
PhD Thesis, Department of Architecture and Built Environment, The University of Nottingham, Oct 2010, p.34

[79] **Pollet, I. V. et al**
Condensation and Radiation Transmittance of Greenhouse Cladding Materials: Part 1, Laboratory Measuring Unit and Performance
Journal of Agricultural Engineering Research, Volume 74, Issue 4, December 1999, pp. 369-377

[80] **Pump Express**
Product Catalogue. 2007,
Pump Express Ltd: 61-62 Lower Dock Street, Kingsway, Newport, South Wales. NP20 1EF, Website:
http://www.pumpexpress.co.uk/multi_800_1300_2500.htmFigures and tables

[81] **Datataker**
DT500/600: specifications 2007
Datataker Pty Ltd: 7 Seismic Court, Rowville, Australia, VIC 3178. Website:
http://www.datataker.com/products/dt500.html

[82] **Datataker, Delogger-Plus**
DeLogger Plus Software
Ed. Software: Discbell Ltd, Manual: Data-Electronics, 1997, Australia
http://www.datataker.com/products/dt500.html,

[83] **CIBSE Guide A Environment design: Supplementary data**
Appendix, Radlat55.txt,
Chartered Institution of Building Services Engineers, CIBSE 1999, UK.

[84] **Xie F. et al**
New evaporative cooling integrated pneumatic clear foil cushion construction
8th International Conference on Sustainable Energy Technologies, .Aachen, Germany, Sept 2009.

[85] **Hughes, J.**
Technology evaluation of thermal destratifiers and other ventilation technologies
Naval Facilities Engineering Service Centre, U.S.A. Website:
http://www.theairpear.com/goopages/pages_downloadgallery/downloadget.php?filename=12425.pdf&orig_name=d1hughes.pdf [last visited: December 2010]

[86] **AEG**
Three phase motors: technical catalogue
Lafert GmbH, Bahnhofstraße 31, D - 73728 Esslingen, Germany. Website:
http://www.lafert.com/lafert/az/products_zoom.php?id_az=6&id=1093

[87] **Allen-Bradley**
Allen-Bradley PowerFlex 4 Adjustable Frequency AC Drive
PowerFlex 4 technical data sheet at website:
http://www.ab.com/en/epub/catalogs/36265/1323285/9463640/tab3.html

[88] **Bentley, J.P.,**
Principles of measurement systems
4Rev Ed edition ed. 2004, Harlow: Pearson Prentice Hall. P. 544.

[89] **BS EN ISO 6946**
Building components and building elements: Thermal resistance and thermal transmittance -Calculation method
British Stands Institution, 2007 , pp.12-17

[90] **Tang, R. et al**
Comparative studies on the water evaporation rate from a wetted surface and that from a free water surface
Building and Environment, Volume 39, Issue 1, January 2004, pp77-86

[91] **Ventilation and Air Conditioning: CIBSE Guide B2**
Chartered Institution of Building Services Engineers
CIBSE 2001, pp3:33-3:37

[92] **Yang, S.M. et al**
Heat Transfer, 3rd edition
Higher Education Press, 1998, pp. 168–169

[93] **Totton-pumps**
Magnetically Coupled Centrifugal Pump
NEMP 40/4 technical data sheet at website:

http://www.totton-pumps.co.uk/product8.html

[94] **Visual Flow Indicators**
Liquid flow indicator (0.2 - 2 l/min. Stock no. 256-281)
Technical overview at website: http:// uk.rs-online.com/

[95] **Barna P.S.**
Fluid Mechanics for Engineers
edition, Butterworths, London, 1964. pp.56-62

[96] **Mayer, D. K**
Transport refrigeration unit combination airflow straightener and defrost damper
United States Patent 4441333, website:
http://www.freepatentsonline.com/4441333.html, [last visited: December 2010]

[97] **Klassen, C.J. and House, J.M.**
Equal Area vs. Log-Tchebycheff,
TAB journal, AABC, Summer 200, pp. 7-11

[98] **Air monitor corporation**
Standards: Velocity Traverse of Air Ducts,
Details at website:
http://www.airmonitor.com/documents/shared/brochures/BRO_Standards_12501300.pdf

[99] **Zhang, X.M. et al**
Fundamentals of Heat Transfer, 3rd edition
China Architecture & Building Press, 1997, pp.143-144

[100] Ibid. Zhang, X.M. et al, Fundamentals of Heat Transfer...pp.208-209

[101] Ibid. Zhang, X.M. et al, Fundamentals of Heat Transfer...pp.113-120

[102] Ibid. Zhang, X.M. et al, Fundamentals of Heat Transfer...Appendix 3, pp.290-291

[103] **Qiu, X.L. et al**
Thermodynamics-Engineering Approach, third edition
China Architecture & Building Press, 1992, pp.61-66

[104] **Croome D, Moseley P**
Environmental design of airhouses
Proceedings of conference "The design of air-supported structures", Bristol, the Institution of Structural Engineers, London, 1984, pp. 213-222

[105] **Hart G, Blancett R, Charter K**
The use of DOE-2 to determine the relative energy performance of daylighted retail stores covered with tension supported fabric roofs
Energy and Buildings, vol. 6, 1984, pp. 343-352

[106] **Howell S, Potts I**
On the natural displacement ventilation flow through a full scale enclosure, driven by a source of buoyancy at floor level
Seventh International IBPSA Conference, Rio de Janeiro, Brazil, August 13-15, 2001, pp. 627-634

[107] **Clarke J**
Energy simulation in building design (2nd edition)
Butterworth-Heinemann, Oxford, 2001, Section 7.4.1

[108] Ibid. Clarke J, Ibid. Clarke J, Energy simulation in building design, Section 7.6.2

[109] **Clarke J**
Radiation modelling
M0404 EEnergy systems modelling, website:
http://www.esru.strath.ac.uk/Courseware/Class-ME404/index.htm [Asseced Jan. 2011]

[110] **Harvie G. N.**
An investigation into the thermal behaviour of spaces enclosed by fabric membranes.
PhD Thesis, Cardiff University of Wales, 1995, p.96

[111] Ibid. Harvie G. N., An investigation into the thermal behaviour... p.130

[112] Ibid. Harvie G. N., An investigation into the thermal behaviour... p.141

[113] **ASHRAE**
ASHRAE handbook: Fundamentals (S.I. edition)
American Society of Heating, Refrigeration and Air-conditioning Engineers, Inc., Atlanta, ISBN 1883413451, 1997. pp. 4:19-4:20

[114] **Devulder T.**
The thermal response of textile membrane constructions
PhD Thesis, School of the Built Environment, The University of Nottingham, 2005, Appendix A.

APPENDIX A

Detailed Specifications of Monitoring Equipment

A.1 Thermocouple Sensors

Thermocouple type	Type K
Temperature measurement range	-40℃ to +1100℃ (operating temp=-50℃ ~200℃)
Accuracy - Class 1	±1.5℃ or 0.0075xT (T in ℃)
+Ve arm	Nickel/Chromium
- Ve arm	Nickel/Aluminium
Wire diameter	0.2mm
Insulation	PTFE
BS specification number	BS4937 Part 30
Extension cables	Solid conductor, shielded, 0.3mm^2 conductor diameter, Miniature connectors and plugs

A.2 Pyranometers

Sensor 1	Kipp & Zonen CM6B
Sensitivity	9-15 μV/W/m^2
Sensitivity calibration	Variable (±0.5%, at normal incidence on horizontal pyranometer): 12.09 μV/W/m
ISO response time (95%)	18s
Zero offset 1: 200W/m^2 thermal radiation 2: 5K/h change in ambient temp	 <15W/m^2 <4W/m^2
Non-stability	<±1% change per year
Non-linearity	±1.2% (<1000W/m^2)
Directional error (beam radiation)	< ±25W/m^2 at 1000 W/m^2
Spectral selectivity	±2% (350-1500nm)
Temp dependence of sensitivity	±2% (-10 to +40℃)
Tilt response	< ±1% (beam light 1000W/m^2)
Impedance	70-100 Ohm
Spectral range	305-2800nm (50% points)

Notes:
The more specification details refer to the "Declaration of conformity, according to EC guideline 89/336/EEC 73/23/EEC, CM6B/7B", from
http://www.kippzonen.com/?downloadcategory/38192/Discontinued+Solar+Instruments.aspx.

Sensor 2	Skye instruments LTD. SKL2650
Sensitivity	0.667mV/W/m^2
ISO response time	50ms
Zero offset	-0.02mV@9Volts
Absolute calibration error	<3%, maximum 5%
Cosine error	3%
Azimuth error	< 1%
Long-term stability	±2%
Temperature co-efficient	±0.1% /℃
Spectral range	700-1100nm
detector	Silicon photocell

Notes:
The more specification details refer to the manual "Skye, high output light sensors, SKL 2610, SKL 2620, SKL 2630, SKL 2640, SKL 2650" , some technical information from *http://www.skyeintrucments.com.*

Sensor 3	Skye instruments LTD. SKL510
Sensitivity	1mV=100W/m^2
Working range	0-5000W/ m^2
ISO response time	10ns
Zero offset	-0.02mV@9Volts
Absolute calibration error	<3%, maximum 5%
Cosine error	3%
Azimuth error	< 1%
Long-term stability	±2%
Temp co-efficient	±0.1% /℃
Sensor pass-band	400-700nm
Internal resistance	c.300 ohm
detector	Silicon photocell

Notes:
The more specification details refer to the manual "Skye, single channel light sensor, SKP210, SKP 215, SKL310, SKL 510, SKL 1110" some technical information from *http://www.skyeintrucments.com.*

A.3 Light Source Simulator

Name	Floddllight luminaire
Type	Tungsten Halogen, encased
Manufacturer	Osram
Wattage	500W
Voltage	230V
Life (Hrs)	2000
Luminous flow	9500 lm
Colour temperature	3000 ℃
Lamp bulb length	114.2mm
Warm up time	20 minutes

Notes:
The specification details refer to the "Bright ideas with OSRAM halogen lamps", from http: *art-rasvjeta.hr/images/download/Katalog-**Osram**.pdf and Website: http://catalog.myosram.com/*

A.4 Velocity Sensors

Name: portable sensor	TA 45 Thermal Anemometer
Manufacturer	Airflow Developments Limited
Velocity ranges (m/s)	0-30
Accuracy (at ambient conditions of 20℃ and 1.013 bar)	±3.0% of reading ±1 digit or ±0.06m/s of reading ±1 digit, whichever is the greater
Operating temperature range	10-50℃
Input power	Four 1.5 volt AA battery

Notes:
The specification details refer to the manual "Airflow, TA45 thermal anemometer operating instructions"
Website: *http://www.airflow.co.uk*

Name	TSI, Air velocity transducer
Models	8455
Manufacturer	TSI Incorporated, USA
Field selectable velocity ranges (m/s)	0.125 to 1.0, 1.25, 1.5, 2.0, 2.5, 3.0, 4.0, 5.0, 7.5, 10.0, 12.5, 15.0, 20.0, 25.0, 30.0, 40.0, 50.0.
Accuracy	±2.0% of reading, ±0.5% of full scale of selected range. (From 18℃ to 28℃, outside this range add 0.2% per ℃, within temperature compensation range.)
Operating temperature range	0-93℃
Input power	11-30VDC

Notes:
The specification details refer to the manual "TSI, Air Velocity transducer technical specifications: Models 8455/8465/8475, 2007, TSI Incorporated: 500 Cardigan Road, Shoreview, MN 55126 U.S.A."
Website: *http://www.tsi.com/documents/2980575_8455-65-75-AVT.pdf*

A.5 Air Pressure Sensors

Model	Digitron pitot tube instrument AF200, multifunction anemometer
Manufacturer	Digitron, U.K.
Measuring range in pressure	0 to 2000Pa
Supply voltage	PP3 battery
Auxiliary component	12 inches diameter pitot tube
Accuracy in pressure measurements	±0.2% rdg ±1 digit (+5 to 25℃)
	±0.3% RDG ±1 digit (-10 to 15℃)
Correction range	static pressure: settable range= 500-1500mbar
	Pitot tube calculation factor(k): settable range= 0.1-3.0

Notes:
The specification details refer to the "Digitron, AF200 datasheet",
Website: www.digitron.co.uk.

A.6 Hygrometer Sensors (Temperature and Humidity Probe)

Model	HMP45A probe
Manufacturer	Vaisala (HUMICAP), Finland
Operating temperature range	-40℃ to 60℃
Supply voltage	7 to 35 VDC
Settling time	500ms
Relative humidity	Measurement range: 0.8 to 100% RH
	Output scale: 0 to 100%=0 to VDC
	Accuracy at 20℃ (including non-linearity and hysteresis): versus factory reference ±1%RH.
	Field calibration versus references ±2% RH (0 to 90%), ±3%RH (90to 100%RH).
	Temperature dependence: ±0.05%RH/℃
	Response time (90%) at 20℃: 15s with membrane filter.
Temperature	Measurement range: -39.2 ℃ to 60℃
	Output scale: -40℃ to 60℃ =0 to 1 VDC
	Accuracy at 20℃: ±0.2℃

Notes:
The specification details refer to the "Vaisala HUMICAP Humidity and Temperature Probes HMP45A/D, User's Guide", Manu direct from manufacturer.

A.7 PVC Technical Data Sheet

三. 奈米遮光隔熱膠布效果測試:

1. 奈米遮光隔熱膠布光穿透率比較:

區分	試樣代號			說　　明
	Blank	IR50	IR70	光線波長測試範圍
紫外光透過率 (%)	10.5%	3.0%	2.2%	250nm~400nm
可見光透過率 (%)	89.6%	64.9%	48.5%	400nm~800nm
紅外光透過率 (%)	73.2%	24.1%	10.7%	800nm~2500nm

2. 奈米遮光隔熱膠布與一般透明膠布對紅外光(IR)遮蔽效果比較: 如下圖

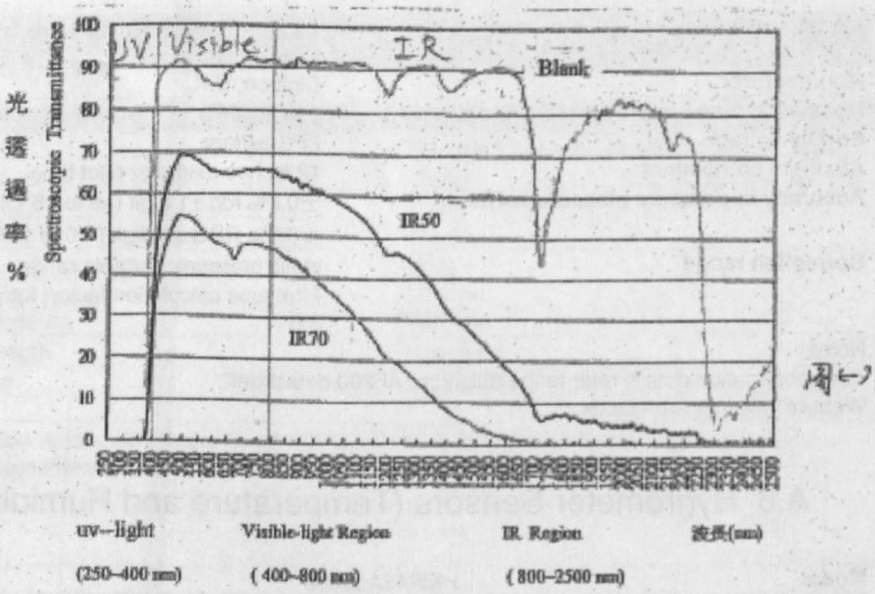

圖七

Note: 上列使用 光穿透率測量儀(Spectrophotometer MPC-3100,Shimadzu)實測數據.
使用不同測量儀器所得數據略有差異.測試結果僅供參考比較.

KAYOSPRUCE LTD

2 Cockerell Close, Segensworth West, Fareham, Hants PO15 5SR
Tel: +44 (0)1489 581696 Fax +44 (0)1489 573489
Web Site: www.sailcloth.co.uk Email: kayospruce@sailcloth.co.uk

- MARINE & TECHNICAL FABRICS
- SAILCLOTH
- HARDWARE & ACCESSORIES
- ACRYLICS

P.V.C Window Material (Taiwan)

Technical Specification

Raw Material	PVC	
Thickness	0.25mm – 10 Thou 0.50mm – 20 Thou 0.75mm – 30 Thou	
Tensile Strength	10 & 20 Thou 30 Thou	Warp - 190kg / cm2 Weft - 180kg / cm2 Warp - 200kg / cm2 Weft - 190kg / cm2
Tear Strength	10 & 20 Thou 30 Thou	Warp - 6kg / mm Weft - 6kg / mm Warp – 7kg / mm Weft - 6kg / mm
Elongation (%)	10 & 20 Thou 30 Thou	Warp - 240 Weft - 260 Warp - 250 Weft – 250
Heat Shrinkage (%)	10 & 20 Thou 30 Thou	Warp - Minus 5 Weft – Plus 2 Warp – Minus 3.5 Weft – Plus 3.0
Width	10, 20 & 30 Thou – 137cm	
Weight	10 Thou – 320g / m2 20 Thou – 640g / m2 30 Thou – 960g / m2	
Fire Retardant	To BS 5438 and MVSS 302	
UV Resistant	Yes	
Roll Length	10 Thou – 100m 20 Thou – 50m 30 Thou – 30m	

Kayospruce Ltd is registered in England and Wales at
2 Cockerell Close, Segensworth West, Fareham, Hampshire PO15 5SR
Director: I. M. Dawson VAT No: 330 0826 21 Reg. No: 1709530

A.8 Fairy Rinse Acid Product Information

1. Identification of the Substance/Preparation	**Fairy Rinse Aid + Active Drying Power**
Company Name:	Procter & Gamble UK
Address:	Brooklands, Weybridge, Surrey KT13 0XP UK
Telephone #:	Tel: 01932 89 6000 Fax: 01932 89 6200
Emergency phone #:	0800 328 5901 (UK); 1800 535 640 (ROI)
Email Address:	rose.yd@pg.com
2. Hazards identification	This product classified as Xi; R36 (Irritant; Irritating to eyes) according to EU Directive 1999/45/EC. Eye contact: Transient superficial irritation. Skin contact: Prolonged exposure may cause skin irritation. Ingestion: Possible mild gastro-intestinal irritation with nausea and vomiting. Inhalation: Inhaling of particles may cause mild irritation of the respiratory system.
3. Composition/information on ingredients	An automatic dishwashing rinse aid containing:

Common Name	CAS	EINECS/ELINCS	Classification	Conc
ETHANOL	64-17-5	200-578-6	R11-F	1-5%
CITRIC ACID MONOHYDRATE	5949-29-1	201-069-1	R36-Xi	1-5%
Trideceth-7 Branched	69011-36-5	Polymer	R22,41-Xn	20-30%
ALCOHOLS, C13-15-BRANCHED AND LINEAR, BUTOXYLATED, ETHOXYLATED	111905-53-4	POLYMER	R50-N	10-20%

8. Exposure controls / Personal protection	Not a hazard in normal use. No personal protective equipment required.
9. Physical and chemical properties	Appearance: Transparent Liquid Odour: perfumed pH (10% solution): 2.5 Flammable: NO Explosive: NO Oxidizing: NO Relative density (g/l): 1.064 Water solubility: High
10. Stability and reactivity	Stable under normal conditions.
11. Toxicological information	Not acutely toxic, may cause vomiting. If very large quantities are ingested, treat symptomatically. Do not induce vomiting. If irritant effects are seen, these will be mild to moderate, depending on exposure. If in contact with eyes flushing with water is recommended. Estimated acute oral toxicity: LD50 (rats) > 2g/kg Eye irritation: Mildly to moderately irritating to eyes Skin irritation: Slightly irritating to skin Chronic toxicity: Repeated exposure to low levels (e.g. residues left on dinnerware) will not cause adverse effects Contact sensitization: Does not provoke a sensitization reaction
12. Ecological information	The product is intended for wide dispersive use and is compatible with the down-the-drain disposal route. The product is not considered harmful to aquatic organisms nor to cause long-term adverse effects in the environment. The surfactants contained in this preparation comply with the biodegradability criteria as laid down in Regulation EC/648/2004 on detergents.
13. Disposal considerations	Consumer products ending up down the drain after use. Observe safe handling precautions and local legislation.
14. Transport information	Not subject to ADR/IATA/IMDG codes.
14. Transport information	Not subject to ADR/IATA/IMDG codes.
15. Regulatory information	This product is classified as Xi; R36 (Irritant; Irritating to eyes) according to EU-Directive 1999/45/EC and national laws. All substances in the preparation are registered in the EU. Label information: Irritant Irritating to eyes. Keep out of reach of children. Avoid contact with eyes. In case of contact with eyes, rinse immediately with plenty of water and seek medical advice. If swallowed, seek medical advice immediately and show this container or label.
16. Other information	This product does not require any special training before use. Usage and handling instructions are mentioned on package and on this Material Safety Data Sheet. Safety Data Sheet available on http://www.scienceinthebox.com/en_UK/product/prodcomp_english_en.html

Notes:

The specification details refer to the "Fairy Rinse Aid + Active Drying Power, Safety data sheet (2001/58/EC)" from http: www.scienceinthebox.com/en_UK/.../FairyRinseAid+ActiveDryingPower.pdf

APPENDIX B

This appendix presents the workflow of the simulation tool implementing the theoretical framework described in Chapter 6. The spreadsheet formant of Microsoft Excel™ (version X or 2003, compatible) is flexible to alter and easy to provide graphical feedback about the behaviour of the analytical model.

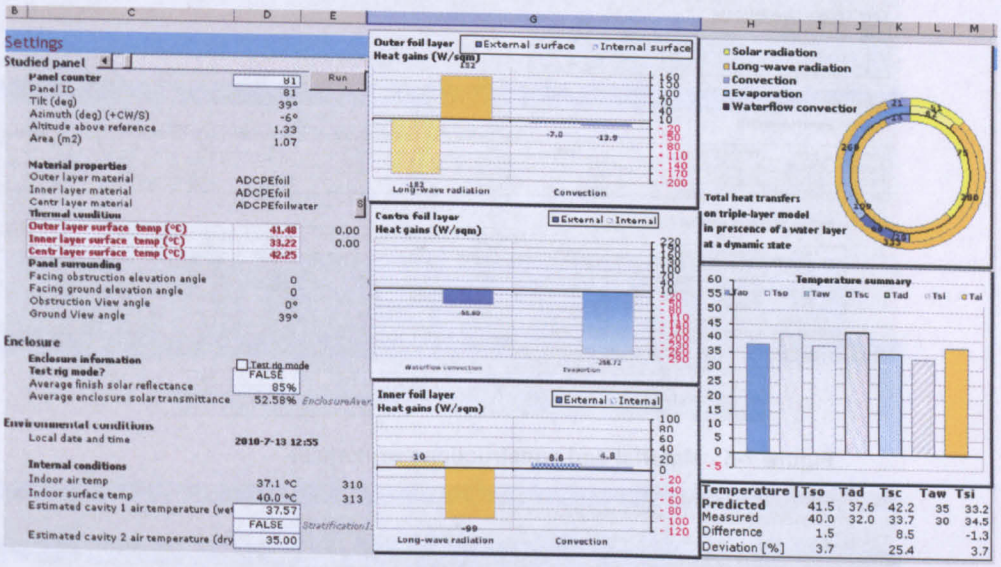

Figure 7-1: Modelling settings worksheet and graphical feedback

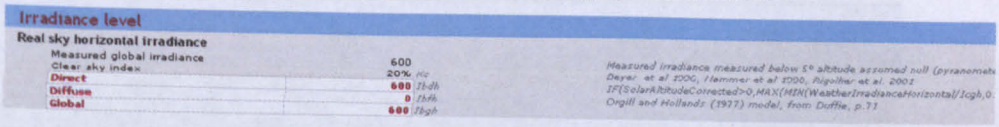

Figure 7-2: Solar simulation model worksheet

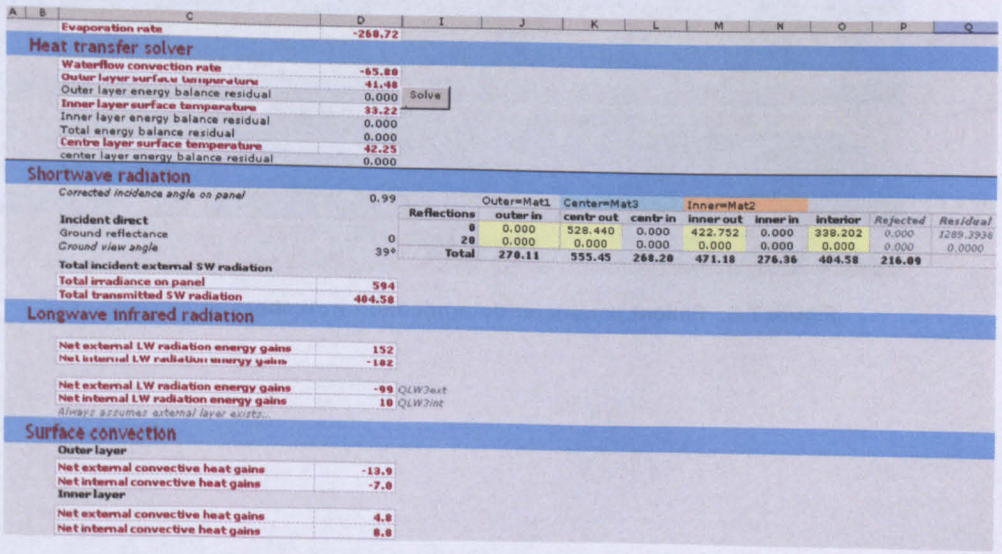

Figure 7-3: Heat transfer model worksheet

Current Panel

Surf ID	Material Code	Surface Orientation on turntable: Azimuth	Surface Orientation on turntable: Tilt	Surface information (Absolute): Area	Perimeter	Rel Altitude	Azimuth	Tilt
81	0.00	-6	39	1.07	4.95	1.33	-6.46	38.52

Figure 7-4: Gometric discription of the foil penal

Constructions

Current construction

ID	Outer	Inner	Centre
4	ADCPE	ADCPE	ADCPEwet

Construction type database

ID	Outer	Inner	Centre
2	PVC	PVC	
3	ADCPE	ADCPE	ADCPE
4	ADCPE	ADCPE	ADCPEwet

Materials

Current panel materials

				Near Normal solar optical properties			Diffuse solar optical properties			LW emittance		
Layer	Code	Product name	Type	Tn	Rn	An	Td	Rd	Ad	Eint	Eext	Data
Outer	ADCPE	ADCPEfoil	foil	89.0%	7.0%	4.0%	80.0%	10.0%	10.0%	33%	33%	
Inner	ADCPE	ADCPEfoil	foil	89.0%	7.0%	4.0%	80.0%	10.0%	10.0%	33%	33%	0
Centre	ADCPEwet	ADCPEfoilwater	foil+water	91.0%	5.0%	4.0%	80.0%	10.0%	10.0%	33%	97%	
						Total	52.58%					

Skins materials property database

			Near Normal solar optical properties			Diffuse solar optical properties			LW emittance		
Code	Product name	Type	Tt	Rt	At	Ts	Rs	As	Int	Ext	Data
SF3	SheerFill III (default)	Membrane	15.0%	70.0%	15.0%	17.0%	70.0%	13.0%	89%	89%	Invar
FF2	Ferrari Fluotop 1202	Membrane	12.0%	61.0%	27.0%	6.0%	72.0%	22.0%	86%	86%	
lowE	Low-e liner (one-sided)	Membrane				3.0%	72.0%	25.0%	85%	35%	Trans
PVC	PVCfoil	foil	89.6%	7.0%	3.4%	81.0%	9.0%	10.0%	62%	62%	
PVCwet	PVCfoilwater	foil+water	53.8%	5.0%	41.2%	50.0%	40.0%	10.0%	62%	97%	
ADCPEwet	ADCPEfoilwater	foil+water	91.0%	5.0%	4.0%	80.0%	10.0%	10.0%	33%	97%	

Angular optical behaviour of generic membranes

From Harvie's Edwards Type Integrating sphere measurements, p.96

Angle of incidence	0	50	60	70	85	90
Transmittance factor	1	0.7	0.6	0.5	0.3	0
Absorptance factor	1	1.05	1.05	1	1	0

Figure 7-5: Material and constructions worksheet

Surrounding surface finishes

Maximum surf temp above and below air temperature

Code	Tmax	Tmin	SR	Material
ConD	7	-1	0.2	Old concrete

External surface convection

	Smooth surface			Rough surface		
Max velocity	a	b	n	a	b	n
4.88	0.99	0.21	1	1.09	0.23	1

Constants

Stefan-Boltzmann	5.67E-08
Celcius to Kelvin	273.15

Velocity define for the Poin2 in Cavity at height of 1.15m

Velocity (m/s)	0 Fanset=5	Fanset=10	Fanset=12	Fanset=	Fanset=1	Fanset=20	Fanset=22	Fanset=25	Fanset=30
Vin	-	0.1700	0.2850	0.3110	0.3680	0.4850	0.5250	0.5910	0.4720	0.8000
V1	-	0.0784	0.1314	0.1434	0.1697	0.2237	0.2421	0.2726	0.3099	0.3690
inlet ar Ain	0.0376									
measur A1	0.075									
1-bend KB	0.7486649									
from 'fl Vel coefficient (k)	0.85									

Water layer velocity relative to the foil surface (mean value)

Water layer velocity	Vol rate [L/m	0.5	0.7	0.9
Vol	0.7		0.2333333	
Thickness of water layer [m	0.1			
width of water layer per len	500			
Relative air flow velocity =	0.4754712			

water convection cooling rate on the triple-layer foil skin construction

	Qw=	hwx=	Rax=	Lx(m)=predicted	Tw=	Twcx=(sur	R=(radium	DelT=(vgh	a=	
After sp	65.79517919	46.04938	218090.9	0.712094335	32.24	33.669	2.04	1.428796	#REF!	
	Ralpha=(thermal conductiv	62.302282								
	Water Viscosity=	0.7618628								
	Nuk=(en at inlet)	20.9								
	Pr=(Prandtl number)	5.0920392								
	Tm=(water and foil layer)	32.954602								
	Vw=(waterflow velocity)	0.2333333								

Evaporation rate in triple-layer foil skin construction

Qe=	Pv=	Pa=	p'=(inches)	Tw=	Tdp=	W=	Tdp=	a=
268.7162591	4667.25	4886.0487	1.443228087	32.24	19.0175	0.007949	10.58499	-0.974056
To=(air at outlet)	26.6							

Solar model / Output / Heat transfers / Weather input / Constants / Geometry input / Materials / Sites / Notepad / Export / Sheet2 / Sheet1

Figure 7-6: Salient parameter determination worksheet